NUREG/CR-4312
EGG-2396

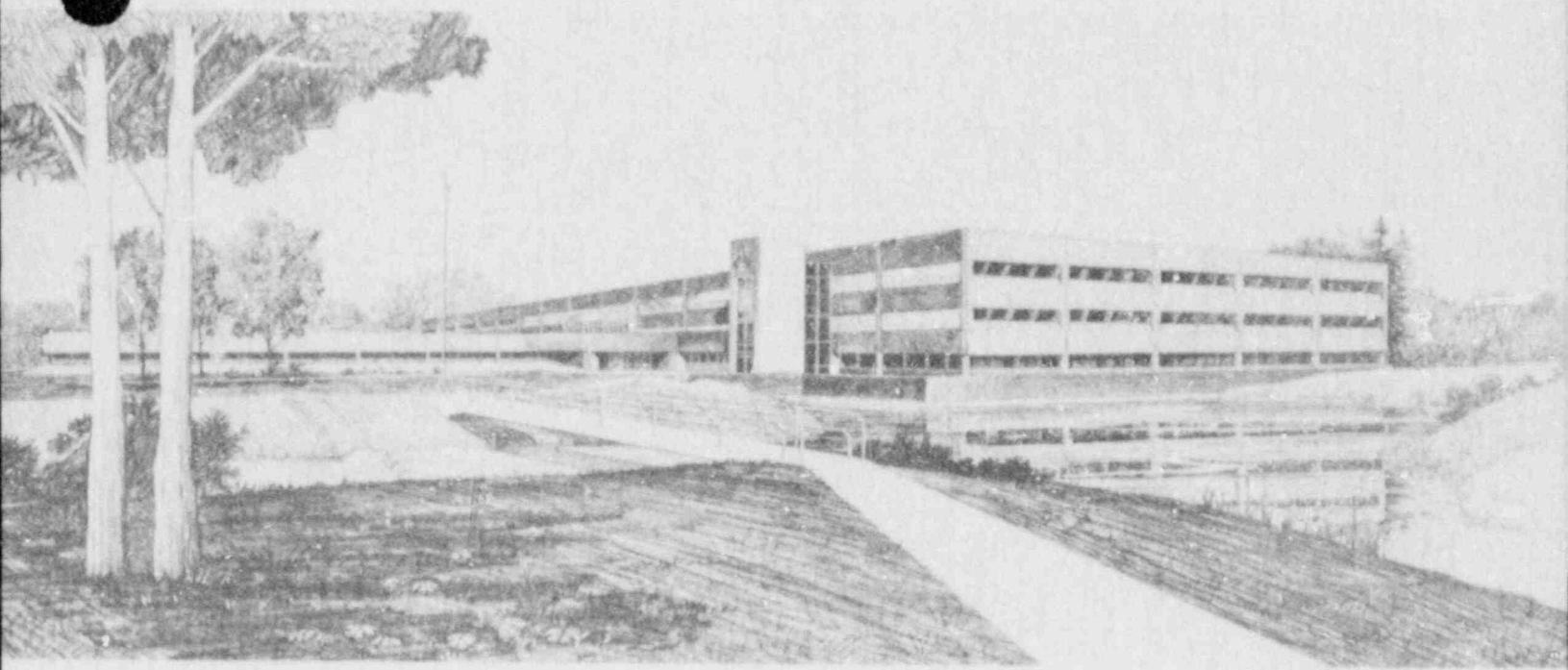

Idaho National Engineering Laboratory
Operated by the U.S. Department of Energy

RELAP5/MOD2 Code Manual
Volume 1: Code Structure, Systems Models, and Solution Methods

Victor H. Ransom, et al.

August 1985

Prepared for the
U.S. Nuclear Regulatory Commission
Under DOE Contract No. DE-AC07-76IDO1570

EG&G Idaho

NOTICE

NUREG/CR-4312
EGG-2396
Limited Distribution

RELAP5/MOD2 CODE MANUAL
VOLUME 1: CODE STRUCTURE, SYSTEMS MODELS, AND SOLUTION METHODS

Victor H. Ransom
Richard J. Wagner
John A. Trapp
Lynn R. Feinauer
Gary W. Johnsen
Dennis M. Kiser
Richard A. Riemke

Published August 1985

EG&G Idaho, Inc.
Idaho Falls, Idaho 83415

Prepared for the
U.S. Nuclear Regulatory Commission
Washington, D.C. 20555
Under DOE Contract No. DE-AC07-76IDO1570
FIN No. A6330

ABSTRACT

The principal objective of the RELAP5 project is to provide the United States Nuclear Regulatory Commission (USNRC) with a fast running and user convenient light water reactor system transient analysis code for use in rule making, licensing audit calculations, evaluation of operator guidelines, and as a basis for a nuclear plant analyzer. The RELAP5/MOD2 code has been developed for best estimate transient simulation of pressurized water reactors and associated systems. The code modeling capabilities are simulation of large and small break loss-of-coolant accidents, as well as operational transients such as anticipated transient without SCRAM, loss-of-offsite power, loss of feedwater, and loss of flow. A generic modeling approach utilizes as much of a particular system to be modeled as necessary. RELAP5/MOD2 extends the modeling base and capabilities offered by previous versions of the code. In particular, MOD2 contains two energy equations, reflood heat transfer, a two-step numerics option, a gap conductance model, revised constitutive models, and additional component and control system models. Control system and secondary system components have been added to permit modeling of plant controls, turbines, condensers, and secondary feedwater conditioning systems.

The modeling theory and associated numerical schemes are documented in Volume 1 to acquaint the user with the modeling base and thus aid in effective use of the code. Volume 2 contains detailed instructions for code application and input data preparation. In addition, Volume 2 contains user guidelines that have evolved over the past several years from application of the code at the Idaho National Engineering Laboratory, at other national laboratories, and by industry users from throughout the world.

EXECUTIVE SUMMARY

The light water reactor transient analysis code, RELAP5, is being developed at the Idaho National Engineering Laboratory (INEL) under the United States Nuclear Regulatory Commission (USNRC) support to provide an advanced best-estimate predictive capability for use in a wide spectrum of applications in support of the regulatory process. Applications of this capability include analytical support for the LOFT and Semiscale experimental programs; support of the relief valve testing program; simulation of design basis loss-of-coolant accidents (DBLOCA), anticipated transients without scram (ATWS), and operational transients in LWR systems for use in regulatory investigations. RELAP5 is a highly generic code that can be used for simulation of a wide variety of hydraulic and thermal transients in both nuclear and nonnuclear systems involving steam-water-noncondensible fluid mixtures.

The RELAP5 code is based on a nonhomogeneous and nonequilibrium model for the two-phase system that is solved by a fast, partially-implicit numerical scheme to permit economical calculation of system transients. The objective of the development effort from the outset has been to produce a code that includes important first-order effects necessary for accurate prediction of system transients, but is sufficiently simple and cost effective such that parametric or sensitivity studies are possible.

The code includes many generic component models from which general systems can be simulated. The component models include pumps, valves, pipes, heat structures, reactor point kinetics, electric heaters, jet pumps, turbines, separators, accumulators, and control system components. In addition, special process models are included for effects such as form loss, flow at an abrupt area change, branching, choked flow, boron tracking, and a noncondensible gas.

The system mathematical models are coupled into an efficient code structure. The code includes extensive input checking capability to help the user discover input errors and inconsistencies. Also included are

free-format input, internal plot capability, restart, renodalization, and variable output edit features. These user conveniences were developed in recognition that generally the major cost associated with the use of a system transient code is in the engineering labor and time involved in accumulating system data and developing system models, while the computer cost associated with generation of the final result is usually small.

The development of RELAP5 has spanned approximately ten years from the early stages of numerical scheme development to the present. RELAP5 represents the aggregate accumulation of experience in modeling two-phase processes, and LWR systems in particular. The code development has benefited from extensive application and comparison to experimental data in the LOFT and Semiscale programs. Additional experience has been gained through use of the code by many research and development institutions in the U.S. and in several foreign countries.

Volume 1 describes the basic theory and numerical methods used for the various system models. Volume 2 gives detailed descriptions of the input preparation and execution procedures, and provides general guidelines on application.

ACKNOWLEDGMENT

Development of a complex computer code such as RELAP5/MOD2 is the result of a team effort. Acknowledgment is also made to those who made significant contributions to the current version, in particular, Drs. J. C. Lin, H. Chow, C. C. Tsai, and W. M. Bryce. Acknowledgment is made to those who made significant contributions to earlier versions, in particular, Mr. K. E. Carlson and Dr. H. H. Kuo. Acknowledgment is also made to Mrs. E. C. Johnson for her work in RELAP5 configuration control and user services.

The RELAP5 Program is indebted to the technical monitors responsible for directing the overall program; Mr. W. Lyon, Drs. R. Landry, R. Lee and Y. Chen of the United States Nuclear Regulatory Commission and Dr. D. Majumdar of the Department of Energy-Idaho Operations Office. Finally, acknowledgment is made of all the code users who have been very helpful in stimulating timely correction of code deficiencies.

CONTENTS

FIGURES

TABLES

NOMENCLATURE (with SI units)

A	Cross-sectional area (m^2), coefficient matrix in hydrodynamics, coefficient in pressure and velocity equations
A_1	Coefficient in heat conduction equation at boundaries
A_L	Surge line cross sectional area (m^2)
A_t	Throat area (m^2)
a	Speed of sound (m/s), interfacial area per unit volume (m^{-1}), coefficient in gap conductance, coefficient in heat conduction equation, absorption coefficient
B	Coefficient matrix, drag coefficient, coefficient in pressure and velocity equations
B_1	Coefficient in heat conduction equation at boundaries
b	Coefficient in heat conduction equation, source vector in hydrodynamics
B_x	Body force in x coordinate direction (m/s^2)
B_y	Body force in y coordinate direction (m/s^2)
C	Coefficient of virtual mass, general vector function, coefficient in pressure, and velocity equations delay neutron precursors in reactor kinetics, concentration
C_0	Coefficient in noncondensible energy equation (J/kg-K)

C_d	Drag coefficient
C_g	Dimensional constant in correlation for r_g
C_p	Specific heat at constant pressure (J/kg-K)
C_v	Specific heat at constant volume (J/kg-K)
c	Coefficient in heat conduction equation, coefficient in new time volume-average velocity equation
D	Coefficient of relative Mach number, diffusivity, diameter (m), heat conduction boundary condition matrix, coefficient in pressure and velocity equations
D_o	Coefficient in noncondensible energy equation ($J/kg-K^2$)
D_1	Coefficient of heat conduction equation at boundaries
d	Coefficient in heat conduction equation, droplet diameter (m)
DISS	Energy dissipation function (W/m^3)
E	Total energy ($U + v^2/2$) (J/kg), emissivity, Young's modulus, term in iterative heat conduction algorithm, coefficient in pressure equation
e	Interfacial roughness
Eu	Euler number

F	Term in iterative heat conduction algorithm, gray-body factor with subscript, frictional loss coefficient, vertical stratification factor
FIF, FIG	Interphase drag coefficients (liquid, vapor) (s^{-1})
FI	Interphase drag coefficient (m^3/kg-s)
FWF, FWG	Wall drag coefficients (liquid, vapor) (s^{-1})
f	Interphase friction factor, vector for liquid velocities in hydrodynamics
G_{head}	Pressure drop across valve due to gravity (Pa)
G	Mass velocity (kg/s), shear stress, gradient, coefficient in heat conduction, vector quantity, fraction of delayed neutrons in reactor kinetics
Gc	Dynamic pressure for valve (Pa)
Gr	Grashof number
g	Gravitational constant (m/s^2), temperature jump distance (m), vector for vapor velocities in hydrodynamics
$g_{Z,g}$	Acceleration due to gravity (m/s^2)
H	Elevation (m), volumetric heat transfer coefficient ($W/K\text{-}m^3$), head (m)
HLOSSF, HLOSSG	Form or frictional losses (liquid, vapor) (m/s)

h	Specific enthalpy (J/kg), heat transfer coefficient (W/m^2-k), energy transfer coefficient for r_g, head ratio
h_L	Dynamic head loss (m)
I	Identity matrix, moment of inertia ($N\text{-}m\text{-}s^2$)
J	Junction velocity (m/s)
K	Energy form loss coefficient
k	Thermal conductivity (W/m-K)
k_B	Boltzmann constant
k_s	Spring constant
L	Length, limit function
L_L	Surge line length (m)
$\ell\ell$	Liquid level (m)
M	Mach number, molecular weight, pump two-phase multiplier, mass transfer rate, mass (kg)
N	Number of system nodes, number density ($\#/m^3$), pump speed (rad/s)
Nu	Nusselt number
n	Unit vector, order of equation system

P_{Br}	Valve closing back pressure (Pa)
P	Pressure (Pa), reactor power (watts), channel perimeter (m), turbine power (J/s)
P_D	Nitrogen pressure in dome (Pa)
P_f	Relates reactor power to heat generation rate in heat structures
P_o	Atmospheric pressure (Pa)
p	Wetted perimeter (m), particle probability function
PCV	Specified pressure required to close a valve (Pa)
Pr	Prandtl number
Q	Volumetric heat addition rate (W/m^3), space dependent function, volumetric flow rate (m^3/s)
Q_D	Total heat transfer to vapor dome (Watts)
q	Heat transfer rate (Watts), heat flux (W/m^2)
q_t	Specified time dependent, space dependent factor in the source term of heat conduction
R	Reynolds number, radius (m), surface roughness in gap conductance, radiation resistance term
Re	Reynolds number
Re_p	The particle Reynolds number

R_n, R_s	Universal gas constants (noncondensible, steam) (N-m/kg-K)
r	Reaction fraction for turbine
S	Chen's boiling suppression factor, stress gradient, specific entropy (J/kg-K), shape factor, real constant, source term in heat conduction or reactor kinetics (Watts)
s	Surface, Laplace transform variable
T	Temperature (K), trip
T_c	Critical temperature (K)
T_R	Reduced temperature (K)
T_t	Specified time dependent function in heat conduction
t	Time (s)
U	Specific internal energy (J/kg), vector of dependent variables
u	Radial displacement in gap conductance (m)
V	Volume (m^3), specific volume (m^3/kg), control quantity
V_v	Volume of noncondensible in accumulator dome (m^3)
VFDP, VGDP	Coefficient for pressure change in momentum equations (liquid, vapor) (m/s/-Pa)
VIS	Numerical viscosity terms in momentum equations (m^2/s^2)

VIS_F, VIS_G	Numerical viscosity terms in momentum equations (liquid, vapor) (m^2/s^2)
VUNDER, VOVER	Separator model parameters (liquid, vapor)
v	Mixture velocity (m/s), phasic velocity (m/s), flow ratio, liquid surge line velocity (m/s)
v_c	Choking velocity (m/s)
W	Weight of valve disk, weighting function in reactor kinetics, relaxation parameter in heat conduction, shaft work per unit mass flow rate
W_{crit}	Critical Weber number
We	Weber number
w	Humidity ratio
X	Static quality, mass fraction, conversion from MeV/s to watts
x	Spatial coordinate (m), vector of hydrodynamic variables
Y	Control variable
Z	Two-phase friction correlation factor, function in reactor kinetics
z	Elevation change coordinate (m)

Symbols

α	Void fraction, subscripted volume fraction, angular acceleration (rad/s^2), coefficient for least squares fit, speed ratio
β	Coefficient of isobaric thermal expansion (K^{-1}), effective delayed neutron fraction in reactor kinetics
Γ	Volumetric mass exchange rate (kg/m^3-s)
ΔP_f	Dynamic pressure loss (Pa)
ΔP_s	Increment in steam pressure (Pa)
ΔV_s	Increment in specific volume of steam (m^3/kg)
Δt	Increment in time variable (s)
Δt_c	Courant time step (s)
Δx	Increment in spatial variable (m)
δ	Area ratio, truncation error measure, film thickness (m), impulse function, Deryagin number
ϵ	Coefficient, strain function, emissivity, tabular function of area ratio, surface roughness, wall vapor generation/condensation flag
ζ	Diffusion coefficient, multiplier or horizontal stratification terms the right side of heat conduction equation in finite difference form

η	Efficiency, bulk/saturation enthalpy flag
θ	Relaxation time in correlation for Γ, angular position (rad)
κ	Coefficient of isothermal compressibility (Pa^{-1})
Λ	Prompt neutron generation time, Baroczy dimensionless property index
λ	Eigenvalue, interface velocity parameter, friction factor, decay constant in reactor kinetics
μ	Viscosity (kg/m•s)
ν	Kinematic viscosity (m^2/s), Poisson's ratio
ξ	Exponential function, RMS precision
π	3.141592654
ρ	Density (kg/m^3), reactivity in reactor kinetics (dollars)
Σ_f	Fission cross section
Σ'	Depressurization rate (Pa/s)
σ	Surface tension (J/m^2), stress, flag used in heat conduction equations to indicate transient or steady state
τ	Shear stresses (N), torque (N-m)
ϕ	Donored property, Lockhart-Martinelli two-phase parameter, neutron flux in reactor kinetics, angle of inclination of valve assembly

χ	Lockhart-Martinelli parameter
Ψ	Coefficient, fission rate (#/s)
ω	ngular velocity (rad/s), function variable in reactor kinetics

Subscripts

a	Average value
B	Boron, dissolved solid
b	Bubble
CHF	Value at critical heat flux
c	Vena contracta, continuous phase, cladding, critical property, cross section
cm	Cladding midpoint
con	Condensation
cr	Critical property or condition
D	Drive line, vapor dome
d	Droplet, delay in control component
e	Thermodynamic equilibrium, equivalent quality in hydraulic volumes, value ring exit, elastic deformation

exp	Used to indicate explicit velocities in choking
F	Wall friction, fuel
FB, FBB	Film boiling, Bromley film boiling
f	Liquid phase
fg	Phasic difference (i.e., vapor term-liquid term)
fp	Onset of vapor pull-through
fr	Frictional
g	Vapor phase, gap
ge	Incipient liquid entrainment
H	Head
HE	Homogeneous equilibrium
HF	Homogeneous frozen
hy	Hydraulic
I	Interface
IB	Incipience of boiling
i	Inlet, interface
j, j+1, j-1	Spatial noding indices, junctions

K	Spatial noding indices, volumes
L	Spatial noding index, volumes, laminar
ℓ	Left boundary in heat conduction
M	Rightmost boundary in heat conduction
m	Mixture property, motor, mesh point
NB	Nucleate boiling
n	Noncondensible component of vapor phase
o	Reference value
R	Rated values
r	Relative Mach number, right boundary in heat conduction
S	Suction region
s	Steam component of vapor phase
sat	Saturated quantity
T	Point of minimum area, turbulent
TB	Transition film boiling
t	Turbulent, tangential
tt	Fully turbulent

up	Upstream quantity
v	Mass mean Mach number, vapor quantity, valve
w	Wall, water
wall	Wall of tank
wg, wf	Wall to vapor, wall to liquid
1	Upstream station, multiple junction index, vector index
10	Single-phase value
2	Downstream station, multiple junction index, vector index
2ϕ	Two-phase value
τ	Torque
$\sim$	Vector
$\approx$	Matrix

Superscripts

b	Boundary gradient weight factor in heat conduction, vector quantities
exp	Old time terms in velocity equation
I	Imaginary part of complex number

m-1, m, m+1	Mesh points in heat conduction finite difference equation or mean value
n, n+1	Time level index
n + 1/2	An average of quantities with superscripts n and n + 1
o	Initial value
R	Real part of complex number
Y	Right boundary in heat conduction
s	Saturation property, space gradient weight factor in heat conduction
v	Volume gradient weight factor in heat conduction
w	Wall
1	Vector index, coefficient in velocity equation
2	Vector index
*	Total derivative of a saturation property with respect to pressure, local variable, bulk/saturation property
'	Derivative
-	Vector, average quantity

.	Donored quantity
~	Unit momentum for mass exchange, intermediate time variable
^	Linearized quantity, quality based on total mixture mass

RELAP5/MOD2 CODE MANUAL

VOLUME 1: CODE STRUCTURE, SYSTEMS MODELS, AND SOLUTION METHODS

1. INTRODUCTION

RELAP5/MOD2 is a pressurized water reactor (PWR) system transient analysis code that can be used for simulation of a wide variety of PWR system transients of interest in light water reactor (LWR) safety. The primary system, secondary system, feedwater train, system controls, and core neutronics can be simulated. The code models have been designed to permit simulation of postulated accidents ranging from large break loss-of-coolant accidents to accidents involving the plant controls and fuel system. Transient conditions can be modeled up to the point of fuel damage.

RELAP5/MOD2 was produced by improving and extending the modeling base that was established with the release of RELAP5/MOD1[1] in December 1980. The modeling approach and instructions for application of the code are documented in a two-volume users manual. In volume 1 the basis for the system models and their numerical implementation is described. Volume 2 contains recommendations for the proper use of the code models and detailed descriptions of the input data requirements for use of the code.

1.1 Project Objectives

The principal objective of the RELAP5 project is to provide the U.S. Nuclear Regulatory Commission (USNRC) with a fast running and user convenient light water reactor system transient analysis code for use in rule making, licensing audit calculations, evaluation of operator guidelines, and as a basis for a nuclear plant analyzer. The code is used extensively at the Idaho National Engineering Laboratory (INEL) for experiment planning, pretest prediction, and posttest analysis in support of the Semiscale, LOFT, and Power Burst Facility (PBF) LWR research projects. A secondary objective is to provide advanced analysis capability to other nuclear power organizations for use in design, safety analysis, and licensing application work. Previous versions of the code have been

made available worldwide through the National Energy Software Center (NESC). RELAP5/MOD2 (and future versions) is available through exchange agreement with the USNRC. The basis for such exchanges is fully established and interested organizations are advised to contact the USNRC Office of Nuclear Regulatory Research.

From the outset of the RELAP5 project the goal has been to establish a reliable analytical capability for use in the nuclear power industry. The approach has been to rely on first principles modeling where possible and thus reduce empiricism. The numerical simulation of transient two-phase flow has been a most challenging task. The RELAP5/MOD2 two-phase flow model provides a significantly improved capability over RELAP5/MOD1 and represents an enhanced understanding of the underlying physics of two-phase flow.

An additional goal of the project has been to provide a more comprehensive and generic modeling of the complete nuclear steam supply system including turbines, generators, condensers, feed systems, and plant controls. The highly generic modeling capability of the code also permits it to be used in many nonnuclear applications of steam-water systems.

1.2 Relationship to Previous Code Versions

The series of RELAP-codes began with RELAPSE (REactor Leak And Power Safety Excursion), which was released in 1966. Subsequent versions of this code are RELAP2,[2] RELAP3,[3] and RELAP4[4] in which the original name was shortened to Reactor Excursion and Leak Analysis Program (RELAP). All of these codes were based on a homogeneous equilibrium model (HEM) of the two-phase flow process. The last code version of this series is RELAP4/MOD7,[5] which was released to NESC in 1980.

In 1976, the development of a nonhomogeneous nonequilibrium model was undertaken for RELAP4. It soon became apparent that a total rewrite of the code was required to efficiently accomplish this goal. The result of this effort was the beginning of the RELAP5 project. As the name implies, this is the fifth in the series of computer codes that was designed to simulate

the transient behavior of LWR systems under a wide variety of postulated accident conditions. RELAP5 follows the naming tradition of previous RELAP codes, i.e., the odd numbered series are complete rewrites of the program while the even numbered versions had extensive model changes, but used the architecture of the previous code. Each version of the code reflects the increased knowledge and new simulation requirements from both large and small scale experiments, theoretical research in two-phase flow, numerical solution methods, computer programming advances, and the increased size and speed of computers.

The principal new feature of the RELAP5 series is the use of a two-fluid nonequilibrium nonhomogeneous hydrodynamic model for transient simulation of the two-phase system behavior. RELAP5/MOD2 employs a full nonequilibrium, six equation, two-fluid model. The use of the two-fluid model eliminates the need for the RELAP4 submodels such as the bubble rise and enthalpy transport models, which were necessary to overcome the limitations of the single fluid model.

1.3 Future Development

RELAP5/MOD2 is the final PWR version of the RELAP5 code. Future embellishments and improvements will be added by updated cycles of the code as needed. In general, these improvements will be made based on the identification of deficiencies by code users.

2. CODE ARCHITECTURE

The RELAP5 code architecture is the result of development experience gained through the RELAP4,[5] CONTEMPT,[6] FRAP,[7] and other large thermal-hydraulic computer codes that have been developed at the INEL. Convenience, design for future growth, and computer efficiency were primary considerations in the structure design. In particular, user experience with the RELAP4 series of codes was used to establish the basic philosophy of a simple and clean interface between the code and user.

2.1 Computer Adaptability

RELAP5/MOD2 is written in FORTRAN V and was developed specifically for a CDC Cyber-176 computer operating under the NOS system. Compile time options are provided to allow operation on Cyber-7600 or -176 machines using SCOPE2 or NOS-BE and machines without large core memory (LCM), such as the Cyber-175. Compile time options are also provided to allow operation on CRAY-1 and CRAY-XMP machines using either COS (default) or the CTSS operating system. Extended core storage (ECS) cannot be used in place of LCM since both block transfers and single level access to LCM is used. Very little testing has been done on the optional versions. However, experience with RELAP5/MOD1 showed a surprisingly low error rate on the optional versions and hopefully RELAP5/MOD2 experience will be similar. The optional versions are maintained and reported errors are resolved.

Compared to large scale scientific machines now available, the small core memory (SCM) accessible for storage of instructions and operand data on the Cyber-176 is relatively small. To conserve memory, RELAP5 uses FORTRAN language extensions to efficiently pack logical (1 bit) and small integer (mostly 12 and 18 bit) quantities into the 60 bit words of the Cyber computer. The packing has permitted additional and more complex models to be added to RELAP5 and execution of more detailed and comprehensive simulations without resorting to extensive swapping of data between SCM and LCM. The penalty is that conversion to other computers is

time consuming due to the dependence on the CDC 60 bit word. Compile time options allow the selection of CRAY compatible coding. Conversion to the CYBER-205 and IBM computers is underway.

2.2 Top Level Organization

RELAP5 is coded in a modular fashion using top down structuring. The various models and procedures are isolated in separate subroutines. The top level structure is shown in Figure 1 and consists of input, steady state, transient, plotting, and stripping blocks.

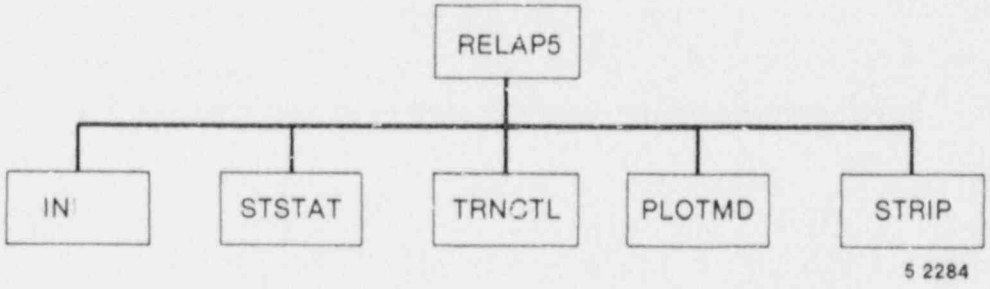

Figure 1. RELAP5 top level structure.

The input block processes input, checks input data, and prepares required data blocks for all program options and is discussed in more detail in Section 2.3.

The steady state block determines the steady state conditions if a properly posed steady state problem is presented. The steady state is obtained by running an accelerated transient until the time derivatives approach zero. Thus, the steady state block is very similar to the transient block but contains convergence testing algorithms to determine satisfactory steady state, divergence from steady state, or cyclic operation. With this technique, approach to steady state from an initial condition would be identical to a plant transient from the initial condition. Pressures, densities, and flow distributions would adjust quickly, but thermal effects would occur more slowly. To reduce the

transient time required to reach steady state, the steady state option artificially accelerates heat conduction by reducing the heat capacity of the conductors.

The transient block advances the transient solution. Further discussion of this and the equivalent portions of the steady state block is given in Section 2.4.

The plotting block produces time history plots of simulation results generated from the steady state or transient blocks. This block can also produce plots from data saved on a restart-plot file from an earlier simulation.

The strip block extracts simulation data from a plot-restart file for convenient passing of RELAP5 simulation results to other computer programs. Brief, one sentence descriptions of all subroutines within RELAP5 are included in Appendix A.

2.3 Input Processing Overview

Input processing has three phases. The first phase reads all input data, checks for punctuation and typing errors such as multiple decimal points and letters in numerical fields, and stores the data keyed by card number such that the data are easily retrieved. A listing of the input data is provided and punctuation errors are noted.

During the second phase, restart data from a previous simulation is read if the problem is a RESTART type, and all the input data are processed. Some processed input is stored in fixed common blocks, but the majority of the data is stored in dynamic data blocks that are created only if needed by a problem and sized to the particular problem. In a NEW type problem, dynamic blocks must be created. In RESTART problems, dynamic blocks may be created, deleted, added to, partially deleted, or modified as modeling features and components within models are added, deleted, or modified. Extensive input checking is done, but at this level, checking is

limited to new data from the cards being processed. Relationships with other data cannot be checked because the latter may not yet be processed. As an illustration of this level of checking, junction data are checked to determine if they are within the appropriate range such as positive, nonzero, or between zero and one, and volume connection codes are checked for proper format. However, no attempt is made at this point to check whether or not the referenced volumes exist in the problem until all input data is processed.

The third phase of processing begins after all input data have been processed. Since all data have been placed in common or dynamic data blocks during the second phase, complete checking of interrelationships can proceed. Examples of cross-checking are: existence of hydrodynamic volumes referenced in junctions and heat structure boundary conditions; entry or existence of material property data specified in heat structures; and validity of variables selected for minor edits, plotting, or used in trips and control systems. As the cross-checking proceeds, cross-linking of the data blocks is done so that it need not be repeated at every time step. The initialization required to prepare the model for start of transient advancement is done at this level.

Input data editing and diagnostic messages can be generated during the second and/or third phases. Input processing for most models generates output and diagnostic messages during both phases. Thus, input editing for these models appears in two sections.

As errors are detected, various recovery procedures are used so that input processing can be continued and a maximum amount of diagnostic information can be furnished. Recovery procedures include supplying default or benign replacement data, marking the data as erroneous so that other models do not attempt use of the data, or deleting the bad data. The recovery procedures sometimes generate additional diagnostic messages. Often after attempted correction of input, different diagnostic messages appear. These can be due to continued incorrect preparation of data, but the diagnostics may result from the more extensive testing permitted as previous errors are eliminated.

The RELAP5 code uses several levels of segmentation to reduce memory requirements. Segmentation is the separation of the coding into segments that reside on disk, and during execution, only those segments needed for a particular processing phase are brought into SCM. During input processing, dynamic blocks are stored on disk and are brought into SCM and LCM only as needed.

2.4 Transient and Steady State Overview

Figure 2 shows the second-level structures for the transient and steady state blocks or subroutines. Since these blocks are nearly identical, the transient blocks are discussed with equivalent steady state block names shown in parentheses.

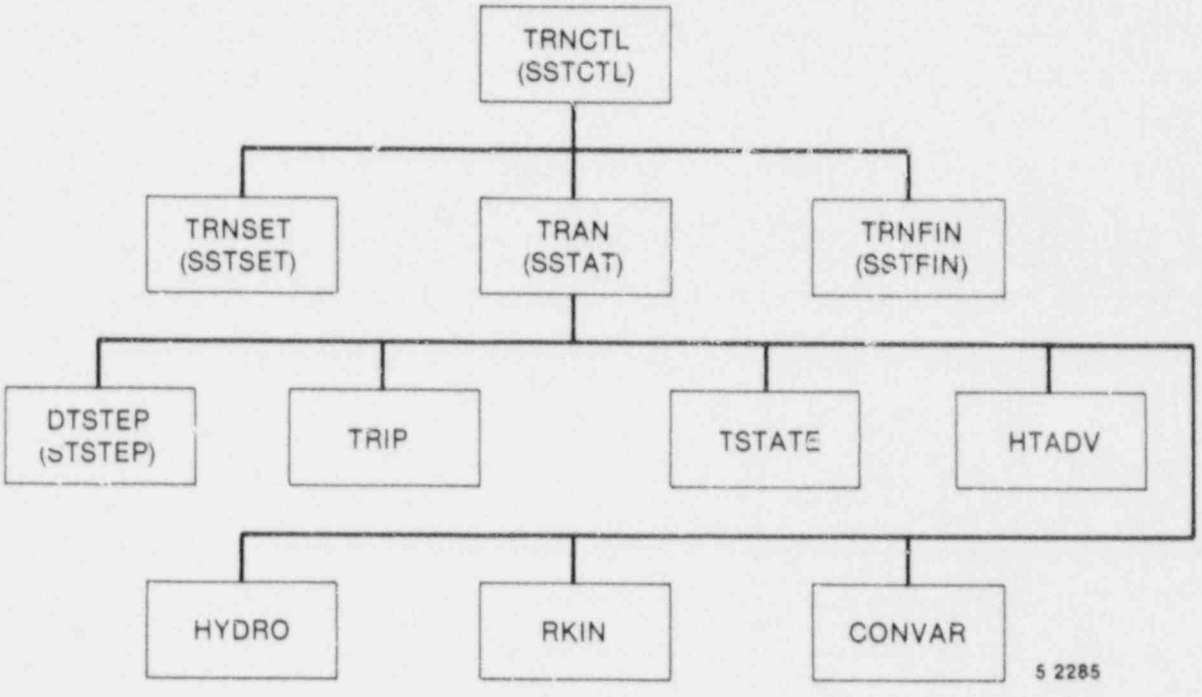

Figure 2. Transient (steady state) structure.

The Subroutine TRNCTL (SSTCTL) consists only of the logic to call the next lower level routines. Subroutine TRNSET (SSTSET) brings dynamic blocks required for transient execution from disk into SCM or LCM, performs final cross-linking of information between data blocks, sets up arrays to

control the sparse matrix solution, establishes scratch work space, and returns unneeded SCM and LCM memory. Subroutine TRAN (SSTAT) controls the transient advancement of the solution. Nearly all the execution time is spent in this block and this block is the most demanding of memory. Nearly all the dynamic data blocks must be in SCM and LCM, and the memory required for instruction storage is high since coding to advance all models resides in this block. The TRAN block is a single segment. Further segmentation results in a significant execution time penalty because the processing time to complete one advancement is of the same order of magnitude as required to load one segment from disk. Some custom installations on the Cyber 7600 (with only 64K SCM) have extensively segmented the TRAN block. In order to avoid the excessive delay in waiting for disk transfers of segments, a segment when first loaded is copied to LCM. Subsequent references to the segment use the fast LCM-SCM transfer. The Subroutine TRNFIN (SSTFIN) releases space for the dynamic data blocks that are no longer needed and prints the transient timing summary.

Figure 2 also shows the structure of the TRAN (SSTAT) block. DTSTEP (STSTEP) determines the time step size and whether transient advancement should be terminated. TSTATE applies hydrodynamic boundary conditions by computing thermodynamic conditions for time dependent volumes and velocities for time dependent junctions. The remaining blocks perform or control the calculations for major models within RELAP5: trip logic (TRIP), heat structure advancement (HTADV), hydrodynamic advancement (HYDRO), reactor kinetics advancement (RKIN), and control system advancement (CONVAR). The blocks are executed in the order shown in the figure from left to right, top to bottom. Although implicit techniques are used within some of the blocks (HTADV and HYDRO), data exchange between blocks is explicit, and the order of block execution dictates the time levels of feedback data between models. Thus, HTADV advances heat conduction/convection solutions using only old time reactor kinetics power and old time hydrodynamic conditions. HYDRO, since it follows HTADV, can use both new and old time heat transfer rates to compute heat transferred into a hydrodynamic volume.

2.5 Computer Requirements

2.5.1 Memory Requirements

The steady state or transient advancement (SSTAT or TRAN blocks) is the most demanding of memory. The transient coding and fixed common on the Cyber-176 version requires approximately 161000_8 words of SCM and steady state coding requires 166000_8. The LCM requirement including the water property table (the standard one in use at INEL and as would be generated by the installation procedure documented in Volume 2) is approximately 33000_8 words of LCM. Remaining SCM and LCM storage requirements are for dynamic blocks, the sizes of which are problem dependent. For example, a small sample problem (Edwards pipe) consisting of 21 hydrodynamic volumes, 20 junctions, 21 heat structures with a total of 231 mesh points, 22 control variables, two trips, reactor kinetics, plots, and a restart-plot file requires 177000_8 words of SCM and 43000_8 words of LCM. The INEL Cyber 176 system allows a user SCM field length of nearly 400000_8. A three loop PWR problem that approaches this limit with 376000_8 words of SCM and 126323_8 words of LCM, has 227 volumes, 241 junctions, 221 heat structures totaling 1002 mesh points, 290 control variables, and 174 trips. A Cyber-7600 or Cyber-176 operating under SCOPE2 would require $\sim 10000_8$ less SCM words. The SCM requirement for a machine without LCM would be approximately the sum of the SCM and LCM requirements given above. Except for the restart-plot file, disk requirements are modest. The length of the restart-plot file is dependent on user input, but is generally large enough that magnetic tapes should be used except for very short term storage.

2.5.2 Computing Time Requirements

Required computing time varies depending on computer type, size of problem, simulation time, and transient scenario. Simulation time for a large break loss-of-coolant accident is usually short, on the order of a few minutes, but small time steps are needed. Larger time steps can be used for small breaks, but simulation time can be hours.

The Edwards Pipe problem previously mentioned represents a pipe blowdown experiment[8] with additional models arbitrarily added for testing. RELAP5 requires under 7 s of Cyber-176 computer time to simulate this pipe blowdown for 0.5 s. The large PWR problem described in the previous section runs to steady state with a time step of 50 ms (which is restricted by the material Courant limit) and runs six times slower than real time on the Cyber-176. Both problems have the number of volumes approximately equal to the number of junctions and also to the number of heat structures. The grind time for these problems is ~1.5 ms per volume per advancement. These examples were run using the semi-implicit hydrodynamic numerical scheme. The user has the option of using the nearly-implicit hydrodynamic numerical scheme which allows violation of the Courant limit and is to be used for quasi-steady problems.

In general, computer run time is roughly proportional to the number of hydrodynamic volumes included in a problem and inversely proportional to the time step size used. The time step size for the semi-implicit scheme is determined by three factors: the user specified maximum time step, the most restrictive material Courant limit in the problem, and the mass truncation error. The overall CPU requirement can be estimated for a particular case by multiplying the grind time (0.0015 s) times the number of hydrodynamic volumes used, times the number of time steps required. The number of time steps required is the most difficult parameter to estimate since it is the total simulation time divided by the average time step size. The maximum average time step can be estimated from material Courant limit considerations, however, a minimum will depend upon the severity of the transient and experience is the best guide. Reference to previous problems is the best guide for estimating run times. For the nearly-implicit scheme the code is allowed to run up to five times the material Courant limit for steady state problems. The grind time for this scheme is 25 to 60% more than the semi implicit grind time.

3. SYSTEM MODELS AND SOLUTION METHODS

In this section each of the major system models, (hydrodynamics, heat structures, controls, trips, and reactor kinetics) is described. The analytical basis for each model and the corresponding numerical solution methods are included.

3.1 Hydrodynamics

The RELAP5/MOD2 hydrodynamic model is a one-dimensional, transient, two-fluid model for flow of a two-phase steam-water mixture that can contain a noncondensible component in the steam phase and/or a nonvolatile component in the liquid phase. The major change from the RELAP5/MOD1 model is the addition of a second energy equation that eliminates the need to constrain one of the phases at the saturated state. Other improvements include a revised interphase drag formulation, a new nonequilibrium wall heat transfer model, a revised wall friction partitioning model, a revised vapor generation model that includes wall heat transfer considerations, and the addition of several new special process/component models.

The RELAP5/MOD2 hydrodynamic model contains several options for invoking simpler hydrodynamic models. These include homogeneous flow, thermal equilibrium, and frictionless flow models. These options can be used independently or in combination. The homogeneous and equilibrium models were included primarily to be able to compare code results with calculations from the older homogeneous equilibrium model (HEM) based codes.

The two-fluid equations of motion that are used as the basis for the RELAP5/MOD2 hydrodynamic model are formulated in terms of area and time average parameters of the flow. Phenomena that depend upon transverse gradients such as friction and heat transfer are formulated in terms of the bulk potentials using empirical transfer coefficient formulations. The system model is solved numerically using a semi-implicit finite difference technique. The user can select an option for solving the system model

using a nearly-implicit finite difference technique, which allows violation of the material Courant limit. This option is suitable for steady state calculations and for slowly-varying, quasi-steady transient calculations.

The basic two-fluid differential equations possess complex characteristic roots that give the system a partially elliptic character and thus constitutes an ill-posed initial boundary value problem. In RELAP5 the numerical problem is rendered well posed by the introduction of artificial viscosity terms in the difference equation formulation that damp the high frequency spatial components of the solution. The ill-posed character of the two-fluid model is a result of the momentum formulation and is introduced as a result of the spatial averaging process and neglect of higher order physical effects. Ransom and Hicks[9] have studied several formulations in which two pressures (one for each fluid) are included in the model, and these models are totally hyperbolic and thus constitute well-posed problems. Limited numerical studies by Ransom and Scofield[10] have shown that solutions for the two-pressure model compare very well to that for the single pressure model with damping. In general, the differences are significant only for short wave-length components of the solution where numerical truncation error is dominant. Thus, either approach provides a valid numerical simulation at solution component wave lengths of interest in most reactor safety problems. The simpler formulation of the single pressure model favors using that approach.

The semi-implicit numerical solution scheme uses a direct sparse matrix solution technique for time step advancement. It is an efficient scheme and results in an overall grind time on the CDC Cyber 176 of ~0.0015 s. The method has a material Courant time step stability limit. However, this limit is implemented in such a way that single node Courant violations are permitted without adverse stability effects. Thus, single small nodes embedded in a series of larger nodes will not adversely affect the time step and computing cost. The nearly-implicit numerical solution scheme also uses a direct sparse matrix solution technique for time step advancement. This scheme has a grind time that is 25 to 60% greater than the semi-implicit scheme but allows violation of the material Courant limit for all nodes.

3.1.1 Field Equations

RELAP5/MOD2 has six dependent variables (seven if a noncondensible component is present, i.e., P, U_g, U_f, α_g, X_n, v_g, and v_f). The noncondensible quality is defined as the ratio of the noncondensible gas mass to the total gaseous phase mass (i.e., $X_n = M_n/(M_n + M_s)$, where M_n = mass of noncondensible in the gaseous phase and M_s = mass of steam in the gaseous phase). The eight secondary dependent variables used in the equations are phasic densities (ρ_g, ρ_f), vapor generation rate per unit volume (Γ_g), phasic interphase heat transfer rates per unit volume (Q_{ig}, Q_{if}), phasic temperatures (T_g, T_f), and saturation temperature (T^s).

The basic two-fluid differential equations that form the basis for the hydrodynamic model are next presented. This discussion will be followed by development of a convenient form of the differential equations that is used as the basis for the numerical solution scheme. The modifications necessary to model horizontal stratified flow are also discussed. Subsequently, the semi-implicit scheme difference equations, the volume-averaged velocity formulations, and the time advancement scheme are discussed. Finally, the nearly-implicit scheme difference equations are presented.

3.1.1.1 Basic Differential Equations. The differential form of the one-dimensional transient field equations is first presented for a one-component system. The modifications necessary to consider noncondensibles as a component of the gaseous phase and boron as a nonvolatile solute component of the liquid phase are discussed separately.

3.1.1.1.1 Vapor/Liquid System--The basic field equations for the two-fluid nonequilibrium model consist of two phasic continuity equations, two phasic momentum equations, and two phasic energy equations. The equations are recorded in differential streamtube form with time and one space dimension as independent variables and in terms of time and

volume-average dependent variables.[a] The development of such equations for the two-phase process has been recorded in several references[11,12] and is not repeated here. The equations are cast in the basic form with discussion of those terms that may differ from other developments. Manipulations required to obtain the form of the equations from which the numerical scheme was developed are described in Section 3.1.1.2.

The phasic continuity equations are

$$\frac{\partial}{\partial t}(\alpha_g \rho_g) + \frac{1}{A}\frac{\partial}{\partial x}(\alpha_g \rho_g v_g A) = \Gamma_g \tag{1}$$

$$\frac{\partial}{\partial t}(\alpha_f \rho_f) + \frac{1}{A}\frac{\partial}{\partial x}(\alpha_f \rho_f v_f A) = -\Gamma_g \ . \tag{2}$$

Generally, the flow does not include mass sources or sinks and overall continuity consideration yields the requirement that the liquid generation term be the negative of the vapor generation; that is,

$$\Gamma_f = -\Gamma_g \ . \tag{3}$$

The interfacial mass transfer model assumes that total mass transfer consists of mass transfer in the bulk fluid (Γ_{ig}) and mass transfer at the wall (Γ_w); that is,

$$\Gamma_g = \Gamma_{ig} + \Gamma_w \tag{4}$$

---

a. In all the field equations shown herein, the correlation coefficients are assumed unity so the average of a product of variables is equal to the product of the averaged variables.

The phasic conservation of momentum equations are used, and recorded here, in the so-called nonconservative form. For the vapor phase it is

$$\alpha_g \rho_g A \frac{\partial v_g}{\partial t} + \frac{1}{2} \alpha_g \rho_g A \frac{\partial v_g^2}{\partial x} = - \alpha_g A \frac{\partial P}{\partial x} + \alpha_g \rho_g B_x A - (\alpha_g \rho_g A) FWG(v_g)$$

$$+ \Gamma_g A(v_{gI} - v_g) - (\alpha_g \rho_g A) FIG(v_g - v_f)$$

$$- C\alpha_g \alpha_f \rho A \frac{\partial (v_g - v_f)}{\partial t} \qquad (5)$$

and for the liquid phase it is,

$$\alpha_f \rho_f A \frac{\partial v_f}{\partial t} + \frac{1}{2} \alpha_f \rho_f A \frac{\partial v_f^2}{\partial x} = - \alpha_f A \frac{\partial P}{\partial x} + \alpha_f \rho_f B_x A - (\alpha_f \rho_f A) FWF(v_f)$$

$$- \Gamma_g A(v_{fI} - v_f) - (\alpha_f \rho_f A) FIF(v_f - v_g)$$

$$- C\alpha_f \alpha_g \rho A \frac{\partial (v_f - v_g)}{\partial t} \quad . \qquad (6)$$

The force terms on the right sides of Equations (5) and (6) are, respectively: the pressure gradient, the body force, wall friction, momenta due to interphase mass transfer, interphase frictional drag, and force due to virtual mass. The terms FWG and FWF are part of the wall frictional drag, which is linear in velocity and are products of the friction coefficient, the frictional reference area per unit volume, and the magnitude of the fluid bulk velocity. The interfacial velocity in the interphase momentum transfer term is the unit momentum with which phase appearance or disappearance occurs. The coefficients FIG and FIF are parts of the interphase frictional drag, which is linear in relative

velocity, and are products of the interphase friction coefficients, tne frictional reference area per unit volume, and the magnitude of interphase relative velocity.

The coefficient of virtual mass is the same as that used by Anderson[13] in the RISQUE code, where the value for C depends on the flow regime. A value of C > 1/2 has been shown to be appropriate for bubbly or dispersed flows,[14,15] while C = 0 may be appropriate for a separated or stratified flow.

The virtual mass term in Equations (5) and (6) is a simplification of the objective formulation[16,17] used in RELAP5/MOD1. In particular, the spatial derivative portion of the term is deleted. The reason for this change is that inaccuracies in approximating spatial derivatives for the relatively course nodalizations used in system representations can lead to nonphysical characteristics in the numerical solution. The primary effect of the virtual mass terms is on the mixture sound speed, thus, the simplified form is adequate since critical flows are calculated in RELAP5 using an integral model[18] in which the sound speed is based on an objective formulation for the added mass terms.

Conservation of interphase momentum requires that the force terms associated with interphase mass and momentum exchange sum to zero, and is shown as

$$\Gamma_g v_{gI} - (\alpha_g \rho_g) FIG(v_g - v_f) - C\alpha_g \alpha_f \rho [\partial(v_g - v_f)/\partial t]$$

$$+ \Gamma_f v_{fI} - (\alpha_f \rho_f) FIF(v_f - v_g) - C\alpha_f \alpha_g \rho [\partial(v_f - v_g)/\partial t] = 0 \quad . \qquad (7)$$

This particular form for interphase momentum balance results from consideration of the momentum equations in conservative form. The force terms associated with virtual mass acceleration in Equation (7) sum to zero identically as a result of the particular form chosen. In addition, it is

usually assumed (although not required by any basic conservation principle) that the interphase momentum transfer due to friction and due to mass transfer independently sum to zero, that is,

$$v_{gI} = v_{fI} = v_I \tag{8}$$

and

$$\alpha_g \rho_g F_{IG} = \alpha_f \rho_f F_{IF} = \alpha_g \alpha_f \rho_g \rho_f F_I \quad . \tag{9}$$

These conditions are sufficient to ensure that Equation (7) is satisfied.

The phasic energy equations are

$$\frac{\partial}{\partial t}(\alpha_g \rho_g U_g) + \frac{1}{A}\frac{\partial}{\partial x}(\alpha_g \rho_g U_g v_g A) = -P\frac{\partial \alpha_g}{\partial t} - \frac{P}{A}\frac{\partial}{\partial x}(\alpha_g v_g A)$$

$$+ Q_{wg} + Q_{ig} + \Gamma_{ig} h_g^* + \Gamma_w h_g^s + DISS_g \tag{10}$$

$$\frac{\partial}{\partial t}(\alpha_f \rho_f U_f) + \frac{1}{A}\frac{\partial}{\partial x}(\alpha_f \rho_f U_f v_f A) = -P\frac{\partial \alpha_f}{\partial t} - \frac{P}{A}\frac{\partial}{\partial x}(\alpha_f v_f A)$$

$$+ Q_{wf} + Q_{if} - \Gamma_{ig} h_f^* - \Gamma_w h_f^s + DISS_f \quad . \tag{11}$$

In the phasic energy equations, Q_{wg} and Q_{wf} are the phasic wall heat transfer rates per unit volume. These phasic wall heat transfer rates satisfy the equation

$$Q = Q_{wg} + Q_{wf} \tag{12}$$

where Q is the total wall heat transfer rate to the fluid per unit volume.

The phasic enthalpies (h_g^*, h_f^*) associated with interphase mass transfer in Equations (10) and (11) are defined in such a way that the interface energy jump conditions at the liquid-vapor interface are satisfied. In particular, the h_g^* and h_f^* are chosen to be h_g^s and h_f respectively for the case of vaporization and h_g and h_f^s respectively for the case of condensation. The logic for this choice will be further explained in the development of the mass transfer model.

The phasic energy dissipation terms, $DISS_g$ and $DISS_f$, are the sums of wall friction and pump effects. The wall friction dissipations are defined as

$$DISS_g = \alpha_g \rho_g FWG\, v_g^2 \tag{13}$$

and

$$DISS_f = \alpha_f \rho_f FWF\, v_f^2 \quad . \tag{14}$$

The phasic energy dissipation terms satisfy the relation

$$DISS = DISS_g + DISS_f \tag{15}$$

where DISS is the energy dissipation. When a pump component is present the associated energy dissipation is also included in the dissipation terms (see Section 3.1.5.4).

The vapor generation (or condensation) consists of two parts, that which results from bulk energy exchange (Γ_{ig}) and that due to wall heat transfer effects (Γ_w). Each of the vapor generation (or condensation) processes involves interface heat transfer effects. The interface heat transfer terms appearing in Equations (10) and (11) include heat transfer

from the bulk states to the interface due to both interface energy exchange and wall heat transfer effects. The vapor generation (or condensation) rates are established from energy balance considerations at the interface.

The summation of Equations (10) and (11) produces the mixture energy equation, from which it is required that the interface transfer terms vanish, that is

$$Q_{ig} + Q_{if} + \Gamma_{ig}(h_g^* - h_f^*) + \Gamma_w(h_g^s - h_f^s) = 0 \quad . \tag{16}$$

The interphase heat transfer terms consist of two parts, that is

$$Q_{ig} = H_{ig}(T^s - T_g) + Q_{ig}^w \tag{17}$$

and

$$Q_{if} = H_{if}(T^s - T_f) + Q_{if}^w \tag{18}$$

H_{ig} and H_{if} are the interphase heat transfer coefficients per unit volume and Q_{ig} and Q_{if}^w are the wall heat transfer terms.

The first term on the right side of Equations (17) and (18) is the thermal energy exchange between the fluid bulk states and the fluid interface, while the second term is that due to wall heat transfer effects and will be defined in terms of the wall vapor generation (or condensation) process.

Although it is not a fundamental requirement, it is assumed that Equation (16) will be satisfied by requiring that the wall heat transfer terms and the bulk exchange terms each sum to zero independently. Thus,

$$H_{ig}(T^s - T_g) + H_{if}(T^s - T_f) + \Gamma_{ig}(h_g^* - h_f^*) = 0 \tag{19}$$

and

$$Q_{ig}^{w} + Q_{if}^{w} + \Gamma_w(h_g^s - h_f^s) = 0 \quad . \tag{20}$$

In addition, it is assumed that $Q_{ig}^{w} = 0$ for boiling processes where $\Gamma_w > 0$. Equation (20) can then be solved for the wall vaporization rate to give

$$\Gamma_w = \frac{- Q_{if}^{w}}{h_g^s - h_f^s} \quad , \quad \Gamma_w > 0 \quad . \tag{21}$$

Similarly, it is assumed that $Q_{if}^{w} = 0$ for condensation processes in which $\Gamma_w < 0$. Equation (20) can then be solved for the wall condensation rate to give

$$\Gamma_w = \frac{- Q_{ig}^{w}}{h_g^s - h_f^s} \quad , \quad \Gamma_w < 0 \quad . \tag{22}$$

The interphase energy transfer terms Q_{ig} and Q_{if} can thus be expressed in a general way as

$$Q_{ig} = H_{ig}(T^s - T_g) - \left(\frac{1 - \varepsilon}{2}\right) \Gamma_w(h_g^s - h_f^s) \tag{23}$$

and

$$Q_{if} = H_{if}(T^s - T_f) - \left(\frac{1 + \varepsilon}{2}\right) \Gamma_w(h_g^s - h_f^s) \tag{24}$$

where $\varepsilon = 1$ for $\Gamma_w > 0$ and $\varepsilon = -1$ for $\Gamma_w < 0$. Finally, Equation (16) can be used to define the interphase vaporization (or condensation) rate

$$\Gamma_{ig} = - \frac{Q_{ig} + Q_{if}}{h_g^* - h_f^*} - \Gamma_w \frac{(h_g^s - h_f^s)}{h_g^* - h_f^*} \tag{25}$$

which, upon substitution of Equations (23) and (24), becomes

$$\Gamma_{ig} = - \frac{H_{ig}(T^s - T_g) + H_{if}(T^s - T_f)}{h_g^* - h_f^*} \quad . \tag{26}$$

The phase change process that occurs at the interface is envisioned as a process in which bulk fluid is heated or cooled to the saturation temperature and phase change occurs at the saturation state. The interphase energy exchange process from each phase must be such that at least the sensible energy change to reach the saturation state occurs. Otherwise, it can be shown that the phase change process implies energy transfer from a lower temperature to a higher temperature. Such conditions can be avoided by the proper choice of the variables h_g^* and h_f^*. In particular, it can be shown that they should be

$$h_g^* = \tfrac{1}{2}[(h_g^s + h_g) + n(h_g^s - h_g)] \tag{27}$$

and

$$h_f^* = \tfrac{1}{2}[(h_f^s + h_f) - n(h_f^s - h_f)] \tag{28}$$

where

$$n = 1 \text{ for } \Gamma_{ig} \geq 0 \tag{29}$$

$$n = -1 \text{ for } \Gamma_{ig} < 0 \quad . \tag{30}$$

Substituting Equation (26) into Equation (4) gives the final expression for the total interphase mass transfer as

$$\Gamma_g = - \frac{H_{ig}(T^s - T_g) + H_{if}(T^s - T_f)}{h_g^* - h_f^*} + \Gamma_w \quad . \tag{31}$$

3.1.1.1.2 Noncondensibles in the Gas Phase--The basic, two-phase, single-component model just discussed can be extended to include a noncondensible component in the gas phase. The noncondensible component is assumed to be in mechanical and thermal equilibrium with the vapor phase, so that

$$v_n = v_g \tag{32}$$

and

$$T_n = T_g \tag{33}$$

where the subscript, n, is used to designate the noncondensible component.

The general approach for inclusion of the noncondensible component consists of assuming that all properties of the gas phase (subscript g) are mixture properties of the steam/noncondensible mixture. The quality, X, is likewise defined as the mass fraction of the entire gas phase. Thus, the two basic continuity equations [Equations (1) and (2)] are unchanged. However, it is necessary to add an additional mass conservation equation for the noncondensible component

$$\frac{\partial}{\partial t}(\alpha_g \rho_g X_n) + \frac{1}{A} \frac{\partial}{\partial x} (\alpha_g \rho_g X_n v_g A) = 0 \tag{34}$$

where X_n is the mass fraction of noncondensible component based on the gaseous phase mass.

The remaining field equations for energy and phasic momentum are unchanged, but the vapor field properties are now evaluated for the steam/noncondensible mixture. The modifications appropriate to the state relationships are described in Section 3.1.2.3.

3.1.1.1.3 Boron Concentration in the Liquid Field--An Eulerian boron tracking model is used in RELAP5 which simulates the transport of a dissolved component in the liquid phase. The solution is assumed to be sufficiently dilute that the following assumptions are valid:

1. Liquid properties are not altered by the presence of the solute
2. Solute is transported only in the liquid phase and at the velocity of the liquid phase
3. Energy transported by the solute is negligible
4. Inertia of the solute is negligible
5. Solute is transported at the velocity of tne vapor phase if no liquid is present.

Under these assumptions, only an additional field equation for the conservation of the solute is required. In differential form, the added equation is

$$\frac{\partial \rho_B}{\partial t} + \frac{1}{A}\frac{\partial (C_B \alpha_f \rho_f v_f A)}{\partial x} = 0 \qquad (35)$$

where the concentration parameter, C_B, is defined as

$$C_B = \frac{\rho_B}{\rho(1 - X)} \qquad (36)$$

C_B is the concentration of dissolved solid in mass units per mass unit of liquid phase.

3.1.1.2 Numerically Convenient Set of Differential Equations. A more convenient set of differential equations upon which to base the numerical scheme is obtained from the basic density and energy differential equations by expanding the time derivative in each equation using the product rule. When the product rule is used to evaluate the time derivative, we will refer to this form as the expanded form.

A sum density equation is obtained by expanding the time derivative in the phasic density equations, Equations (1) and (2), adding these two new equations, and using the relation

$$\frac{\partial \alpha_f}{\partial t} = - \frac{\partial \alpha_g}{\partial t} \quad . \tag{37}$$

This gives

$$\alpha_g \frac{\partial \rho_g}{\partial t} + \alpha_f \frac{\partial \rho_f}{\partial t} + (\rho_g - \rho_f)\frac{\partial \alpha_g}{\partial t} + \frac{1}{A} \frac{\partial}{\partial x}(\alpha_g \rho_g v_g A + \alpha_f \rho_f v_f A) = 0 \quad . \tag{38}$$

A difference density equation is obtained by expanding the time derivative in the phasic density equations, Equations (1) and (2), subtracting these two new equations, again using the relation

$$\frac{\partial \alpha_f}{\partial t} = - \frac{\partial \alpha_g}{\partial t} \tag{39}$$

and substituting Equation (31) for Γ_g. This gives

$$\alpha_g \frac{\partial \rho_g}{\partial t} - \alpha_f \frac{\partial \rho_f}{\partial t} + (\rho_g + \rho_f)\frac{\partial \alpha_g}{\partial t} + \frac{1}{A} \frac{\partial}{\partial x}(\alpha_g \rho_g v_g A - \alpha_f \rho_f v_f A)$$

$$= - \frac{2[H_{ig}(T^s - T_g) + H_{if}(T^s - T_f)]}{h_g^* - h_f^*} + 2\Gamma_w \quad . \tag{40}$$

The time derivative of the noncondensible density equation, Equation (34), is expanded to give

$$\rho_g X_n \frac{\partial \alpha_g}{\partial t} + \alpha_g X_n \frac{\partial \rho_g}{\partial t} + \alpha_g \rho_g \frac{\partial X_n}{\partial t} + \frac{1}{A} \frac{\partial}{\partial x}(\alpha_g \rho_g X_n v_g A) = 0 \quad . \tag{41}$$

The momentum equations are also rearranged into a sum and difference form. The sum momentum equation is obtained by direct summation of Equations (5) and (6) with the interface conditions [Equations (7), (8), and (9)] substituted where appropriate and the cross-sectional area canceled throughout. The resulting sum equation is

$$\alpha_g \rho_g \frac{\partial v_g}{\partial t} + \alpha_f \rho_f \frac{\partial v_f}{\partial t} + \frac{1}{2}\alpha_g \rho_g \frac{\partial \hat{v}_g^2}{\partial x} + \frac{1}{2}\alpha_f \rho_f \frac{\partial v_f^2}{\partial x} = - \frac{\partial P}{\partial x} + \rho B_x$$

$$- \alpha_g \rho_g v_g FWG - \alpha_f \rho_f v_f FWF - \Gamma_g (v_g - v_f) \quad . \tag{42}$$

The difference of the phasic momentum equations is obtained by first dividing the vapor and liquid phasic momentum equations by $\alpha_g \rho_g$ and $\alpha_f \rho_f$, respectively, and subsequently subtracting. Here again, the interface conditions are used and the common area is divided out. The resulting equation is

$$\frac{\partial v_g}{\partial t} - \frac{\partial v_f}{\partial t} + \frac{1}{2}\frac{\partial v_g^2}{\partial x} - \frac{1}{2}\frac{\partial v_f^2}{\partial x} = - \left(\frac{1}{\rho_g} - \frac{1}{\rho_f}\right)\frac{\partial P}{\partial x} - v_g FWG + v_f FWF$$

$$+ \Gamma_g [\rho v_I - (\alpha_f \rho_f v_g + \alpha_g \rho_g v_f)]/(\alpha_g \rho_g \alpha_f \rho_f) - \rho FI(v_g - v_f)$$

$$- C[\rho^2/(\rho_g \rho_f)] \frac{\partial (v_g - v_f)}{\partial t} \tag{43}$$

where the interfacial velocity, v_I, is defined as

$$v_I = \lambda v_g + (1 - \lambda) v_f \quad . \tag{44}$$

This definition for v_I has the property that if $\lambda = 1/2$, the interphase momentum transfer process associated with mass transfer is reversible. This value leads to either an entropy sink or source, depending on the sign of Γ_g. However if λ is chosen to be 0 for positive values of Γ_g and +1 for negative values of Γ_g (that is, a donor formulation), the mass exchange process is always dissipative. The latter model for v_I is the most realistic for the momentum exchange process and is used for the numerical scheme development.

To develop an expanded form of the vapor energy Equation (10) the time derivative of the vapor energy equation, Equation (10), is expanded, the Q_{ig} Equation (23) and the Γ_{ig} Equation (26) are substituted, and the H_{ig}, H_{if}, $\partial\alpha_g/\partial t$, and convective terms are collected. This gives the desired form for the vapor energy equation

$$(\rho_g U_g + P)\frac{\partial \alpha_g}{\partial t} + \alpha_g U_g \frac{\partial \rho_g}{\partial t} + \alpha_g \rho_g \frac{\partial U_g}{\partial t} + \frac{1}{A}\left[\frac{\partial}{\partial x}(\alpha_g \rho_g U_g v_g A) + P\frac{\partial}{\partial x}(\alpha_g v_g A)\right]$$

$$= -\left(\frac{h_f^*}{h_g^* - h_f^*}\right) H_{ig}(T^s - T_g) - \left(\frac{h_g^*}{h_g^* - h_f^*}\right) H_{if}(T^s - T_f)$$

$$+ \left[\left(\frac{1+\varepsilon}{2}\right)h_g^s + \left(\frac{1-\varepsilon}{2}\right)h_f^s\right]\Gamma_w + Q_{wg} + DISS_g \quad . \tag{45}$$

To develop an expanded form of the liquid energy Equation (11) the time derivative is expanded, the Q_{if} Equation (24) and the Γ_{ig} Equation (26) are substituted, and

$$\frac{\partial \alpha_f}{\partial t} = -\frac{\partial \alpha_g}{\partial t} \tag{46}$$

is used, then the H_{ig}, H_{if}, $\partial\alpha_g/\partial t$, and convective terms are collected. This gives the desired form for the liquid energy equation

$$- (\rho_f U_f + P) \frac{\partial \alpha_g}{\partial t} + \alpha_f U_f \frac{\partial \rho_f}{\partial t} + \alpha_f \rho_f \frac{\partial U_f}{\partial t} + \frac{1}{A} \left[\frac{\partial}{\partial x}(\alpha_f \rho_f U_f v_f A + P \frac{\partial}{\partial x}(\alpha_f v_f A)\right]$$

$$= \left(\frac{h_f^*}{h_g^* - h_f^*}\right) H_{ig}(T^s - T_g) + \left(\frac{h_g^*}{h_g^* - h_f^*}\right) H_{if}(T^s - T_f)$$

$$- \left[\left(\frac{1 + \varepsilon}{2}\right) h_g^s + \left(\frac{1 - \varepsilon}{2}\right) h_f^s\right] \Gamma_w + Q_{wf} + DISS_f \quad . \tag{47}$$

The basic density and energy differential equations are used in nonexpanded form in the back substitution part of the numerical scheme. When the product rule is not used to evaluate the time derivative, we will refer to this form as the nonexpanded form.

The vapor, liquid, and noncondensible density equations, Equations (1), (2), and (34), are in nonexpanded form. The Γ_g, Equation (31), is not substituted into the vapor and liquid density equations (the reason will be apparent in the Time Step Solution Scheme, Section 3.1.1.6). The vapor energy equation, Equation (10), is altered by substituting Equation (23) for Q_{ig}, substituting Equation (26) for Γ_{ig} and collecting the H_{ig}, H_{if}, and convective terms. This gives

$$\frac{\partial}{\partial t}(\alpha_g \rho_g U_g) + \frac{1}{A}\left[\frac{\partial}{\partial x}(\alpha_g \rho_g U_g v_g A) + P \frac{\partial}{\partial x}(\alpha_g v_g A)\right]$$

$$= - P \frac{\partial \alpha_g}{\partial t} - \left(\frac{h_f^*}{h_g^* - h_f^*}\right) H_{ig}(T^s - T_g) - \left(\frac{h_g^*}{h_g^* - h_f^*}\right) H_{if}(T^s - T_f)$$

$$+ \left[\left(\frac{1 + \varepsilon}{2}\right) h_g^s + \left(\frac{1 - \varepsilon}{2}\right) h_f^s\right] \Gamma_w + Q_{wg} + DISS_g \quad . \tag{48}$$

The liquid energy equation, Equation (11), is also altered by substituting Equation (24) for Q_{if}, substituting Equation (26) for Γ_{ig}, using

$$\frac{\partial \alpha_f}{\partial t} = - \frac{\partial \alpha_g}{\partial t} \tag{49}$$

and collecting the H_{ig}, H_{if}, and convective terms. This gives

$$\frac{\partial}{\partial t}(\alpha_f \rho_f U_f) + \frac{1}{A}\left[\frac{\partial}{\partial x}(\alpha_f \rho_f U_f v_f A) + P\frac{\partial}{\partial x}(\alpha_f v_f A)\right]$$

$$= P\frac{\partial \alpha_g}{\partial t} + \left(\frac{h_f^*}{h_g^* - h_f^*}\right) H_{ig}(T^s - T_g) + \left(\frac{h_g^*}{h_g^* - h_f^*}\right) H_{if}(T^s - T_f)$$

$$- \left[\left(\frac{1 + \epsilon}{2}\right) h_g^s + \left(\frac{1 - \epsilon}{2}\right) h_f^s\right] \Gamma_w + Q_{wf} + DISS_f \quad . \tag{50}$$

3.1.1.3 Horizontal Stratified Flow. Flow at low velocity in a horizontal passage can be stratified as a result of buoyancy forces caused by density differences between vapor and liquid. When the flow is stratified, the area average pressures are affected by nonuniform transverse distribution of the phases. Appropriate modifications to the basic field equations when stratified flow exists are obtained by considering separate area average pressures for the vapor and liquid phases, and the interfacial pressure between them. Using this model, the pressure gradient force terms of Equations (5) and (6) become

$$- \alpha_g A\left(\frac{\partial P}{\partial x}\right) \rightarrow - \alpha_g A\left(\frac{\partial P_g}{\partial x}\right) + (P_I - P_g) A\left(\frac{\partial \alpha_g}{\partial x}\right) \tag{51}$$

and

$$- \alpha_f A\left(\frac{\partial P}{\partial x}\right) \rightarrow - \alpha_f A\left(\frac{\partial P_f}{\partial x}\right) + (P_I - P_f) A\left(\frac{\partial \alpha_f}{\partial x}\right) \quad . \tag{52}$$

The area average pressure for the entire cross section of the flow is expressed in terms of the phasic area average pressures by

$$P = \alpha_g P_g + \alpha_f P_f \quad . \tag{53}$$

With these definitions, the sum of the phasic momentum equations, written in terms of the cross section average pressure [Equation (42)] remains unchanged. However, the difference of the phasic momentum equations [Equation (43)], contains on the right side the following additional terms

$$[\rho/(\alpha_g \alpha_f \rho_g \rho_f)] \left[- \alpha_f \partial(\alpha_g P_g)/\partial x + \alpha_g \partial(\alpha_f P_f)/\partial x + P_I(\partial \alpha_g/\partial x)\right] \quad . \tag{54}$$

The interface and phasic cross-sectional average pressures, P_I, P_g, and P_f, can be found by means of the assumption of a transverse hydrostatic pressure in a round pipe. For a pipe having diameter D, pressures P_I, P_g, and P_f are given by

$$P_g = P_I - \rho_g B_y D \left[\sin^3\theta/(3\pi\alpha_g) - \cos\theta/2\right] \tag{55}$$

$$P_f = P_I + \rho_f B_y D \left[\sin^3\theta/(3\pi\alpha_f) + \cos\theta/2\right] \quad . \tag{56}$$

The angle, θ, is defined by the void fraction as illustrated in Figure 3. The algebraic relationship between α_g and θ is

$$\alpha_g \pi = (\theta - \sin\theta \cos\theta) \quad . \tag{57}$$

The additional term in the momentum difference equation [Equation (54)] can be simplified using Equations (55), (56), and (57) to obtain

$$- [\rho/(\rho_g \rho_f)] (\rho_f - \rho_g) \pi D B_y/(4\sin\theta) (\partial \alpha_g/\partial x) \tag{58}$$

where θ is related to the void fraction using Equation (57).

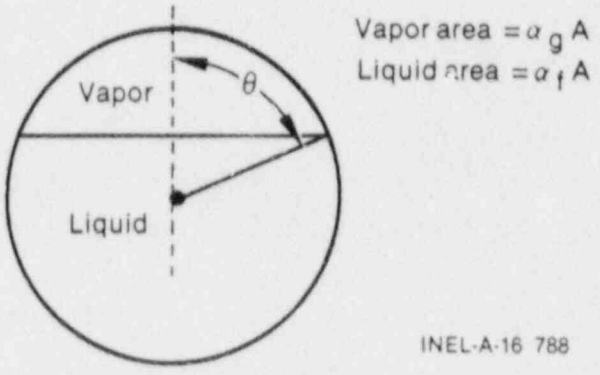

Figure 3. Relation of central angle θ to void fraction α_g.

The additional force term that arises for a stratified flow geometry in horizontal pipes is added to the basic equation when the flow is established to be stratified from flow regime considerations.

3.1.1.4 Semi-Implicit Scheme Difference Equations. The semi-implicit numerical solution scheme is based on replacing the system of differential equations with a system of finite-difference equations partially implicit in time. The terms evaluated implicitly are identified as the scheme is developed. In all cases, the implicit terms are formulated to be linear in the dependent variables at new time. This results in a linear time-advancement matrix that is solved by direct inversion using a sparse matrix routine.[19] An additional feature of the scheme is that implicitness is selected such that the field equations can be reduced to a single difference equation per fluid control volume or mesh cell, which is in terms of the hydrodynamic pressure. Thus, only an N x N system of the difference equations must be solved simultaneously at each time step (N is the total number of control volumes used to simulate the fluid system).

It is well known[13,20] that the system of differential equations constitutes an ill-posed, initial-value problem. This fact is of little concern physically since the addition of any second-order differential effect (regardless of how small) such as viscosity or surface tension,

results in a well-posed problem.[21] However, the ill-posedness is of some concern numerically since it is necessary that the numerical problem be well-posed. The approximations inherent in any numerical scheme modify the solution somewhat (truncation error); these effects can be either stabilizing or destabilizing.

A well-posed numerical problem is obtained by several means. These include the selective implicit evaluation of spatial gradient terms at the new time, donor formulations for the mass and energy flux terms, and use of a donor-like formulation for the momentum flux terms. The term, donor-like, is used because the momentum flux formulation consists of a centered formulation for the spatial velocity gradient plus a numerical viscosity term similar to the form obtained when the momentum flux terms are donored with the conservative form of the momentum equations. The well-posedness of the final numerical scheme (as well as its accuracy) has been demonstrated by extensive numerical testing during development.

The difference equations are based on the concept of a control volume (or mesh cell) in which mass and energy are conserved by equating accumulation to rate of influx through the cell boundaries. This model results in defining mass and energy volume average properties and requiring knowledge of velocities at the volume boundaries. The velocities at boundaries are most conveniently defined through use of momentum control volumes (cells) centered on the mass and energy cell boundaries. This approach results in a numerical scheme having a staggered spatial mesh. The scalar properties (pressure, energies, and void fraction) of the flow are defined at cell centers, and vector quantities (velocities) are defined on the cell boundaries. The resulting one-dimensional spatial noding is illustrated in Figure 4. The term, cell, means an increment in the spatial variable, x, corresponding to the mass and energy control volume.

The difference equations for each cell are obtained by integrating the mass and energy equations [Equations (38), (40), (41), (45), and (47)] with respect to the spatial variable, x, from the junction at x_j to x_{j+1}. The momentum equations [Equations (42) and (43)] are integrated with

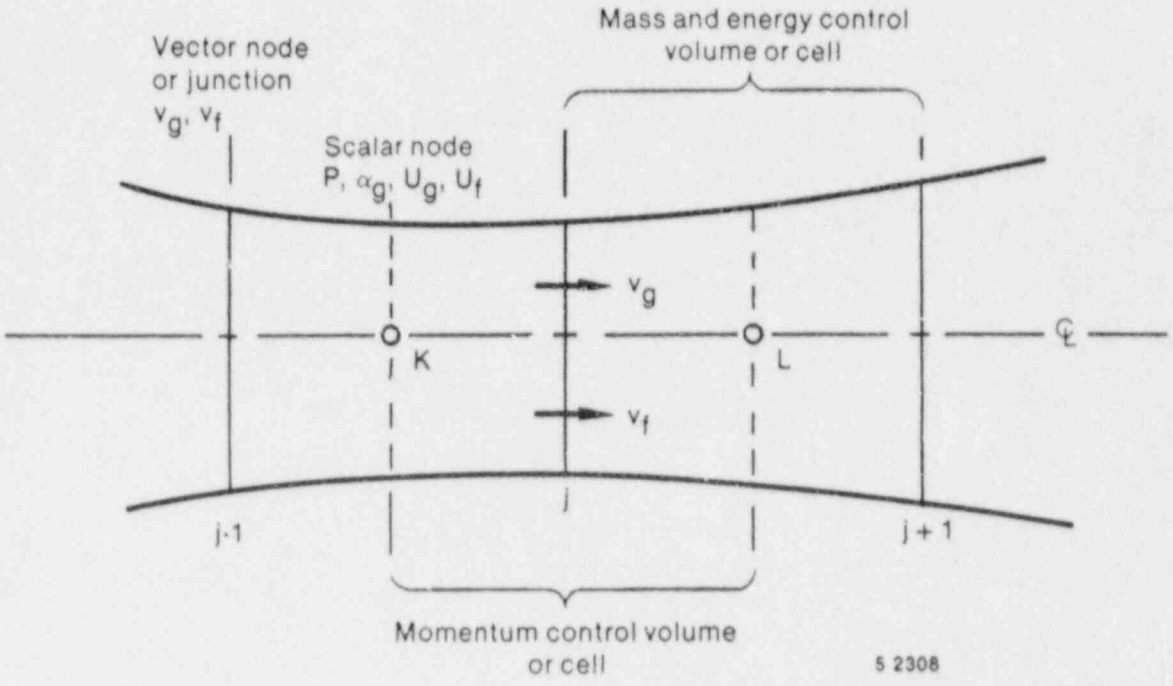

Figure 4. Difference equation nodalization schematic.

respect to the spatial variable from cell center to adjoining cell center (x_K to x_L, Figure 4). The equations are listed for the case of a pipe with no branching.

When the mass and energy equations [Equations (38), (40), (41), (45), and (47)] are integrated with respect to the spatial variable from junction j to j+1, differential equations in terms of cell-average properties and cell boundary fluxes are obtained. The subscripts and superscripts within the parentheses indicate integration limits for the enclosed quantity. The quantities not enclosed in parentheses are volume averages.

The sum density Equation (38) becomes

$$V\left[\alpha_g \frac{\partial \rho_g}{\partial t} + \alpha_f \frac{\partial \rho_f}{\partial t} + (\rho_g - \rho_f) \frac{\partial \alpha_g}{\partial t}\right]$$

$$+ (\alpha_g \rho_g v_g A)_{x_j}^{x_{j+1}} + (\alpha_f \rho_f v_f A)_{x_j}^{x_{j+1}} = 0 \quad . \tag{59}$$

The difference density Equation (40) becomes

$$V\left[\alpha_g \frac{\partial \rho_g}{\partial t} - \alpha_f \frac{\partial \rho_f}{\partial t} + (\rho_g + \rho_f) \frac{\partial \alpha_g}{\partial t}\right] + (\alpha_g \rho_g v_g A)_{x_j}^{x_{j+1}} - (\alpha_f \rho_f v_f A)_{x_j}^{x_{j+1}}$$

$$= - V \left\{ \frac{2[H_{ig} (T^s - T_g) + H_{if} (T^s - T_f)]}{h_g^* - h_f^*} + 2\Gamma_w \right\} \quad . \tag{60}$$

The noncondensible density Equation (41) becomes

$$V\left(\rho_g X_n \frac{\partial \alpha_g}{\partial t} + \alpha_g X_n \frac{\partial \rho_g}{\partial t} + \alpha_g \rho_g \frac{\partial X_n}{\partial t}\right) + [(\alpha_g \rho_g X_n v_g A)]_{x_j}^{x_{j+1}} = 0 \quad . \tag{61}$$

The vapor energy Equation (45) becomes

$$V\left[(\rho_g U_g + P) \frac{\partial \alpha_g}{\partial t} + \alpha_g U_g \frac{\partial \rho_g}{\partial t} + \alpha_g \rho_g \frac{\partial U_g}{\partial t}\right] + \left[(\alpha_g \rho_g U_g v_g A) + P(\alpha_g v_g A)\right]_{x_j}^{x_{j+1}}$$

$$= V \left\{ - \left(\frac{h_f^*}{h_g^* - h_f^*}\right) H_{ig} (T^s - T_g) - \left(\frac{h_g^*}{h_g^* - h_f^*}\right) H_{if} (T^s - T_f) \right.$$

$$\left. + \left[\left(\frac{1 + \varepsilon}{2}\right) h_g^s + \left(\frac{1 - \varepsilon}{2}\right) h_f^s\right] \Gamma_w + Q_{wg} + DISS_g \right\} \quad . \tag{62}$$

The liquid energy Equation (47) becomes

$$V\left[-(\rho_f U_f + P)\frac{\partial \alpha_g}{\partial t} + \alpha_f U_f \frac{\partial \rho_f}{\partial t} + \alpha_f \rho_f \frac{\partial U_f}{\partial t}\right] + \left[(\alpha_f \rho_f U_f v_f A) + P(\alpha_f v_f A)\right]_{x_j}^{x_{j+1}}$$

$$= V\left\{\left(\frac{h_f^*}{h_g^* - h_f^*}\right) H_{ig}\,(T^s - T_g) + \left(\frac{h_g^*}{h_g^* - h_f^*}\right) H_{if}\,(T^s - T_f)\right.$$

$$\left. - \left[\left(\frac{1+\epsilon}{2}\right) h_g^s + \left(\frac{1-\epsilon}{2}\right) h_f^s\right] \Gamma_w + Q_{wf} + DISS_f\right\} . \qquad (63)$$

The sum and difference momentum equations [Equations (42) and (43)] are integrated from cell center-to-cell center to obtain

$$\left(\frac{V}{A}\right)\left[(\alpha_g \rho_g)\frac{\partial v_g}{\partial t} + (\alpha_f \rho_f)\frac{\partial v_f}{\partial t}\right] + \frac{1}{2}\alpha_g \rho_g \left(v_g^2\right)_{x_K}^{x_L} + \frac{1}{2}\alpha_f \rho_f \left(v_f^2\right)_{x_K}^{x_L}$$

$$= -(P)_{x_K}^{x_L} + \rho B_x (x_L - x_K) - (\alpha_g \rho_g v_g FWG + \alpha_f \rho_f v_f FWF)(x_L - x_K)$$

$$- \Gamma_g (v_g - v_f)(x_L - x_K) \qquad (64)$$

and

$$\left(\frac{V}{A}\right)\left[1 + C\rho^2/(\rho_g \rho_f)\right]\left(\frac{\partial v_g}{\partial t} - \frac{\partial v_f}{\partial t}\right) + \frac{1}{2}\left(v_g^2\right)_{x_K}^{x_L} - \frac{1}{2}\left(v_f^2\right)_{x_K}^{x_L}$$

$$= -\left(\frac{1}{\rho_g} - \frac{1}{\rho_f}\right)(P)_{x_K}^{x_L} - (v_g FWG - v_f FWF)(x_L - x_K) + \left\{\Gamma_g\left[\rho v_I\right.\right.$$

$$\left.\left. - (\alpha_f \rho_f v_g + \alpha_g \rho_g v_f)\right]/(\alpha_g \rho_g \alpha_f \rho_f)\right\}(x_L - x_K) - \rho FI(v_g - v_f)(x_L - x_K) . \qquad (65)$$

Here, the common area term, A, has been factored from most terms. The quantities shown in brackets with limits are evaluated at the indicated limits, while the coefficients are averaged over the cell or integration interval. The indicated derivatives are now derivatives of cell average quantities. Since the integration interval is centered on the junction, the coefficient averages are approximated by the junction values. In all cases, the correlation coefficients for averaged products are taken as unity so averaged products are replaced directly with products of averages.

Several general guidelines were followed in developing numerical approximations for Equations (59), (60), (61), (62), (63), (64), and (65). These guidelines are summarized below.

1. Mass and energy inventories are very important quantities in water reactor safety analysis. The numerical scheme should be consistent and conservative in these quantities (a greater degree of approximation for momentum effects is considered acceptable). Both mass and energy are convected from the same cell and each is evaluated at the same time level that is, mass density is evaluated at old time level so energy density is also evaluated at old time).

2. To achieve fast execution speed, implicit evaluation is used only for those terms responsible for the sonic wave propagation time step limit, and those phenomena known to have small time constants. Thus, implicit evaluation is used for the velocity in mass and energy transport terms, the pressure gradient in the momentum equations, and the interphase mass and momentum exchange terms.

3. To further increase computing speed, time-level evaluations are selected so the resulting implicit terms are linear in the new time variables. Where it is necessary to retain nonlinearities, Taylor series expansions about old time values are used to obtain a formulation linear in the new time variables (higher-order

terms are neglected). Linearity results in high computing speed by eliminating the need to iteratively solve systems of nonlinear equations.

4. To allow easy degeneration to homogeneous, or single-phase formulations, the momentum equations are used as a sum and a difference equation. The particular difference equation used is obtained by first dividing each of the phasic momentum equations by $\alpha_g\rho_g$ and $\alpha_f\rho_f$ for the vapor and liquid phase equations, respectively, and then subtracting.

Using the above guidelines the finite-difference equations for the mass and energy balances, corresponding to Equations (59) ,(60), (61). (62), and (63) are listed below. Some of the terms are intermediate time variables, which are written with a tilde ($\sim$). The reason for their use will be explained in the Time Advancement Scheme, Section 3.1.1.6.

The sum density equation is

$$V_L[\alpha^n_{g,L}(\tilde{\rho}^{n+1}_{g,L} - \rho^n_{g,L}) + \alpha^n_{f,L}(\tilde{\rho}^{n+1}_{f,L} - \rho^n_{f,L}) + (\rho^n_{g,L} - \rho^n_{f,L})(\tilde{\alpha}^{n+1}_{g,L} - \alpha^n_{g,L})]$$

$$+ (\dot{\alpha}^n_{g,j+1}\dot{\rho}^n_{g,j+1}v^{n+1}_{g,j+1}A_{j+1} - \dot{\alpha}^n_{g,j}\dot{\rho}^n_{g,j}v^{n+1}_{g,j}A_j)\Delta t$$

$$+ (\dot{\alpha}^n_{f,j+1}\dot{\rho}^n_{f,j+1}v^{n+1}_{f,j+1}A_{j+1} - \dot{\alpha}^n_{f,j}\dot{\rho}^n_{f,j}v^{n+1}_{f,j}A_j)\Delta t = 0 \quad . \tag{66}$$

The difference density equation is

$$V_L[\alpha^n_{g,L}(\tilde{\rho}^{n+1}_{g,L} - \rho^n_{g,L}) - \alpha^n_{f,L}(\tilde{\rho}^{n+1}_{f,L} - \rho^n_{f,L}) + (\rho^n_{g,L} + \rho^n_{f,L})(\tilde{\alpha}^{n+1}_{g,L} - \alpha^n_{g,L})]$$

$$+ (\dot{\alpha}^n_{g,j+1}\dot{\rho}^n_{g,j+1}v^{n+1}_{g,j+1}A_{j+1} - \dot{\alpha}^n_{g,j}\dot{\rho}^n_{g,j}v^{n+1}_{g,j}A_j)\Delta t$$

$$- (\dot{\alpha}^n_{f,j+1}\dot{\rho}^n_{f,j+1}v^{n+1}_{f,j+1}A_{j+1} - \dot{\alpha}^n_{f,j}\dot{\rho}^n_{f,j}v^{n+1}_{f,j}A_j)\Delta t$$

$$= \cdot \left(\frac{2}{h^*_g - h^*_f}\right)^n_L V_L \Delta t[H^n_{ig,L}(\tilde{T}^{s,n+1}_L - \tilde{T}^{n+1}_{g,L})$$

$$+ H^n_{if,L}(\tilde{T}^{s,n+1}_L - \tilde{T}^{n+1}_{f,L})] + 2V_L \Delta t\ \Gamma^n_{w,L} \qquad (67)$$

The noncondensible density equation is

$$V_L[\rho^n_{g,L}X^n_{n,L}(\tilde{\alpha}^{n+1}_{g,L} - \alpha^n_{g,L}) + \alpha^n_{g,L}X^n_{n,L}(\tilde{\rho}^{n+1}_{g,L} - \rho^n_{g,L})$$

$$+ \alpha^n_{g,L}\rho^n_{g,L}(\tilde{X}^{n+1}_{n,L} - X^n_{n,L})] + (\dot{\alpha}^n_{g,j+1}\dot{\rho}^n_{g,j+1}\dot{X}^n_{n,j+1}v^{n+1}_{g,j+1}A_{j+1}$$

$$- \dot{\alpha}^n_{g,j}\dot{\rho}^n_{g,j}\dot{X}^n_{n,j}v^{n+1}_{g,j}A_j)\Delta t = 0 \quad . \qquad (68)$$

The vapor energy equation is

$$V_L\left[(\rho^n_{g,L}U^n_{g,L} + P^n_L)(\tilde{\alpha}^{n+1}_{g,L} - \alpha^n_{g,L}) + \alpha^n_{g,L}U^n_{g,L}(\tilde{\rho}^{n+1}_{g,L} - \rho^n_{g,L})\right.$$

$$\left. + \alpha^n_{g,L}\rho^n_{g,L}(\tilde{U}^{n+1}_{g,L} - U^n_{g,L})\right] + \left[\dot{\alpha}^n_{g,j+1}(\dot{\rho}^n_{g,j+1}\dot{U}^n_{g,j+1} + P^n_L)v^{n+1}_{g,j+1}A_{j+1}\right.$$

$$\left. - \dot{\alpha}^n_{g,j}(\dot{\rho}^n_{n,j}\dot{U}^n_{g,j} + P^n_L)v^{n+1}_{g,j}A_j\right]\Delta t = \left\{-\left(\frac{h^*_f}{h^*_g - h^*_f}\right)^n_L H^n_{ig,L}(\tilde{T}^{s,n+1}_L - \tilde{T}^{n+1}_{g,L})\right.$$

$$\left. - \left(\frac{h^*_g}{h^*_g - h^*_f}\right)^n_L H^n_{if,L}(\tilde{T}^{s,n+1}_L - \tilde{T}^{n+1}_{f,L}) + [(\frac{1+\varepsilon}{2})h^{s,n}_{g,L} + (\frac{1-\varepsilon}{2})h^{s,n}_{f,L}]\Gamma^n_{w.L}\right.$$

$$+ Q^n_{wg,L} + DISS^n_{g,L}\Big\}V_L\Delta t \quad . \tag{69}$$

The liquid energy equation is

$$V_L[-(\rho^n_{f,L}U^n_{f,L} + P^n_L)(\tilde{\alpha}^{n+1}_{g,L} - \alpha^n_{g,L}) + \alpha^n_{f,L}U^n_{f,L}(\tilde{\rho}^{n+1}_{f,L} - \rho^n_{f,L})$$

$$+ \alpha^n_{f,L}\rho^n_{f,L}(\tilde{U}^{n+1}_{f,L} - U^n_{f,L})] + [\dot{\alpha}^n_{f,j+1}(\dot{\rho}^n_{f,j+1}\dot{U}^n_{f,j+1} + P^n_L)v^{n+1}_{f,j+1}A_{j+1}$$

$$- \dot{\alpha}^n_{f,j}(\dot{\rho}^{n}_{f,j}\dot{U}^n_{f,j} + P^n_L)v^{n+1}_{f,j}A_j]\Delta t = \Bigg\{\left(\frac{h^*_f}{h^*_g - h^*_f}\right)^n_L H^n_{ig,L}(\tilde{T}^{s,n+1}_L - \tilde{T}^{n+1}_{g,L})$$

$$+ \left(\frac{h^*_g}{h^*_g - h^*_f}\right)^n_L H^n_{if,L}(\tilde{T}^{s,n+1}_L - \tilde{T}^{n+1}_{f,L}) - [(\frac{1+\varepsilon}{2})h^{s,n}_{g,L} + (\frac{1-\varepsilon}{2})h^{s,n}_{f,L}]\Gamma^n_{w,L}$$

$$+ Q^n_{wf,L} + DISS^n_{f,L}\Big\}V_L\Delta t \quad . \tag{70}$$

The quantities having a dot overscore are donored quantities based on the junction velocities, v_g and v_f. The donored quantities are volume average scalar quantities defined analytically as

$$\dot{\phi} = \frac{1}{2}(\phi_K + \phi_L) + \frac{1}{2}\frac{|v|}{v}(\phi_K - \phi_L), \; v \neq 0 \tag{71}$$

where ϕ is any of the donored properties and v is the appropriate velocity (that is, vapor or liquid). For the degenerate case of $v = 0$, a density-weighted average formulation is used

$$\dot{\phi} = \frac{\rho_K\phi_K + \rho_L\phi_L}{\rho_K + \rho_L}, \; v = 0 \tag{72}$$

for all donored properties except for the densities (a simple average is used for the donored densities). In this equation ρ_K and ρ_L are the appropriate density (that is, vapor or liquid). Where donored values are not used at junctions, linear interpolations between neighboring cell values are used.

The intermediate time phasic densities used in Equations (66) through (70) are obtained by linearizing the phasic state relations about the old time values (see State Relationships, Section 3.1.2).

$$\tilde{\rho}^{n+1}_{g,L} = \rho^{n}_{g,L} + \left(\frac{\partial \rho_g}{\partial P}\right)^{n}_{L} (P^{n+1}_{L} - P^{n}_{L}) + \left(\frac{\partial \rho_g}{\partial X_n}\right)^{n}_{L} (\tilde{X}^{n+1}_{n,L} - X^{n}_{n,L})$$

$$+ \left(\frac{\partial \rho_g}{\partial U_g}\right)^{n}_{L} (\tilde{U}^{n+1}_{g,L} - U^{n}_{g,L}) \qquad (73)$$

$$\tilde{\rho}^{n+1}_{f,L} = \rho^{n}_{f,L} + \left(\frac{\partial \rho_f}{\partial P}\right)^{n}_{L} (P^{n+1}_{L} - P^{n}_{L}) + \left(\frac{\partial \rho_f}{\partial U_f}\right)^{n}_{L} (\tilde{U}^{n+1}_{f,L} - U^{n}_{f,L}) \quad . \qquad (74)$$

The method of obtaining the state derivatives used in Equations (73) and (74) is also indicated in the State Relationships, Section 3.1.2.

Intermediate time interphase heat transfer rates can be written using the finite difference form of Equations (23) and (24).

$$\tilde{Q}^{n+1}_{ig,L} = H^{n}_{ig,L}(\tilde{T}^{s,n+1}_{L} - \tilde{T}^{n+1}_{g,L}) - (\frac{1 - \epsilon}{2}) \Gamma^{n}_{w,L}(h^{s,n}_{g,L} - h^{s,n}_{f,L}) \qquad (76)$$

$$\tilde{Q}^{n+1}_{if,L} = H^{n}_{if,L}(\tilde{T}^{s,n+1}_{L} - \tilde{T}^{n+1}_{f,L}) - (\frac{1 + \epsilon}{2}) \Gamma^{n}_{w,L}(h^{s,n}_{g,L} - h^{s,n}_{f,L}) \qquad (77)$$

The intermediate time temperatures are obtained by linearizing the temperature relations about the old time values (see State Relationships, Section 3.1.2).

$$\tilde{T}^{s,n+1}_{L} = T^{s,n}_{L} + \left(\frac{\partial T^{s}}{\partial P}\right)^{n}_{L} (P^{n+1}_{L} - P^{n}_{L}) + \left(\frac{\partial T^{s}}{\partial X_{n}}\right)^{n}_{L} (\tilde{X}^{n+1}_{n,L} - X^{n}_{n,L})$$

$$+ \left(\frac{\partial T^{s}}{\partial U_{g}}\right)^{n}_{L} (\tilde{U}^{n+1}_{g,L} - U^{n}_{g,L}) \qquad (78)$$

$$\tilde{T}^{n+1}_{g,L} = T^{n}_{g,L} + \left(\frac{\partial T_{g}}{\partial P}\right)^{n}_{L} (P^{n+1}_{L} - P^{n}_{L}) + \left(\frac{\partial T_{g}}{\partial X_{n}}\right)^{n}_{L} (\tilde{X}^{n+1}_{n,L} - X^{n}_{n,L})$$

$$+ \left(\frac{\partial T_{g}}{\partial U_{g}}\right)^{n}_{L} (\tilde{U}^{n+1}_{g,L} - U^{n}_{g,L}) \qquad (79)$$

$$\tilde{T}^{n+1}_{f,L} = T^{n}_{f,L} + \left(\frac{\partial T_{f}}{\partial P}\right)^{n}_{L} (P^{n+1}_{L} - P^{n}_{L}) + \left(\frac{\partial T_{f}}{\partial U_{f}}\right)^{n}_{L} (\tilde{U}^{n+1}_{f,L} - U^{n}_{f,L}) \quad . \qquad (80)$$

The method of obtaining the temperature derivatives used in Equations (78) through (80) is also indicated in the State Relationships, Section 3.1.2.

A similar approach is used to obtain the finite-difference form for the phasic momentum equations. In this case, volume-average properties for the momentum control volume are taken as junction properties (that is, linear interpolations between mass and energy control volume centers). The momentum flux terms are approximated using a donor-like formulation that results in a centered velocity gradient term and a viscous-like term. The difference equations for the sum and difference momentum equations, Equations (42) and (43), are

$$(\alpha_g\rho_g)_j^n\,(v_g^{n+1} - v_g^n)_j\Delta x_j + (\alpha_f\rho_f)_j^n\,(v_f^{n+1} - v_f^n)_j\Delta x_j$$

$$+ \tfrac{1}{2}(\dot{\alpha}_g\dot{\rho}_g)_j^n\left[(v_g^2)_L^n - (v_g^2)_K^n\right]\Delta t + \tfrac{1}{2}(\dot{\alpha}_f\dot{\rho}_f)_j^n\left[(v_f^2)_L^n - (v_f^2)_K^n\right]\Delta t$$

$$- \tfrac{1}{2}\left[(\dot{\alpha}_g\dot{\rho}_g)_j^n VISG_j^n + (\dot{\alpha}_f\dot{\rho}_f)_j^n VISF_j^n\right]\Delta t$$

$$= -(P_L - P_K)^{n+1}\Delta t + \left[\rho_j^n B_x - (\alpha_g\rho_g)_j^n (v_g)_j^{n+1} FWG_j^n\right.$$

$$\left. - (\alpha_f\rho_f)_j^n (v_f)_j^{n+1} FWF_j^n - (Q_g)_j^n (v_g - v_f)_j^{n+1}\right]\Delta x_j\Delta t$$

$$- \left[(\alpha_g\rho_g)_j^n HLOSSG_j^n\, v_{g,j}^{n+1} + (\alpha_f\rho_f)_j^n HLOSSF_j^n\, v_{f,j}^{n+1}\right]\Delta t \qquad (81)$$

and

$$\left[1 + C\rho^2/(\rho_g\rho_f)\right]_j^n\left[(v_g^{n+1} - v_g^n) - (v_f^{n+1} - v_f^n)\right]_j\Delta x_j$$

$$+ \tfrac{1}{2}\left[(\dot{\alpha}_g\dot{\rho}_g)/(\alpha_g\rho_g)\right]_j^n\left[(v_g^2)_L^n - (v_g^2)_K^n\right]\Delta t - \tfrac{1}{2}\left[(\dot{\alpha}_g\dot{\rho}_g)/(\alpha_g\rho_g)\right]_j^n VISG_j^n\Delta t$$

$$- \tfrac{1}{2}\left[(\dot{\alpha}_f\dot{\rho}_f/(\alpha_f\rho_f)\right]_j^n\left[(v_f^2)_L^n - (v_f^2)_K^n\right]\Delta t + \tfrac{1}{2}\left[(\dot{\alpha}_f\dot{\rho}_f)/(\alpha_f\rho_f)\right]_j^n VISF_j^n\Delta t$$

$$= -\left[(\rho_f - \rho_g)/(\rho_g\rho_f)\right]_j^n (P_L - P_K)^{n+1}\Delta t - \left\{FWG_j^n (v_g)_j^{n+1} - FWF_j^n (v_f)_j^{n+1}\right.$$

$$- \left[\Gamma_g^n\left(\rho^n v_I^{n+1} - \alpha_f^n\rho_f^n v_g^{n+1} - \alpha_g^n\rho_g^n v_f^{n+1}\right)/(\alpha_g\rho_g\alpha_f\rho_f)^n\right]_j$$

$$\left. + (\rho FI)_I^n (v_g - v_f)_j^{n+1}\right\}\Delta x_j\Delta t - \left(HLOSSG_j^n v_{g,j}^{n+1} - HLOSSF_j^n v_{f,j}^{n+1}\right)\Delta t \qquad (82)$$

where the viscous terms are defined as

$$VISG_j^n = \frac{1}{2}\left\{ \left|v_{g,L}^n\right| \left[(v_g^n)_{j+1}(A_{j+1}/A_j) - (v_g^n)_j\right] \right.$$

$$\left. - \left|v_{g,K}^n\right| \left[(v_g^n)_j - (v_g^n)_{j-1}(A_{j-1}/A_j)\right]\right\} \tag{83}$$

and

$$VISF_j^n = \frac{1}{2}\left\{ \left|v_{f,L}^n\right| \left[(v_f^n)_{j+1}(A_{j+1}/A_j) - (v_f^n)_j\right] \right.$$

$$\left. - \left|v_{f,K}^n\right| \left[(v_f^n)_j - (v_f^n)_{j-1}(A_{j-1}/A_j)\right]\right\} \quad . \tag{84}$$

In Equations (81) and (82), the scalar or thermodynamic variables needed at the junctions are either linear interpolations between the neighboring cell values or donored quantities. The $HLOSSG_j$ and $HLOSSF_j$ terms contain both code calculated abrupt area change loss terms and user specified loss terms.

Using the same averaging techniques the nonexpanded form of the mass and energy equations [Equations (1), (2), (34), (48), and (50)] are next presented in their final finite difference form.

The nonexpanded vapor density Equation (1) becomes

$$V_L[(\alpha_g\rho_g)_L^{n+1} - (\alpha_g\rho_g)_L^n] + (\dot{\alpha}_{g,j+1}^n \dot{\rho}_{g,j+1}^n v_{g,j+1}^{n+1} A_{j+1} - \dot{\alpha}_{g,j}^n \dot{\rho}_{g,j}^n v_{g,j}^{n+1} A_j)\Delta t$$

$$= \hat{\Gamma}_{g,L}^{n+1} V_L \Delta t \quad . \tag{85}$$

The intermediate time variable, $\tilde{\Gamma}^{n+1}_{g,L}$, is obtained using the finite difference form of Equation (31), and is written

$$\tilde{\Gamma}^{n+1}_{g,L} = - \frac{H^n_{ig,L}(\tilde{T}^{s,n+1}_L - \tilde{T}^{n+1}_{g,L}) + H^n_{if,L}(\tilde{T}^{s,n+1}_L - \tilde{T}^{n+1}_{f,L})}{h^{*,n}_{g,L} - h^{*,n}_{f,L}} + \Gamma^n_{w,L} \quad . \tag{86}$$

The nonexpanded liquid density Equation (2) becomes

$$V_L[(\alpha_f \rho_f)^{n+1}_L - (\alpha_f \rho_f)^n_L] + (\dot{\alpha}^n_{f,j+1} \dot{\rho}^n_{f,j+1} v^{n+1}_{f,j+1} A_{j+1} - \dot{\alpha}^n_{f,j} \dot{\rho}^n_{f,j} v^{n+1}_{f,j} A_j) \Delta t$$

$$= - \tilde{\Gamma}^{n+1}_{g,L} V_L \Delta t \quad . \tag{87}$$

The nonexpanded noncondensible density Equation (34) becomes

$$V_L[(\alpha_g \rho_g X_n)^{n+1}_L - (\alpha_g \rho_g X_n)^n_L] + (\dot{\alpha}^n_{g,j+1} \dot{\rho}^n_{g,j+1} \dot{X}^n_{n,j+1} v^{n+1}_{g,j+1} A_{j+1}$$

$$- \dot{\alpha}^n_{g,j} \dot{\rho}^n_{g,j} \dot{X}^n_{n,j} v^{n+1}_{g,j} A_j) \Delta t = 0 \quad . \tag{88}$$

The nonexpanded vapor energy Equation (48) becomes

$$V_L[(\alpha_g \rho_g U_g)^{n+1}_L - (\alpha_g \rho_g U_g)^n_L] + [\dot{\alpha}^n_{g,j+1}(\dot{\rho}^n_{g,j+1} \dot{U}^n_{g,j+1} + P^n_L) v^{n+1}_{g,j+1} A_{j+1}$$

$$- \dot{\alpha}^n_{g,j}(\dot{\rho}^n_{g,j} \dot{U}^n_{g,j} + P^n_L) v^{n+1}_{g,j} A_j] \Delta t = -V_L P^n_L (\tilde{\alpha}^{n+1}_{g,L} - \alpha^n_{g,L})$$

$$+ \left[- \left(\frac{h^*_f}{h^*_g - h^*_f} \right)^n_L H^n_{ig,L}(\tilde{T}^{s,n+1}_L - \tilde{T}^{n+1}_{a,L}) - \left(\frac{h^*_g}{h^*_g - h^*_f} \right)^n_L H^n_{if,L}(\tilde{T}^{s,n+1}_L - \tilde{T}^{n+1}_{f,L}) \right.$$

$$+\left[\left(\frac{1+\varepsilon}{2}\right)h_{g,L}^{s,n}+\left(\frac{1-\varepsilon}{2}\right)h_{f,L}^{s,n}\right]\Gamma_{w,L}^{n}+Q_{wg,L}^{n}+DISS_{g,L}^{n}\Bigg]V_L\,\Delta t \quad . \tag{89}$$

The variables $\tilde{\alpha}_{g,L}^{n+1}$, $\tilde{T}_L^{s,n+1}$, $\tilde{T}_{g,L}^{n+1}$, and $\tilde{T}_{f,L}^{n+1}$ are written with a tilde ($\sim$) to indicate they are intermediate time variables. The nonexpanded liquid energy Equation (50) becomes

$$V_L[(\alpha_f\rho_f U_f)_L^{n+1}-(\alpha_f\rho_f U_f)_L^{n}]+[\dot{\alpha}_{f,j+1}^{n}(\dot{\rho}_{f,j+1}^{n}\dot{U}_{f,j+1}^{n}+P_L^{n})v_{f,j+1}^{n+1}A_{j+1}$$

$$-\dot{\alpha}_{f,j}^{n}(\dot{\rho}_{f,j}^{n}\dot{U}_{f,j}^{n}+P_L^{n})v_{f,j}^{n+1}A_j]\Delta t = V_L P_L^{n}(\tilde{\alpha}_{g,L}^{n+1}-\alpha_{g,L}^{n})$$

$$+\left[\left(\frac{h_f^*}{h_g^*-h_f^*}\right)_L^{n}H_{ig,L}^{n}(\tilde{T}_L^{s,n+1}-\tilde{T}_{g,L}^{n+1})+\left(\frac{h_g^*}{h_g^*-h_f^*}\right)_L^{n}H_{if,L}^{n}(\tilde{T}_L^{s,n+1}-\tilde{T}_{f,L}^{n+1})\right.$$

$$\left.-\left[\left(\frac{1+\varepsilon}{2}\right)h_{g,L}^{s,n}+\left(\frac{1-\varepsilon}{2}\right)h_{f,L}^{s,n}\right]\Gamma_{w,L}^{n}+Q_{wf,L}^{n}+DISS_{f,L}^{n}\right]V_L\,\Delta t \quad . \tag{90}$$

3.1.1.5 Volume-Average Velocities. Volume-average velocities are required for the momentum flux calculation, evaluation of the frictional forces and the Courant time step limit. In a simple constant area passage, the arithmetic-average between the inlet and outlet is a satisfactory approximation. However, at branch volumes with multiple inlets and/or outlets, or for volumes with abrupt area change, use of the arithmetic average results in nonphysical behavior.

The RELAP5 volume-average velocity formulas have the form

$$(v_f)_L^{n}=\frac{\left\{\sum_j(\alpha_f\rho_f v_f)_j^{n}A_j\cdot\sum_j A_j\right\}_{\text{inlets}}}{\left\{\sum_j(\alpha_f\rho_f)_j^{n}A_j\cdot A_L\right\}_{\substack{\text{inlets and}\\ \text{outlets}}}}$$

$$+\frac{\left\{\sum_j (\alpha_f \rho_f v_f)_j^n A_j \cdot \sum_j A_j\right\}_{\text{outlets}}}{\left\{\sum_j (\alpha_f \rho_f)_j^n A_j \cdot A_L\right\}_{\text{inlets and outlets}}} \tag{91}$$

and

$$(v_g)_L^n = \frac{\left\{\sum_j (\alpha_g \rho_g v_g)_j^n A_j \cdot \sum_j A_j\right\}_{\text{inlets}}}{\left\{\sum_j (\alpha_g \rho_g)_j^n A_j \cdot A_L\right\}_{\text{inlets and outlets}}}$$

$$+\frac{\left\{\sum_j (\alpha_g \rho_g v_g)_j^n A_j \cdot \sum_j A_j\right\}_{\text{outlets}}}{\left\{\sum_j (\alpha_g \rho_g)_j^n A_j \cdot A_L\right\}_{\text{inlets and outlets}}} \tag{92}$$

3.1.1.6 Semi-Implicit Scheme Time Advancement. The solution scheme will be discussed with regard to the state of the fluid in a control volume for two successive time steps. There are four possible transition cases. They are:

1. Two-phase to two-phase, where two-phase conditions exist at both old time (n) and new time (n+1).

2. One-phase to one-phase, where one-phase conditions (either pure gas or pure liquid) exist at both old time (n) and new time (n+1).

3. Two-phase to one-phase (disappearance), where two-phase conditions exist at old time (n) and one-phase conditions exist at new time (n+1).

4. One-phase to two-phase (appearance), where one-phase conditions exist at old time (n) and two-phase conditions exist at new time (n+1).

The solution scheme will first be presented for the two-phase to two-phase case, because it is the most general. Then, the solution scheme for the other 3 cases will be presented.

3.1.1.6.1 Two-Phase To Two-Phase--First, the state and temperature Equations (73), (74), (78), (79) and (80) are substituted into the five expanded density and energy difference Equations (66), (67), (68), (69), and (70). The equations then are ordered so that the noncondensible density equation is first, the vapor energy equation is second, the liquid energy equation is third, the difference density equation is fourth, and the sum density equation is fifth. The five density and energy variables are expressed as differences, and the order is

$$(\tilde{X}^{n+1}_{n,L} - X^{n}_{n,L}) \quad , (\tilde{U}^{n+1}_{g,L} - U^{n}_{g,L}) \quad , (\tilde{U}^{n+1}_{f,L} - U^{n}_{f,L}) \quad , (\tilde{\alpha}^{n+1}_{g,L} - \alpha^{n}_{g,L}) \quad ,$$

and

$$(P^{n+1}_{L} - P^{n}_{L}) \quad .$$

The tilde ($\sim$) is used for X_n, U_g, U_f, and α_g to indicate that these are intermediate new time variables, and they do not represent the final new time variables for the two-phase to two-phase case. The ordering of the variables and equations was selected so that a given equation is dominated by its corresponding variable (e.g., the vapor energy equation is second and the vapor energy variable U_g is also second). The noncondensible equation is placed first for ease of degeneration when a noncondensible component is not specified in the problem, and the pressure variable is placed last for numerical convenience in the pressure solution. The system of equations has the following form, where 0 indicates a zero entry in the matrix $\underset{\approx}{A}$ and the vectors

$\underset{\sim}{b}$, $\underset{\sim}{g}^1$, $\underset{\sim}{g}^2$, $\underset{\sim}{f}^1$, $\underset{\sim}{f}^2$ contain only old-time level variables:

$$\underset{\approx}{A}\,\underset{\sim}{x} = \underset{\sim}{b} + \underset{\sim}{g}^{1} v^{n+1}_{g,j+1} + \underset{\sim}{g}^{2} v^{n+1}_{g,j} + \underset{\sim}{f}^{1} v^{n+1}_{f,j+1} + \underset{\sim}{f}^{2} v^{n+1}_{f,j} \qquad (93)$$

where

$$\underset{\approx}{A} = \begin{bmatrix} A_{11} & A_{12} & 0 & A_{14} & A_{15} \\ A_{21} & A_{22} & A_{23} & A_{24} & A_{25} \\ A_{31} & A_{32} & A_{33} & A_{34} & A_{35} \\ A_{41} & A_{42} & A_{43} & A_{44} & A_{45} \\ A_{51} & A_{52} & A_{53} & A_{54} & A_{55} \end{bmatrix} \qquad \underset{\sim}{x} = \begin{bmatrix} \tilde{x}^{n+1}_{n,L} - x^{n}_{n,L} \\ \tilde{U}^{n+1}_{g,L} - U^{n}_{g,L} \\ \tilde{U}^{n+1}_{f,L} - U^{n}_{f,L} \\ \tilde{\alpha}^{n+1}_{g,L} - \alpha^{n}_{g,L} \\ P^{n+1}_{L} - P^{n}_{L} \end{bmatrix}$$

$$\underset{\sim}{b} = \begin{bmatrix} 0 \\ b_2 \\ b_3 \\ b_4 \\ 0 \end{bmatrix} \quad \underset{\sim}{g}^{1} = \begin{bmatrix} g^1_1 \\ g^1_2 \\ 0 \\ g^1_4 \\ g^1_5 \end{bmatrix} \quad \underset{\sim}{g}^{2} = \begin{bmatrix} g^2_1 \\ g^2_2 \\ 0 \\ g^2_4 \\ g^2_5 \end{bmatrix} \quad \underset{\sim}{f}^{1} = \begin{bmatrix} 0 \\ 0 \\ f^1_3 \\ f^1_4 \\ f^1_5 \end{bmatrix} \quad \underset{\sim}{f}^{2} = \begin{bmatrix} 0 \\ 0 \\ f^2_3 \\ f^2_4 \\ f^2_5 \end{bmatrix}$$

A Gaussian elimination system solver[22,23] is used to obtain the bottom row of $\underset{\approx}{A}^{-1}$. Multiplying Equation (93) by $\underset{\approx}{A}^{-1}$, one can verify that just the bottom row of $\underset{\approx}{A}^{-1}$ is needed to obtain an equation that involves only the unknown variables $(P^{n+1}_L - P^{n}_L)$, $v^{n+1}_{g,j+1}$, $v^{n+1}_{g,j}$, $v^{n+1}_{f,j+1}$, and $v^{n+1}_{f,j}$. Substituting the velocity equations [solving Equations (81) and (82) for $v^{n+1}_{f,j}$ and $v^{n+1}_{g,j}$] into this equation results in a single equation involving only pressures. This is done for each volume giving rise to an N x N system of linear equations for the new time pressure. Next, a sparse matrix solver[19] is used to obtain

$(P_L^{n+1} - P_L^n)$ for each volume. Then, the pressure differences $(P_L^{n+1} - P_L^n)$ are substituted into the velocity Equations (81) and (82) to obtain the new time velocities.

Now, the new time velocities are substituted back into Equation (93) to obtain a single vector on the right side. The Gaussian elimination system solver[22,23] is called again to obtain the intermediate time

variables $\tilde{X}_{n,L}^{n+1}$, $\tilde{U}_{g,L}^{n+1}$, $\tilde{U}_{f,L}^{n+1}$, and $\tilde{\alpha}_{g,L}^{n+1}$.

A mixture density, $\rho_{m,L}^{n+1}$, is then calculated from a numerically mass-preserving mixture density equation and compared with the mixture density, ρ_L^{n+1}, which is calculated from the state relations. The difference between these two mixture densities is used to provide a time step control based on mass error. The quantity $\rho_{m,L}^{n+1}$ is calculated as follows: Adding the phasic density Equations (1) and (2), and letting $\rho_m = \alpha_g\rho_g + \alpha_f\rho_f$, gives the differential equation,

$$\frac{\partial \rho_m}{\partial t} + \frac{1}{A}\frac{\partial}{\partial x}(\alpha_g\rho_g v_g A + \alpha_f\rho_f v_f A) = 0 \quad . \tag{94}$$

The numerically mass-preserving finite difference equation corresponding to Equation (94) is

$$V_L[\rho_{m,L}^{n+1} - \rho_L^n] + (\dot{\alpha}_{g,j+1}^n \dot{\rho}_{g,j+1}^n v_{g,j+1}^{n+1} A_{j+1} - \dot{\alpha}_{g,j}^n \dot{\rho}_{g,j}^n v_{g,j}^{n+1} A_j)\Delta t$$

$$+ (\dot{\alpha}_{f,j+1}^n \dot{\rho}_{f,j+1}^n v_{f,j+1}^{n+1} A_{j+1} - \dot{\alpha}_{f,j}^n \dot{\rho}_{f,j}^n v_{f,j}^{n+1} A_j)\Delta t = 0 \tag{95}$$

from which $p_{m,L}^{n+1}$ is obtained.

Next, $\tilde{\Gamma}_{g,L}^{n+1}$ is calculated using Equations (86),

where $\tilde{T}_L^{s,n+1}$, $\tilde{T}_{g,L}^{n+1}$ and $\tilde{T}_{f,L}^{n+1}$ are obtained from Equations (78) through (80)

using the newly calculated variables P_L^{n+1} , $\tilde{U}_{g,L}^{n+1}$, $\tilde{U}_{f,L}^{n+1}$, and $\tilde{X}_{n,L}^{n+1}$.

To obtain the new time variables $X_{n,L}^{n+1}$, $U_{g,L}^{n+1}$, $U_{f,L}^{n+1}$, and $\alpha_{g,L}^{n+1}$ the nonexpanded difference equations, Equations (85), (87), (88), (89), and (90), are used. Using the phasic convective terms along with $\tilde{\Gamma}_{g,L}^{n+1}$ from Equation (86), the nonexpanded phasic density Equations (85) and (87) are used to obtain $(\alpha_g\rho_g)_L^{n+1}$ and $(\alpha_f\rho_f)_L^{n+1}$.

Next, the nonexpanded noncondensible density Equation (88) is used to calculate $(\alpha_g\rho_g X_n)_L^{n+1}$, which is then divided by $(\alpha_g\rho_g)_L^{n+1}$ to obtain $X_{n,L}^{n+1}$.

Following this, the nonexpanded vapor energy Equation (89) is used with the old time vapor energy source and convective terms as well as the intermediate time variables for T_s, T_g, and T_f to obtain $(\alpha_g\rho_g U_g)_L^{n+1}$ which is divided by $(\alpha_g\rho_g)_L^{n+1}$ to give $U_{g,L}^{n+1}$.

Analogously, the nonexpanded liquid energy Equation (90) is used to obtain $(\alpha_f\rho_f U_f)_L^{n+1}$, which is divided by $(\alpha_f\rho_f)_L^{n+1}$ to give $U_{f,L}^{n+1}$.

Finally, $\alpha_{g,L}^{n+1}$ is calculated from $(\alpha_f\rho_f)_L^{n+1}$ using the equation

$$\alpha_{g,L}^{n+1} = 1 - \alpha_{f,L}^{n+1} = 1 - \frac{(\alpha_f\rho_f)_L^{n+1}}{\hat{\rho}_f^{n+1}} \qquad (96)$$

where $\hat{\rho}_f^{n+1}$ is obtained using the linearized state Equation (74) and the new time variables P_L^{n+1} and $U_{f,L}^{n+1}$.

3.1.1.6.2 One-Phase to One-Phase--For this case, the pressure calculation remains the same as in the two-phase to two-phase case. For the densities and energies, however, the nonexpanded equations are not used and the intermediate time variables obtained from the expanded equations are taken to be the new time variables. For the phase that is not present, a large interfacial heat transfer coefficient (10^{12}) is used that results in the internal energy of that phase being very close to saturation conditions. Slight numerical variations from saturation occur due to linearization, and the phasic energy, temperature, and density of the missing phase are reset to the saturation values in the state subroutine. This insures agreement with saturation conditions. For the phase that is present, a value of 0.0 for the interfacial heat transfer coefficient is used since there is no mass transfer occurring.

3.1.1.6.3 Two-Phase to One-Phase (Disappearance)--For this case, the calculation is carried out in the same way as in the two-phase to two-phase case, where expanded calculations followed by nonexpanded calculations are used. Then, for the phase that disappears, the phasic energy, temperature, and density are reset to saturation values in the state subroutine as is done with the one-phase to one-phase case.

3.1.1.6.4 One-Phase to Two-Phase (Appearance)--Here the calculation proceeds in the same way as in the one-phase to one-phase case. A large interfacial heat transfer coefficient (10^{12}) is used for the appearing phase that results in the energy and temperature of that phase being very close to saturation. Because the phase that is appearing is assumed to appear at saturation conditions, an error can be made if, in reality, the phase appeared by convection from a neighboring volume that was at a temperature different from saturation. The magnitude of the potential error is controlled by letting the phase appear at saturation, but restricting the amount that can appear by time step control (corresponds to a typical thermal boundary layer thickness). If more than the limiting amount appears, an error is assumed to have occurred, and the time step is reduced and repeated. This approach is modified when a noncondensible component is present. For the case when vapor appears with

noncondensible present, the old time saturation temperature ($T_L^{s,n}$) is set to the old time liquid temperature ($T_{f,L}^n$) if it is smaller. This is then used to recalculate the old time vapor energy ($U_{g,L}^n$).

3.1.1.7 Nearly-Implicit Scheme Difference Equations and Time Advancement. For problems where the flow is expected to change very slowly with time, it is possible to obtain adequate information from an approximate solution based on very large time steps. This would be advantageous if a reliable and efficient means could be found for solving difference equations treating all terms--phase exchanges, pressure propagation, and convection--by implicit differences. Unfortunately, the state-of-the-art is less satisfactory here than in the case of semi-implicit (convection-explicit) schemes. A fully-implicit scheme for the six equation model of a 100 cell problem would require the solution of 600 coupled algebraic equations. If these equations were linearized for a straight pipe, inversion of a block tri-diagonal 600 x 600 matrix with 6 x 6 blocks would be required. This would yield a matrix of bandwidth 23 containing ∿13,800 nonzero elements, resulting in an extremely costly time advancement scheme.

To reduce the number of calculations required for solving fully implicit difference schemes, fractional step (sometimes called multiple step) methods have been tried. The equations can be split into fractional steps based upon physical phenomena. This is the basic idea in the nearly-implicit scheme. Fractional step methods for two-phase flow problems have been developed in References 24 and 25. These earlier efforts have been used to guide the development of the nearly-implicit scheme. The fractional step method described here differs significantly from prior efforts in the reduced number of steps used to evaluate the momentum equations.

The nearly-implicit scheme consists of a first step that solves all seven conservation equations treating all interphase exchange processes, the pressure propagation process, and the momentum convection process implicitly. These finite difference equations are exactly the expanded ones [Equations (66), (67), (68), (69), (70), (81), and (82)] solved in the

semi-implicit scheme with one major change. The convective terms in the momentum Equations (81) and (82) are evaluated implicitly (in a linearized form) instead of in an explicit donored fashion as is done in the semi-implicit scheme.

The linearized implicit technique used for the convective terms can be seen by examining the convective terms in the vapor part of the sum momentum Equation (64). An analogous result occurs for the liquid part as well as for the difference momentum Equation (65). The convective term is

$$\frac{1}{2}\,\alpha_g\rho_g\,(v_g^2)_{x_K}^{x_L} \quad . \tag{97}$$

In the nearly-implicit formulation the VISF and VISG terms that result from the donor cell formulation are not used. Evaluating the velocities at new time gives the finite difference form as

$$\frac{1}{2}\left(\dot{\alpha}_g\dot{\rho}_g\right)_j^n \left[\left(v_{g,L}^{n+1}\right)^2 - \left(v_{g,K}^{n+1}\right)^2\right] \quad . \tag{98}$$

This term can be rewritten as

$$\frac{1}{2}\left(\dot{\alpha}_g\dot{\rho}_g\right)_j^n \left[\left(v_{g,L}^{n+1} - v_{g,L}^{n}\right)^2 + 2v_{g,L}^{n}\left(v_{g,L}^{n+1} - v_{g,L}^{n}\right) + \left(v_{g,L}^{n}\right)^2 - \left(v_{g,K}^{n+1} - v_{g,K}^{n}\right)^2 - 2v_{g,K}^{n}\left(v_{g,K}^{n+1} - v_{g,K}^{n}\right) - \left(v_{g,K}^{n}\right)^2\right] \quad . \tag{99}$$

Assuming that the leading quadratic term for L and K is small compared to the others results in the following form

$$\frac{1}{2}\left(\dot{\alpha}_g\dot{\rho}_g\right)_j^n \left[2v_{g,L}^{n}\left(v_{g,L}^{n+1} - v_{g,L}^{n}\right) + \left(v_{g,L}^{n}\right)^2 - 2v_{g,K}^{n}\left(v_{g,K}^{n+1} - v_{g,K}^{n}\right) - \left(v_{g,K}^{n}\right)^2\right] \quad . \tag{100}$$

Using this linearized implicit form the explicit convective and viscous terms in the sum momentum finite difference Equation (81) are replaced by

$$\frac{1}{2}(\dot{\alpha}_g\dot{\rho}_g)_j^n\left[2v_{g,L}^n(v_{g,L}^{n+1}-v_{g,L}^n)+(v_{g,L}^n)^2-2v_{g,K}^n(v_{g,K}^{n+1}-v_{g,K}^n)-(v_{g,K}^n)^2\right]\Delta t$$

$$+\frac{1}{2}(\dot{\alpha}_f\dot{\rho}_f)_j^n\left[2v_{f,L}^n(v_{f,L}^{n+1}-v_{f,L}^n)+(v_{f,L}^n)^2\right.$$

$$\left.-2v_{f,K}^n(v_{f,K}^{n+1}-v_{f,K}^n)-(v_{f,K}^n)^2\right]\Delta t \quad . \tag{101}$$

Similarly, for the difference momentum finite difference Equation (82), the convective terms become

$$\frac{1}{2}\left[(\dot{\alpha}_g\dot{\rho}_g)/(\alpha_g\rho_g)\right]_j^n\left[2v_{g,L}^n(v_{g,L}^{n+1}-v_{g,L}^n)+(v_{g,L}^n)^2\right.$$

$$\left.-2v_{g,K}^n(v_{g,K}^{n+1}-v_{g,K}^n)-(v_{g,K}^n)^2\right]\Delta t$$

$$-\frac{1}{2}\left[(\dot{\alpha}_f\dot{\rho}_f)/(\alpha_f\rho_f)\right]_j^n\left[2v_{f,L}^n(v_{f,L}^{n+1}-v_{f,L}^n)+(v_{f,L}^n)^2\right.$$

$$\left.-2v_{f,K}^n(v_{f,K}^{n+1}-v_{f,K}^n)-(v_{f,K}^n)^2\right]\Delta t \quad . \tag{102}$$

The new time volume-averaged velocities ($v_{f,L}^{n+1}$ and $v_{g,L}^{n+1}$) in Equations (101) and (102) use the same equations as the old time volume-averaged velocities [Equations (91) and (92)], except that the junction velocities are at new time. Thus the new time volume-averaged velocities have the form

$$v_{f,L}^{n+1} = \left(\sum_j c_{f,j}^n \; v_{f,j}^{n+1}\right)_{inlets} + \left(\sum_j c_{f,j}^n \; v_{f,j}^{n+1}\right)_{outlets} \tag{103}$$

and

$$v_{g,L}^{n+1} = \left(\sum_j c_{g,j}^n \; v_{g,j}^{n+1}\right)_{inlets} + \left(\sum_j c_{g,j}^n \; v_{g,j}^{n+1}\right)_{outlets} \tag{104}$$

where $c_{f,j}^n$ and $c_{g,j}^n$ contain all old time quantities.

Although this additional implicitness involves only the momentum convective terms, it has a large impact on the algebraic solution algorithm in the first step. In the semi-implicit scheme, Equations (66) through (70) are solved locally to give a single equation of the form

$$P_L^{n+1} = A \; v_{g,j+1}^{n+1} + B \; v_{g,j}^{n+1} + C \; v_{f,j+1}^{n+1} + D \; v_{f,j}^{n+1} + E \tag{105}$$

for pressure where A, B, C, D, and E contain old time variables only (see Figure 4 for cell indexes).

In the semi-implicit scheme, the momentum equations are also solved locally to obtain

$$v_{g,j}^{n+1} = A^1 \left(P_L^{n+1} - P_K^{n+1}\right) + C^1 \tag{106}$$

$$v_{f,j}^{n+1} = B^1 \left(P_L^{n+1} - P_K^{n+1}\right) + D^1 \tag{107}$$

where A^1, B^1, C^1, and D^1 again contain only n time level variables. If the momentum Equations (106) and (107) are used to eliminate the n+1 level velocities from Equation (105), we get the normal pressure

equation used in the semi-implicit scheme to obtain all the n+1 pressures. For a 100 cell straight pipe problem, this results in a 100 x 100 tri-diagonal matrix system to solve for all the P^{n+1}.

In the nearly-implicit scheme, because the momentum flux terms are implicit, the momentum Equations (81) and (82) [using the convective terms from Equations (101) and (102)] cannot be locally solved to get Equations (106) and (107). The new-time convective terms bring in n+1 level upstream and downstream velocities. Equations (66) through (70) are still used to obtain Equation (105). In the nearly-implicit scheme, Equation (105) is used to eliminate the n+1 level pressure terms from Equations (81) and (82), [using the convective terms from Equations (101) and (102)], and a coupled pair of momentum equations involving only n+1 level velocities is obtained. Because of the n+1 level flux terms, this is a globally coupled system. For a straight pipe of 100 junctions, a block tri-diagonal 200 x 200 matrix system with 2 x 2 blocks is obtained. This system of equations is solved using a sparse matrix solution algorithm.[19] Once the v_f^{n+1} and v_g^{n+1} solution is obtained, P^{n+1} is obtained by back substitution into Equation (105). Using Equations (66) through (70) intermediate/provisional n+1 values for α_g, U_g, U_f, X_n denoted by $\tilde{\alpha}_g^{n+1}$, $\tilde{U}_g^{n+1}$, $\tilde{U}_f^{n+1}$, $\tilde{X}_n^{n+1}$ can also be obtained.

The second step in the nearly-implicit scheme is used to stabilize the convective terms in the mass and energy balance equations. This step uses the final n+1 level velocities from the first step along with the interphase exchange terms resulting from the first step, i.e., the interphase heat and mass exchanges for step two are calculated using P^{n+1}, $\tilde{U}_g^{n+1}$, $\tilde{U}_f^{n+1}$, $\tilde{X}_n^{n+1}$ from step one. The phasic continuity and energy equations in this second step have the fluxed variables evaluated at the n+1 time level, i.e., implicitly as compared to their explicit evaluation in the first step.

The vapor density equation is

$$V_L[(\alpha_g\rho_g)_L^{n+1} - (\alpha_g\rho_g)_L^n] + \left[(\dot{a}\rho)_{g,j+1}^{n+1} v_{g,j+1}^{n+1} A_{j+1} - (\dot{a}\rho)_{g,j}^{n+1} v_{g,j}^{n+1} A_j\right]\Delta t$$

$$= \tilde{\Gamma}^{n+1}_{g,L} V_L \Delta t \quad . \tag{108}$$

The liquid density equation is

$$V_L\left[(\alpha_f\rho_f)^{n+1}_L - (\alpha_f\rho_f)^n_L\right] + \left[(\dot{\alpha}\rho)^{n+1}_{f,j+1} v^{n+1}_{f,j+1} A_{j+1} - (\dot{\alpha}\rho)^{n+1}_{f,j} v^{n+1}_{f,j} A_j\right]\Delta t$$

$$= -\tilde{\Gamma}^{n+1}_{g,L} V_L \Delta t \quad . \tag{109}$$

In Equations (108) and (109) the mass exchange $\tilde{\Gamma}^{n+1}_g$ is evaluated using the provisional values from the first step, and is written

$$\tilde{\Gamma}^{n+1}_{g,L} = -\frac{H^n_{ig,L}(\tilde{T}^{s,n+1}_L - \tilde{T}^{n+1}_{g,L}) + H^n_{if,L}(\tilde{T}^{s,n+1}_L - \tilde{T}^{n+1}_{f,L})}{h^{*,n}_{g,L} - h^{*,n}_{f,L}} + \Gamma^n_{w,L} \tag{110}$$

where the provisional temperatures from the linearized state relationship are known as functions of $\tilde{U}^{n+1}_g$, $\tilde{U}^{n+1}_f$, $\tilde{X}^{n+1}_n$, and P^{n+1}.

The noncondensible density equation is

$$V_L\left[(\alpha_g\rho_g X_n)^{n+1}_L - (\alpha_g\rho_g X_n)^n_L\right] + \left[(\alpha_g\dot{\rho}_g X_n)^{n+1}_{j+1} v^{n+1}_{g,j+1} A_{j+1}\right.$$

$$\left. - (\alpha_g\dot{\rho}_g X_n)^{n+1}_j v^{n+1}_{g,j} A_j\right]\Delta t = 0 \quad . \tag{111}$$

The vapor energy equation is given by

$$V_L\left[(\alpha_g\rho_g U_g)^{n+1}_L - (\alpha_g\rho_g U_g)^n_L\right] + \left[(\alpha\dot{\rho}U)^{n+1}_{g,j+1} v^{n+1}_{g,j+1} A_{j+1} - (\alpha\dot{\rho}U)^{n+1}_{g,j} v^{n+1}_{g,j} A_j\right]\Delta t$$

$$= -V_L P^n_L(\tilde{\alpha}^{n+1}_{g,L} - \alpha^n_{g,L}) - P^n_L\left(\dot{\alpha}^n_{g,j+1} v^{n+1}_{g,j+1} A_{j+1} - \dot{\alpha}^n_{g,j} v^{n+1}_{g,j} A_j\right)\Delta t$$

$$+\left\{-\left(\frac{h_f^*}{h_g^* - h_f^*}\right)_L^n H_{ig,L}^n \left(\tilde{T}_L^{s,n+1} - \tilde{T}_{g,L}^{n+1}\right) - \left(\frac{h_g^*}{h_g^* - h_f^*}\right) H_{if,L}^n \left(\tilde{T}_L^{s,n+1} - \tilde{T}_{f,L}^{n+1}\right)\right.$$

$$\left. + \left[\left(\frac{1+\varepsilon}{2}\right) h_{g,L}^{s,n} + \left(\frac{1-\varepsilon}{2}\right) h_{f,L}^{s,n}\right] \Gamma_{w,L}^n + Q_{wg,L}^n + DISS_{g,L}^n \right\} V_L \Delta t \quad . \qquad (112)$$

The liquid energy equation is given by

$$V_L \left[(\alpha_f \rho_f U_f)_L^{n+1} - (\alpha_f \rho_f U_f)_L^n\right] + \left[(\alpha\dot{\rho}U)_{f,j+1}^{n+1} v_{f,j+1}^{n+1} A_{j+1} - (\alpha\dot{\rho}U)_{f,j}^{n+1} v_{f,j}^{n+1} A_j\right] \Delta t$$

$$= V_L P_L^n \left(\tilde{\alpha}_{g,j}^{n+1} - \alpha_{g,L}^n\right) - P_L^n \left(\dot{\alpha}_{f,j+1}^n v_{f,j+1}^{n+1} A_{j+1} - \dot{\alpha}_{f,j}^n v_{f,j}^{n+1} A_j\right) \Delta t$$

$$+\left\{\left(\frac{h_f^*}{h_g^* - h_f^*}\right)_L^n H_{ig,L}^n \left(\tilde{T}_L^{s,n+1} - \tilde{T}_{g,L}^{n+1}\right) + \left(\frac{h_g^*}{h_g^* - h_f^*}\right)_L^n H_{if,L}^n \left(\tilde{T}_L^{s,n+1} - \tilde{T}_{f,L}^{n+1}\right)\right.$$

$$\left. - \left[\left(\frac{1+\varepsilon}{2}\right) h_{g,L}^{s,n} + \left(\frac{1-\varepsilon}{2}\right) h_{f,L}^{s,n}\right] \Gamma_{w,L}^n + Q_{wf,L}^n + DISS_{f,L}^n \right\} V_L \Delta t \quad . \qquad (113)$$

This second step uses the mass and energy balance equations only. If the structure of Equations (108) through (113) is examined, it is seen that each equation only involves one unknown variable:
Equation (108) - $(\alpha\rho)_g^{n+1}$,

Equation (109) - $(\alpha\rho)_f^{n+1}$, Equation (111) - $(\alpha_g \rho_g X_n)^{n+1}$,

Equation (112) - $(\alpha\rho U)_g^{n+1}$, and Equation (113) - $(\alpha\rho U)_f^{n+1}$.

This is because the new time velocities v_g^{n+1}, v_f^{n+1} are known from step one and provisional n+1 values from step one are used in the exchange terms. Hence, each equation is uncoupled from the others and can be solved independently. In addition, the three equations involving the

gas phase, Equations (108), (111), and (112), have the same structural form for the convective terms, i.e., each equation convects with velocity v_g^{n+1}. Equation (108) is inverted once and then this inverse may be used with different right sides to solve Equations (111) and (112). Hence, for a straight pipe problem of 100 cells, only one 100 x 100 tri-diagonal system is inverted to obtain $(\alpha\rho)_g^{n+1}$, $(\alpha_g\rho_g X_n)^{n+1}$, and $(\alpha\rho U)_g^{n+1}$. In like manner, the liquid phase Equations (109) and (113) have the same structure and require only one inversion to be carried out to solve both equation sets giving $(\alpha\rho)_f^{n+1}$ and $(\alpha\rho U)_f^{n+1}$.

With the above five new time variables known, we obtain X_n^{n+1}, U_g^{n+1}, and U_f^{n+1} from

$$X_n^{n+1} = (\alpha_g\rho_g X_n)^{n+1}/(\alpha\rho)_g^{n+1} \tag{114}$$

$$U_g^{n+1} = (\alpha\rho U)_g^{n+1}/(\alpha\rho)_g^{n+1} \tag{115}$$

$$U_f^{n+1} = (\alpha\rho U)_f^{n+1}/(\alpha\rho)_f^{n+1} \quad . \tag{116}$$

The void fraction, α_g^{n+1}, is obtained from

$$\alpha_g^{n+1} = \frac{\rho_m^{n+1} - \hat{\rho}_f^{n+1}}{\hat{\rho}_g^{n+1} - \hat{\rho}_f^{n+1}} = \frac{(\alpha\rho)_g^{n+1} + (\alpha\rho)_f^{n+1} - \hat{\rho}_f^{n+1}}{\hat{\rho}_g^{n+1} + \hat{\rho}_f^{n+1}} \tag{117}$$

where ρ_m^{n+1} is the mixture density, ρ_f is the liquid density calculated from the linearized state relationship [Equation(74)] using U_f^{n+1} and ρ^{n+1}, and $\hat{\rho}_g^{n+1}$ is the vapor density calculated from the linearized state relationship [Equation(73)] using U_g^{n+1} and ρ^{n+1}.

Up to this point of this section on the nearly-implicit scheme, the difference equations have been recorded along with the time advancement for the case of two-phase to two-phase only. As indicated in the Semi-Implicit Scheme Time Advancement Section 3.1.1.6, there are three other possible transaction cases (one-phase to one-phase, two-phase to one-phase, and one-phase to two-phase). These three cases will now be presented for the nearly-implicit scheme.

For the one-phase to one-phase case, both the first step and the second step are carried out as in the two-phase to two-phase case. For the phase that is not present α is zero and thus $(\alpha\rho)^{n+1}$ equals zero for that phase. The provisional n+1 value of the corresponding variable is used in order to avoid the zero divide in Equations (114) through (116). For the phase that is not present, a large interfacial heat transfer coefficient (10^{12}) is used, and for the phase that is present, a value of 0.0 is used for the interfacial heat transfer coefficient. The first step quantities are used for the appearing phase. As with the semi-implicit time advancement, phasic energy, temperature, and density of the missing phase are reset to the saturation values in the state subroutine.

For the two-phase to one-phase case (disappearance), the calculation is carried out the same as in the two-phase to two-phase case. Then, for the phase that is missing, the phasic energy, temperature, and density of the missing phase are reset to saturation values in the state subroutine as is done with the one-phase to one-phase case. This is the same approach used in the semi-implicit scheme time advancement.

For the one-phase to two-phase case (appearance), the first step quantities are used for the appearing phase. A large interfacial heat transfer coefficient (10^{12}) is used for the appearing phase that results in the energy and temperature of that phase being very close to saturation. Because the phase that is appearing is assumed to appear at saturation conditions, an error can be made if, in reality, the phase appeared by convection from a neighboring volume that was at a temperature different from saturation. The magnitude of the potential error is controlled by letting the phase appear at saturation, but restricting the

amount that can appear by time step control (corresponds to a typical thermal boundary layer thickness). If more than the limiting amount appears, an error is assumed to have occurred, and the time step is reduced and repeated. This is the same approach used in the semi-implicit scheme time advancement.

In summary, the second step stabilizes the convective terms in the mass and energy equations, and it does so with very little computational effort due to the fractional step nature of the scheme. If the nearly-implicit method is compared with the fully-implicit method for a straight pipe problem of 100 cells, we have the following efficiency estimates. The fully-implicit method requires the inversion of a banded block tri-diagonal 600 x 600 matrix of bandwidth 23 containing 13,800 nonzero elements. The nearly-implicit method requires the inversion of one block tri-diagonal 200 x 200 matrix with 2 x 2 blocks and bandwidth 7 containing 1,400 nonzero elements plus two 100 x 100 tri-diagonal matrices with 300 nonzero elements. The nearly-implicit method thus requires about 1/10 the number of storage locations required by the fully-implicit method. If the computational efficiency is estimated by counting the number of multiplications in the forward part of a Gaussian elimination algorithm, then the fully-implicit method for this problem requires about 450,000 multiplications, whereas the nearly-implicit method requires about 2,000 multiplications. Thus, the nearly-implicit method requires about 1/200 of the computational time needed for a fully-implicit scheme.

3.1.2 State Relationships

The six equation model with an additional equation for the noncondensible gas component has five independent state variables. The independent variables are chosen to be P, α_g, U_g, U_f, and X_n. All the remaining thermodynamic variables (temperatures, densities, partial pressures, qualities, etc.) are expressed as functions of these five independent properties. In addition to these properties several state derivatives are needed because of the linearization used in the numerical scheme. This section contains three parts. The first discusses the state

property derivatives needed in the numerical scheme. The second section develops the appropriate derivative formulas for the single component case and the third section does the same for the two-phase, two-component case.

3.1.2.1 State Equations. To expand the time derivatives of the phasic densities in terms of these dependent variables using two-term Taylor series expansions, the following derivatives of the phasic densities are needed

$$\left(\frac{\partial \rho_g}{\partial P}\right)_{U_g, X_n}, \left(\frac{\partial \rho_g}{\partial U_g}\right)_{P, X_n}, \left(\frac{\partial \rho_g}{\partial X_n}\right)_{P, U_g}, \left(\frac{\partial \rho_f}{\partial P}\right)_{U_f}, \left(\frac{\partial \rho_f}{\partial U_f}\right)_{P} .$$

The interphase mass and heat transfer requires an implicit (linearized) evaluation of the interphase temperature potentials $T_f - T_I$ and $T_g - T_I$. T_I is the temperature that exists at the phase interface. For a single component mixture we have

$$T_I = T^s(P) \tag{118}$$

where the superscript s denotes a saturation value. In the presence of a noncondensible mixed with the steam we have

$$T_I = T^s(P_s) \tag{119}$$

where P_s is the partial pressure of the steam in the gaseous phase. The gaseous phase properties for a two-component mixture can be described with three independent properties. In particular, the steam partial pressure, P_s, can be expressed as

$$P_s = P_s(P, X_n, U_g) . \tag{120}$$

Substituting Equation (120) into Equation (119) gives the interface temperature, T_I, as the desired function of P and X_n, U_g.[a] The implicit evaluation of the temperature potential in the numerical scheme requires the following derivatives of the phasic and interface temperatures, such as

$$\left(\frac{\partial T_g}{\partial P}\right)_{U_g,X_n}, \left(\frac{\partial T_g}{\partial U_g}\right)_{P,X_n}, \left(\frac{\partial T_g}{\partial X_n}\right)_{P,U_g},$$

$$\left(\frac{\partial T_f}{\partial P}\right)_{U_f}, \left(\frac{\partial T_f}{\partial U_f}\right)_{P}, \left(\frac{\partial T^S}{\partial P}\right)_{U_g,X_n}, \left(\frac{\partial T^S}{\partial U_g}\right)_{P,X_n}, \left(\frac{\partial T^S}{\partial X_n}\right)_{P,U_g}.$$

If we have a single component mixture the X_n derivatives are zero and

$$\left(\frac{\partial T^S}{\partial U_g}\right)_P = 0 \tag{121}$$

since T^S is only a function of P for this case.

In addition to these derivatives, the basic phasic properties as a function of P, α_g, U_g, U_f, and X_n are needed along with the homogeneous equilibrium sound speed for the critical flow model.

The basic properties are obtained from steam tables that tabulate for each phase the phasic properties and three phasic derivatives; the isobaric thermal expansion coefficient (β), the isothermal compressibility (κ), and the specific heat at constant pressure (C_p).

3.1.2.2 Single Component Two-Phase Mixture. For the purposes of this report a single component two-phase mixture will be referred to as Case 1. Case 1 is straight forward. Liquid properties are obtained from the steam

---

a. ρ_g and T_g could have initially been written with P_s, X_n, U_g as the independent arguments. Equation (120) would then be used to write ρ_g and T_g with P, X_n, and U_g as the independent variables.

tables given P and U_f. All the desired density and temperature derivatives can then be obtained from κ_f, β_f, and C_{pf}. The desired derivatives are given as

$$\left(\frac{\partial \rho_f}{\partial U_f}\right)_P = -\left(\frac{V_f \beta_f}{C_{pf} - V_f \beta_f P}\right) / V_f^2 \tag{122}$$

$$\left(\frac{\partial T_f}{\partial U_f}\right)_P = \frac{1}{C_{pf} - V_f \beta_f P} \tag{123}$$

$$\left(\frac{\partial \rho_f}{\partial P}\right)_{U_f} = \left[\frac{C_{pf} V_f \kappa_f - T_f (V_f \beta_f)^2}{C_{pf} - V_f \beta_f P}\right] / V_f^2 \tag{124}$$

$$\left(\frac{\partial T_f}{\partial P}\right)_{U_f} = -\left(\frac{P V_f \kappa_f - T V_f \beta_f}{C_{pf} - V_f \beta_f P}\right) \quad . \tag{125}$$

Parallel formulas hold for the vapor phase with P and U_g as the independent variables.

The only nonstandard feature involved in the evaluation of the formulas in Equation (125) is the calculation of V, T, κ, β, and C_p if the steam is subcooled or the liquid is superheated, i.e., metastable states. The extrapolation used for these cases is a constant pressure extrapolation from the saturation state for the temperature and specific volume. Using the first two terms of a Taylor series this gives

$$T = T(P) + \frac{1}{C_p(P) - PV(P)\beta(P)} [U - U(P)] \tag{126}$$

$$V = V(P) + V(P)\beta(P)[T - T(P)] \quad . \tag{127}$$

In Equations (126) and (127) the argument P indicates a saturation value.

To obtain the β, κ, and C_p corresponding to the extrapolated V and T the extrapolation formulas are differentiated. Taking the appropriate derivatives of Equation (126) and (127) gives

$$C_p(P,T) \overset{\Delta}{=} \left(\frac{\partial h}{\partial T}\right)_P = \left(\frac{\partial U}{\partial T}\right)_P + P\left(\frac{\partial V}{\partial T}\right)_P = C_p(P) \tag{128}$$

$$\beta(P,T) \overset{\Delta}{=} \frac{1}{V}\left(\frac{\partial V}{\partial T}\right)_P = \frac{V(P)\beta(P)}{V(P,T)} \tag{129}$$

$$\kappa(P,T) \overset{\Delta}{=} -\frac{1}{V}\left(\frac{\partial V}{\partial P}\right)_T = [V(P) + [T - T(P)]V(P)\beta(P)]\frac{\kappa(P)}{V(P,T)}$$

$$- [T - T(P)]\, V(P)\left[\frac{d\beta(P)}{dP} + \beta^2(P)\frac{dT}{dP}(P)\right]/V(P,T) \quad . \tag{130}$$

Equation (128) shows that a consistently extrapolated C_p is just the saturation value $C_p(P)$. Equation (129) gives the extrapolated β as a function of the saturation properties and the extrapolated V. Equation (130) gives the consistently extrapolated κ as a function of the extrapolated and saturation properties. The extrapolated κ in Equation (130) involves a change of saturation properties along the saturation line. In particular, $\frac{d\beta}{dP}(P)$ involves a second derivative of specific volume. Since no second-order derivatives are available from the steam property tables this term was approximated for the vapor phase by assuming the fluid behaves as an ideal gas. With this assumption the appropriate formula for the vapor phase κ is

$$\kappa_g(P,T) = \left\{V_g(P) + [T_g - T(P)]\, V_g(P)\beta_g(P)\right\} \kappa_g(P)/V_g(P,T) \quad . \tag{131}$$

For the liquid phase extrapolation (superheated liquid) only the specific volume correction factor in Equation (130) was retained, i.e.,

$$\kappa_f(P,T) = \frac{V_f(P)\kappa_f(P)}{V_f(P,T)} \quad . \tag{132}$$

The homogeneous equilibrium sound speed is calculated from standard formulas using the saturation κ's, β's, and C_p's. The sound speed formula

$$a^2 = V^2 \left(\frac{dP^s}{dT}\right)^2 \Bigg/ \left\{ X\left[\frac{C_{pg}}{T_g} + V_g \frac{dP^s}{dT}\left(\kappa_g \frac{dP^s}{dT} - 2\beta_g\right)\right] + (1 - X)\left[\frac{C_{pf}}{T_f} + V_f \frac{dP^s}{dT}\left(\kappa_f \frac{dP^s}{dT} - 2\beta_f\right)\right]\right\} \quad (133)$$

is used, where from Clapeyron's equation

$$\frac{dP^s}{dT} = \frac{h_g^s - h_f^s}{T^s(V_g^s - V_f^s)} \quad (134)$$

and X is the steam quality based on the mixture mass.

3.1.2.3 Two Component, Two-Phase Mixture. This case is referred to as Case 2. The liquid phasic properties and derivatives are calculated in exactly the same manner as described in Case 1 (see Section 3.1.2.2); we assume the noncondensible component is present only in the gaseous phase.

The properties for the gaseous phase are calculated assuming a Gibbs-Dalton mixture of steam and an ideal noncondensible gas. A Gibbs-Dalton mixture is based upon the following assumptions:

1. $$P = P_n + P_s \quad (135)$$

2. $$U_g = X_n U_n + (1 - X_n) U_s \quad (136)$$

3. $$X_n V_n = (1 - X_n) V_s = V_g \quad (137)$$

where P_s and P_n are the partial pressures of the steam and noncondensible components, respectively. The internal energies U_s, U_n,

and the specific volumes V_s, V_n are evaluated at the gas temperature and the respective partial pressures. The vapor properties are obtained from the steam tables and the noncondensible state equations are,[a]

$$P_n V_n = R_n T_g \tag{138}$$

$$U_n = \begin{cases} C_o T_g + U_o & T_g < T_o \\ C_o T_g + \frac{1}{2} D_o (T_g - T_o)^2 + U_o & T_g \geq T_o \end{cases} . \tag{139}$$

Given P, U_g, and X_n we must solve Equations (135) through (137) implicitly to find the state of the gaseous phase. If Equation (135) is used to eliminate P_n and Equation (138) is used for V_n, Equations (136) and (137) can be written as

$$(1 - X_n) U_s + X_n U_n \left[T_g(U_s, P_s) \right] - U_g = 0 \tag{140}$$

$$(1 - X_n) \left[\frac{V_s(U_s, P_s) P_s}{T_g(U_s, P_s)} \right] (P - P_s) - X_n R_n P_s = 0 . \tag{141}$$

Given P, U_g, and X_n, Equations (140) and (141) implicitly determine U_s and P_s. [Equation (137) was divided by the temperature and multiplied by the partial pressures to obtain Equation (141).]

To obtain the derivatives needed in the numerical scheme, we must evaluate the derivatives of U_s and P_s with respect to P, U_g, and X_n. These derivatives can be obtained from Equations (140) and (141) by the use of the chain rule and implicit differentiation. For example,

---

a. The code input permits selection of any one of six noncondensible gases. The constants used to represent air are in SI units; T_o = 250.0 K, C_o = 715.0 J/(kg K), U_o = 158990.52 J/kg, D_o = 0.10329 J/(kg K^2), and R_n = 287.066 N m/(kg K).

taking the derivative of Equations (140) and (141) with respect to P [recall that $P_s = P_s(P, U_g, X_n)$ and $U_s = U_s(P, U_g, X_n)$] we obtain

$$\begin{bmatrix} X_n\left(\frac{dU_n}{dT_g}\right)\left(\frac{\partial T_g}{\partial P_s}\right) & 1 - X_n + X_n\left(\frac{dU_n}{dT_g}\right)\left(\frac{\partial T_g}{\partial U_s}\right) \\ -X_n R_n - (1 - X_n)R_s & 0 + TERM2 \\ + R_s + TERM1 & \end{bmatrix} \times \begin{bmatrix} \left(\frac{\partial P_s}{\partial P}\right)_{U_g, X_n} \\ \left(\frac{\partial U_s}{\partial P}\right)_{U_g, X_n} \end{bmatrix}$$

$$= \begin{bmatrix} 0 \\ \\ (1 - X_n)R_s \end{bmatrix} \qquad (142)$$

as a linear system of two equations determining

$$\left(\frac{\partial P_s}{\partial P}\right)_{U_g, X_n} \quad \text{and} \quad \left(\frac{\partial U_s}{\partial P}\right)_{U_g, X_n} .$$

In Equation (142),

$$R_s = \frac{P_s V_s}{T_g} \qquad (143)$$

is the equivalent gas constant for the steam vapor,

$$TERM1 = (1 - X_n)P_{rl}R_s\left[\frac{1}{P_s} + \frac{1}{V_s}\left(\frac{\partial V_s}{\partial P_s}\right)_{U_s} - \frac{1}{T_g}\left(\frac{\partial T_g}{\partial P_s}\right)_{U_s}\right] \qquad (144)$$

and

$$\text{TERM2} = (1 - X_n)P_n R_s \left[\frac{1}{V_s}\left(\frac{\partial V_s}{\partial U_s}\right)_{P_s} - \frac{1}{T_g}\left(\frac{\partial T_g}{\partial U_s}\right)_{P_s} \right] . \tag{145}$$

The TERM factors have been singled out as they are treated in a special manner in the numerical scheme. To obtain the derivatives of P_s and U_s with respect to U_g and X_n we repeat the above development taking derivatives of Equations (140) and (141) with respect to U_g and X_n. In each case, linear equations parallel to those in Equation (142) are obtained. In fact, the left side matrix is exactly the same, only the right side vector changes.

Having obtained all the derivatives of P_s and U_s, it is relatively easy to obtain the derivatives needed for the gaseous phase. From the chain rule we have

$$\left(\frac{\partial T_g}{\partial P}\right)_{U_g, X_n} = \left(\frac{\partial T_g}{\partial P_s}\right)_{U_s}\left(\frac{\partial P_s}{\partial P}\right)_{U_g, X_n} + \left(\frac{\partial T_g}{\partial U_s}\right)_{P_s}\left(\frac{\partial U_s}{\partial P}\right)_{U_g, X_n} \tag{146}$$

$$\left(\frac{\partial T_g}{\partial U_g}\right)_{P, X_n} = \left(\frac{\partial T_g}{\partial P_s}\right)_{U_s}\left(\frac{\partial P_s}{\partial U_g}\right)_{P_g, X_n} + \left(\frac{\partial T_g}{\partial U_s}\right)_{P_s}\left(\frac{\partial U_s}{\partial U_g}\right)_{P, X_n} \tag{147}$$

$$\left(\frac{\partial T_g}{\partial X_n}\right)_{P, U_g} = \left(\frac{\partial T_g}{\partial P_s}\right)_{U_s}\left(\frac{\partial P_s}{\partial X_n}\right)_{P, U_g} + \left(\frac{\partial T_g}{\partial U_s}\right)_{P_s}\left(\frac{\partial U_s}{\partial X_n}\right)_{P, U_g} \tag{148}$$

where

$$\left(\frac{\partial T_g}{\partial P_s}\right)_{U_s} \quad \text{and} \quad \left(\frac{\partial T_g}{\partial U_s}\right)_{P_s}$$

are the standard phasic derivatives for the vapor phase. Equations (146) through (148) give all the desired gaseous temperature derivatives. The interface temperature derivatives are obtained from Clapeyron's equation and the known P_s derivatives, i.e.,

$$\left(\frac{\partial T_I}{\partial P}\right)_{U_g,X_n} = \frac{dT_I}{dP_s}\left(\frac{\partial P_s}{\partial P}\right)_{U_s,X_n} \tag{149}$$

$$\left(\frac{\partial T_I}{\partial U_g}\right)_{P,X_n} = \frac{dT_I}{dP_s}\left(\frac{\partial P_s}{\partial U_g}\right)_{P,X_n} \tag{150}$$

$$\left(\frac{\partial T_I}{\partial X_n}\right)_{P,U_g} = \frac{dT_I}{dP_s}\left(\frac{\partial P_s}{\partial X_n}\right)_{P,U_g} \tag{151}$$

where dT_I/dP_s is given by the reciprocal of Equation (134).

The density derivatives can be obtained from $V_g = X_n V_n$ or $V_g = (1 - X_n)V_s$ as these two formulas for the gaseous specific volume are equivalent [see Equation (137)]. A symmetric formula can be obtained by eliminating X_n from the above two formulas giving

$$V_g = \frac{V_s V_n}{V_s + V_n} \quad . \tag{152}$$

Using Equation (152) we have for the ρ_g derivatives with respect to P

$$\left(\frac{\partial \rho_g}{\partial P}\right)_{U_g,X_n} = -\frac{1}{V_n^2}\left(\frac{\partial V_n}{\partial P}\right)_{U_g,X_n} - \frac{1}{V_s^2}\left(\frac{\partial V_s}{\partial P}\right)_{U_g,X_n} \quad . \tag{153}$$

Parallel formulas are obtained when U_g or X_n is the independent variable. The partial derivatives on the right side of Equation (153) are

obtained from formulas exactly parallel to those in Equations (146) through (148) with T_g replaced by V_s or V_n. When taking the derivatives of V_n remember that

$$V_n = \frac{R_n T_g(P_s, V_s)}{P - P_s} \quad . \tag{154}$$

Hence, an additional term appears in Equation (146) due to the direct dependence of V_n on P.

The homogeneous equilibrium sound speed for a noncondensible-steam-water mixture is derived in Reference 26.

The sound speed formula in Reference 26 is

$$a^2 = V^2 (P_s')^2 / \left(\left[-\hat{X}_n V_n P_s' \beta_n - \hat{X}_f V_f P_s' (\beta_f - P_s' \kappa_f) \right] \right.$$
$$+ \left\{ \hat{X}_s P_s' \left[\frac{C_{ps}}{T^s} + P_s' V_s (-2\beta_s + \kappa_s P_s') \right] + \hat{X}_n P_s' \left(\frac{C_{pn}}{T^s} + P_s' V_n \beta_n \right) \right.$$
$$\left. \left. + \hat{X}_f P_s' \left(\frac{C_{pf}}{T^s} - P_s' V_s \beta_s \right) \right\} \left(\frac{\partial T}{\partial P} \right)_{S, X_n} \right) \tag{155}$$

where

$$P_s' = \frac{dP^s}{dT} = \frac{h_s^s - h_f^s}{T^s (V_s^s - V_f^s)} \tag{156}$$

and

$$\left(\frac{\partial T}{\partial P} \right)_{S, X_n} = \left\{ 1 + \left[\hat{X}_n V_n \beta_n + X_f V_f \beta_f \right] / \left[\hat{X}_s \kappa_n (S_s - S_f) \right] \right\} /$$

$$\left(P_s' + \left(\frac{\kappa_s}{\kappa_n}\right)\left\{P_s' + \left(\frac{\beta_n - \beta_s}{\kappa_s}\right) + \left[(\hat{X}_n V_n \beta_n - \hat{X}_s V_s \beta_s) P_s' + (\hat{X}_n C_{pn} + \hat{X}_s C_{ps}\right.\right.\right.$$

$$\left.\left.\left. + \hat{X}_f C_{pf})/T^s\right]/[\hat{X}_s \kappa_s (S_s - S_f)]\right\}\right). \qquad (157)$$

In the above formulas, $\hat{X}_s$, $\hat{X}_n$, and $\hat{X}_f$ are mass qualities based on the total mixture mass.

Evaluation of the sound speed formulas at the saturated equilibrium state requires a second iteration. To avoid this extra iteration the sound speed formulas were evaluated using the nonequilibrium state properties.

The liquid properties and derivatives are obtained as above for Case 1. To obtain the gaseous properties, Equations (140) and (141) must be solved iteratively. A standard Newton iteration in two variables is used. The iteration variables are P_s and U_s. The steam table Subroutine STH2X6 is called once during each iteration to obtain all the needed steam vapor properties and Equations (138) and (139) are used to obtain the air properties. To save calculation time only an approximate Jacobian is used inside the iteration loop. From Equation (141), it is clear that if the steam behaves as an ideal gas i.e., $R_s = (V_s P_s/T_g)$ is constant, then Equation (141) is a simple linear equation determining P_s directly in terms of P and X_n. It simplifies the iteration if we neglect the derivatives of R_s in the Jacobian. This makes the Jacobian matrix equal the left side matrix in Equation (142) with TERM1 and TERM2 terms absent. This iteration has been tested with P_s ranging from 2000 Pa to P and has always converged. The iteration is terminated when $|\Delta P_s|/P$ and $|\Delta V_s|/V_g$ are both <0.0005. Hand calculations have been performed to compare both the properties and derivatives with the code calculations. In all cases the scheme converged in 4 iterations or less.

Once the iteration has converged the gaseous properties are determined from the formulas in this section. In the evaluation of all these derivatives the full matrix in Equation (142) is used including TERM1 and TERM2.

3.1.3 Constitutive Models

The constitutive relations include models for defining flow regimes and flow regime related models for interphase drag, wall friction, heat transfer, interphase heat and mass transfer and reflood heat transfer.

3.1.3.1 Flow Regime Maps. In RELAP5 the constitutive relations include flow regime effects for which simplified mapping techniques have been developed to control the use of constitutive relation correlations. The flow regime maps are based on the work of Taitel and Dukler[27,28] and Ishii.[29-31]

Taitel and Dukler have simplified flow regime classification and developed semi-empirical relations to describe flow regime transitions. However, some of their transition criteria are quite complex and further simplification has been carried out in order to efficiently apply these criteria in RELAP5. In addition, post-CHF regimes as suggested by Ishii[29] are included.

Three flow regime maps are utilized. They are vertical and horizontal maps for flow in pipes, and a high mixing map for flow in pumps.

3.1.3.1.1 Vertical Flow Regime Map--The vertical flow regime map is modeled as seven regimes, three of which are for pre-CHF heat transfer, three of which are for post-CHF heat transfer, and one of which is for vertical stratification. For pre-CHF heat transfer, the regimes modeled are the bubbly, slug, and annular mist regimes. Formulations for these three regimes were utilized by Vince and Lahey[32] to analyze their data. For post-CHF heat transfer, the bubbly, slug, and annular mist regimes are transformed to the inverted annular, inverted slug, and mist regimes, respectively, as suggested by Ishii.[29] Unheated components are also

modeled utilizing the pre-CHF map. A schematic representing the pre- and post-CHF regimes of the vertical flow regime map is shown in Figure 5. The vertically stratified regime may exist at low flow conditions and a schematic showing its relationship in the vertical flow regime map is given in Figure 6. The criteria for defining the boundaries for transition from one regime to another are given by the following correlations.

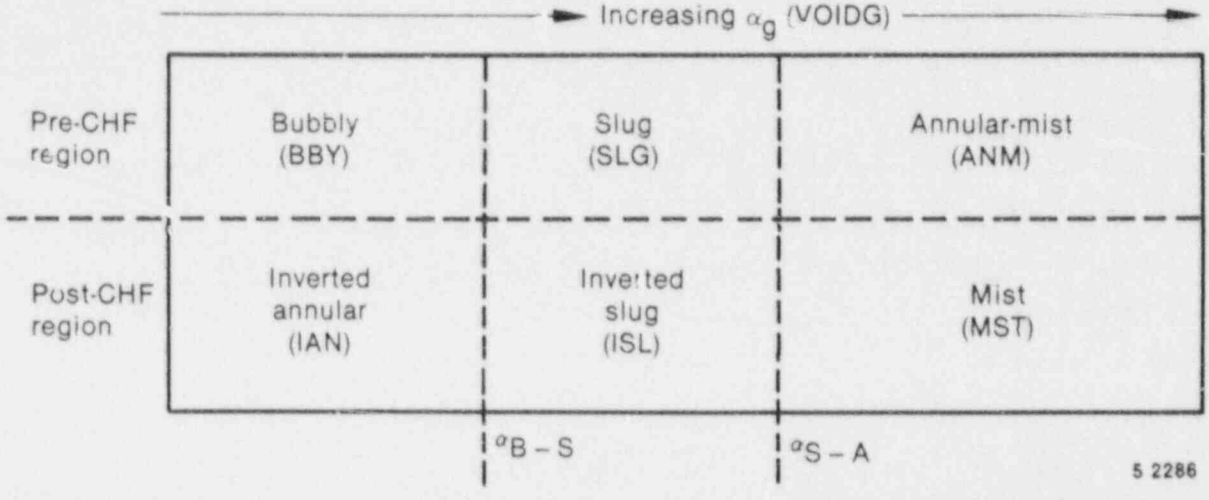

Figure 5. Sketch of vertical flow regime map.

For the bubbly to slug transition, Taitel and Dukler[27,28] suggested that bubbly flow may not exist in tubes of small diameter where the rise velocity of small bubbles exceeds that of Taylor bubbles. The small bubble rise velocity is given by the correlation[28]

$$V_{sb} = 1.53\left[g(\rho_f - \rho_g)\sigma\rho_f^2\right]^{1/4} \tag{158}$$

and the Taylor bubble rise velocity is given by the correlation[11]

$$V_{Tb} = 0.35[gD(\rho_f - \rho_g)\rho_f]^{1/2} . \tag{159}$$

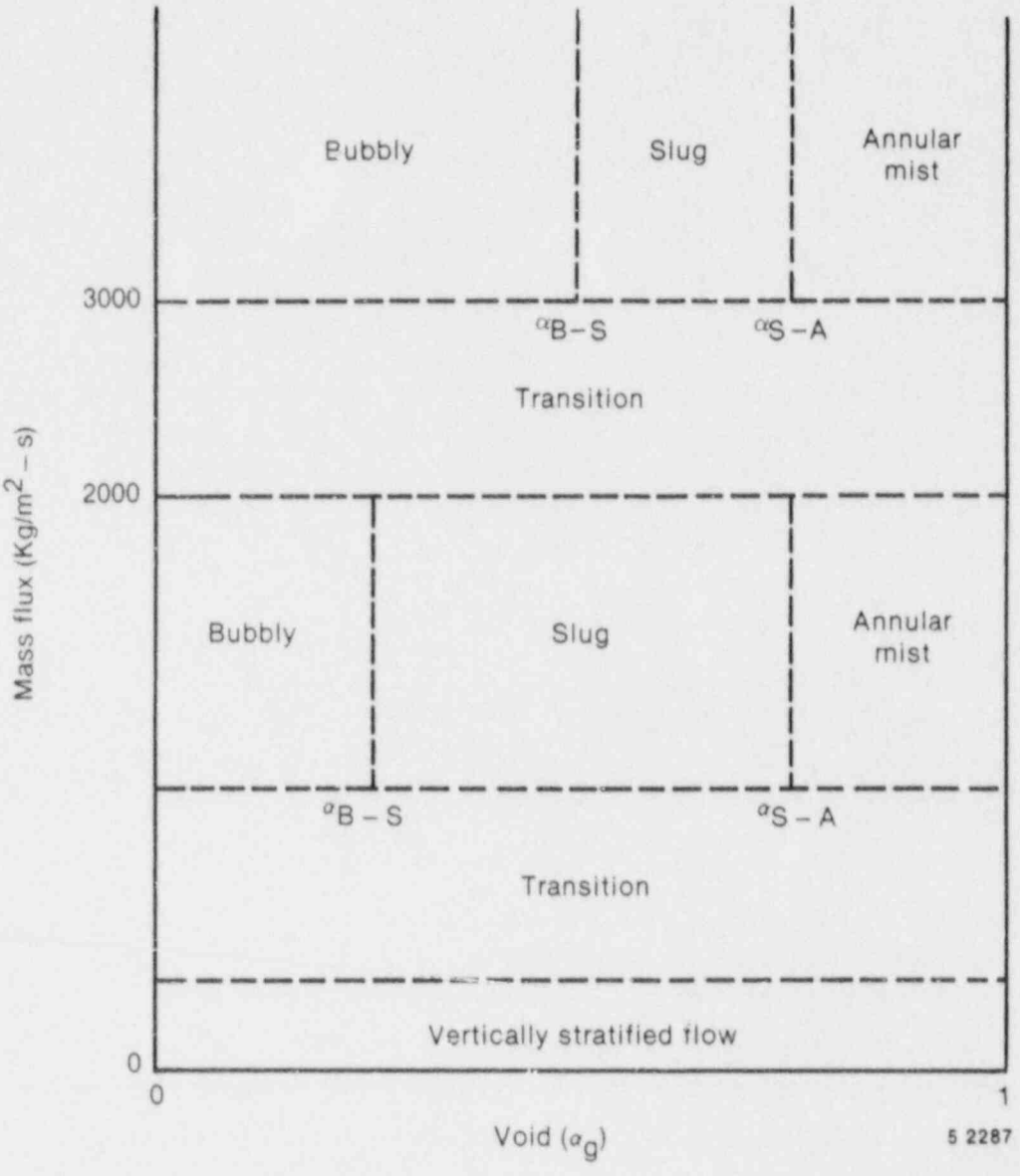

Figure 6. Vertical flow regime map including the vertically stratified regime.

(Note: in Reference 28, $\rho_f - \rho_g$ is approximated as ρ_f, see also References 30 and 33). Accordingly, the limiting tube diameter allowing the presence of bubbly flow is

$$D^* \geq 19 \quad , \tag{160}$$

where D^* is the dimensionless tube diameter,

$$D^* = D[g(\rho_f - \rho_g) \ \sigma]^{1/2} \quad . \tag{161}$$

Equation (159) is the dimensionless ratio of tube diameter to film thickness times the Deryagin number, where the Deryagin number is the ratio of film thickness to capillary length. Also, in the limit, as the fluid properties approach the thermodynamic critical pressure, $D^* = D$.

For tubes with diameters satisfying the condition of Equation (160), the bubble-slug transition occurs at a void fraction $\alpha_g = 0.25$ for low mass fluxes of $G \leq 2000$ kg/m^{2}s. By combining this void criterion with Equation (160) the bubble-slug transition criterion can be defined such that

$$\alpha_L = 0.25 \ \text{MIN} \ [1.0, \ (D^*/19)^8] \quad . \tag{162}$$

Hence, if the local void fraction, α_g^v, exceeds the criterion of Equation (162) then bubbly flow cannot exist since the rise velocity of small bubbles exceeds that of Taylor bubbles. The exponential power of 8 is used to provide a smooth variation of α_L as D^* decreases.

At high mass fluxes of $G \geq 3000$ kg/m^{2}s, bubbly flow with finely-dispersed bubbles can exist up to a void fraction, α_g, of 0.5. Then, if the criterion is linearly interpolated between the upper and lower void limits, the bubbly-slug transition criterion can be written as

$$\alpha_{B\text{-}S} = \alpha_L \tag{163}$$

for mass fluxes of $G \leq 2000$ kg/m^{2}s,

$$\alpha_{B-S} = \alpha_L + 0.001\,(G - 2000)\,(0.5 - \alpha_L) \tag{164}$$

for mass fluxes of $2000 < G < 3000$ kg/m^{2}s and

$$\alpha_{B-S} = 0.5 \tag{165}$$

for mass fluxes of $G \leq 3000$ kg/m^{2}s. The flow regime can therefore be said to be in the bubbly regime if $\alpha_g < \alpha_{B-S}$ and in the slug regime if $\alpha_g \leq \alpha_{B-S}$.

The bubble-slug transition defined by Equations (163) to (165) is similar to that given by Taitel and Dukler,[28] except that their void fraction relation is converted into a form based on liquid and vapor superficial velocities and finely dispersed bubbles are also distinguished from ordinary bubbles.

For the slug to annular flow transition, Taitel and Dukler[28] developed a criterion based on the critical vapor velocity required to suspend a liquid droplet. The critical velocity, u_c, is written as

$$u_c = 3.1[\sigma g(\rho_f - \rho_g)]^{1/4} \Big/ \rho_g^{1/2} = (\alpha_g v_g)_c \,. \tag{166}$$

The value 3.1 for the numerical coefficient is somewhat larger than the value of 1.4 reported by Wallis[34] but is a better fit to the data reported by Vince and Lahey.[32] In comparing RELAP5 code results to data, however, the coefficient value of 1.4 gives better results. The void fraction must also be >0.75 in order to get good comparisons between code results and data. Hence, solving Equation (166) for void fraction and imposing a lower void limit of 0.75 yields the slug to annular transition criterion for which

$$\alpha_{S-A} = \text{MAX}\left\{0.75,\ 1.4[\sigma g(\rho_f - \rho_g)]^{1/4} \Big/ (v_g\, \rho_g^{1/2})\right\} \tag{167}$$

where the flow regime is said to be in the slug regime if $\alpha_g \leq \alpha_{S-A}$ and in the annular-mist regime if $\alpha_g > \alpha_{S-A}$.

For post-CHF heat transfer the same formulations are used to define the inverted flow regime transition criteria in that Equations (163) through (165) also define the inverted annular to inverted slug regime transition and Equation (167) defines the inverted slug to mist regime transition.

At low mass fluxes the possibility exists for vertically stratified conditions. In RELAP5 vertical flow in a volume cell is considered to be stratified if the difference in void fraction of the volumes above and below is >0.5 and if the magnitude of the volume average mixture mass flux is less than the Taylor bubble rise velocity mass flux. The Taylor bubble criterion is based on the Taylor bubble velocity given by Equation (158) such that

$$|G| < \rho v_{Tb} \tag{168}$$

where v_{Tb} is the Taylor bubble velocity and

$$|G| = |\alpha_g \rho_g v_g + \alpha_f \rho_f v_f| \quad . \tag{169}$$

Hence, if Equation (168) is true, then transition to vertical stratification exists and if Equation (168) is false, then transition to vertical stratification does not exist.

3.1.3.1.2 Horizontal Flow Regime Map--The horizontal flow regime map is similar to the vertical flow regime map except that the post-CHF regimes are not included and a horizontal stratification regime is modeled that replaces the vertical stratification regime. The horizontal flow regime map therefore consists of horizontally stratified, bubbly, slug and annular mist regimes. The criteria for the bubbly to slug and the slug to annular mist regimes are also similar to those for the vertical map except that the bubbly to slug transition criterion is a constant

$$\alpha_{B\text{-}S} = \alpha_L = 0.25 \tag{170}$$

and the slug to annular mist transition criterion is a constant

$$\alpha_{S\text{-}A} = 0.8 \quad . \tag{171}$$

The criterion defining the horizontally stratified regime is one developed by Taitel and Dukler.[27]

According to Taitel and Dukler, the flow field is horizontally stratified if the vapor velocity satisfies the condition that

$$v_g < v_{gL} \tag{172}$$

where

$$v_{gL} = \frac{1}{2}\left[\frac{(\rho_f - \rho_g) g \alpha A}{\rho_g D \sin\theta}\right]^{1/2} (1 - \cos\theta) \quad . \tag{173}$$

The angle θ is related to the liquid level, $\ell\ell$, and the void fraction, α_g, by the relationships

$$\ell\ell = D\,(1 + \cos\theta)/2 \tag{174}$$

and

$$\alpha_g \pi = \theta - \sin\theta \cos\theta \quad . \tag{175}$$

If the horizontal stratification condition of Equation (172) is met, then the flow field undergoes a transition to horizontally stratified. If the condition of Equation (172) is not met, then the flow field undergoes a transition to the bubbly, slug, or annular mist flow regime.

3.1.3.1.3 High Mixing Flow Regime Map--The high mixing flow regime map is based on vapor void fraction, α_g, and consists of a bubbly regime for $\alpha_g \leq 0.5$, a mist regime for $\alpha_g \geq 0.95$, and a transition regime for $0.5 < \alpha_g < 0.95$. The transition regime is modeled as a mixture of bubbles dispersed in liquid and droplets dispersed in vapor.

3.1.3.2 Interphase Drag. The interphase drag force per unit volume expressed in terms of relative phasic velocity is

$$FI_{gf} = - f_{gf} \left| v_g - v_f \right| (v_g - v_f) \tag{176}$$

with

$$f_{gf} = \frac{1}{8} \rho_c S_F a_{gf} C_D \tag{177}$$

where

ρ_c = density of the continuous phase

C_D = drag coefficient

a_{gf} = interfacial area per unit volume

S_F = shape factor.

The shape factor 30, S_F, is assumed to be unity (1.0). The evaluation of a_{gf} and C_D for different flow regimes is covered in the following discussion.

3.1.3.2.1 Dispersed Flow--The bubbly and mist flow regimes are both considered as dispersed flow. According to Wallis[34] and Shapiro,[35] the dispersed bubbles or droplets can be assumed to be spherical particles with a size distribution of the Nukiyama-Tanasawa form. The Nukiyama-Tanasawa distribution function in nondimensional form is

$$p^* = 4d^{*2}\, e^{-2d^*} \tag{178}$$

where $d^* = d/d'$; d' is the most probable particle diameter, and p^* is the probability of particles with nondimensional diameter of d^*. With this distribution, it can be shown that the average particle diameter $d_o = 1.5\, d'$, and the surface area per unit volume is

$$a_{gf} = \frac{6\bar{\alpha}}{d'} \frac{\int d^{*2}\, p^*\, dd^*}{\int d^{*3}\, p^*\, dd^*} = \frac{2.4\bar{\alpha}}{d'} \tag{179}$$

where $\bar{\alpha} = \alpha_g$ for bubbles and $\bar{\alpha} = \alpha_f$ for droplets. In terms of the average diameter, d_o, the interfacial area per unit volume, a_{gf}, is

$$a_{gf} = 3.6\bar{\alpha}/d_o \quad . \tag{180}$$

The average diameter d_o is obtained by assuming that $d_o = 1/2\, d_{max}$. The maximum diameter, d_{max}, is related to the critical Weber number, We, by

$$We = d_{max}\, \rho_c\, (v_g - v_f)^2/\alpha \quad . \tag{181}$$

The values for We are presently taken as We = 10 for bubbles and We = 3.0 for droplets.

The drag coefficient is given by Ishii and Chawla[30] for the viscous regime as

$$C_D = 24(1 + 0.1\, Re_p^{0.75})/\, Re_p \tag{182}$$

where the particle Reynolds number Re_p is defined as

$$Re_p = \left| v_g - v_f \right| d_o \rho_c / \mu_m \quad . \tag{183}$$

The mixture viscosity, μ_m, is $\mu_m = \mu_f / \alpha_f$ for bubbles and $\mu_m = \mu_g / (\alpha_g)^{2.5}$ for droplets.

3.1.3.2.2 Slug Flow--Slug flow is modeled as a series of Taylor bubbles separated by liquid slugs containing small bubbles. A sketch of a slug flow pattern is shown in Figure 7. The Taylor bubble has a diameter nearly equal to the pipe diameter and a length varying from one to one hundred pipe diameters.

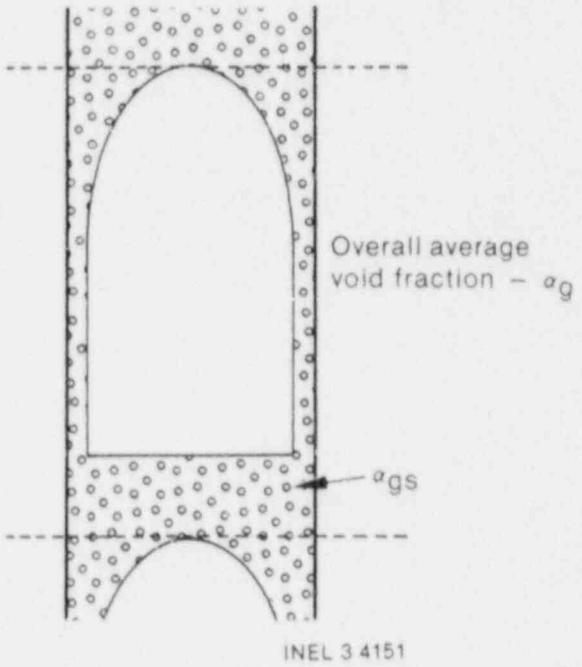

Figure 7. Slug-flow pattern.

Let α_{gs} be the average void fraction in the liquid film and slug region. The void fraction of a single Taylor bubble, α_b, in the total mixture is then

$$\alpha_b = (\alpha_g - \alpha_{gs}) / (1 - \alpha_{gs}) \quad . \tag{184}$$

By approximating the ratio of the Taylor bubble diameter to the tube diameter and the diameter to length ratio of a Taylor bubble, Ishii and Mishima[31] obtained the surface to volume ratio of a Taylor bubble as 4.5/D. Consequently, the interfacial area per unit volume, a_{gf}, for slug flow is

$$a_{gf} = (4.5\ C_t/D)\alpha_b + (3.6\ \alpha_{gs}/d_o)(1 - \alpha_b) \quad (185)$$

where C_t is a roughness parameter that is introduced to account for irregularities in the surface of large Taylor bubbles. At the present time, C_t is assumed to be unity (1.0).

To provide a smooth transition into and out of slug flow, α_{gs}, in Equation (184), is considered as a free parameter varying from α_{B-S} at the bubbly to slug flow regime transition to nearly zero at the slug to annular mist flow regime transition. The variation is represented by the exponential expression

$$\alpha_{gs} = \alpha_{B-S} \exp[-10(\alpha_g - \alpha_{B-S})/(\alpha_{S-A} - \alpha_{B-S})] \ . \quad (186)$$

The drag coefficient for Taylor bubbles is given by Ishii and Chawla[30] as

$$C_D = 9.8\ (1 - \alpha_b)^3 \quad (187)$$

where α_b is given by combining Equations (184) and (186).

3.1.3.2.3 Annular Mist Flow--Annular mist flow is characterized by a liquid film along the wall and a vapor core containing entrained liquid droplets. Let α_{ff} be the average liquid volume fraction of the liquid film along the wall. Then, from simple geometric considerations, the interfacial area per unit volume can be shown to be

$$a_{gf} = (4C_{an}/D)(1 - \alpha_{ff})^{1/2} + (3.6\alpha_{fd}/d_o)(1 - \alpha_{ff}) \quad (188)$$

where C_{an} is a roughness parameter introduced to account for waves in the liquid wall film and α_{fd} is the average liquid volume fraction in the vapor core, for which

$$\alpha_{fd} = (\alpha_f - \alpha_{ff})/(1 - \alpha_{ff}) \quad . \tag{189}$$

A simple relation based on the flow regime transition criterion and liquid Reynolds number is used to correlate the average liquid film volume fraction. For vertical flow regimes, the entrainment relation is

$$\alpha_{ff} = \alpha_f C_f \exp\left[-7.5 \times 10^{-5} (\alpha_g v_g / u_c)^6\right] \tag{190}$$

where u_c is the entrainment critical velocity given by Equation (166) with the coefficient 3.1 replaced by 1.4. For horizontal flow regimes, the entrainment relation is

$$\alpha_{ff} = \alpha_f C_f \exp\left[-4.0 \times 10^{-5} (v_g / v_{gL})^6\right] \tag{191}$$

where v_{gL} is the horizontal stratification critical velocity given by Equation (173). The term C_f is expressed as

$$C_f = 10^{-4} \rho_f \alpha_f v_f \frac{D}{\mu_f} \quad .$$

The interfacial friction factor, f_i, for the liquid film takes the place of C_D in Equation (177), and is described by a correlation obtained by Bharathan et al.[36] for which

$$f_i = 4\left[0.005 + A(\delta^*)^B\right] \tag{192}$$

where

$$\log_{10} A = -0.56 + 9.07/D^* \quad (193)$$

$$B = 1.63 + 4.74/D^* \quad (194)$$

$$\delta^* = \delta\left[\frac{(\rho_f - \rho_g)g}{\sigma}\right]^{1/2} . \quad (195)$$

The term δ^* is the liquid wall film Deryagin number for which δ is the film thickness, and D^* is the dimensionless diameter given by Equation (162).

3.1.3.2.4 Vertical Stratified Flow--For vertically stratified flow the previously discussed interphase drag relationships are applied except that a low interphase drag coefficient of 0.1 N-s^2/m^5 is imposed for the junction above the vertically stratified volume.

3.1.3.2.5 Horizontal Stratified Flow--By simple geometric consideration, one can show that the interfacial area per unit volume is

$$a_{gf} = 4C_{st} \sin\theta \, (\pi D) \quad (196)$$

where C_{st} is a roughness parameter introduced to account for surface waves and is set to 1 at the present time.

The interface Reynolds number is defined with the vapor properties and regarding liquid as the continuous phase for which

$$Re_i = D_i \rho_g \left| v_g - v_f \right| \mu_g \quad (197)$$

where the equivalent wetted diameter, D_i, for the interface is

$$D_i = \alpha\pi D/(\theta + \sin\theta) . \quad (198)$$

The interfacial friction factor, f_i, replaces C_D in Equation (177) and is obtained by assuming typical friction factor relationships for which

$$f_i = 64/Re_i \tag{199}$$

for laminar flow, where $Re_i \leq 1187$

$$f_i = 0.3164/Re_i^{0.25} \tag{200}$$

for turbulent flow, where $Re_i \geq 4000$ and

$$f_i = 0.0539 \tag{201}$$

for the laminar to turbulent transition where $1187 < Re_i < 4000$.

3.1.3.2.6 Inverted Flow Regimes--The interphase drag relationships for post-CHF inverted flow regimes are treated in a similar fashion to the corresponding pre-CHF flow regimes except that the roles of vapor and liquid are interchanged.

3.1.3.3 Wall Friction. In RELAP5, the wall friction force terms include only wall shear effects. Losses due to abrupt area change are calculated using mechanistic form loss models. Other losses due to elbows or complicated flow passage geometry are modeled using energy loss coefficients that must be input by the user.

In the development of the RELAP5/MOD2 wall friction model, emphasis was placed on obtaining reasonable values for wall friction in all flow regimes. The flow regime models are discussed in the previous Section 3.1.3.1.

The wall friction model is based on a two-phase multiplier approach in which the two-phase multiplier is calculated from the Heat Transfer and Fluid Flow Service (HTFS) modified BAROCZY correlation.[37] The individual

phasic wall friction components are calculated by apportioning the two-phase friction between the phases using a technique derived from the Lockhart-Martinelli[38] model. The model is based on the assumption that the frictional pressure drop may be calculated using a quasi-steady form of the momentum equation.

3.1.3.3.1 The Two-Phase Friction Multiplier Approach--The overall friction pressure drop can be expressed in terms of the liquid-alone wall friction pressure drop

$$\left(\frac{\partial P}{\partial x}\right)_{2\phi} = \phi_f^2 \left(\frac{\partial P}{\partial x}\right)_f \tag{202}$$

or the vapor-alone wall friction pressure drop

$$\left(\frac{\partial P}{\partial x}\right)_{2\phi} = \phi_g^2 \left(\frac{\partial P}{\partial x}\right)_g \tag{203}$$

where ϕ_f and ϕ_g are the liquid-alone and vapor-alone two-phase friction multipliers, respectively. The phasic wall friction pressure gradients are expressed as

$$\left(\frac{\partial P}{\partial x}\right)_f = \frac{\lambda_f' M_f^2}{2D\rho_f A^2} \tag{204}$$

for the liquid-alone, and

$$\left(\frac{\partial P}{\partial x}\right)_g = \frac{\lambda_g' M_g^2}{2D\rho_g A^2} \tag{205}$$

for the vapor-alone, where the prime indicates the liquid and vapor-alone friction factors, respectively, calculated at the respective Reynold's numbers

$$Re'_f = \frac{\alpha_f \rho_f |v_f| D}{\mu_f} \tag{206}$$

and

$$Re'_g = \frac{\alpha_g \rho_g |v_g| D}{\mu_g} \quad . \tag{207}$$

The liquid and vapor mass flow rates, respectively, are defined as

$$M_f = \alpha_f \rho_f v_f A \tag{208}$$

and

$$M_g = \alpha_g \rho_g v_g A \quad . \tag{209}$$

Throughout the current literature the overall two-phase friction pressure gradient is calculated using two-phase friction multiplier correlations. However, regardless of the correlation used, the multipliers may be interrelated using Equations (202) through (205) and the Lockhart-Martinelli[38] ratio defined as

$$X \equiv \frac{\left(\frac{dP}{dx}\right)_f}{\left(\frac{dP}{dx}\right)_g} = \frac{\phi_g^2}{\phi_f^2} \quad . \tag{210}$$

In RELAP5 these equations are used to apportion the overall wall friction into liquid and vapor wall friction coefficients.

3.1.3.3.2 Flow Regime Effects--Two-phase friction can be modeled in terms of two-phase friction multipliers and known friction factors using the method developed by Lockhart-Martinelli.[38] Chisholm[38] also developed a theoretical basis for the Lockhart-Martinelli model that provides a rationale for relating the equations to empirical results.

From the theoretical basis developed by Chisholm, irrespective of flow regime, the quasi-steady phasic momentum equations can be expressed in scaler form as

$$\alpha_f A(\frac{\partial P}{\partial x})_{2\phi} - \tau_f p_f + S_{FI} = 0 \tag{211}$$

for the liquid, and

$$\alpha_g A(\frac{\partial P}{\partial x})_{2\phi} - \tau_g p_g - S_{FI} = 0 \tag{212}$$

for the vapor, where τ_f and τ_g are the liquid and vapor wall shear stresses, respectively, p_f and p_g are the liquid and vapor wetted wall perimeter, respectively and S_{FI} is a stress gradient due to interphase friction. These equations can be expressed in terms of Darcy friction factors and simplified so that

$$(\frac{dP}{dx})_{2\phi}(1 + S_R \frac{\alpha_g}{\alpha_f}) = \frac{\lambda_f \rho_f v_f^2}{2D} (\frac{\alpha_{fw}}{\alpha_f}) \tag{213}$$

for the liquid, and

$$(\frac{dP}{dx})_{2\phi}(1 - S_R) = \frac{\lambda_g \rho_g v_g^2}{2D} (\frac{\alpha_{gw}}{\alpha_g}) \tag{214}$$

for the vapor, where the interphase friction term, S_R, is defined as

$$S_R = \frac{S_{FI}}{\alpha_g A(\frac{\partial P}{\partial x})_{2\phi}} \quad . \tag{215}$$

The terms α_{fw} and α_{gw} are the liquid and vapor volume fractions, respectively, at the wall, and α_f and α_g are the overall liquid and vapor volume fractions, respectively. Taking the ratio of Equation (213) to (214) gives

$$Z^2 = \frac{\lambda_f \rho_f v_f^2 (\frac{\alpha_{fw}}{\alpha_f})}{\lambda_g \rho_g v_g^2 (\frac{\alpha_{gw}}{\alpha_g})} = \frac{1 + S_R \frac{\alpha_g}{\alpha_f}}{(1 - S_R)} \quad . \tag{216}$$

Consider the pure liquid case where $\alpha_g = 0$ and $\alpha_{fw} = \alpha_f$ and for which Equation (213) reduces to

$$(\frac{\partial P}{\partial x})_{2\phi} = (\frac{\partial P}{\partial x})_f = \frac{\lambda_f \rho_f v_f^2}{2D} \quad . \tag{217}$$

For this case, the friction factor, λ_f, can be precisely calculated based on a Reynolds number expressed in terms of D. Similarly, for the two-phase case, liquid and vapor friction factors can be calculated based on Reynolds number of

$$R_f = \frac{\rho_f (\frac{\alpha_f}{\alpha_{fw}}) D | v_f |}{\mu_f} \quad , \quad R_g = \frac{\rho_g (\frac{\alpha_g}{\alpha_{gw}}) D | v_g |}{\mu_g} \tag{218}$$

for the liquid and vapor, respectively. These terms have the property that as one phase or the other disappears the friction factors calculated reduce to their single-phase formulations.

Equations (213) and (214) can be rewritten as

$$(\frac{dP}{dx})_{2\phi} \frac{Z^2}{\alpha_g + \alpha_f Z^2} = \frac{\lambda_f \rho_f v_f^2}{2D} (\frac{\alpha_{fw}}{\alpha_f}) \tag{219}$$

$$\left(\frac{dP}{dx}\right)_{2\phi} \frac{1^2}{\alpha_g + \alpha_f Z^2} = \frac{\lambda_g \rho_g v_g^2}{2D}\left(\frac{\alpha_{gw}}{\alpha_g}\right) \tag{220}$$

for the liquid and vapor, respectively. However, these equations are now flow regime dependent since knowledge of the wetted wall and overall void fractions is required in order to calculate the friction factors. The term Z^2 can also be considered as a correlating factor relating the overall two-phase friction pressure gradient to the known phasic friction factors.

The quasi-steady phasic momentum equations similar to Equations (219) and (220) can also be written in terms of the RELAP5 friction coefficient, where

$$\alpha_f\left(\frac{dP}{dx}\right)_{2\phi} \frac{Z^2}{\alpha_g + \alpha_f Z^2} = FWF(\alpha_f \rho_f v_f) \tag{221}$$

for the liquid, and

$$\alpha_g\left(\frac{dP}{dx}\right)_{2\phi} \frac{1}{\alpha_g + \alpha_f Z^2} = FWG(\alpha_g \rho_g v_g) \tag{222}$$

for the vapor. Taking the sum of these two equations gives the overall quasi-steady two-phase pressure gradient as

$$\left(\frac{dP}{dx}\right)_{2\phi} = FWF(\alpha_f \rho_f v_f) + FWG(\alpha_g \rho_g v_g) \quad . \tag{223}$$

It should be noted that the calculation of the phasic friction factors using the Reynolds numbers given by Equation (218) and the assumption that two-phase flows behave similarly to single-phase flows in the laminar, transition, and turbulent regimes provides the rationale relating Equations (219) and (220) to empirical data. It is this same rationale that allows expressing the correlating term, Z^2, in terms of friction

factors that are independent of interphase friction as given by Equation (216). It is this equation that forms the basis for apportioning the overall two-phase wall friction between the phases.

3.1.3.3.3 Apportioning Wall Friction--Overall two-phase wall friction can be apportioned into phasic components by combining Equations (221) and (222) with Equations (202) through (205) and (216), (219), and (220) which results in

$$\phi_f^2 \frac{\lambda'_f \rho_f (\alpha_f v_f)^2}{2D} \quad \frac{\alpha_{fw} \lambda_f \rho_f v_f^2}{\alpha_{gw} \lambda_g \rho_g v_g^2 + \alpha_{fw} \lambda_f \rho_f v_f^2} = FWF(\alpha_f \rho_f v_f) \tag{224}$$

for the liquid, and

$$\phi_g^2 \frac{\lambda'_g \rho_g (\alpha_g v_g)^2}{2D} \quad \frac{\alpha_{gw} \lambda_g \rho_g v_g^2}{\alpha_{gw} \lambda_g \rho_g v_g^2 + \alpha_{fw} \lambda_f \rho_f v_f^2} = FWG(\alpha_g \rho_g v_g) \tag{225}$$

for the vapor, where the two-phase multiplier terms are calculated using a two-phase friction multiplier correlation. Flow regime effects are also included in the relationships between wetted wall and overall void fractions and their effect in calculating the friction factor terms.

3.1.3.3.4 The H.T.F.S. Two-Phase Friction Multiplier Correlation--In RELAP5 only the H.T.F.S. correlation[37] is used to calculate two-phase friction multipliers. This correlation was chosen because it is correlated to empirical data over very broad ranges of phasic volume fractions, phasic flowrates and flow regimes. The correlation has also been shown to give good agreement with empirical data.

The H.T.F.S. correlation for two-phase friction multiplier[38] is expressed as

$$\phi_f^2 = 1 + \frac{C}{X} + \frac{1}{X^2} \tag{226}$$

for the liquid-alone multiplier, or

$$\phi_g^2 = \chi^2 + C\chi + 1 \tag{227}$$

for the vapor-alone multiplier, where C is the correlation term and χ is the Lockhart-Martinelli ratio given by Equation (210). The correlation term is expressed in terms of scalar mass flux, G, and the Baroczy dimensionless property index, Λ, such that

$$2 \leq C = -2 + f_1(G)\, T_1 \tag{228}$$

where

$$f_1(G) = 28 - 0.3\ G \tag{229}$$

$$T_1 = EXP\left[- \frac{(\log_{10}\Lambda + 2.5)^2}{2.4 - G(10^{-4})} \right] \tag{230}$$

$$\Lambda = \frac{\rho_g}{\rho_f} \left(\frac{\mu_f}{\mu_g}\right)^{0.2} \tag{231}$$

$$G = \alpha_f \rho_f v_f + \alpha_g \rho_g v_g \quad . \tag{232}$$

The terms ρ, μ, α and v denote the density, viscosity, volume fraction and velocity, respectively.

If the H.T.F.S. correlation is combined with the wall friction formulations by combining Equations (202) through (205), (208) through (210), (226), and (227), then

$$\left(\frac{dP}{dx}\right)_{2\phi} = \phi_f^2 \left(\frac{dP}{dx}\right)_f = \phi_g^2 \left(\frac{dP}{dx}\right)_g$$

$$= \frac{1}{2D}\left[\lambda_f'\rho_f(\alpha_f v_f)^2 + C\sqrt{\lambda_f'\rho_f(\alpha_f v_f)^2\lambda_f'\rho_f(\alpha_g v_g)^2} + \lambda_g'\rho_g(\alpha_g v_g)^2\right] . \quad (233)$$

Equation (233) can then be combined with Equation (224) and (225) and simplified such that

$$FWF(\alpha_f\rho_f) = \alpha_{fw}\frac{\rho_f\lambda_f|v_f|}{2D}\left[\lambda_f'\rho_f(\alpha_f v_f)^2 + C\sqrt{\lambda_f'\rho_f(\alpha_f v_f)^2\lambda_g'\rho_g(\alpha_g v_g)^2}\right.$$
$$\left. + \lambda_g'\rho_g(\alpha_g v_g)^2\right] \Big/ \left[\alpha_{gw}\lambda_g\rho_g v_g^2 + \alpha_{fw}\lambda_f\rho_f v_f^2\right] \quad (234)$$

for the liquid, and

$$FWG(\alpha_g\rho_g) = \alpha_{gw}\frac{\rho_g\lambda_g|v_g|}{2D}\left[\lambda_f'\rho_f(\alpha_f v_f)^2 + C\sqrt{\lambda_f'\rho_f(\alpha_f v_f)^2\lambda_g'\rho_g(\alpha_g v_g)^2}\right.$$
$$\left. + \lambda_g'\rho_g(\alpha_g v_g)^2\right] \Big/ \left[\alpha_{gw}\lambda_g\rho_g v_g^2 + \alpha_{fw}\lambda_f\rho_f v_f^2\right] \quad (235)$$

for the vapor.

In RELAP5 the friction factor and velocity terms are calculated in such a manner that as the velocity terms disappear the equations give the correct limits. For example, the friction factor terms are evaluated such that

$$\lim_{|(\frac{\alpha_f}{\alpha_{fw}})v_f|\to 0}(\lambda_f|(\frac{\alpha_f}{\alpha_{fw}})v_f|) = \frac{64\mu_f}{D\rho_f} = \lim_{|\alpha_f v_f|\to 0}(\lambda_f'|\alpha_f v_f|)$$

$$\lim_{|(\frac{\alpha_g}{\alpha_{gw}})v_g|\to 0}(\lambda_g|(\frac{\alpha_g}{\alpha_{gw}})v_g|) = \frac{64\mu_g}{D\rho_g} = \lim_{|\alpha_g v_g|\to 0}(\lambda_g'|\alpha_g v_g|) \quad (236)$$

and the velocity terms are evaluated such that

$$\lim_{|v_f| \to 0} |v_f| = \varepsilon = \lim_{|v_g| \to 0} |v_g| \quad . \tag{237}$$

Hence, for stagnant flow or single-phase conditions, a positive and finite friction coefficient is always calculated. Thus, the numerical possibility of an infinite or negative friction coefficient is eliminated.

In Equations (234) and (235), flow regime effects are included in the terms (α_{fw}/α_f) and (α_{gw}/α_g) for the liquid and vapor, respectively. These terms are such that

$$\alpha_{fw} = 1 - \alpha_{gw} \tag{238}$$

$$\alpha_f = 1 - \alpha_g \quad . \tag{239}$$

Equations (236) and (239) are restricted such that as overall phasic volume fraction disappears its corresponding wall film volume fraction disappears so that

$$\lim_{\alpha_f \to 0} \left(\frac{\alpha_{fw}}{\alpha_f}\right) = 1, \quad \lim_{\alpha_f \to 0} \left(\frac{\alpha_{gw}}{\alpha_g}\right) = 1 \tag{240}$$

and similarly,

$$\lim_{\alpha_g \to 0} \left(\frac{\alpha_{gw}}{\alpha_g}\right) = 1, \quad \lim_{\alpha_g \to 0} \left(\frac{\alpha_{fw}}{\alpha_f}\right) = 1 \quad . \tag{241}$$

3.1.3.3.5 Flow Regime Factors for Phasic Wall Friction--Phasic wall friction is expressed in terms of wall shear stress, which in turn requires knowledge of the surface area wetted by each phase. From the flow regime model discussed in Section 3.1.3.1, expressions for the wall film

phasic volume fractions can be derived. Using these expressions, the phasic wall friction factors that appear in Equations (213) and (214) may then be computed.

In the flow regime map, seven flow regimes are modeled, which are; for pre-CHF heat transfer, the bubbly, slug, and annular mist; for post-CHF heat transfer, the inverted-annular, inverted-slug and mist; and for stratified flow, the vertically and horizontally stratified. For the transition regime between pre- and post-CHF heat transfer, an interpolation scheme is also implemented in the code.

To implement flow regime effects in the two-phase wall friction model, first consider the wall liquid and vapor volume fractions. These terms are

$$\frac{p_f}{p} = \alpha_{fw} \tag{242}$$

which represents the liquid volume fraction in the wall film, and

$$\frac{p_g}{p} = \alpha_{gw} \tag{243}$$

which represents the vapor volume fraction in the wall film where the terms p_f, p_g, and p are the perimeters wetted by the liquid, vapor, and mixture, respectively. Then, from the flow regime model these are formulated for all of the flow regimes as follows:

For the bubbly regime

$$\alpha_{fw} = \alpha_f \text{ and } \alpha_{gw} = \alpha_g \ , \tag{244}$$

where α_f, α_g are the overall liquid vapor volume fraction, respectively.

For the slug regime

$$\alpha_{fw} = 1 - \alpha_{gs} \text{ and } \alpha_{gw} = \alpha_{gs} \quad , \tag{245}$$

where α_{gs} is given by Equation (186). For the annular-mist regime

$$\alpha_{fw} = (\alpha_{ff})^{\frac{1}{4}} \text{ and } \alpha_{gw} = 1 - (\alpha_{ff})^{\frac{1}{4}} \quad , \tag{246}$$

where α_{ff} is given by Equation (191). For the inverted-annular regime

$$\alpha_{gw} = (\alpha_{gg})^{\frac{1}{4}} \text{ and } \alpha_{fw} = 1 - (\alpha_{gg})^{\frac{1}{4}} \quad , \tag{247}$$

where α_{gg} is the inverted form of Equation (191).

For the inverted-slug regime

$$\alpha_{fw} = \alpha_{fs} \text{ and } \alpha_{gw} = 1 - \alpha_{fs} \quad , \tag{248}$$

where α_{fs} is the inverted form of Equation (186). For the mist regime

$$\alpha_{fw} = \alpha_f \text{ and } \alpha_{gw} = \alpha_g \quad , \tag{249}$$

similar to the bubbly regime. For the vertically stratified regime

$$\alpha_{fw} = \alpha_f \text{ and } \alpha_{gw} = \alpha_g \quad . \tag{250}$$

For the horizontally stratified regime

$$\alpha_{fw} = 1 - \frac{\theta}{\pi} \text{ and } \alpha_{gw} = \frac{\theta}{\pi} \quad , \tag{251}$$

where θ results from the solution of Equations (174) and (175).

3.1.3.3.6 The Friction Factor Model--In RELAP5, the friction factor is computed using a high speed calculational scheme representing an engineering approximation to the Colebrook correlation.[39]

The friction factor model is simply an interpolation scheme linking the laminar, laminar-turbulent transition, and turbulent-full turbulent transition regimes. The laminar friction factor is calculated as

$$\lambda_L = \frac{64}{R}, \quad 0 \leqq R \leqq 2000 \tag{252}$$

where R is the Reynolds number. The laminar-turbulent friction factor is interpolated as

$$\lambda_{L,T} = [1.189 - (4000/R)0.25] (\lambda_{t,tt} - \lambda_{L,2000}) + \lambda_{L,2000}, \quad 2000 < R < 4000 \tag{253}$$

where $\lambda_{L,2000}$ is the laminar factor at a Reynolds number of 2000 and where $\lambda_{t,4000}$ is the turbulent friction factor at a Reynolds number of 4000. The interpolation factor is defined such that

$$0 \leqq (2 - 4000/R) \leqq 1 \quad . \tag{254}$$

The turbulent-full turbulent friction factor is interpolated as

$$\lambda_{t,tt} = \frac{\left[1 - \left(\frac{4000}{R}\right)^{0.25}\right]}{\left[1 - \left(\frac{4000}{R_c}\right)^{0.25}\right]} (\lambda_{tt} - \lambda_{t,4000}) + \lambda_{t,4000}, \quad 4000 \leqq R \leqq R_c \tag{255}$$

where the interpolation factor is defined such that

$$0 \leqq = \frac{\left[1 - \left(\frac{4000}{R}\right)^{0.25}\right]}{\left[1 - \left(\frac{4000}{R_c}\right)^{0.25}\right]} \leqq 1 \tag{256}$$

and R_c is the critical Reynolds number at which the Colebrook equation gives a constant friction factor of

$$\lambda_{tt} = [1.74 - 2\text{Log}_{10}(2\varepsilon/D)]^{-2} \tag{257}$$

and where ε is the surface roughness.

The critical Reynolds number is given as

$$R_c = \frac{378.3}{\lambda_{tt}} \left(\frac{2\varepsilon}{D}\right) \quad . \tag{258}$$

If precise values for $\lambda_{t,4000}$ are used, Equations (252) and (253) are identical to the formulations used in the Colebrook friction factor model for the laminar and transition regimes. Equation (257) is also identical to the solution of the Colebrook model for Reynolds numbers greater than the critical Reynolds number. Therefore, the interpolation scheme in the friction factor model lies in the formulation of Equation (255), which is linear in $(1/R)^{0.25}$. The maximum deviation between the friction factor calculated using Equation (255) and that calculated using the Colebrook correlation is within the third significant figure for a moderate ε/D of 0.0003, and as ε/D increases the deviation decreases until at an ε/D such that $R_c < 4000$ the value given by Equation (255) is precisely that of Equation (257). In any case, the results calculated using Equation (255) are negligibly different from those calculated by the Colebrook equation. This accuracy is achieved using a good estimate for $\lambda_{t,4000}$ given by

$$\lambda_{t,4000} \sim \lambda_o + K(\lambda_{tt} - \lambda_1) \tag{259}$$

where λ_o is a constant evaluated from the Blasius smooth pipe formula at a Reynolds number of 4000, such that

$$\lambda_o = 0.0398 \quad . \tag{260}$$

The coefficients have been evaluated as

$$K = 0.558, \quad \lambda_1 = 0.0158 \tag{261}$$

by the method of least squares.

In calculational schemes, it is desirable to evaluate the friction factor in terms of $\lambda|\psi v|$ so that the limiting terms will be correctly calculated as defined by Equations (236). For this case, the Reynolds number must be defined as

$$R = \frac{\rho D}{\mu} |\psi v| \tag{262}$$

and Equation (255) can be rewritten as

$$\lambda|\psi v| = \lambda_L^* + L(2 - R^*) \left\{ L[(1 - R^*)/(1 - R_c^*)] \right.$$

$$\left. (\lambda_{tt} - \lambda_{t,4000})|\psi v| + \lambda_{t,4000}|\psi v| - \lambda_L^* \right\} \tag{263}$$

where $L(y)$ denotes a general limit function such that

$$0 \leq L(y) \leq 1 \quad , \tag{264}$$

$$R^* = (4000/R)^{.25} \quad , \quad R_c^* = (4000/R_c)^{.25} \quad , \tag{265}$$

and

$$R \geq 2000 \quad , \quad R_c \geq 4000 \quad , \tag{266}$$

and where the laminar term is

$$\lambda_L^* = \frac{64\mu}{\rho D} \quad . \tag{267}$$

The accuracy of the improved friction factor model can be observed in Figure 8, which is a plot of results calculated by Equation (263) compared to similar results calculated by the Colebrook equation. Four curves are plotted for each model representing roughness to diameter ratios of $2\varepsilon/D = 0.0$, 0.0006, 0.02, and 0.1, respectively. Equation (263) results are plotted as dotted lines and labeled as INTERP in the plot legend. Colebrook equation results are plotted as solid lines and labeled as COLBRK in the plot legend. The axes of the plot are scaled logarithmically.

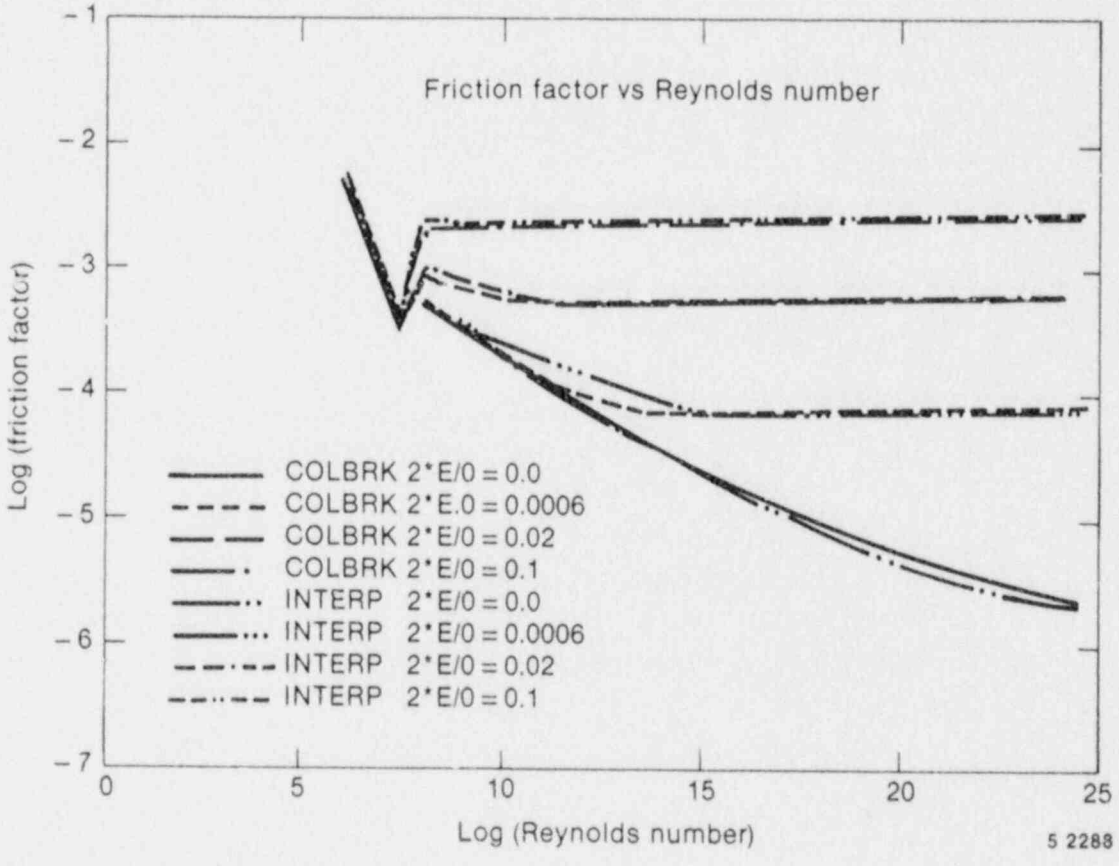

Figure 8. Comparison of firction factors for the Colebrook and the improved RELAP5 friction factor models.

3.1.3.4 Heat Transfer Models. A boiling curve is used in RELAP5 to govern the selection of heat transfer correlations. In particular, the heat transfer regimes modeled are classified as pre-CHF, CHF and post-CHF

regimes. Condensation heat transfer is also modeled and the effects of noncondensible gases are modeled. Figure 9 gives a chart of the logic scheme for selecting the heat transfer models.

The pre-CHF regime consists of models for single phase liquid convection, subcooled nucleate boiling, and saturated nucleate boiling. The model assumes that the wall is totally wetted by liquid and that the wall is not wetted by vapor. Therefore, the heat transfer from the wall to the vapor, Q_{wg}, is equal to zero. Heat transfer from the wall to the liquid, Q_{wf}, is given by the expression

$$Q_{wf} = h_{wf} A_{wf} (T_w - T_f)/V \tag{268}$$

where h_{wf} is the heat transfer coefficient, A_{wf} is the heat transfer area between the wall and liquid, and T_w and T_f are the wall and liquid temperatures, respectively. The heat transfer coefficients used for this regime are the Dittus-Boelter[40] and the Chen[41] correlations for the single-phase liquid convective heat transfer and the nucleate boiling regimes, respectively. It should be noted that the Chen correlation is also extended into the subcooled boiling regime by setting the Reynolds number factor to one.

The post-CHF regime consists of models for transition film boiling, film boiling, and single-phase vapor convection. A mechanistic model developed by Tong and Young[42] is adapted so that

$$Q_{wf} = h_{wf} A_w F_f (T_w - T_f)/V \tag{269}$$

$$Q_{wg} = h_{wg} A_w (1 - F_f) (T_w - T_g)/V \tag{270}$$

where A_w is the total wall heat transfer area and F_f is the fraction of wall surface contacted by the liquid. The heat transfer correlation and the liquid contact area correlation developed by Chen[43] are used in both the transition film boiling and the film boiling regime. For single-phase

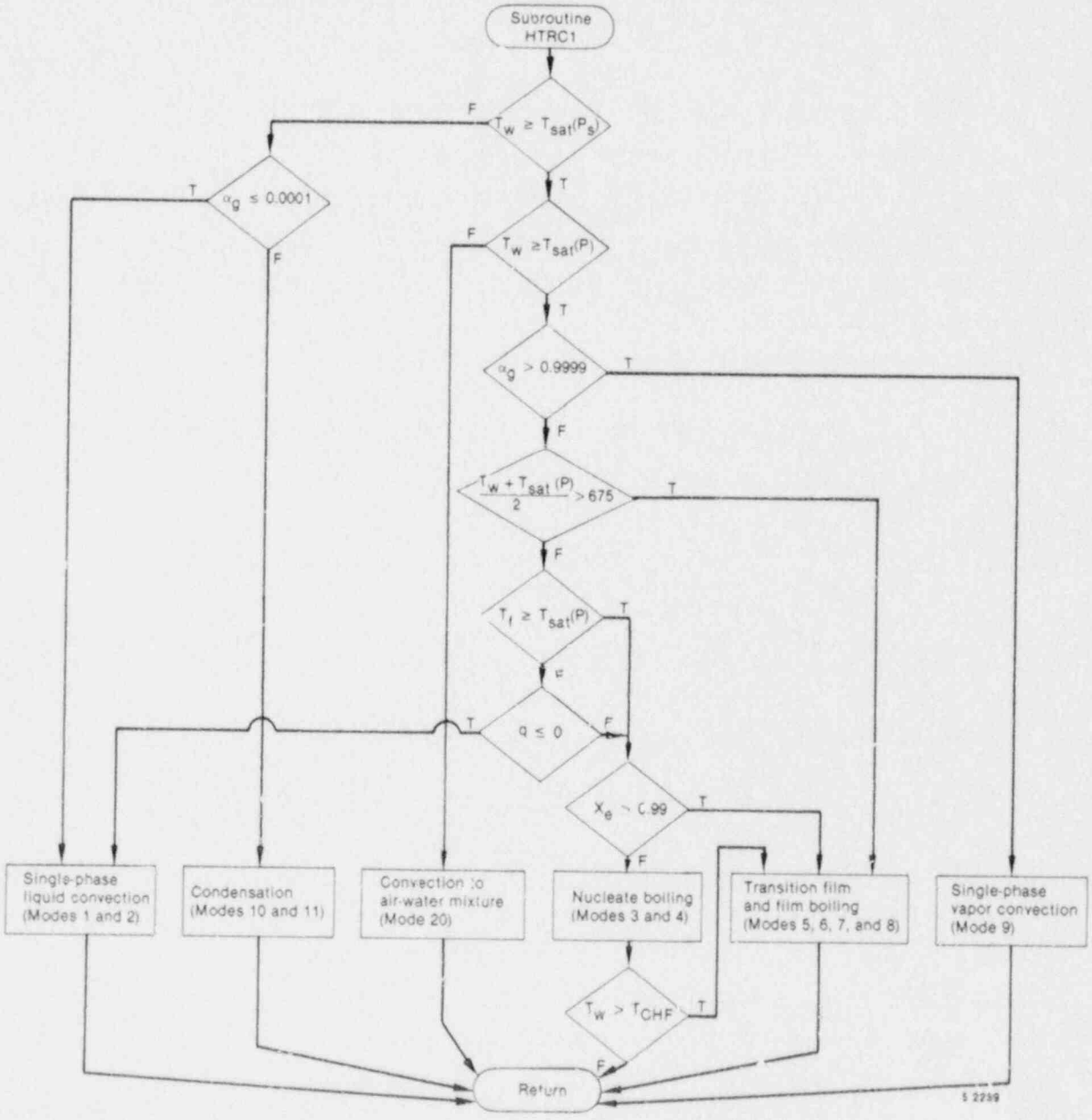

Figure 9. Logic chart for wall heat transfer regime selection.

vapor convective heat transfer, the wall is assumed to be dry and the heat transfer area between the wall and the liquid is negligible. Therefore, the heat transfer from the wall to the liquid is negligible and the heat transfer from the wall to the vapor is given by the expression

$$Q_{wg} = h_{wg} A_w (T_w - T_g) \quad . \tag{271}$$

The Dittus-Boelter correlation is used for h_{wg}.

In the condensation regime, heat transfer to the wall from liquid and vapor is dependent on the flow regime. Heat transfer from liquid to the wall is modeled by convection in the low void regime and heat transfer from vapor to the wall is modeled by condensation in the high void regime. A void fraction weighting scheme is used to include the effects of condensate in the heat transfer from liquid to the wall for which the expression is

$$Q_{wf} = [(1 - \alpha_g) h_{\text{Dittus-Boelter}}(T_w - T_f) + \alpha_g h_{con}(T_w - T_g)]A_w/V \tag{272}$$

where h_{con} is the condensation heat transfer coefficient. Heat transfer from vapor to the wall is modeled by convection and expressed as

$$Q_{wg} = [\alpha_g h_{con} (T_w - T_g)]A_w/V \quad . \tag{273}$$

The correlations used to calculate wall heat transfer are summarized in Table 1.

3.1.3.5 Interphase Mass Transfer. The interface mass transfer is modeled according to the thermodynamic process, interphase heat transfer regime and flow regime. After the thermodynamic process is decided, the flow regime map discussed in Section 3.1.3.1 is used to determine the phasic interfacial area and to select the interphase heat transfer correlation.

TABLE 1. RELAP5/MOD2 HEAT TRANSFER

Single-Phase Forced Convection for Wall to Liquid, Liquid to Wall, Vapor to Wall, or Wall to Vapor: Dittus-Boelter[40]

$$h = 0.023 \frac{k}{D_e} Pr^{0.4} Re^{0.8}$$

where the physical properties are evaluated at fluid temperature (T_f or T_g) and where

h = heat transfer coefficient ($W/m^2 \cdot K$)

k = thermal conductivity ($W/m \cdot K$)

D_e = equivalent diameter (m)

Pr = Prandtl number = $C_p \mu / k$

C_p = specific heat at constant pressure ($J/kg \cdot K$)

μ = viscosity ($kg/m \cdot s$)

G = mass flux ($kg/m^2 \cdot s$)

Re = Reynolds number = GD_e/μ.

For single-phase liquid

$$Q_{wf} = h \cdot A_{wf} (T_w - T_f)/V$$

TABLE 1. (continued)

$Q_{wg} = h \cdot A_{wg} (T_w - T_g)/V = 0$

where

$A_{wf} = A_w$

$A_{wg} = 0$

Q_{wf} = wall to liquid volumetric heat flux (W/m^3)

Q_{wg} = wall to vapor volumetric heat flux (W/m^3)

A_w = total heat transfer area (m^2)

A_{wf} = wall to liquid heat transfer area (m^2)

A_{wg} = wall to vapor heat transfer area (m^2)

V = hydraulic volume (m^3)

T_w = wall temperature (K)

For single-phase vapor

$Q_{wf} = h \cdot A_{wf} (T_w - T_f)/V = 0$

TABLE 1. (continued)

$$Q_{wg} = h \cdot A_{wg} (T_w - T_g)/V$$

where

$$A_{wf} = 0$$

$$A_{wg} = A_w \ .$$

Saturated Nucleate Boiling: Chen[41]

$$h = h_{mic} + h_{mac}$$

where

$$h_{mic} = 0.00122 \frac{k_f^{0.79} C_{pf}^{0.45} \rho_f^{0.49}}{\sigma^{0.5} \mu_f^{0.29} h_{fg}^{0.24} \rho_g^{0.24}} \Delta T_{sat}^{0.24} \Delta p^{0.75} S$$

$$h_{mac} = 0.023 \frac{k_g}{D_e} (Pr)_f^{0.4} (Re)_f^{0.8} F$$

F = Reynolds number factor

$$F = \begin{cases} 1.0 & X_{tt}^{-1} \leq 0.10 \\ 2.35 (X_{tt}^{-1} + 0.213)^{0.736} & X_{tt}^{-1} > 0.10 \end{cases}$$

$$X_{tt}^{-1} = \left\{ \frac{\alpha_g \rho_g v_g}{(1-\alpha_g) \rho_f v_f} \right\}^{0.9} \left(\frac{\rho_f}{\rho_g} \right)^{0.5} \left(\frac{\mu_g}{\mu_f} \right)^{0.1}$$

TABLE 1. (continued)

S = suppression factor

$$S = \begin{cases} [1 + 0.12\ (Re_{TP})^{1.14}]^{-1} & Re_{TP} < 32.5 \\ [1 + 0.42\ (Re_{TP})^{0.78}]^{-1} & 32.5 \leq Re_{TP} \leq 70.0 \\ 0.1 & Re_{TP} \geq 70 \end{cases}$$

$$Re_{TP} = \left(\frac{v_f \rho_f \alpha_f D_e}{\mu_f} \right) F^{1.25} \times 10^{-4}$$

ρ = density (kg/m^3)

σ = surface tension (N/m)

h_{fg} = latent heat of vaporization (J/kg)

ΔT_{sat} = $T_w - T_{sat}$

T_{sat} = saturation temperature (K)

ΔP = difference in vapor pressure corresponding to ΔT_{sat} (Pa)

v = velocity (m/s)

α_g = void fraction

f = saturated liquid condition (subscript)

g = saturated vapor condition (subscript).

TABLE 1. (continued)

$$Q_{wf} = h \cdot A_{wf} \cdot (T_w - T_f)/V$$

$$Q_{wg} = h \cdot A_{wg} \cdot (T_w - T_f)/V = 0$$

where

$$A_{wf} = A_w$$

$$A_{wg} = 0 \ .$$

Subcooled Nucleate Boiling: Modified Chen[44]

$$Q_{wf} = \left[h_{mic} \ \Delta T_{sat} + h_{mac} \ (T_w - T_f)\right] A_{wf}/V$$

$$Q_{wg} = h \cdot A_{wg} \cdot (T_w - T_g)/V = 0$$

where

$$A_{wf} = A_w$$

$$A_{wg} = 0 \ .$$

The modified Chen correlation is obtained by setting $F = 1$ in h_{mac} and evaluating the properties at T_f.

TABLE 1. (continued)

Critical Heat Flux (CHF) Correlation:

1. High Flow CHF correlation: Biasi[44] (for mass flux (G) $\geq$ 200 kg/m^2-s)

$$q_{crit} = \frac{1.883 \times 10^7}{D_e^n \, G^{1/6}} \left[\frac{f(P)}{G^{1/6}} - X_e \right]$$

for the low quality region

$$q_{crit} = \frac{3.78 \times 10^7 h(P)}{D_e^n \, G^{0.6}} \left[1 - X_e \right]$$

for the high quality region

where the maximum value of the above q_{crit}'s is used and

where

n = 0.4, for $D_e \geq 1$ cm

n = 0.6, for $D_e < 1$ cm

$f(P)$ = $0.7249 + 0.099 \, P \exp(-0.032P)$

$h(P)$ = $-1.159 + 0.149 \, P \exp(-0.019P) + 8.99P/(10 + P^2)$

D_e = hydraulic diameter (cm)

P = pressure (bar)

X_e = equilibrium equality

TABLE 1. (continued)

q_{crit} = critical heat flux (W/m^2)

G = mass flux (g/cm^2-s) .

2. Low Flow CHF Correlation: Modified Zuber[23] (for G $\leq$ 100 kg/m^2-s)

$$q_{crit} = 0.131\, h_{fg}\, \rho_g^{0.5} [\sigma g (\rho_f - \rho_g)]^{0.25} \left(\frac{\rho_f}{\rho_f + \rho_g}\right)^{0.5} (0.96 - \alpha_g)$$

If mass flux, G, is between 100 and 200 ($kg/m^2 \cdot s$) a linear interpolation with respect to G is used to evaluate q_{crit}.

Transition Film Boiling: Chen[43]

$$Q_{wf} = q_{crit} \cdot A_{wf}/V + q_{rad,f} (A_{wf})_{rad}/V$$

where

A_{wf} = $A_w \cdot e^{-\lambda \Delta T_{sat}}$

λ = λ_1 or λ_2, which ever is greater

where the exponential term is the liquid contact area weighting factor and where

$$\lambda_1 = C_1 - C_2 \cdot \frac{G}{10^5}$$

$$\lambda_2 = C_3 \cdot \frac{G}{10^5}$$

TABLE 1. (continued)

$$C_2 = \frac{0.05}{1 - \alpha_g^{40}} + 0.075\alpha_g$$

$$C_1 = 2.4\ C_2$$

$$C_3 = 0.2\ C_2$$

also,

$$q_{rad,f} = \varepsilon_f B(T_w^4 - T_s^4) \quad (\varepsilon \text{ is the gray factor})$$

$$(A_{wf})_{rad} = A_w \cdot (1-\alpha_g) \quad .$$

It should be noted that the Chen transition film boiling correlation is expressed here in British Units.

$$Q_{wg} = q_{vc}\ A_{wg}/V + q_{rad,g}\ (A_{wg})_{rad}/V$$

where

$$q_{vc} = 0.023\ (\frac{k_g}{D_e}) \left[\left(\frac{\rho_g v_g \alpha_g}{\mu_g}\right) D_e\right]^{0.8} (Pr)_g^{0.4}\ (T_w - T_g)$$

$$A_{wg} = A_w\ (1 - e^{-\lambda\sqrt{\Delta T_{sat}}})$$

$$q_{rad,g} = \varepsilon_g B(T_w^4 - T_g^4)$$

$$(A_{wg})_{rad} = A_w \cdot \alpha_g$$

$$B = \text{Boltzmann constant}$$

TABLE 1. (continued)

Film Boiling: Bromley Pomeranz[45] and Dougall-Rohsenow[46]

$$Q_{wf} = q_{film} \cdot A_{wf}/V$$

where

$$A_{wf} = (1 - \alpha_g)\, A_w$$

$$q_{film} = h_{Bromely\text{-}Pomeranz}\, (\Delta T_{sat})$$

$$h_{Bromley\text{-}Pomeranz} = 0.620 \left(\frac{D_e}{\lambda_c}\right)^{0.172} \left[\frac{k_g^3\, \rho_g\, (\rho_f - \rho_g)\, h_{fg} g}{D_e\, \mu_g\, \Delta T_{sat}}\right]^{0.25}$$

$$\lambda_c = 2\pi \left[\frac{\sigma}{g(\rho_f - \rho_g)}\right]^{0.5}$$

g = acceleration due to gravity (m/s^2)

$$Q_{wg} = q_{DFG} \cdot A_{wg}/V + q_{rad,g}\, (A_{wg})_{rad}/V$$

where

$$A_{wg} = \alpha_g\, A_w$$

$$A_{wg,rad} = \alpha_g\, A_w$$

$$q_{DFG} = h_{Dougall\text{-}Rohsenow}\, (T_w - T_g)$$

$$h_{Dougall\text{-}Rohsenow} = 0.023\, \frac{k_g}{D_e} \left\{\frac{\rho_g[\alpha_g v_g + (1-\alpha_g)\, v_f]\, D_e}{\mu_g}\right\}^{0.8} \left[\frac{\mu_g (C_p)_g}{k_g}\right]^{0.4}$$

$$q_{rad,g} = \varepsilon_g\, (T_w^4 - T_g^4)$$

TABLE 1. (continued)

Condensation heat transfer: (See Reference 44)

$$Q_{wf} = \left[(1 - \alpha_g)\, h_{\text{Dittus-Boelter}} \cdot (T_w - T_f) + \alpha_g\, h_{con} \cdot (T_w - T_g)\right] A_w/V$$

where

$$h_{con} = \begin{cases} \max & \\ & \frac{3}{4}\,(1.47)\,(Re)_f^{-0.333} \left[\frac{\rho_f\,(\rho_f - \rho_g)\,g}{\mu_f^2}\right]^{0.333} k_f \quad \text{(free flow condensation)} \\ & 0.065\,\frac{\rho_f^{0.5}}{\mu_f}\,(Pr)_f^{0.5}\,\tau_i^{0.5}\,k_f \quad \text{(free flow condensation)} \end{cases}$$

$$\tau_i = \frac{0.0792}{(Re)_g^{0.25}} \left(\frac{\rho_g\, v_g^2}{2}\right)$$

$$Q_{wg} = \alpha_g \cdot h_{con} \cdot (T_w - T_g)\, A_w/V$$

The mass transfer model is formulated so that the net interfacial mass transfer rate is composed of two components which are the mass transfer rate at the wall and the mass transfer rate in the bulk fluid, which is expressed as

$$\Gamma_g = \Gamma_w + \Gamma_{ig} \quad . \tag{274}$$

For system components in which wall heat transfer is modeled, mass transfer at the wall is calculated according to the wall heat transfer model and mass transfer to the bulk fluid is calculated according to the interphase heat transfer regime and flow regime. For system components in which wall heat transfer is not modeled, mass transfer at the wall is ignored and mass transfer in the bulk fluid is modeled according to the interphase heat transfer regime and flow regime.

For components modeling wall heat transfer processes, the interfacial mass transfer at the wall is calculated from the total wall to liquid heat transfer minus the wall to liquid convective heat transfer. For these processes, the heat transfer model developed by Chen, as discussed in Section 3.1.3.4, is used to model the total wall to liquid heat transfer. The Chen model assumes that the total wall to liquid heat transfer is composed of boiling and convective heat transfer and that the interfacial mass transfer at the wall is mainly due to boiling heat transfer. Consequently, the contribution due to convective heat transfer must be subtracted from the total wall to liquid heat transfer in order to calculate the interfacial mass transfer at the wall. Correlations used to calculate interfacial mass transfer at the wall for different heat transfer regimes are summarized in Table 2.

For components not modeling wall heat transfer and for the general bulk mass transfer processes, the interfacial mass transfer in the bulk fluid is modeled according to the flow regime. In the bubbly flow regime, for the liquid side, interfacial mass transfer is the larger of either the model for bubble growth developed by Plesset and Zwick[47] or the model for convective heat transfer for a spherical bubble,[48] and for the vapor

TABLE 2. RELAP5/MOD2 INTERFACIAL MASS TRANSFER AT WALL

Subcooled and Saturated Boiling Heat Transfer Regimes:

$$\Gamma_{wf} = (Q_{wf} - Q_c)/h_{fg}$$

$$\Gamma_{wg} = 0$$

where

Q_{wf} is defined in Table 1 for corresponding regimes

and

$Q_c = h_{mac} \cdot (T_w - T_f) \cdot A_w/V$

h_{mac} = convective part of the Chen correlation (see Table 1)

h_{fg} = specific latent heat (J/kg)

Transition Film and Film Boiling Regimes:

$$\Gamma_{wf} = \frac{Q_{wf}}{h_{fg}\,(1 + 0.5\, C_{pg} \cdot \Delta T_{sat}/h_{fg})}$$

$$\Gamma_{wg} = 0$$

Condensation Regime:

$$\Gamma_{wg} = \frac{Q_{wf} - Q_c}{h_{fg}\,[1 + 0.375\, C_{pg}\,(T_g - T_s)/h_{fg}]}$$

TABLE 2. (continued)

$\Gamma_{wf} = 0$

where

$$Q_c = (1 - \alpha_s)\, h_{\text{Dittus-Boelter}}\, (T_w - T_f) \cdot A_w/V$$

side, an interphase heat transfer coefficient is assumed that is high enough to drive the vapor temperature toward saturation. Analogously, in the annular mist regime, for the vapor side, a convective heat transfer model for a spherical droplet is used for the interphase heat transfer coefficient, and for the liquid side, an interphase heat transfer coefficient is assumed that is high enough to drive the liquid temperature toward saturation. Correlations used to calculate interfacial mass transfer in the bulk fluid are summarized in Table 3.

For condensation processes, the interfacial mass transfer in the bulk fluid, for the liquid side, is calculated by the Unal bubble collapse model[49] in the bubbly flow regime and by the Theofanous interfacial condensation model[51] in the annular mist flow regime and for the vapor side, a large interphase heat transfer coefficient is assumed in order to drive the vapor temperature toward saturation.

3.1.3.6 Reflood Heat Transfer. A special reflood model is designed to specifically analyze the reflood process, which occurs normally at low pressures and low mass flow rates. To increase computational efficiency in the nucleate boiling and transition boiling regimes, the heat transfer correlations known to apply for the reflood process are employed. These correlations and a model for radiation heat transfer are described in the following.

The wall temperature, T_{IB}, at the incipience of boiling is determined by a criterion developed by Bergles and Rohsenow[52] expressed in British Units as

$$T_{IB} = T_{sat} + \left(\frac{q}{15.6\ P^{1.156}}\right)^{\left(\frac{P\ 3.034}{2.30}\right)} \qquad (275)$$

where the heat flux, q, is computed from the Dittus-Boelter correlation for single-phase convection to liquid. For wall temperatures higher than that at the incipience of boiling, the heat flux is computed from the equation,

TABLE 3. RELAP5/MOD2 INTERFACIAL MASS TRANSFER IN BULK FLUID

Depressurization Process ($T_f > T_{sat}$)

1. Bubbly Flow Regimes:

$$Q_{if} = H_{if} (T_s - T_f)$$

where

$$H_{if} = MAX \begin{cases} \dfrac{12}{\pi d_b^2} \Delta T_{sat} \dfrac{\rho_f \cdot (C_p)_f k_f}{\rho_g h_{fg}} \text{ (Plesset-Zwick)}^{47} \ (W/m^3\text{-}K) \\ \dfrac{6\alpha_g K_f}{d_b^2} (2 + 0.74 Re_b^{0.5} Pr_f^{0.333}) \text{ (Force convection for single bubble)}^{42} \end{cases}$$

$$Re_b = \frac{\rho_f d_b |v_g - v_f|}{\mu_f} \text{ (Bubble Reynolds number)}$$

$$d_b = \text{bubble diameter (m)}$$

$$Q_{ig} = H_{ig} (T_s - T_g)$$

where

$$H_{ig} = \frac{6\alpha_g}{d_b^2} k_g Nu_{ib}$$

$$Nu_{ib} = 10^4$$

TABLE 3. (continued)

2. Annular-Mist Regime:

$$Q_{if} = H_{if} (T_s - T_f)$$

where

$$H_{if} = \frac{6 (1-\alpha_g)}{d_b^2} k_f Nu_{id}$$

$$Nu_{id} = 10^5$$

$$Q_{ig} = H_{ig} (T_s - T_g)$$

where

$$H_{ig} = \frac{6 (1-\alpha_g)}{d_d^2} \cdot k_g (2. + 0.74 Re_d^{0.5} Pr_g^{0.33})$$

$$+ \quad 0.0023 (Re)_g^{0.8} \cdot k_g \cdot \frac{(\alpha_g)^{0.5}}{D_e^2}$$

$$Re_d = \frac{\rho_g d_d |v_g - v_f|}{\mu_g} \quad \text{(Droplet Reynolds Number)}$$

d_d = drop diameter (m)

Heat Transfer Process ($T_f \leq T_{sat}$)

1. Bubbly Flow Regime:

$$Q_{if} = H_{if} (T_s - T_f)$$

TABLE 3. (continued)

---

where

$$H_{if} = \frac{3\phi\ C\ h_{fg}\ \alpha_g}{\frac{1}{\rho_g} - \frac{1}{\rho_f}} \qquad \text{(Unal's correlation)}^{49}$$

where

$$\phi = \begin{cases} 1 & v_f \leq 0.61\ \text{(m/s)} \\ [1.639\ v_f]^{0.47} & v_f > 0.61\ \text{(m/s)} \end{cases}$$

$$C = \begin{cases} 61 - 6.489 \times 10^{-5}\ (P - 1.7 \times 10^5) & P \leq 10^6\ \text{(Pa)} \\ 2.3 \times 10^9 / P^{1.418} & P > 10^6\ \text{(Pa)} \end{cases}$$

P = pressure (Pa)

$$Q_{ig} = H_{ig}\ (T_s - T_g)$$

where

$$H_{ig} = \frac{6\alpha_g}{d_b^2}\ k_g\ Nu_{ib}$$

$$Nu_{ib} = 10^4$$

TABLE 3. (continued)

2. Annular-Mist Flow Regime:

Similar as the depressurization process.

Condensation Process

1. Bubbly Flow Regime:

Similar as the heat transfer process.

2. Annular-Mist Flow Regime:

$$Q_{if} = H_{if} (T_s - T_f)$$

where

$$H_{if} = 6 \left[2. + \frac{8. (T_s - T_f)}{T_m - T_f}\right] k_f (1-\alpha_g)/d_d^2 + 10^{-3} \cdot \rho_f \cdot v_f \cdot C_{pf} \cdot A_{film}$$

A_{film} = area of film per unit volume

$$T_m = \frac{T_s - T_f}{1 + C_{pg}(T_g - T_s)/h_{fg}}$$

The first term of right side uses the condensation of a single droplet in superheated steam model developed by Brown.[50] The second term of right side uses the film condensation model developed by Theofanous.[51]

$$Q_{ig} = H_{ig} (T_s - T_f)$$

TABLE 3. (continued)

where

$$H_{ig} = \frac{6 \cdot (1-\alpha)}{d_d^2} k_g \cdot Nu_{id}$$

$$Nu_{id} = 10^5$$

$$q = h_c(T_w - T_f) + h_{NB}(T_w - T_{sat}) \quad (276)$$

where h_c is a Dittus-Boelter convective heat transfer coefficient and h_{NB} is a nucleate boiling heat transfer coefficient. The nucleate boiling heat transfer coefficient is obtained utilizing the McAdams[53] nucleate boiling correlation for low pressures, for which

$$q_{NB} = h_{NB}(T_w - T_{sat}) = 2.253(T_w - T_{sat})^{3.86} \quad . \quad (277)$$

Nucleate boiling prevails up to a temperature, T_{CHF}, at which the boiling heat flux is equal to the critical heat flux, q_{CHF}, where

$$h_{NB}(T_{CHF} - T_{sat}) = q_{CHF} \quad . \quad (278)$$

The critical heat flux, q_{CHF}, is calculated according to the modified Zuber correlation,[54-57] expressed as

$$q_{CHF} = 0.131(1-\alpha_g) h_{fg} \left(\frac{\rho_g \rho_f}{\rho_f + \rho_g}\right)^{1/2} \left[\sigma g (\rho_f - \rho_g)\right]^{1/4}$$

$$X\left\{\max\left[1, (G/G_{ref})^{0.33}\right]\right\} \quad , \quad (279)$$

where G is mass flux and G_{ref} is a reference mass flux and is equal to 67.8 kg/m^2s.

For wall temperatures higher than the temperature, T_{CHF}, the heat flux is computed using the equation

$$q = h_c(T_w - T_g) + h_{TB}(T_w - T_{sat}) \quad (280)$$

where the convective heat transfer coefficient, h_c, is of a Dittus-Boelter form given by the Dougall-Rohsenow correlation shown in

Table 1. The transition boiling heat transfer coefficient, h_{TB}, is calculated using a correlation developed by Weisman.[55] for which

$$h_{TB} = h_m \exp(-0.055\Delta T) + 4500 (G/G_{ref})^{0.2} \exp(-0.012\Delta T) \quad . \tag{281}$$

Here h_m and ΔT are

$$h_m = q_{cr}/\Delta t_m \tag{282}$$

and

$$\Delta T = T_w - T_{sat} - \Delta T_m \quad , \tag{283}$$

respectively, and where

$$\Delta T_m = S (q_{cr}/2.253)^{1/3.86} \quad . \tag{284}$$

The term, S, is Chen's boiling suppression factor shown in Table 1.

The transition boiling and film boiling formulas intersect at a temperature, T_Q, which is called the rewetting or quench temperature. The quench temperature is currently computed using the formula

$$T_Q = (T_{CHF} + T_{sat})/2 + 125.0 \tag{285}$$

where T_{sat} is the saturation temperature at atmospheric pressure. Equation (285) yields a value of about 520 K, which is close to the value of 260°C suggested by Arrieta and Yadigaroglu.[58]

For film boiling, the heat transfer coefficient, h_{FB}, is obtained from

$$h_{FB} = \text{MAX}(h_{TB}, h_{FBB}) \quad . \tag{286}$$

Here, h_{TB} is defined by Equation (281) and h_{FBB} is given by the modified Bromley correlation[59] for which

$$h_{FBB} = 0.62 \left[\frac{k_g^3 \rho_g^3 (\rho_f - \rho_g) h_{fg} g}{\mu_g (T_w - T_{Sat})} \frac{1}{2\pi} \sqrt{\frac{g (\rho_f - \rho_g)}{\sigma}} \right]^{0.25} \quad (287)$$

where

$$h'_{fg} = h_{fg} [1 + 0.68 C_{pv} (T_w - T_{sat})/h_{fg}] \quad , \quad (288)$$

and where h_{fg} is the heat of vaporization. In Equations (287) and (288) all of the vapor properties are evaluated at the film temperature, $(T_w + T_{sat})/2$. Note also that the true quench temperature is implied by the minimum film boiling heat transfer coefficient given by Equation (286). The value of T_Q defined by Equation (285) is for convenience and its value is not important in the calculated results as long as the actual quench temperature implied from Equation (286) is higher than T_Q from Equation (285).

At high wall temperatures radiation heat transfer is treated using a model developed by Sun.[60] The model considers the vapor-droplet mixture as an optically thin medium and uses an electric network analogy to analyze the radiation energy exchange among the wall, the liquid droplets, and the vapor. The radiation fluxes are expressed as

$$q_{we} = F_{wf} \sigma (T_w^4 - T_{sat}^4) \quad , \quad (289)$$

$$q_{wg} = F_{wg} \sigma (T_w^4 - T_g^4) \quad \text{and} \quad (290)$$

$$q_{gf} = F_{gf} \sigma (T_w^4 - T_{sat}^4) \quad . \quad (291)$$

In Equations (289) through (291) the term σ is the Stefan-Boltzman constant, T_g is the vapor temperature, and F_{we}, F_{wg} and F_{gf} are gray body factors for which

$$F_{we} = 1/[R_2 (1 + R_3/R_1 + R_3/R_2)] \quad , \tag{292}$$

$$F_{wg} = 1/[R_1 (1 + R_3/R_1 + R_3/R_2)] \quad \text{and} \tag{293}$$

$$F_{gf} = 1/[R_2 (1 + R_1/R_2 + R_2/R_3)] \quad . \tag{294}$$

In Equations (292) through (294) the resistance terms in the electrical analogy are given as

$$R_1 = (1 - \varepsilon_g)/[\varepsilon_g (1 - \varepsilon_g \varepsilon_g)] \quad , \tag{295}$$

$$R_2 = (1 - \varepsilon_g)/[\varepsilon_g (1 - \varepsilon_g \varepsilon_f)] \quad \text{and} \tag{296}$$

$$R_3 = 1/(1 - \varepsilon_g \varepsilon_f) + (1 - \varepsilon_w)/\varepsilon_w \tag{297}$$

for which the emissivities are given as

$$\varepsilon_g = 1 - \exp(-a_g L_m) \quad , \tag{298}$$

$$\varepsilon_f = 1 - \exp(-a_f L_m) \quad \text{and} \tag{299}$$

$$\varepsilon_w = 0.8 \quad , \tag{300}$$

where L_m is a mean length and a_g and a_f are vapor and liquid absorption coefficients, respectively. The mean length L_m is roughly equal to 0.9 D_{hy}, where D_{hy} is the hydraulic diameter of the fluid channel. The absorption coefficient, a_f, for droplets is given by

$$a_f = 1.11\ \alpha_f / D_d \quad , \tag{301}$$

where α_f is the liquid volume fraction and D_d is the droplet diameter. The absorption coefficient, a_g, for vapor[61] is given by

$$a_g = 1.3 \times 10^{-4}\ P\ (555.56/T_g)^2\ [1 - 0.054(555.56/T_g)^2] \quad , \tag{302}$$

where P is pressure.

3.1.4 Special Process Models

Certain models in RELAP5/MOD2 have been developed to simulate the special processes. These models are described in the following subsections.

3.1.4.1 Choked Flow. A choked flow model developed by Ransom and Trapp[62,18] is included in RELAP5 primarily for calculation of the mass discharge from the system at a pipe break or a nozzle. Generally, the flow at the break or nozzle is choked until the system pressure nears the containment pressure. The choked flow model is used to predict if the flow is choked at break or nozzle and, if it is, to establish the discharge boundary condition. In addition, the choked flow model can be used to predict existence of and calculate choked flow at internal points in the system.

Choking is defined as the condition wherein the mass flow rate becomes independent of the downstream conditions (that point at which further reduction in the downstream pressure does not change the mass flow rate). The fundamental reason that choking occurs is that acoustic signals can no longer propagate upstream. This occurs when the fluid velocity equals or exceeds the propagation velocity. The choked flow model is based on a definition that is established by a characteristic analysis using the time-dependent differential equations.

Consider a system of n first-order quasi-linear, partial differential equations of the form

$$A(U)\,(\partial U/\partial t) + B(U)\,(\partial U/\partial x) + C(U) = 0 \quad . \tag{303}$$

The characteristic directions (or characteristic velocities) of the system are defined[63,64] as the roots, $\lambda_i (i \leq n)$, of the characteristic polynomial

$$(A\lambda - B) = 0 \quad . \tag{304}$$

The real part of any root, λ_i, gives the velocity of signal propagation along the corresponding characteristic path in the space/time plane. The imaginary part of any complex root, λ_i, gives the rate of growth or decay of the signal propagating along the respective path. For a hyperbolic system in which all the roots of Equation (304) are real and nonzero, the number of boundary conditions required at any boundary point equals the number of characteristic lines entering the solution region as time increases. If we consider the system [Equation (303)] for a particular region $0 \leq x \leq L$, and examine the boundary conditions at $x = L$, as long as any λ_i are less than zero, we must supply some boundary information to obtain the solution. If λ_i are greater than or equal to zero, no boundary conditions are needed at $x = L$, and the interior solution is unaffected by conditions beyond this boundary.

A choked condition exists when no information can propagate into the solution region from the exterior. Such a condition exists at the boundary point, $x = L$, when

$$\lambda_j \geq 0 \text{ for all } j \leq n \quad . \tag{305}$$

These are the mathematical conditions satisfied by the equations of motion for a flowing fluid when reduction in downstream pressure ceases to result in increased flow rate. It is well-known[65] that the choked condition for single-phase flow occurs when the fluid velocity just equals the local

sound speed. For this case, one of the λ_j's is just equal to zero. For the two-phase case, it is possible for all λ_j's to be greater than zero under special conditions which can exist during discharge of a subcooled liquid.

During the course of the RELAP5 development, extensive investigation was carried out to determine two-phase choked flow criterion under two assumed conditions:[a] (a) thermal equilibrium between phases, and (b) adiabatic phases without phase change (frozen).[66] The frozen assumption was in poor agreement with data, compared to the thermal equilibrium assumption. Therefore, the thermal equilibrium assumption with slip is used as the basis for the RELAP5 choked flow criterion. In the following subsections, theoretical aspects of choked flow are discussed.

3.1.4.1.1 Choking Criterion for Nonhomogeneous, Equilibrium Two-Phase Flow--The two-fluid model for the conditions of thermal equilibrium (equilibrium interphase mass transfer) is described by the overall mass continuity equation, two phasic momentum equations, and the mixture entropy equation. This system of equations is

$$\partial(\alpha_g\rho_g + \alpha_f\rho_f)/\partial t + \partial(\alpha_g\rho_g v_g + \alpha_f\rho_f v_f)/\partial x = 0 \tag{306}$$

$$\alpha_g\rho_g[\partial v_g/\partial t + v_g(\partial v_g/\partial x)] + \alpha_g(\partial P/\partial x) + C\alpha_g\alpha_f\rho(\partial v_g/\partial t - \partial v_f/\partial t) = 0 \tag{307}$$

$$\alpha_f\rho_f[\partial v_f/\partial t + v_f(\partial v_f/\partial x)] + \alpha_f(\partial P/\partial x) + C\alpha_f\alpha_g\rho(\partial v_f/\partial t - \partial v_g/\partial t) = 0 \tag{308}$$

---

a. The hydrodynamic model is not based on either of these assumptions; however, the purpose of this analysis is simply to establish a criterion for a choked flow and thus, there is no conflict with the basic hydrodynamic model.

$$\partial(\alpha_g \rho_g S_g + \alpha_f \rho_f S_f)/\partial t + \partial(\alpha_g \rho_g S_g v_g + \alpha_f \rho_f S_f v_f)/\partial x = 0 \quad . \tag{309}$$

The momentum equations include the interphase force terms due to relative acceleration.[16] These force terms have a significant effect on wave propagation velocity and consequently on the choked flow velocity. The particular form chosen is frame invariant and symmetrical, and the coefficient of virtual mass, $C\alpha_g \alpha_f \rho$, is chosen to ensure a smooth transition between pure vapor and pure liquid. For a dispersed flow, the constant, C, has a theoretical value of 0.5, whereas for a separated flow, the value may approach zero. The energy equation is written in terms of mixture entropy, which is constant for adiabatic flow (the energy dissipation associated with interphase mass transfer and relative phase acceleration is neglected).

The nondifferential source terms, C(U), in Equation (303) do not enter into the characteristic analysis or affect the propagation velocities. For this reason, the source terms associated with wall friction, interphase drag, and heat transfer are omitted for brevity in Equations (306) through (309).

In the thermal equilibrium case, ρ_g, ρ_f, S_g, and S_f are known functions of the pressure only (the vapor and liquid values along the saturation curve). The derivatives of these variables are designated by an asterisk as follows

$$\rho_f^* = d\rho_f^S/dP, \quad \rho_g^* = d\rho_g^S/dP \tag{310}$$

$$S_f^* = dS_f^S/dP, \quad S_g^* = dS_g^S/dP \quad . \tag{311}$$

The system of governing equations [Equations (306) through (309)] can be written in terms of the four dependent variables, α_g, P, v_g, and v_f, by application of the chain rule and the property derivatives

[Equations (310) and (311)]. Thus, the system of equations can be written in the form of Equation (303) where the A and B are fourth-order square coefficient matrices.

The characteristic polynomial that results is fourth-order in λ and factorization can only be carried out approximately to obtain the roots for λ, and establish the choking criterion. The first two roots are

$$\lambda_{1,2} = \frac{\left(\left\{ \alpha_f \rho_g + \rho C/2 \pm \left[(\rho C/2)^2 - \alpha_g \alpha_f \rho_g \rho_f \right]^{1/2} \right\} v_g \right.}{\left. + \left\{ \alpha_g \rho_f + \rho C/2 + \left[(\rho C/2)^2 - \alpha_g \alpha_f \rho_g \rho_f \right]^{1/2} \right\} v_f \right)} \Big/ \left((\alpha_f \rho_g + \rho C/2) + (\alpha_g \rho_f + \rho C/2) \right) . \quad (312)$$

These two roots are obtained by neglecting the fourth-order factors relative to the second-order factors in $(\lambda - v_g)$ and $(\lambda - v_f)$. There are no first- or third-order factors. Inspection of Equation (312) shows that $\lambda_{1,2}$ have values between v_g and v_f, thus the fourth-order factors, $(\lambda - v_g)$ and $(\lambda - v_f)$, are small (i.e., neglecting these terms is justified). The values for $\lambda_{1,2}$ may be real or complex depending on the sign of the quantity $[(\rho C/2)^2 - \alpha_g \alpha_f \rho_g \rho_f]$.

The remaining two roots are obtained by dividing out the quadratic factor containing $\lambda_{1,2}$, neglecting the remainder, and subsequent factorization of the remaining quadratic terms. [This procedure can be shown to be analogous to neglecting the second- and higher-order terms in the relative velocity, $(v_g - v_f)$.] The remaining roots are

$$\lambda_{3,4} = v + D(v_g - v_f) \pm a \quad (313)$$

where

$$v = (\alpha_g \rho_g v_g + \alpha_f \rho_f v_f)/\rho \quad (314)$$

$$a = a_{HE}\left\{\left[C_\rho{}^2 + \rho(\alpha_g\rho_f + \alpha_f\rho_g)\right]/(C_\rho^2 + \rho_g\rho_f)\right\}^{1/2} \tag{315}$$

and

$$D = 0.5\left[\frac{(\alpha_g\rho_f - \alpha_f\rho_g)}{(\rho C + \alpha_f\rho_g + \alpha_g\rho_f)} + \frac{\rho_g\rho_f(\alpha_f\rho_f - \alpha_g\rho_g)}{\rho\left(\rho_g\rho_f + C_\rho{}^2\right)} - a_{HE}^2\,\frac{\rho\left(\alpha_g\rho_g{}^2S_g^* + \alpha_f\rho_f{}^2S_f^*\right)}{\rho_g\rho_f(S_g - S_f)}\right] . \tag{316}$$

The quantity, a_{HE}, is the homogeneous equilibrium speed of sound. The roots, $\lambda_{3,4}$, have only real values.

The general nature and significance of these roots is revealed by applying the characteristic considerations. The speed of propagation of small disturbances is related to the values of the characteristic roots. In general, the velocity of propagation corresponds to the real part of a root and the growth or attenuation is associated with the complex part of the root. Choking will occur when the signal, which propagates with the largest velocity relative to the fluid, is just stationary, i.e.,

$$\lambda^R = 0 \text{ for } j \leq 4 \tag{317}$$

and

$$\lambda^R \geq 0 \text{ for all } i \neq j \quad . \tag{318}$$

The existence of complex roots for $\lambda_{1,2}$ makes the initial boundary value problem ill-posed. This problem has been discussed by many investigators[13,20] and the addition of any small, second-order viscous effects renders the problem well-posed.[13,21] The whole phenomenon of systems with mixed orders of derivatives and a first-order system with the addition of a small, second-order term, has been discussed and analyzed by

Whitham.[64] He has shown that the second-order viscous terms give infinite characteristic velocities. However, very little information is propagated along these characteristic lines and the bulk of the information is propagated along characteristic lines defined by the first-order system. We conclude that the ill-posed nature of Equations (306) through (309) can be removed by the addition of small, second-order viscous terms that have little effect upon the propagation of information. Therefore, the choking criterion for the two-phase flow system analyzed here is established from Equation (317).

The explicit character of the choking criterion for the two-phase flow model defined by Equations (306) through (309) is examined. Since the two roots, $\lambda_{1,2}$, are between the phase velocities, v_f and v_g, the choking criterion is established from the roots, $\lambda_{3,4}$, and Equation (317). The choking criterion is

$$v + D(v_g - v_f) = \pm a \quad . \tag{319}$$

The choking criterion can be rewritten in terms of the mass mean and relative Mach numbers

$$M_v = v/a, \; M_r = (v_g - v_f)/a \tag{320}$$

as

$$M_v + DM_r = \pm 1 \quad . \tag{321}$$

This relation is similar to the choking criterion for single-phase flow where only the mass average Mach number appears and choking corresponds to a Mach number of unity.

The choking criterion [Equation (321)] is a function of the two parameters, D and a. In Figure 10, a is plotted as a function of the void fraction, α_g, for a typical steam/water system at 7.5 MPa with C equal to zero (the stratified equilibrium sound speed), C equal to 0.5 (the

typical value for a dispersed flow model), and in the limiting case when C becomes infinite (homogeneous equilibrium sound speed). From Figure 10 it is evident that the virtual mass coefficient has a significant effect upon the choked flow dynamics in two-phase flow.[14]

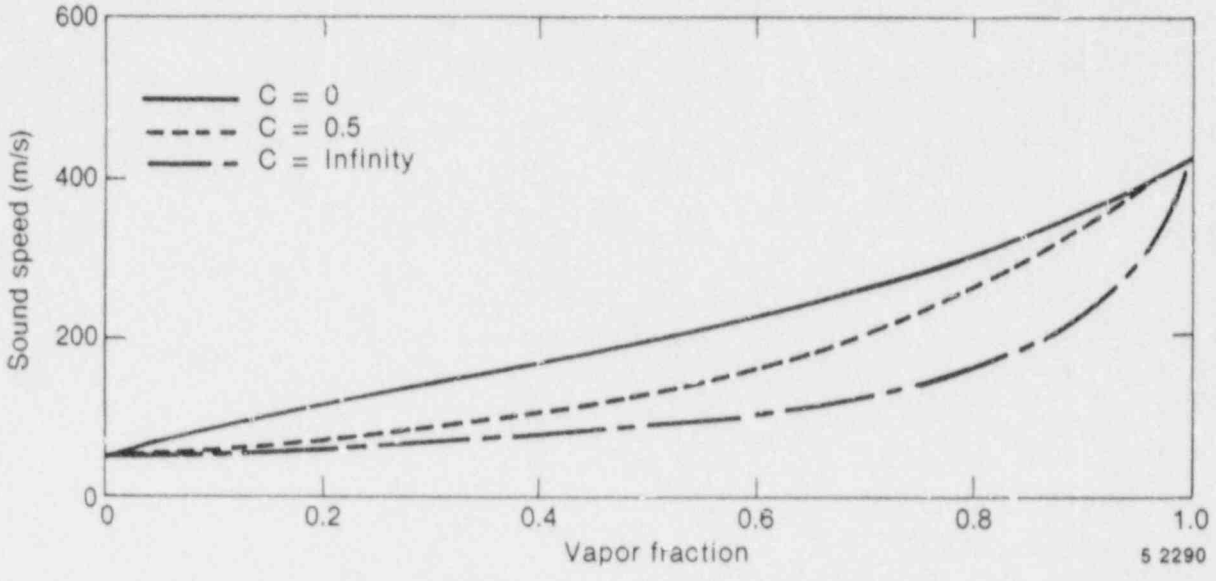

Figure 10. Equilibrium speed of sound as a function of void fraction and virtual mass coefficient.

To establish the actual choked flow rate for two-phase flow with slip, the relative velocity term in Equation (321) must also be considered. The relative Mach number coefficient, D, is shown plotted in Figure 11 for values of C equal to 0, 0.5 and ∞. It is evident from these results that the choked flow velocity can differ appreciably from the mass mean velocity when slip occurs. It is significant that the variation of the choked flow criterion from the homogeneous result is entirely due to velocity nonequilibrium, since these results have been obtained under the assumption of thermal equilibrium. The particular values of these parameters used in the model are further discussed later in this Section.

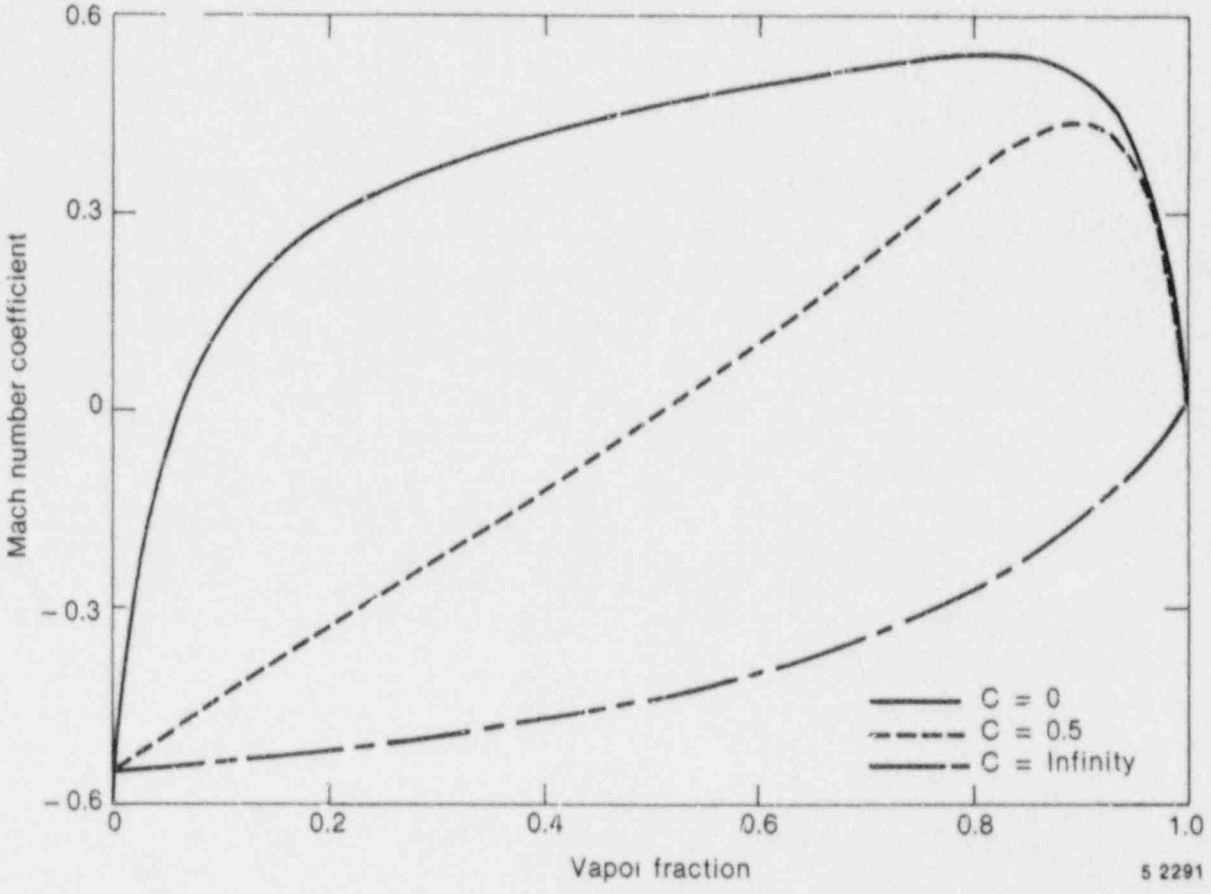

Figure 11. Coefficient of relative Mach number for thermal equilibrium flow as a function of void fraction and virtual mass coefficient.

3.1.4.1.2 Subcooled Choking Criterion--The previous analysis assumes two-phase conditions exist throughout the break flow process. However, initially and in the early phase of blowdown, the flow approaching the break or break nozzle will be subcooled liquid. Under most conditions of interest in LWR systems, the fluid undergoes a phase change at the break. The transition from single- to two-phase flow is accompanied by a discontinuous change in the fluid bulk modulus. This is especially true for the liquid-to-liquid/vapor transition. For example, at 600 KPa, the ratio of the single- to two-phase sound speed at the liquid boundary is 339.4. Thus, considerable care must be exercised when analyzing a flow having transitions to or from a pure phase (a discontinuity is also present at the vapor boundary, but the ratio is only 1.069).

To understand the physical process that occurs for subcooled upstream conditions, consider the flow through a converging/diverging nozzle connected to an upstream plenum with subcooled water at a high pressure. For a downstream pressure only slightly lower than the upstream pressure, subcooled liquid flow will exist throughout the nozzle. Under these conditions the flow can be analyzed using Bernoulli's equation, which predicts a minimum pressure, P_t, at the throat.[a] As the downstream pressure is lowered further, a point is reached where the throat pressure equals the local saturation pressure, P_{sat}. If the downstream pressure is lowered further, vaporization will take place at the throat.[b] When this happens, the fluid sound speed lowers drastically, but continuity considerations dictate that the velocity, v_t, of the two-phase mixture (at the point of minuscule void fraction) just equals the velocity of the subcooled water slightly upstream of the throat. When this occurs, v_t in the subcooled region is less than the water sound speed, but in the two-phase region, v_t can be greater than the two-phase sound speed. Hence, the subcooled water has a Mach number (M) less than one, whereas the two-phase mixture at the throat has a Mach number greater than one. Under these conditions (Mach numbers greater than one in the two-phase region), downstream pressure effects are not propagated upstream and the flow is choked. In particular, the supersonic two-phase fluid at the throat must increase in velocity and the pressure drop as it expands in the diverging section[c] (transition back to subsonic flow can occur in the nozzle as a result of a shock wave). The choked condition is shown in Figure 12(a). Contrary to the usual single-phase choked flow in a converging/diverging nozzle, there is no point in the flow field where M = 1. This is because in the homogeneous equilibrium model the fluid undergoes a discontinuous

---

a. For all practical cases of choking, the subcooled water can be considered incompressible with infinite sound speed.

b. An idealized one-dimensional homogeneous equilibrium model is assumed in the example.

c. In a supersonic flow, a diverging nozzle implies an increase in velocity.

change in sound speed from single-phase subcooled conditions to two-phase conditions, although the fluid properties are continuous through the transition point.

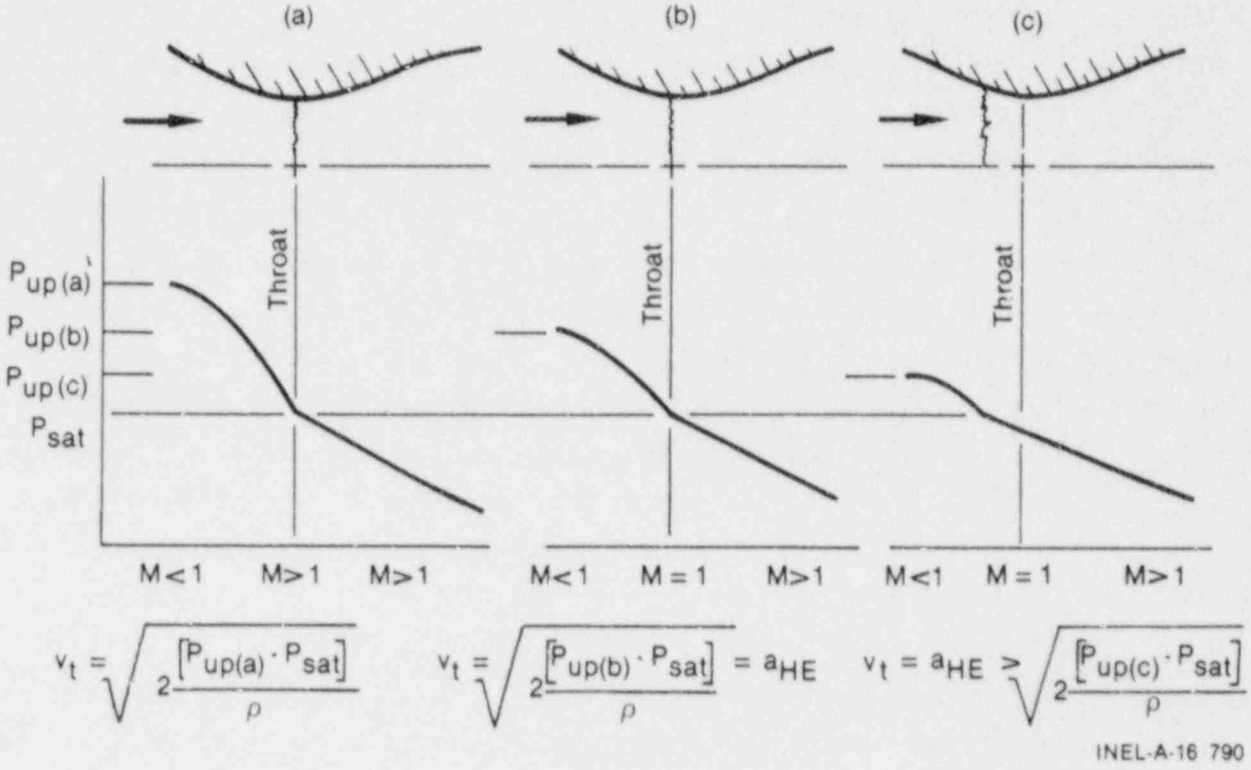

Figure 12. Subcooled choking process.

When this condition prevails, the flow rate can be established from application of Bernoulli's equation ($1/2\ \rho v_t^2 = P_{up} - P_{sat}$). For further decrease in the downstream pressure, no further increase in upstream fluid velocity will occur as long as the upstream conditions are maintained constant.

Now consider the process where a subcooled choked flow, as described above, initially exists (with a very low downstream pressure) and the upstream pressure is lowered. As the upstream pressure decreases, the pressure at the throat will remain at P_{sat} and Bernoulli's equation will give a smaller subcooled water velocity (v_t) at the throat. As P_{up} is lowered further, a point is reached where $v_t = a_{HE}$ and M = 1 on the

two-phase side of the throat (the Mach number in the subcooled portion upstream of the throat is much less than one). This situation is shown schematically in Figure 12(b).

As the upstream pressure is lowered further, the point where the pressure reaches P_{sat} must move upstream of the throat [see Figure 12(c)]. The subcooled water velocity at the P_{sat} location is smaller than the two-phase sound speed and the flow is subsonic. In the two-phase region between the point at which P_{sat} is reached and the throat, the Mach number is less than 1, but increases to M = 1 at the throat, that is, the two-phase sonic velocity is reached at the throat (as in the case of choked flow having a continuous variation of sound speed with pressure). As P_{up} is lowered still further, the P_{sat} point moves upstream until the flow becomes completely two-phase.

The homogeneous assumption applied in the above subcooled choking description is very close to the real situation when vapor is first formed. However, nonequilibrium can result in a superheated liquid state at a throat pressure, P_t, much lower than the saturation pressure, P_{sat}. The onset of vaporization occurs at P_t instead of P_{sat}.

The pressure undershoot, $P_{sat} - P_t$, can be described by the Alamgir-Lienhard-Jones correlation[67-69]

$$P_{sat} - P_t = \max(\Delta P, 0) \tag{322}$$

with

$$\Delta P = 0.258\,\sigma^{3/2} T_R^{13.76} \left(1 + 13.25 \sum{}'^{0.8}\right)^{1/2} \Big/ \left[(k_B T_c)^{1/2} (1 - V_f/V_g)\right]$$

$$- 0.07 (A_t/A)^2 \left(\rho v_c^2/2\right) . \tag{323}$$

The first term in ΔP represents the static depressurization effect and is derived by Alamgir and Lienhard[68] based on classical nucleation theory. For a steady flow in a nozzle, the depressurization rate, Σ', can be shown to be

$$\Sigma' = \left(\rho v_c^3 / A_t\right) (dA/dx)_t \quad . \tag{324}$$

Note that in Equation (323) Σ' is in units of Matm/s; but in Equation (324), Σ' is in units of Pa/s. Here, $(dA/dx)_t$ is the variation of area with respect to axial length and is to be evaluated at the throat. The second term in ΔP [Equation (323)] represents the turbulence effect and is developed by Jones.[69]

The choking velocity, based upon the process shown in Figure 12(a), can be calculated by applying Bernoulli's equation

$$v_c = \left[v_{up}^2 + 2\,(P_{up} - P_t)/\rho\right]^{1/2} \tag{325}$$

where P_t is to be computed from Equation (322).

For the process shown in Figure 12(b) and (c)

$$v_c = a_{HE} \tag{326}$$

and the two-phase choking criterion applies.

To determine which of the above situations exists, both v_c's are calculated and the larger is used as the choking velocity to be imposed at the throat. This velocity is imposed numerically at the throat in exactly the same manner as the choking criterion used for the two-phase condition described previously.

The subcooled choking model is very similar to models proposed by Burnell[70] and Moody;[71] however, the criterion for transition from subcooled choking to two-phase choking is now better understood and is in agreement with the physics of two-phase flow. The model here is also in agreement with cavitating venturi experience (experimentally confirmed behavior).

3.1.4.1.3 Horizontal Stratified Choked Flow--Under stratified conditions, the void fraction of the flow out of a small break may be quite different from the upstream void fraction. The usual definition of the outlet void fraction as a donored void fraction is no longer applicable. A simple approach based on the height of the liquid level and a criterion for the stability of small disturbances is used to determine the junction void fraction for stratified break flow.

By balancing the upward pressure force due to the Bernoulli effect and the downward gravitational force acting on a small surface perturbation, Taitel and Dukler[27] developed the following criterion for transition from the stratified horizontal flow regime in a round pipe

$$v_g > \left[\frac{(\rho_f - \rho_g)\, B_y A_g}{\rho_g dA_f/dH_f}\right]^{1/2} \left(1 - \frac{H_f}{D}\right) \quad . \tag{327}$$

In Equation (327), A_g and A_f are the flow areas of vapor and liquid, respectively. The right side of Equation (327) is the limiting vapor velocity designated by v_{gL}. The following geometrical relationships define H_g and H_f:

$$H_g = D\,(1 - \cos\theta)/2 \quad , \tag{328}$$

and

$$H_f = D\,(1 + \cos\theta)/2 \tag{329}$$

where θ is the central angle formed by a vertical cord and a radius to the liquid vapor interface. It can be shown that dA_f/dH_f equals $D \sin\theta$ and hence v_{gL} becomes

$$v_{gL} = 1/2 \left[\frac{(\rho_f - \rho_g) B_y \alpha_g A}{\rho_g D \sin\theta} \right]^{1/2} (1 - \cos\theta) \quad . \tag{330}$$

Let D_t be the diameter of the break area. When the liquid level is above the break [that is, $H_f > (D + D_t)/2$], the outlet void fraction, $\alpha_{g,j}$, which accounts for the pull-through of vapor, is defined as

$$\alpha_{g,j} = \alpha_{g,K} (v_g / v_{gL})^{1/2} \tag{331}$$

where $\alpha_{g,K}$ and v_g are the void fraction and vapor velocity upstream of the outlet. If the liquid level falls below the break [that is, $H_f < (D - D_t)/2$], liquid entrainment is modeled by defining the outlet liquid fraction, $\alpha_{f,j}$, as

$$\alpha_{f,j} = \alpha_{f,K} (v_g / v_{gL})^{1/2} \tag{332}$$

where $\alpha_{f,K}$ is the liquid volume fraction upstream of the outlet. The equality, $\alpha_{g,j} + \alpha_{f,j} = 1$, is used to obtain $\alpha_{g,j}$ ($\alpha_{f,j}$), if $\alpha_{f,j}$ ($\alpha_{g,j}$) is known. When the liquid level lies within the outlet area [that is, $(D + D_t)/2 > H_f > (D - D_t)/2$], the void fraction is obtained by interpolation of the two void fractions computed at the boundaries.

3.1.4.1.4 Implementation of Choked Flow Model--Ideally, the two-phase choking criterion [Equation (319)] can be used as a boundary condition for obtaining flow solutions. However, the applicability of Equation (319) has not been fully explored. Instead, an approximate criterion

$$(\alpha_g \rho_f v_g + \alpha_f \rho_g v_f)/(\alpha_g \rho_f + \alpha_f \rho_g) = \pm a_{HE} \tag{333}$$

has been applied extensively and has produced good code/data comparisons. Equation (333) can be derived from Equation (319) by neglecting the third term in D and setting C = 0 (stratified) on the right side of Equation (319) and C = ∞ (homogeneous) on the left side. Because of extensive experience with this approximate model, Equation (333) is currently used in RELAP5/MOD2 choked flow calculations.

At each time step and at each flow junction where two-phase cocurrent flow exists, the choking criterion [Equation (333)] is checked using explicitly calculated values. When choking occurs, Equation (333) is solved semi-implicitly with the upstream vapor and liquid momentum equations for v_g, v_f, and P_t, throat pressure, at the point of flow choking (upstream is with reference to v_g and v_f). As P_t is not needed in system calculations, we can eliminate $\partial P/\partial x$ from the vapor and liquid momentum equations to obtain

$$\rho_g\left(\partial v_g/\partial t + 1/2\ \partial v_g^2/\partial x\right) - \rho_f\left(\partial v_f/\partial t + 1/2\ \partial v_f^2/\partial x\right)$$

$$= \rho_g - \rho_f B_x + \Gamma_g(v_I - \alpha_f v_g - \alpha_g v_f)/\alpha_f \alpha_g$$

$$- \rho_g v_g F_{WG} + \rho_f v_f F_{WF} - \rho_f \rho_g (v_g - v_f)\, F_I$$

$$- C\, \rho a (v_g - v_f)/\partial t \quad . \tag{334}$$

The finite-difference form of this equation is obtained by integrating with respect to the spatial variable from the upstream volume center to the junction. In this finite-difference equation, all junction velocities are evaluated implicitly;[72] a_{HE}^{n+1} is approximated by

$$a_{HE}^{n+1} = a_{HE}^{n} + (\partial a_{HE}/\partial P)\ (P^{n+1} - P^{n}) \tag{335}$$

where P is the upstream volume pressure. The finite-difference equations corresponding to Equations (333) and (334) can be solved for v_g^{n+1} and v_f^{n+1} in terms of P^{n+1} and old time values.

In the case of subcooled choking, the choking criterion [Equation (333)] and the velocity equation [Equation (334)] reduce to

$$v_f = v_g = \pm v_c \quad . \tag{336}$$

Here, v_c is determined according to the procedures described previously. The frictional pressure losses and gravity head, which do not appear in ideal Equation (325) are properly taken into account in the actual calculation.

In general, there is a large drop in critical velocity when the fluid changes from a subcooled state to a two-phase state. This sudden change often leads to unrealistic velocity oscillations and causes the time step size to be reduced considerably. To provide a smooth transition from subcooled to two-phase, a transition region is defined as in the low void region. Within the transition region, an underrelaxation scheme,

$$v_g^{n+1} = v_g^n + 0.1\left(v_g^{n+1} - v_g^n\right)$$

$$v_f^{n+1} = v_f^n + 0.1\left(v_f^{n+1} - v_f^n\right) \tag{337}$$

is implemented. Experience with this scheme indicates that it works satisfactorily.

3.1.4.2 Horizontal Stratification Entrainment Model. Under stratified conditions in horizontal components, the void fraction of flow through a junction may be different from the upstream volume void fraction. Consequently, the regular donoring scheme for junction void fraction is no longer appropriate because vapor may be pulled through the

junction and liquid may also be entrained and pulled through the junction. The correlations describing the onset of vapor pull through and liquid entrainment for various geometrical conditions were summarized by Zuber.[73]

The incipient liquid entrainment is determined by the criterion that

$$v_g \geq v_{ge} \tag{338}$$

where, v_{ge} is given by the expressions

$$v_{ge} = 5.7 \left(\frac{D-\ell\ell}{d}\right)^{3/2} \left[\frac{B_y (\rho_f-\rho_g) (D-\ell\ell)}{\rho_g}\right]^{1/2} \tag{339}$$

for an upwardly oriented junction[73], and

$$v_{ge} = 3.25 \left(\frac{D/2-\ell\ell}{d}\right)^{2} \left[\frac{B_y (\rho_f-\rho_g) (D/2-\ell\ell)}{\rho_g}\right]^{1/2} \tag{340}$$

for a centrally oriented junction,[74,75] where d is the junction diameter and $\ell\ell$ is the liquid level.

The condition for the onset of vapor pull-through is determined by the criterion

$$v_f > v_{fp} \tag{341}$$

where

$$v_{fp} = 3.25 \left[\frac{\ell\ell - D\zeta/2}{d}\right]^{5/2} \left[\frac{B_y (\rho_f - \rho_g)d}{\rho_f}\right]^{1/2} \tag{342}$$

and where

ζ = 1 for a centrally located or side junction

ζ = 0 for downward oriented junction.[76,77]

Equations (338) through (342) together with the horizontal stratification criterion [Equation (172)] from Section 3.1.3.1, form the basis for calculating the junction void fraction under stratification conditions.

For liquid entrainment, the junction liquid fraction, $\alpha_{f,j}$, is related to the donor volume liquid fraction, $\alpha_{f,K}$, by the expression

$$\alpha_{f,j} = \alpha_{f,K} \left[1 - \exp\left(-C_1 v_g / v_{ge} - 10 v_g^2 / v_{gL}^2\right)\right] \quad (343)$$

where v_{gL} is from Equation (173). For vapor pull-through, the junction void fraction, $\alpha_{g,j}$, is given by the expression

$$\alpha_{g,j} = \alpha_{g,K} \left[1 - \exp\left(-C_2 v_f / v_{fp} - 10 v_g^2 / v_{gL}^2\right)\right] \quad . \quad (344)$$

The constants C_1 and C_2 for Equations (343) and (344) are obtained by comparisons of code calculations with experimental data.[78-80] Currently, C_1 and C_2 are both equal to 1.

3.1.4.3 Abrupt Area Change. The general reactor system contains piping networks with many sudden area changes and orifices. To apply the RELAP5 hydrodynamic model to such systems, analytical models for these components have been developed.[81] The basic hydrodynamic model is formulated for slowly varying (continuous) flow area variations; therefore, special models are not required for this case.

The abrupt area change model discussed here and developed in detail in Reference 81, is based on the Bourda-Carnot[82] formulation for a sudden enlargement and standard pipe flow relations, including the vena-contracta effect for a sudden contraction or an orifice or both. Quasi-steady continuity and momentum balances are employed at points of abrupt area change. The numerical implementation of these balances is such that hydrodynamic losses are independent of upstream and downstream nodalization. In effect, the quasi-steady balances are employed as jump conditions that couple fluid components having abrupt changes in cross-sectional area. This coupling process is achieved without change to the basic linear semi-implicit numerical time-advancement scheme.

3.1.4.3.1 Abrupt Area Change Modeling Assumptions--The basic assumption used for the transient calculation of two-phase flow in flow passages with points of abrupt area change is: the transient flow process can be approximated as a quasi-steady flow process that is instantaneously satisfied by the upstream and downstream conditions (that is, transient inertia, mass, and energy storage are neglected at abrupt area changes). However, the upstream and downstream flows are treated as fully transient flows.

There are several bases for the above assumption. A primary consideration is that available loss correlations are based on data taken during steady flow processes; however, transient investigations[83] have verified the adequacy of the quasi-steady assumption. The volume of fluid and associated mass, energy, and inertia at points of abrupt area change is generally small compared with the volume of upstream and downstream fluid components. The transient mass, energy, and inertia effects are approximated by lumping them into upstream and downstream flow volumes. Finally, the quasi-steady approach is consistent with modeling of other important phenomena in transient codes (that is, heat transfer, pumps, and valves).

3.1.4.3.2 Review of Single-Phase Abrupt Area Change Models--The modeling techniques used for dynamic pressure losses associated with abrupt area change in a single-phase flow are reviewed briefly before discussing

the extension of these methods to two-phase flows. In a steady incompressible flow, losses at an area change are modeled by the inclusion of an appropriate dynamic head loss term, h_L, in the one-dimensional modified Bernoulli equation

$$(v^2/2 + P/\rho)_1 = (v^2/2 + P/\rho)_2 + h_L \quad . \tag{3-67}$$

The particular form of the dynamic head loss is obtained by employing the Bourda-Carnot[82] assumption for calculating losses associated with the expansion part of the flow process. Losses associated with the contracting part of the flow process are small relative to the expansion losses, and are neglected.

The most general case of an abrupt area change is a contraction with an orifice at the point of contraction. Such a configuration is shown in Figure 13. Three area ratios are used throughout this development. The first is the contraction area ratio at the vena-contracta relative to the minimum physical area, $\varepsilon_c = A_c/A_T$. The second is the ratio of the minimum physical area to the upstream flow area, $\varepsilon_T = A_T/A_1$. The third is the ratio of the downstream to upstream area, $\varepsilon = A_2/A_1$.

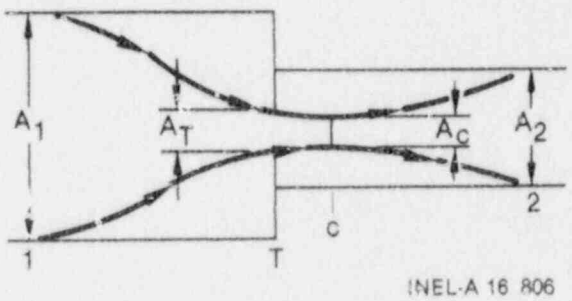

Figure 13. Orifice at abrupt area change.

The loss associated with the contracting fluid stream from Station 1 to c (the point of vena-contracta) is neglected [measurements indicate that the contracting flow experiences a loss no larger than $\Delta P_f \sim 0.05$

$(1/2\ \rho v_c^2)$ where v_c is the velocity at the vena-contracta whereas the dynamic pressure loss associated with the expansion from the vena-contracta to the downstream section is given by

$$\Delta P_f = 1/2\ \rho(1 - A_c/A_2)^2\ v_c^2 \quad . \tag{346}$$

The contraction ratio, $\varepsilon_c = A_c/A_T$, is an empirical function of $\varepsilon_T = A_T/A_1$. Using the continuity equations, $v_c = \frac{A_T v_T}{A_c} = v_T/\varepsilon_c$, and $v_T = \frac{A_2 v_2}{A_T} = \frac{\varepsilon}{\varepsilon_T} v_2$, Equation (346) can be written as

$$\Delta P_f = 1/2\ \rho \left(1 - \frac{\varepsilon}{\varepsilon_c \varepsilon_T}\right)^2 v_2^2 \quad . \tag{347}$$

Equation (347) is applicable to all the cases of interest. For a pure expansion, $\varepsilon_T = 1$, $\varepsilon_c = 1$, and $\varepsilon > 1$; for a contraction, $\varepsilon_T = \varepsilon < 1$ and $\varepsilon_c < 1$. Each of these is a special case of Equation (347). The two-phase dynamic pressure loss model is based on an adaptation of the general single-phase head loss given by Equation (347).

3.1.4.3.3 Two-Phase Abrupt Area Change Model--The two-phase flow through an abrupt area change is modeled in a manner very similar to that for single-phase flow by defining phasic flow areas. The two phases are coupled through the interphase drag, a common pressure gradient, and the requirement that the phases coexist in the flow passage.

The one-dimensional phasic stream-tube momentum equations are given in Section 3.1.1.1. The flow at points of abrupt area change is assumed to be quasi-steady and incompressible. In addition, the terms in the momentum equations due to body force, wall friction, and mass transfer are assumed to be small in the region affected by the area change. The interphase drag terms are retained since the gradient in relative velocity can be large at points of abrupt area changes.

Equations (5) and (6) can be integrated approximately for a steady incompressible, smoothly varying flow to obtain modified Bernoulli-type equations

$$\left(1/2\ \rho_f v_f^2 + P\right)_1 = \left(1/2\ \rho_f v_f^2 + P\right)_2 + \left(\frac{FI'}{\alpha_f}\right)_1 (v_{f1} - v_{g1})\ L_1$$

$$+ \left(\frac{FI'}{\alpha_f}\right)_2 (v_{f2} - v_{g2})\ L_2 \qquad (348)$$

and

$$\left(1/2\ \rho_g v_g^2 + P\right)_1 = \left(1/2\ \rho_g v_g^2 + P\right)_2 + \left(\frac{FI'}{\alpha_f}\right)_1 (v_{g1} - v_{f1})\ L_1$$

$$+ \left(\frac{FI'}{\alpha_f}\right)_2 (v_{g2} - v_{f2})\ L_2 \qquad (349)$$

where $FI' = \alpha_f\ \alpha_g\ \rho_f\ \rho_g\ FI$. The interphase drag is divided into two parts associated with the upstream and downstream parts of the flow affected by the area change.

3.1.4.3.4 General Model--Consider the application of Equations (348) and (349) to the flow of a two-phase fluid through a passage having a generalized abrupt area change (the flow passage shown in Figure 14[a]). Here, the area A_T is the throat or minimum area associated with an orifice located at the point of the abrupt area change. Since each phase is governed by a modified Bernoulli-type equation, it is reasonable to assume that losses associated with changes in the phasic flow area can be modeled by separate dynamic pressure loss terms for both the

---

a. In Figure 14, the flow is shown as a separated flow for clarity. The models developed are equally applicable to separated and dispersed flow regimes.

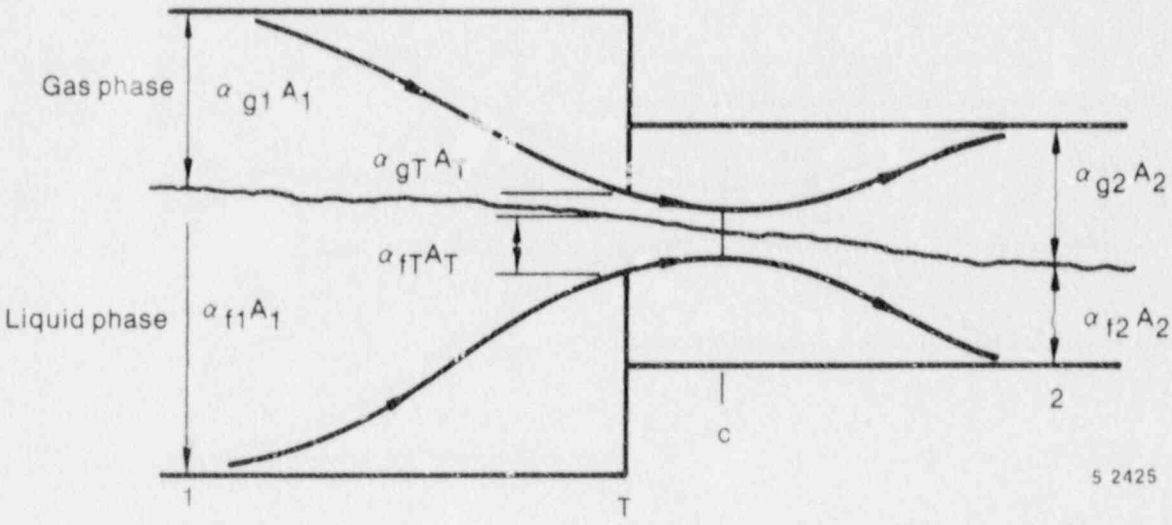

Figure 14. Schematic flow of two-phase mixture at abrupt area change.

liquid and gas phases. Hence, we assume that the liquid sustains a loss as if it alone (except for interphase drag) were experiencing an area change from $\alpha_{f1} A_1$ to $\alpha_{fT} A_T$ to $\alpha_{f2} A_2$, and the gas phase experiences a loss as if it alone were flowing through an area change from $\alpha_{g1} A_1$ to $\alpha_{gT} A_T$ to $\alpha_{g2} A_2$. The area changes for each phase are the phasic area changes (see Figure 14). When the losses for these respective area changes [based on the Bourda-Carnot model and given by Equation (347)] are added to Equations (348) and (349), the following phasic momentum equations are obtained

$$\left(1/2\ \rho_f v_f^2 + P\right)_1 = \left(1/2\ \rho_f v_f^2 + P\right)_2 + 1/2\ \rho_f \left(1 - \frac{\alpha_{f2}\ \varepsilon}{\alpha_{fT}\ \varepsilon_{fc}\ \varepsilon_T}\right)^2 (v_{f2})^2$$

$$+ \left(\frac{FI'}{\alpha_f}\right)_2 (v_{f1} - v_{g1})\ L_1 + \left(\frac{FI'}{\alpha_f}\right)_2 (v_{f2} - v_{g2})\ L_2 \qquad (350)$$

and

$$\left(1/2\ \rho_g v_g^2 + P\right)_1 = \left(1/2\ \rho_g v_g^2 + P\right)_2 + 1/2\ \rho_g \left(1 - \frac{\alpha_{f2}\ \varepsilon}{\alpha_{gT}\ \varepsilon_{gc}\ \varepsilon_T}\right)^2 (v_{g2})^2$$

$$+\left(\frac{FI'}{\alpha_g}\right)_2 (v_{g1} - v_{f1})\, L_1 + \left(\frac{FI'}{\alpha_g}\right)_2 (v_{g2} - v_{f2})\, L_2 \quad . \quad (351)$$

These phasic momentum equations are used across an abrupt area change. In Equations (350) and (351), ε_{fc} and ε_{gc} are the same tabular function of area ratio as in the single-phase case except the area ratios used are the phasic area ratios

$$\varepsilon_{fT} = (\alpha_{fT}/\alpha_{f1})\, \varepsilon_T \quad (352)$$

and

$$\varepsilon_{gT} = (\alpha_{gT}/\alpha_{g1})\, \varepsilon_T \quad (353)$$

respectively. The area ratios, $\varepsilon = A_2/A_1$ and $\varepsilon_T = A_T/A_1$, are the same as for single-phase flow.

The interphase drag effects in Equations (350) and (351) are important. These terms govern the amount of slip induced by an abrupt area change, and if they are omitted, the model will always predict a slip at the area change appropriate to a completely separated flow situation and give erroneous results for a dispersed flow.

3.1.4.3.5 Model Application--A few remarks concerning the way Equations (350) and (351) are applied to expansions and contractions, both with and without an orifice, are necessary. In a single-phase steady flow situation, given the upstream conditions, v_1 and P_1, using the continuity equation ($v_1A_1 = v_2A_2$) and Equation (345) one can solve for v_2 and P_2. Equations (350) and (351) along with the two phasic continuity equations can be used in a similar manner except now the downstream void fraction is an additional unknown which must be determined.

3.1.4.3.5.1 Expansion--For the purpose of explanation, consider the case of an expansion ($\alpha_{fT} = \alpha_{f1}$, $\varepsilon > 0$, $\varepsilon_T = 1$, $\varepsilon_{fc} = \varepsilon_{gc} = 1$, $FI'_1 = 0$, $L1 = 0$) for which Equations (350) and (351) reduce to

$$\left(1/2\ \rho_f v_f^2 + P\right)_1 = \left(1/2\ \rho_f v_f^2 + P\right)_2 + 1/2\ \rho_f \left(1 - \frac{\alpha_{f2}\varepsilon}{\alpha_{f1}}\right)^2 (v_{f2})^2 + \left(\frac{FI'}{\alpha_f}\right)_2 (v_{f2} - v_{g2})\ L_2 \tag{354}$$

and

$$\left(1/2\ \rho_g v_g^2 + P\right)_1 = \left(1/2\ \rho_g v_g^2 + P\right)_2 + 1/2\ \rho_g \left(1 - \frac{\alpha_{g2}\varepsilon}{\alpha_{g1}}\right)^2 (v_{g2})^2 + \left(\frac{FI'}{\alpha_g}\right)_2 (v_{g2} - v_{f2})\ L_2 \tag{355}$$

These two equations with the incompressible continuity equations

$$\alpha_{f1} v_{f1} A_1 = \alpha_{f2} v_{f2} A_2 \tag{356}$$

and

$$\alpha_{g1} v_{g1} A_1 = \alpha_{g2} v_{g2} A_2 \tag{357}$$

are a system of four equations having four unknowns, α_{f2} ($\alpha_{g2} = 1 - \alpha_{f2}$), v_{f2}, v_{g2}, and P_2, in terms of the upstream conditions, α_{f1} ($\alpha_{g1} = 1 - \alpha_{f1}$), v_{f1}, v_{g1}, and P_1. (The interphase drag, FI', is a known function of the flow properties.) It is important to note that the downstream value of the liquid fraction (α_{f2}) is an additional unknown compared with the

single-phase case and is determined (with the downstream velocities and pressure) by simultaneous solution of Equations (354), (355), (356), and (357) without additional assumptions. It is reassuring that by taking a proper linear combination of Equations (350) and (351) the usual overall momentum balance obtained using the Bourda-Carnot[82] assumption can be obtained.[84-85]

If, as in the cited literature,[84-87] only the overall momentum balance is used at an expansion, there will be an insufficient number of equations to determine all the downstream flow parameters, α_{f2}, v_{f2}, v_{g2}, and P_2. The indeterminacy has been overcome in cited works by means of several different assumptions concerning the downstream void fraction.[a] In the model developed here [Equations (354) and (355)], division of the overall loss into liquid and gas parts, respectively, results in sufficient conditions to determine all downstream flow variables including α_{f2}. In addition, the present model includes force terms due to interphase slip in Equations (354) and (355), which are necessary to predict the proper amount of slip and void redistribution that occurs at points of area change.

3.1.4.3.5.2 Contraction--Consider the application of Equations (353) and (354) to a contraction. To determine both the downstream conditions and throat conditions from the upstream values of $\alpha_{f1}(\alpha_{g1})$, v_{f1}, v_{g1}, and P_1, an additional consideration needs to be made. To obtain the throat values, apply the momentum equations valid for the contracting section of flow (here, the L_1 portion of the interphase force is associated with the contraction)

$$\left(1/2\ \rho_f v_f^2 + P\right)_1 = \left(1/2\ \rho_f v_f^2 + P\right)_T + \left(\frac{FI'}{\alpha_f}\right)_1 (v_{f1} - v_{g1})\ L_1 \qquad (358)$$

---

a. J. G. Collier[84] mentions three different assumptions that have been used: (i) $\alpha_{f2} = \alpha_{f1}$, (ii) α_{f2} is given by a homogeneous model, and (iii) α_{f2} is given by the Hughmark void fraction correlation.

$$\left(1/2\ \rho_g v_g^2 + P\right)_1 = \left(1/2\ \rho_g v_g^2 + P\right)_T + \left(\frac{FI'}{\alpha_f}\right)_1 (v_{g1} - v_{f1})\ L_1 \qquad (359)$$

$$\alpha_{f1} v_{f1} A_1 = \alpha_{fT} v_{fT} A_T \qquad (360)$$

$$\alpha_{g1} v_{g1} A_1 = \alpha_{gT} v_{gT} A_T \ . \qquad (361)$$

These four equations are solved simultaneously for the values of $\alpha_{fT}(\alpha_{gT})$, v_{fT}, v_{gT}, P_T at the throat section (the minimum physical area). No additional or special assumptions are made concerning the throat conditions since they follow as a direct consequence of the unique head loss models for each phase. After the throat values have been obtained, the conditions at the point of vena-contracta are established assuming the void fraction is the same as at the throat. Thus, ε_{fc} and ε_{gc} are established using the tabular function in Appendix A of Reference 81 and the throat area ratios, ε_{fT} and ε_{gT}, defined by Equations (352) and (353). To determine the downstream values, Equations (350) and (351) can be applied directly from Stations 1 to 2 with the throat values known or the expansion loss equations can be used from the throat section to Station 2. Both approaches produce identical downstream solutions. As in the case of an expansion, because the proper upstream and downstream interphase drag is included, this modeling approach establishes the phase slip and resulting void redistribution. An orifice at an abrupt area change is treated exactly as the contraction explained above (that is, with two separate calculations to establish first the throat and then the downstream flow variables).

3.1.4.3.5.3 Countercurrent Flow--The preceding development implicitly assumed a cocurrent flow. For countercurrent flow, Equations (350) and (351) are applied exactly as in cocurrent flow except the upstream sections for the respective phases are located on different sides of the abrupt area change. The difference appears in how the throat and downstream voids are determined. To determine the throat properties, equations similar to Equations (358), (359), (360), and (361) are used with the upstream values appropriate for each phase. These four equations are

then solved for $\alpha_{fT}(\alpha_{gT})$, v_{fT}, v_{gT}, and P_T. To determine the downstream values for each phase, only the head loss terms are needed for the downstream voids (the downstream v_f, v_g, and P do not appear). For countercurrent flow, these voids are set such that the downstream void of each phase plus the upstream void of the opposite phase adds to one (both phases together must fill the flow channel). With the throat and downstream voids now known, Equations (350) and (351) can be used directly to determine the total loss for each phase at the abrupt area change.

3.1.4.4 Crossflow Junction. The RELAP5 numerical scheme is generally formulated using one-dimensional elements. However, there are several applications where an approximate treatment of crossflow provides an improved physical simulation. Three different applications for a crossflow formulation are described in the following paragraphs.

The first application concerns a small crossflow between two essentially axial flow streams. This situation is typical of regions such as a reactor core or a steam generator because the component geometry provides a large resistance to crossflow and a small resistance to axial flow. Hence, simplified crossflow momentum equations can be used to couple a hot flow channel to a bulk flow channel.

The second application of a crossflow junction is to provide a tee model. In this case, the momentum flux in the side branch is assumed to be perpendicular to the main stream and thus the main stream momentum flux does not contribute to the crossflow momentum formulation.

The third application is modeling of leak flow paths. In this case, the flow is small and governed primarily by pressure differential, gravity and flow resistance. Thus the momentum flux terms can be neglected.

The vapor momentum finite difference equation used in the basic numerical scheme is

$$(\alpha_g\rho_g)_j^n\,(v_g^{n+1} - v_g^n)_j\,\Delta x_j^n + \frac{1}{2}(\alpha_g\rho_g)_j^n\left[(v_g^2)_L^n - (v_g^2)_K^n\right]\Delta t + \text{VISCOUS TERMS}$$

$$= - \alpha_{g,j}^{n}(P_L^{n+1} - P_K^{n+1})\Delta t$$

$$- (\alpha_g \rho_g)_j^n \left[(FWG_K^n + FWG_L^n)\Delta x_j + HLOSSG_j^n\right] v_{g,j}^{n+1} \Delta t$$

$$- (\alpha_g \rho_g)_j^n FIG_j^n (v_{g,j}^{n+1} - v_{f,j}^{n+1})\Delta x_j \Delta t + (\alpha_g \rho_g)_j^n B_x \Delta x_j \Delta t$$

ADDED MASS + MASS TRANSFER MOMENTUM

+ HORIZONTAL STRATIFIED PRESSURE GRADIENT EFFECT (362)

where

$$\Delta x_j = \frac{1}{2}(\Delta x_K + \Delta x_L) \quad . \tag{363}$$

A parallel equation holds for the liquid phase. It should be noted that the momentum Equation (362) is in reality the sum of half the K cell momentum plus half the L cell momentum. This is the reason for Equation (363).

There are two areas in which the crossflow modeling affects the numerical scheme. One concerns the approximations made in the junction momentum equations the other concerns the volume average velocities in a volume.

If the junction is to model crossflow perpendicular to the main or axial-flow direction then the volume average velocity in the K and L cells, which represent the axial flow velocity, should not include crossflow junction velocity components. For the simple leak flow situation shown in Figure 15, this requires that $v_{J,3}$ not be included in the volume average (axial) velocity calculation for Cell L.

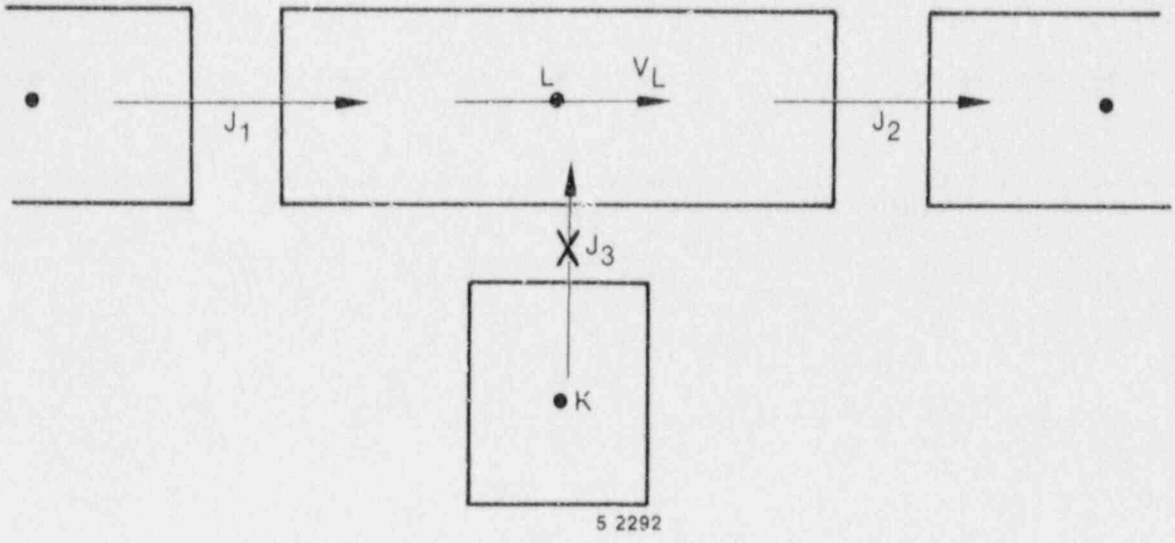

Figure 15. Simplified tee crossflow.

The second area of numerical modification relates to the reduced form of the momentum equations to be used at a crossflow junction. In crossflow junctions, just as in the normal junctions, the cross product momentum flux terms are neglected, i.e., there is no x-direction transport of momentum due to the y velocity.

For the case of a small crossflow junction between two axial-flow streams (J2 in Figure 16) all the geometric input (AVOL, DX, DZ) for both of the volumes relates to the axial flow direction as does the wall drag and code calculated form losses. Since the crossflow has a different flow geometry and resistance (for example, crossflow resistance in a rod bundle) the friction and form losses must be user input and must be appropriate for the crossflow direction geometry. For crossflow junctions the user input form losses should include all crossflow resistance (form losses and wall drag). The normal terms representing wall drag and abrupt area change losses are not included in the formulation of the momentum equation at a crossflow junction as these refer to the axial properties of the K and L volumes.

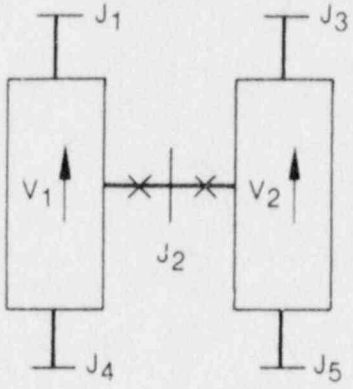

Figure 16. Modeling of crossflows or leak.

Since the connecting K and L volumes are assumed to be predominately axial-flow volumes, the crossflow junction momentum flux (related to the axial volume velocity in K and L) is neglected along with the associated numerical viscous term. In addition, the horizontal stratified pressure gradient is neglected.

All lengths and elevation changes in the one-dimensional representation are based upon the axial geometry of the K and L volumes and the crossflow junction is assumed to be perpendicular to the axial direction and of zero elevation change, thus, no gravity force term is included.

The resulting vapor momentum finite difference equation for a crossflow junction is

$$(\alpha_g \rho_g)_j^n (v_g^{n+1} - v_g^n)_j \Delta x_j = - \alpha_{g,j}^n (P_L - P_K)^{n+1} \Delta t - (\alpha_g \rho_g)_j^n \, HLOSSG_j^n \, v_{g,j}^{n+1} \Delta t$$

$$- (\alpha_g \rho_g)_j^n \, FIG_j^n \, (v_{g,j}^{n+1} - v_{f,j}^{n+1}) \Delta x_j \Delta t$$

$$+ \text{ADDED MASS} + \text{MASS TRANSFER MOMENTUM} \quad . \qquad (364)$$

A similar equation can be written for the liquid phase. In Equation (364), $HLOSSG_j^n$ contains only the user input crossflow

resistance. The Δx_j term that is used to estimate the inertial length associated with crossflow is defined using the diameters of volumes K and L,

$$\Delta x_j = \frac{1}{2} [D(K) + D(L)] \quad . \tag{365}$$

The crossflow option can be used with the crossflow junction perpendicular to the axial flow in Volume L (or K) but parallel to the axial flow in Volume K (or L) (see Figure 15). Here, the situation regarding the half cell momentum contribution in Volume L is the same as described above. The half cell momentum contribution associated with Volume K is the same as for a normal junction. Hence, this crossflow junction has all the terms in Equation (362) except that; (a) wall friction, momentum flux, and gravity only include the K cell contribution, (b) the $HLOSSG_j^n$ term is only the user input loss and (c) the Δx used in the inertial term and interphase drag includes the normal K cell contribution and a term of the form in Equation (365) for the L cell. This type of crossflow modeling can be used for a 90 degree tee simulation.

For leak flows and minor flow paths the modeling approach shown in Figure 17 is recommended. Here, J_3 is the normal flow path, whereas Junction J_1, Volume M, and Junction J_2 represent the leak flow path. Junctions J_1 and J_2 should be modeled as tee junctions described above. The only reason for using Volume M is to obtain a correct representation of the gravity head from K to L. If a crossflow junction were modeled directly between Volumes K and L then there would be no gravity head in the leak flow junction equation. Leak paths may also be modeled using a crossflow junction that is perpendicular to both the K and L volumes when the leak flow is between volumes having the same volume center elevation.

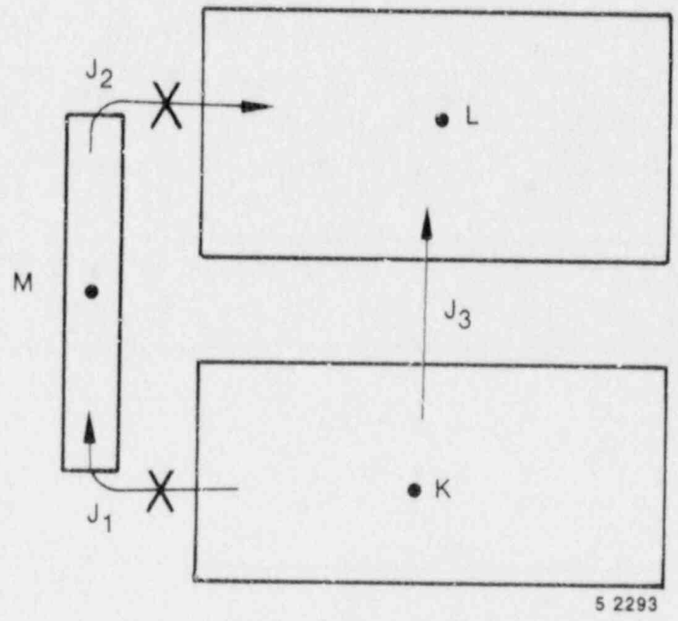

Figure 17. Leak flow modeling.

3.1.4.5 Vertical Stratification Model. The vertical stratification model has been installed so that the nonequilibrium modeling capability can include repressurization transients in which subcooled liquid and superheated vapor may coexist in the pressurizer and/or other locations in the primary coolant system. A preliminary version[88] of this model has been modified, and this modified version is described in this section.

For this model, a vertically stratified flow regime is included in the vertical flow regime map as shown in Figure 6. A vertical volume is detected as being vertically stratified when the difference between the void fraction in the volume above and that in the volume below is >0.50.

The criterion is based on the Taylor bubble velocity in Reference 28. Calculated first is the factor F,

$$F = \left\{ \frac{v_g}{0.35\,[gD(\rho_f - \rho_g)/\rho_f]^{\frac{1}{2}}} \right\}^3 . \qquad (366)$$

If $F \leq 1$, then the vertical stratification model is not used and the normal vertical flow regime map is used. If $F > 1$, then a linear interpolation is used between the normal flow regime values and the vertical stratification flow regime values for the interphase mass transfer, wall heat transfer, and the interphase drag coefficients.

For a vertically stratified volume, the interphase mass transfer, wall heat transfer, and interphase drag coefficients are modified. The interphase mass transfer is given in terms of the interphase heat transfer [see Equation (25)]. The interphase heat transfer rate per unit volume (neglecting contribution from the wall) is given as

$$Q_{if} = h_{if} \frac{A_c}{V} (T^s - T_f) \tag{367}$$

$$Q_{ig} = h_{ig} \frac{A_c}{V} (T^s - T_g) \tag{368}$$

where h_{if} and h_{ig} are the liquid side and vapor side interface heat transfer coefficients, A_c is the cross-sectional flow area (equal to the interfacial area when stratified), and V is the volume. A value of 10 $W/m^2 \cdot K$ is used for both h_{if} and h_{ig} in the vertical stratification model. The wall heat transfer coefficients h_{wf} and h_{wg} are partitioned with respect to their corresponding vapor and liquid fractions (α_f and α_g) when vertical stratification occurs. For the junction above the vertically stratified volume, an interphase drag coefficient of 10^{-1} $N\text{-}s^2/m^5$ is used.

There is no specific edit information output for a vertically stratified volume.

3.1.4.6 Water Packing Mitigatior Scheme. Large pressure spikes that cannot be explained by known physical phenomena are at times encountered when Eulerian type codes are used to analyze integral systems tests or reactor accidents. These spikes usually do not affect overall transient behavior, but in some cases may affect important localized behavior (e.g. delivery of coolant to the reactor core). A water packing scheme has been installed to mitigate these spikes.

The water packing scheme closely follows the method used in the TRAC code.[89,90] It involves a detection scheme to determine when a pressure change occurs in a volume containing mostly liquid. It then imposes changes to the momentum equations, followed by a recalculation of the pressure solution using the sparse matrix solver.

The detection logic used in the water packing scheme evolved from experience gained in running a vertical fill problem.[91] The scheme requires a pressure increase of 0.23% or more, a void fraction (α_g) $\leq$0.12, the liquid temperature (T_f) to be less than the saturation temperature (T^s), the volume to be flagged as vertically stratified, and the volume above to be highly voided. Thus a legitimate water hammer would not be detected in the water packing scheme.

The next part of the scheme involves altering the momentum equations so that only small pressure changes will occur in the volume that fills with water. The scheme involves modifying the coefficient that multiplies the pressure change in the filling volume. The modification multiplies this coefficient by 10^6. This is discussed in more detail in the next paragraph. Since the pressure solution is rejected when water packing occurs, the pressure calculation is repeated using the sparse matrix solver.

The finite difference form of the phasic momentum equations used can be written

$$v_{f,j}^{n+1} = v_{f,j}^{n,exp} - (VFDP)_j^n \left[(P_L^{n+1} - P_L^n) - (P_K^{n+1} - P_K^n) \right] \quad (369)$$

$$v_{g,j}^{n+1} = v_{g,j}^{n,exp} - (VGDP)_j^n \left[(P_L^{n+1} - P_L^n) - (P_K^{n+1} - P_K^n) \right] \quad (370)$$

where $v_{f,j}^{n,exp}$ and $v_{g,j}^{n,exp}$ contain all the old time terms and $(VFDP)_j^n$ and $(VGDP)_j^n$ contain all the terms that multiply the pressure change. Consider the filling example in Figure 18 where Volume K is full of liquid and Volume L is full of steam. The change to the momentum equations is to multiply the $(P_K^{n+1} - P_K^n)$ terms by 10^6, which forces P_K^{n+1} to be approximately the same as P_K^n. Thus, the water filled K volume will not show a pressure spike. The momentum equations then have the form

$$v_{f,j}^{n+1} = v_{f,j}^{n,exp} - (VFDP)_j^n (P_L^{n+1} - P_L^n) + (VFDP)_j^n (10^6) (P_K^{n+1} - P_K^n) \quad (371)$$

$$v_{g,j}^{n+1} = v_{g,j}^{n,exp} - (VGDP)_j^n (P_L^{n+1} - P_L^n) + (VGDP)_j^n (10^6) (P_K^{n+1} - P_K^n) \quad (372)$$

In addition to the modification of the momentum equation, the interphase drag is reduced to 10^{-1} $(N - s^2)/m^5$ for Junction j.

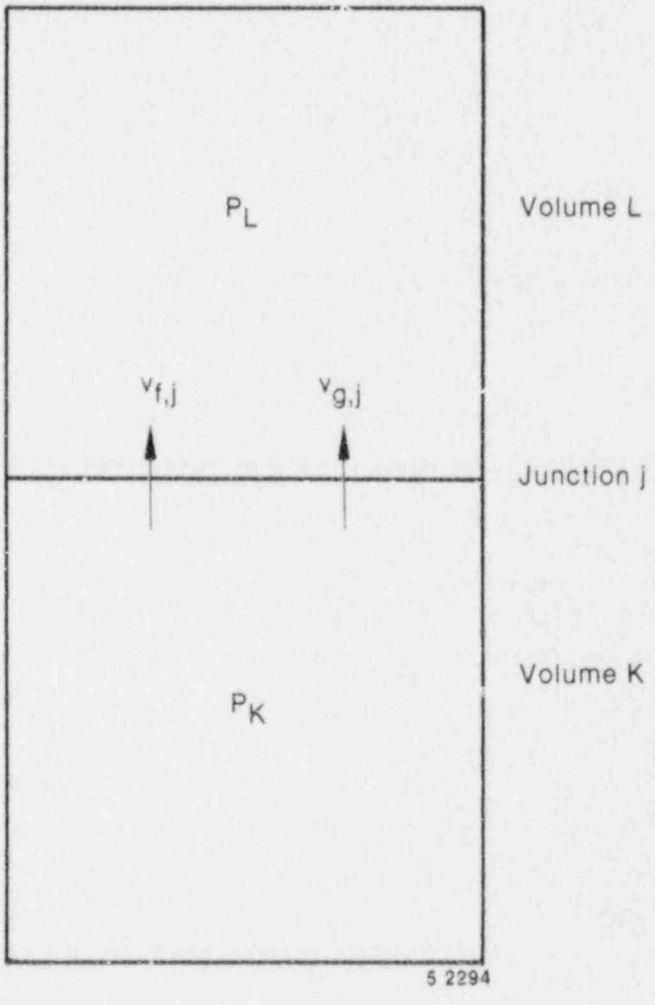

Figure 18. Two vertical vapor/liquid volumes.

3.1.5 Component Models

RELAP5 consists of a variety of generic models which are used to build system models. These include the pipe, annulus, branch, single volume, single junction, etc. These will be discussed in more detail in Volume 2

of this manual. The general philosophy has been to avoid system component models such as pressurizer, steam generator, core, etc. However, certain subsystem components are unavoidable due to unique processes or performance. RELAP5 contains models for subsystem components such as a branch, separator, jet mixer, pump, turbine, valve, and accumulator. A brief summary of each of these models is included here.

3.1.5.1 Branch. The branch component is a model designed for convenient interconnection of hydrodynamic components. The identical result can be obtained by using a single volume component and several single junction components. Thus the branch is a separate component only in the input processing scheme.

In RELAP5/MOD2 the crossflow junction has been added in which the junction velocities are assumed to be normal to the one-dimensional flow path of the hydrodynamic volume. Thus, the branch component can include multiple connections at the inlet, outlet, or in the crossflow direction.

Specialized modeling considerations are applied to any volume having multiple junctions connected at either volume end (the ends of a hydrodynamic volume are the inlet and outlet as defined in Section 3.1.1.1).

These special calculations include both the method for calculating the volume average velocities and the method for partitioning the volume cross-sectional area between the multiple inlet or multiple outlet junctions. The partitioned volume areas are used both in the abrupt area change model to calculate junction kinetic loss factors and in the momentum equations to simulate the stream-tube area.

In applications, the multiple junction and crossflow models are used in three distinct ways to model branching flows. These are the one-dimensional branching, a tee branch, and a crossflow branch. Combination of the three basic branches may also occur. Each of the three basic models will be discussed in turn.

3.1.5.1.1 One-Dimensional Branching--This basic branch model is consistent with the one-dimensional approximation for a piping network and assumes that multidimensional effects at branches are small compared to system interaction effects. In the case of branched flows that occur in headers or plena, the model gives an accurate physical description of the flow division or merging process and the one-dimensional branch model is intended primarily for use in modeling such branched flows. Examples of such situations in LWR systems are flow division at the core inlet if parallel flow paths through the core are modeled, steam generator inlet and outlet plena when several parallel tube groups are modeled (for the effect of tube height and length), or at a wye connection.

The one-dimensional branch is illustrated in Figure 19 for a volume having two inlet junctions and one outlet junction. The Junctions J_1 and J_2 are the inlet junctions and Junction J_3 is the outlet junction. The multiple flows are assumed to merge in such a way that they come to the common velocity equal to the inlet volume average velocity for Volume V_3. The volume cross-sectional area is then divided in proportion to the volume flow of the respective inlet junctions. This method of apportioning volume cross-sectional area satisfies continuity but does not conserve momentum, particularly for high velocity differences between the merging streams (for flow splitting, however, the method does preserve momentum). For this reason the special jet mixer component was developed for merging flows having high relative velocities such as in a jet pump. The jet-mixer can be used for one-dimensional mixing, but is limited to two inlet streams and a single outlet stream (see Section 3.1.5.3 for a description of the jet mixer model). The volume partitioned areas are calculated as follows:

$$(A_K)_j = \left[\left|(\alpha_f)_j^n (v_f)_j^n\right| + \left|(\alpha_g)_j^n (v_g)_j^n\right|\right] A_j A_k \Big/$$

$$\sum_{i=J_1}^{J_N} \left[\left|(\alpha_f)_i^n (v_f)_i^n\right| + \left|(\alpha_g)_i^n (v_g)_i^n\right|\right] A_i \quad . \tag{373}$$

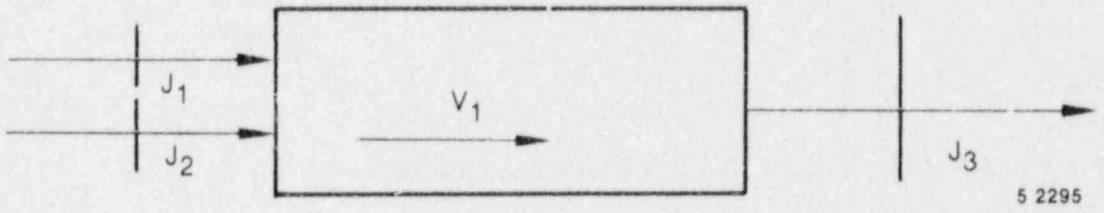

Figure 19. One-dimensional branch.

The apportioned volume areas for each junction are used with the abrupt area change model, Section 3.1.4.2, to calculate energy loss coefficients for the liquid and vapor streams at each junction.

3.1.5.1.2 Ninety-Degree Tee Model--The crossflow junction (see Section 3.1.4.4) is used to form a 90-degree tee as shown in Figure 15. In this particular application the side connection to the tee is modeled using a junction in which only one-half of the junction momentum equation has the crossflow form (the half of Junction J_3 associated with Volume V_L is a crossflow junction and is designated by an X, see Figure 15).

No special component is provided to accomplish the input associated with a model such as illustrated in Figure 15. The Volume V_L may be specified as a branch with the associated junctions or as a single volume with single junctions used to specify the connecting junctions. In either case, Junctions J_1 and J_2 should be specified as smooth unless actual abrupt changes in area occur at either junction. The Junction J_3 should be specified as smooth with a user input form loss factor to account for the turning and entrance losses. In addition, Junction J_3 must be specified so that the half of the junction associated with volume V_L is modeled as a crossflow junction and the half associated with Volume V_K is a normal junction. These options are specified through input of junction control flags.

It is also possible to model a 90-degree tee with the RELAP5/MOD2 code, however, unphysical numerical results have been obtained at times for reasons that are not fully understood. Thus, the 90-degree tee model described previously is recommended and is a closer approximation to the actual fluid momentum interaction which occurs at a tee.

3.1.5.1.3 Gravity Effects at a Tee--In some branching situations where the through flow is small or where the flow is constrained by the geometry, body force effects may be significant. Examples that occur in PWR systems are the cold leg connections to the inlet annulus and downcomer, and the hot leg connection to the upper plenum and core. This type of branched flow is modeled as shown in Figure 20. Here the vertical direction is modeled as the through flow direction (indicated by the volume orientation arrows). The cold or hot leg connections are modeled by crossflow junctions. The through flow direction of Volume V_3 is chosen to correspond to the major flow path. In the case of a PWR inlet annulus through flow in the horizontal direction is inhibited by the annular structure and in the case of the upper plenum to core connection the area for flow in the vertical direction is large compared to the flow area in the horizontal direction. Some judgment is required to select the orientation. However, the crossflow branch connection will permit through flow in the horizontal direction but with some accompanying pressure rise and drop associated with the fact that the momentum flux terms are neglected in the crossflow part of the junction.

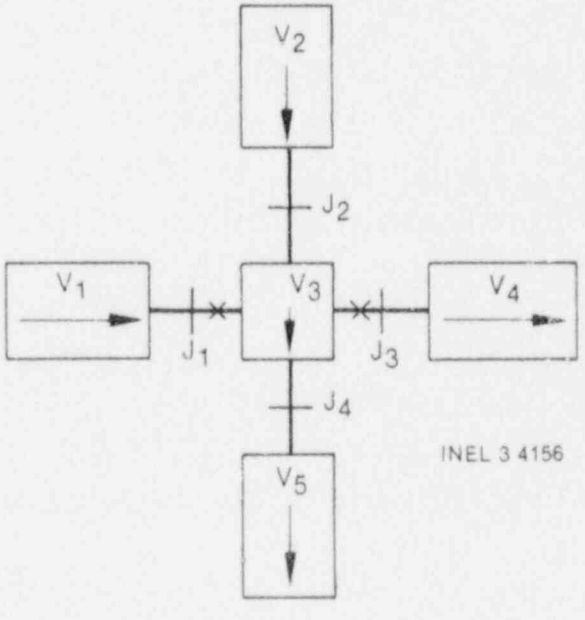

Figure 20. Gravity effects on a tee.

The model illustrated in Figure 20 has the additional advantage that the effect of vertical void gradients in the flow out of the horizontal connections may be more sharply defined as a result of the central volume, V_3, which has a vertical height equal to the diameter of branch Volumes V_1 and V_4.

No special component model is provided for modeling the vertical tee and either a branch or a single volume may be used for Volume V_3. The branch component is more convenient since all junctions connecting to Volume V_3 can be specified with the branch component.

3.1.5.1.4 Crossflow Branch--A fourth type of branched flow path can be created by the use of a crossflow junction to couple two volumes. This type of branch is used to model crossflow between parallel core channels and leak paths between volumes having centers at the same vertical elevation. The crossflow junction is assumed to have no elevation change, thus one limitation of this type of branch is that the volume centers that are coupled must be at the same elevation. If volumes of differing elevation are coupled, an input processing error will occur in the loop elevation checking routines. The application of the crossflow junction for cross flow or leak path modeling is illustrated in Figure 16. The length scale associated with the crossflow junction is one half the diameter of the K volume plus one half the diameter of the L volume. This length is only used for modeling the fluid inertia terms in the momentum equation and is always assumed to lie in a horizontal plane.

The pure crossflow branch is most easily modeled using a single junction component for the crossflow junction. However, either volume, V_1 or V_2 in Figure 16, can be modeled using the branch component and specifying the coupling junctions with that component.

3.1.5.2 Separator. The RELAP5 separator model is a nonmechanistic or black box model consisting of a special volume with junction flows as pictured in Figure 21. A steam-water inflowing mixture is separated by

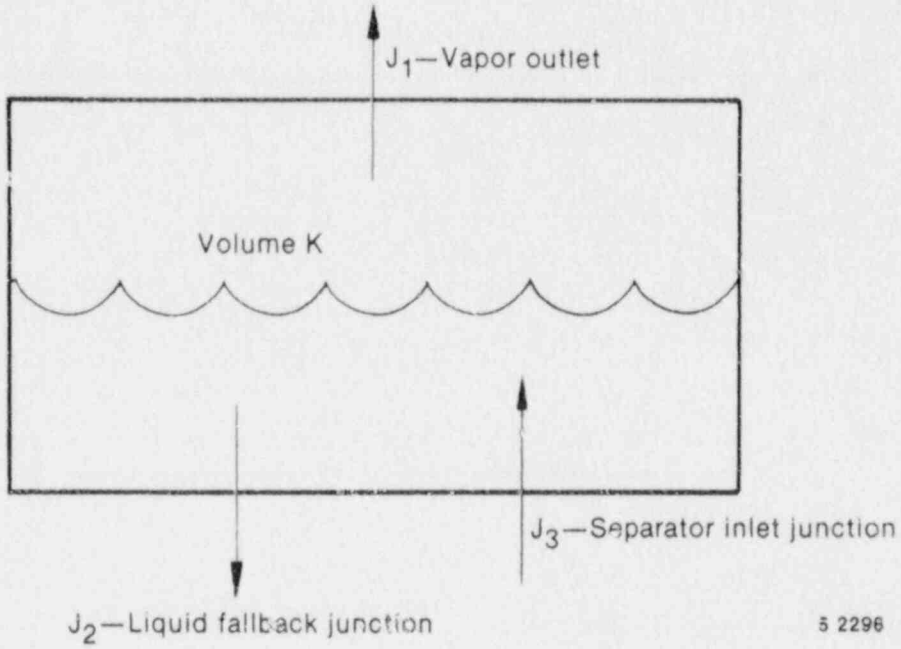

Figure 21. Typical separator volume and junctions.

defining the quality of the outflow streams using empirical functions. No attempt is made to model the actual separation process from first principles.

The separator vapor outlet performance is defined by means of a special function for the vapor void fraction at J_1. The donored junction vapor void fraction used to flux mass through the steam outlet is related to the vapor void fraction in the separator volume using the curve in Figure 22(a). For separator volume void fractions above the value of VOVER (an input parameter) a perfect separation is assumed and pure vapor is fluxed out Junction J_1. For separator volume void fractions less than VOVER a two phase mixture is fluxed out. The VOVER parameter governs the vapor void fraction of the outflow. If VOVER is small the vapor outflow corresponds to an ideal separator. IF VOVER equals 1.0 the vapor outlet junction behaves as a normal junction and the vapor outlet junction void fraction is equal to the separator volume average void fraction.

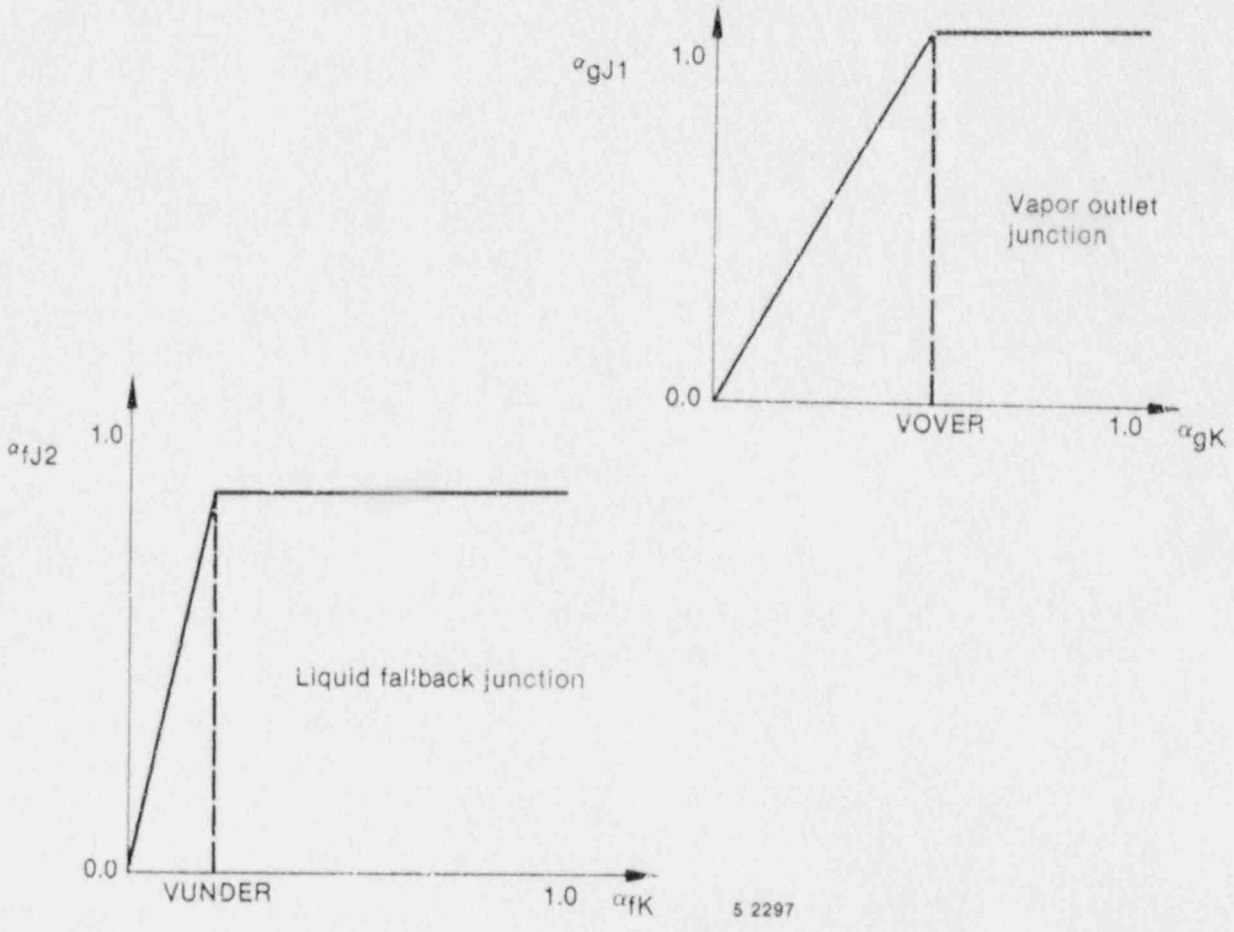

Figure 22. Donor junction voids for outflow.

The flow of the separator liquid drain junction is modeled in a manner similar to the steam outlet except pure liquid outflow is assumed when the volume void fraction is less than the value of VUNDER, see Figure 22(b). Normal donored fluxes are used for the separator inlet junction. Although the void fractions used to flux mass and energy from the separator volumes are modified the normal junction momentum equations are used to calculate the flow velocities.

3.1.5.3 Jet Mixer. There are several components in a typical reactor plant where the momentum effects due to the mixing of two parallel streams of fluid at different velocities may be important. An example of this is the jet pump in a BWR. In this component the pumping action is caused by

the momentum transfer between the two fluid streams. Momentum effects may also be important for mixing at ECC injection points or for the aspirators present in some steam generators. The JETMIXER component was developed for these cases.

3.1.5.3.1 Basic Jet Mixing Model--To derive the momentum equations needed to model a jet mixing situation, consider the schematic shown in Figure 23 which illustrates a mixing volume connected to a drive and a suction volume.[a] The suction junction (with velocity v_S and area A_S) connects the last upstream suction region volume, KS, to the mixing volume, L. The drive junction (with velocity v_D and area A_D) connects the last upstream drive line volume, KD, to the mixing volume, L. Figure 23 shows the drive junction as a smooth junction and the suction

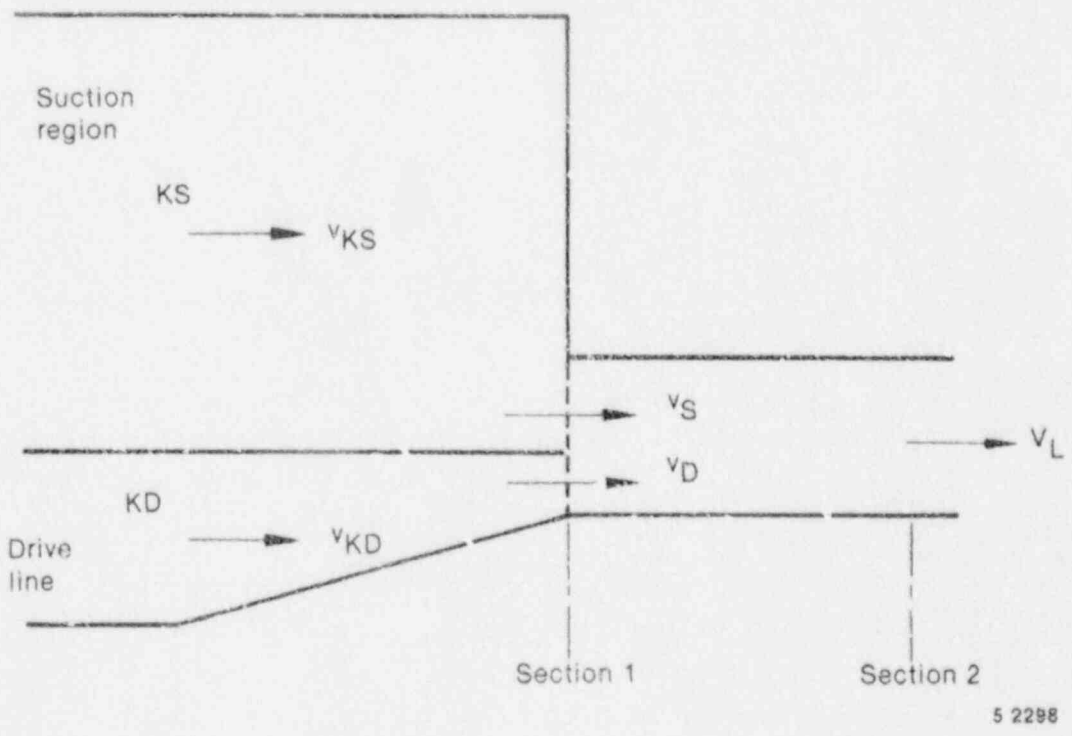

Figure 23. Schematic of mixing junctions.

a. The drive and suction junctions should be the high speed and low speed junctions respectively when the JETMIXER component is used for other than jet pump applications.

junction as abrupt. The user can model either junction either way if the appropriate loss factors are included (see input guidelines in Volume 2 of this manual). Void fractions and densities subscripted by a D or S are donored values, a subscript a indicates an average value.

The mixing of the drive and suction flows between cross section 1 and 2 requires a reevaluation of the momentum flux terms. The wall drag, interphase drag, temporal acceleration, momentum exchange due to mass transfer, and gravity head terms for the drive and suction junctions are treated exactly as they are at any other junction. Only the pressure and momentum flux terms will be examined in the following momentum equation development.

Consider a control volume in the mixing region between cross sections 1 and 2. If we apply the conservation of momentum principle for this control volume with the following assumptions: (a) Steady single-phase flow, (b) One-dimensional flow at cross sections 1 and 2, (c) Pressures at junctions D and S are equal, the momentum equation becomes

$$(P_L - P_1) A_L + \rho_L v_L^2 A_L - \rho_S v_S^2 A_S - \rho_D v_D^2 A_D = 0 \quad . \tag{374}$$

Conservation of mass applied with these same assumptions gives

$$\rho_L v_L A_L - \rho_S v_S A_S - \rho_D v_D A_D = 0 \quad . \tag{375}$$

Equation (375) can be used to write Equation (374) in its nonconservative form, obtaining

$$(P_L - P_1) + \rho_S v_S A_S (v_L - v_S)/A_L + \rho_D v_D A_D (v_L - v_D)/A_L = 0 \quad . \tag{376}$$

Equation (376) gives the momentum equation (pressure and flux terms) for the upstream half of the mixing volume. To develop the momentum equation for the suction junction a normal half cell momentum equation is written from KS to cross Section 1, i.e.,

$$(P_1 - P_{KS}) + 1/2\ \rho_{KS}(v_S^2 - v_{KS}^2) = 0 \quad . \tag{377}$$

Adding this to the half cell momentum Equation (376) for cross section 1 to L, gives

$$P_L - P_{KS} + 1/2\ \rho_{KS}(v_S^2 - v_{KS}^2)$$

$$+ \rho_S v_S A_S(v_L - v_S)/A_L + \rho_D v_D A_D(v_L - v_D)/A_L = 0 \quad . \tag{378}$$

This equation shows how the pressure and momentum flux terms should be calculated for the suction junction equation.

If the suction junction was a normal junction its momentum equation (pressure and flux terms) would be

$$(P_L - P_{KS}) + 1/2\ \rho_{Sa}(v_L^2 - v_{KS}^2) = 0 \quad . \tag{379}$$

The velocity terms in Equation (379) must be replaced by the velocity terms in Equation (378) to correctly model the momentum equation at the suction junction. Similar equations for the drive junction can be obtained.

3.1.5.3.2 Jet Mixing in Two-Phase Flows--If a derivation similar to the previous section is carried out for the pressure and momentum flux terms in the two-phase case the following equations are obtained for the liquid phase in the mixing region:

1. Conservation of momentum (from cross section 1 to L)

$$\alpha_{fL} A_L (P_L - P_1) + \alpha_{fL} \rho_{fL} v_{fL}^2 A_L$$

$$- \alpha_{fS} \rho_{fS} v_{fS}^2 A_S - \alpha_{fD} \rho_{fD} v_{fD}^2 A_D = 0 \tag{380}$$

2. Conservation of mass (from cross section 1 to L)

$$\alpha_{fL}\rho_{fL}v_{fL}A_L - \alpha_{fS}\rho_{fS}v_{fS}A_S - \alpha_{fD}\rho_{fD}v_{fD}A_D = 0 \quad . \tag{381}$$

Using Equation (381) in Equation (380) and rewriting Equation (380) in nonconservative form, yields

$$\alpha_{FL}(P_L - P_1) + \alpha_{fS}\rho_{fS}v_{fS}A_S(v_{fL} - v_{fS})/A_L$$

$$+ \alpha_{fD}\rho_{fD}v_{fD}A_D(v_{fL} - v_{fD})/A_L = 0 \quad . \tag{382}$$

Equation (382) can now be combined with the appropriate half cell momentum equation for the upstream volume to obtain the final momentum equation for the liquid flow at the suction junction. A parallel development gives the gas phase momentum equation at the suction junction.

In RELAP5 the momentum equations used consist of the sum of the phasic momentum equations and the difference of the phasic momentum equations. To derive the sum momentum equation (pressure and flux terms only) for the suction junction, Equation (382) for the liquid phase is added to a similar equation for the gas phase to obtain

$$(P_L - P_1) + \alpha_{fS}\rho_{fS}v_{fS}A_S(v_{fL} - v_{fS})/A_L + \alpha_{fD}\rho_{fD}v_{fD}A_D(v_{fL} - v_{fD})/A_L$$

$$+ \alpha_{gS}\rho_{gS}v_{gS}A_S(v_{gL} - v_{gS})/A_L + \alpha_{gD}\rho_{gD}v_{gD}A_D(v_{gL} - v_{gD})/A_L = 0 \quad . \tag{383}$$

The normal half cell sum momentum equation (pressure and flux terms only) for the upstream suction volume can then be added to Equation (383) to give

$$(P_L - P_{KS}) + \alpha_{fS}\rho_{fS}v_{fS}A_S(v_{fL} - v_{fS})/A_L + \alpha_{fD}\rho_{fD}v_{fD}A_D(v_{fL} - v_{fD})/A_L$$

$$+ \alpha_{gS}\rho_{gS}v_{gS}A_S(v_{gL} - v_{gS})/A_L + \alpha_{gD}\rho_{gD}v_{gD}A_D(v_{gL} - v_{gD})/A_L$$

$$+ 1/2\ \alpha_{fKS}\rho_{fKS}(v_{fS}^2 - v_{fKS}^2) + 1/2\ \alpha_{gKS}\rho_{gKS}(v_{gS}^2 - v_{gKS}^2) = 0 \qquad (384)$$

as the final form for the pressure and momentum flux terms in the new sum momentum equation for the suction junction. The pressure term in this equation has exactly the same form as the pressure term in the normal sum momentum equation. A parallel equation holds for the drive junction. Hence, at the drive and suction mixing junctions the normal momentum flux terms in the sum momentum equation must be replaced by those in Equation (384).

The difference momentum equation for the suction junction is derived by dividing the liquid momentum mixing Equation (382) by α_{fL} and adding it to the half cell liquid momentum equation for the upstream suction volume (also divided by the appropriate void fraction, α_{fKS}) to obtain

$$(P_L - P_{KS}) + \alpha_{fS}\rho_{fS}v_{fS}A_S(v_{fL} - v_{fS})/\alpha_{fL}A_L + \alpha_{fD}\rho_{fD}v_{fD}A_D(v_{fL} - v_{fD})/\alpha_{fL}A_L$$

$$+ 1/2\ \rho_{fKS}(v_{fS}^2 - v_{fKS}^2) = 0 \quad . \qquad (385)$$

Next, Equation (385) is divided by the average junction liquid density, ρ_{fa}, and subtracted from the corresponding gas equation to obtain

$$\left(\frac{\rho_f - \rho_g}{\rho_f\rho_g}\right)_a (P_L - P_{KS}) + \alpha_{gS}\rho_{gS}v_{gS}A_S(v_{gL} - v_{gS})/\alpha_{gL}\rho_{ga}A_L$$

$$+ \alpha_{gD}v_{gD}A_D(v_{gL} - v_{gD})/\alpha_{gL}\rho_{ga}A_L + \frac{1}{2}\rho_{gKS}(v_{gS}^2 - v_{gKS}^2)/\rho_{ga}$$

$$- \alpha_{fS}\rho_{fS}v_{fS}A_S(v_{fL} - v_{fS})/\alpha_{fL}\rho_{fa}A_L - \alpha_{fD}\rho_{fD}v_{fD}A_D(v_{fD} - v_{fD})/\alpha_{fL}\rho_{fa}A_L$$

$$- \frac{1}{2}\rho_{fKS}(v_{fS}^2 - v_{fKS}^2)/\rho_{fa} = 0 \qquad (386)$$

as the final difference momentum equation to be used at Junction S. A parallel equation must be used at the drive junction. The pressure term in Equation (386) has exactly the same form as the pressure term in the normal difference momentum equation. Hence, at the drive and suction mixing junctions the normal momentum flux terms in the difference momentum equation must be replaced by those in Equation (386).

3.1.5.3.3 Associated Flow Losses--The flow in the mixing region of Volume L can in reality be either a true jet mixing or a flow split (for reverse flow). The flow split case is governed by different physics than the jet mixing case considered in the previous discussions. The redistribution that occurs when the flow splits is primarily determined by the effective resistances downstream of the separation point in the suction and drive flow paths. The mixing terms derived above do not apply. For this reason we apply the additional mixing terms only for the positive drive flow regimes. We use the normal momentum flux calculations for the negative drive flow regimes.

The junctions associated with the JETMIXER component can be modeled as smooth or abrupt. If the junctions are input as smooth then the appropriate flow resistances should be calculated in a standard fashion and input as form loss coefficients at the appropriate junctions by the user.

If the junctions in the JETMIXER component are input as abrupt area changes then the code will calculate form loss coefficients as usual except that: (a) the forward loss coefficients at the drive and suction junctions are set to zero and (b) the reverse loss coefficients for the suction and drive junctions are those associated with the expansions from the junction areas to the suction or drive volume areas. The forward losses at these junctions are actually associated with the expansion from the vena contract

to the downstream mixing volume flow area. For parallel mixing streams, this loss is no longer appropriate. The losses associated with any contraction from the mixing volume to the suction or drive junctions are neglected for the same reason.

If the above normal flow losses are used when the suction flow reverses, it will be found that jet pump performance (head ratio) in this regime is significantly below the experimental data. The reverse flow loss coefficient applied in the suction junction has a significant effect on the jet pump performance in this flow situation. This loss coefficient (in addition to the normal loss coefficient associated with the expansion from A_S to area A_{KS}) represents all the irreversible losses associated with the turning and expansion of the flow from the drive junction. Because this flow regime is an important regime in the accident analysis of a BWR it was decided to include an approximation for this flow dependent loss in the jet mixing model.

This reverse suction flow loss was based upon the expansion losses experienced by the flow as it moves from the drive to the suction junction. Two flow situations with reversed suction flow and positive drive flow are possible depending upon the flow direction in the mixing section (Figure 24). In the first situation the expansion loss associated with the area change A_D to A_S, i.e.,

$$K = (A_S/A_D - 1)^2 \tag{387}$$

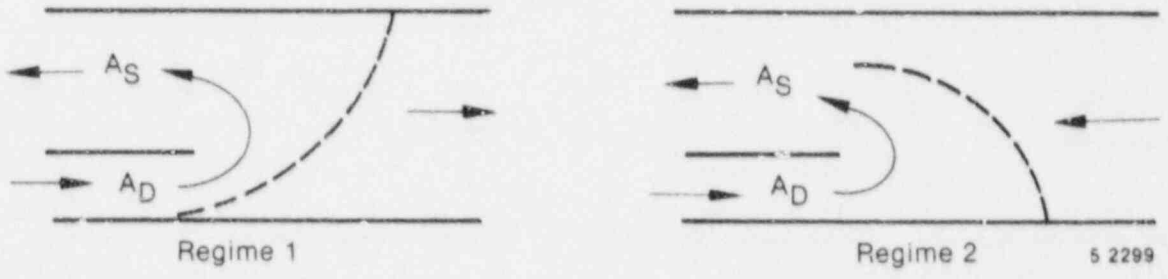

Figure 24. Flow regimes and dividing streamline.

is added to the user input reverse loss coefficient (or the standard abrupt area change loss factor if the junction is input as abrupt) for the suction junction. In the second situation the effective area for the suction flow that comes from the drive junction is less than A_S because the discharge flow is reversed. In this situation the effective areas for the expansion loss are A_D and $A_S|W_D/W_S|$. Hence, for the second situation the loss coefficient

$$K = \left(\frac{A_S|W_D/W_S| - 1}{A_D}\right)^2 \tag{388}$$

is added to the user input reverse loss coefficient (or the abrupt area loss factor if the junction is input as abrupt) at the suction junction only if $A_S|W_D/W_S|$ is $>A_D$. If $A_S|W_D/W_S|$ is $<A_D$, the drive to suction flow is effectively a contraction and the additional loss coefficient is set to zero.

Since the jet mixing and effective resistances are modeled by special terms in the suction and drive junction momentum equations the normal losses associated with the partitioning of volume L are not included in these junction equations. However, the normal losses associated with the area ratios experienced by the flow upstream of the suction and drive junctions are retained in the junction momentum equations.

3.1.5.3.4 Numerical Implementation--The basic numerical algorithm used to evaluate the new momentum flux terms in Equations (384) and (386) is similar to the numerical evaluation of the normal momentum flux terms. The normal momentum flux terms are calculated explicitly at the n^{th} time level. The new momentum flux terms in Equation (384) and (386) are also explicitly evaluated and the spatial location of each variable is indicated by its subscript.

3.1.5.4 Pump Model. The RELAP5/MOD2 pump model is almost identical to the RELAP5/MOD1 pump model,[1] which was originally taken from the RELAP4 pump model.[92] The only difference is that in RELAP5/MOD2 a shaft

component has been added to the control system component and the pump can be linked to the shaft and thus driven by either a motor or a turbine. However, the RELAP5/MOD1 options for a motor driven pump were retained so that input changes to an existing plant model using the pump are not required unless it is desired to make use of the shaft coupling.

The pump is a volume oriented component and the head developed by the pump is apportioned equally between the suction and discharge junctions that connect the pump volume to the system. The pump model is interfaced with the two fluid hydrodynamic model by assuming the head developed by the pump is similar to a body force. Thus, the head term appears in the mixture momentum equation, but like the gravity body force, it does not appear in the difference of momentum equation used in RELAP5. The term that is added to the mixture momentum equation is

$$\frac{1}{2} \rho g H \tag{389}$$

where H is the total head rise of the pump (m), ρ is the fluid density (kg/m^3), and g is the acceleration due to gravity (m/s^2). The factor 1/2 is needed because the term is applied at both the suction and discharge junctions.

In the semi-implicit numerical scheme, the pump is coupled explicitly so the numerical equivalent of Equation (389) is

$$\frac{1}{2} \rho^n g H^n \Delta t \tag{390}$$

where the n designates the previous time level and Δt is the time integration interval. This term is added to the right side of the mixture momentum equation, Equation (81).

In the nearly-implicit numerical scheme, the pump is coupled implicitly by way of its dependence on the volumetric flow rate (Q). It is assumed that the head depends on the volumetric flow rate, and a first order Taylor series expansion is used,

$$H^{n+1} = H^n + \left(\frac{dH}{dQ}\right)^n (Q^{n+1} - Q^n) \quad . \tag{391}$$

Thus, the numerical equivalent of Equation (389) in the nearly-implicit scheme is

$$\frac{1}{2} \rho_g^n g H^n \Delta t + \frac{1}{2} \rho^n g \left(\frac{dH}{dQ}\right)^n (Q^{n+1} - Q^n) \Delta t \quad . \tag{392}$$

This term is added to the right side of the mixture momentum Equation (81), which uses the linear implicit convection term from Equation (101).

The pump dissipation is calculated for the pump volume as

$$\tau\omega - \frac{gH}{\rho} (\alpha_f \rho_f v_f + \alpha_g \rho_g v_g) A \tag{393}$$

where τ is the pump torque and ω is the pump speed.

This term is evaluated explicitly in both the semi-implicit and nearly-implicit schemes, and it is partitioned between the liquid and vapor thermal energy equations in such a way that the rise in temperature due to dissipation is equal in each phase (the details of the dissipation mechanism in a two phase system are unknown so the assumption is made that the mechanism acts in such a way that thermal equilibrium between the phases is maintained without phase change). Thus the terms that are added to the right sides of the liquid and vapor thermal energy equations, Equations (69) and (70), are

$$\left[\tau^n \omega^n - \frac{gH^n}{\rho^n}\left(\alpha_f^n \rho_f^n \bar{v}_f^n + \alpha_g^n \rho_g^n \bar{v}_g^n\right) A\right] \Delta t \left(\alpha_f^n \rho_f^n C_{pf}^n\right) \Big/$$

$$\left(\alpha_f^n \rho_f^n C_{pf}^n + \alpha_g^n \rho_g^n C_{pg}^n\right) \tag{394}$$

and

$$\left[\tau^n \omega^n - \frac{gH^n}{\rho^n}\left(\alpha_f^n \rho_f^n \bar{v}_f^n + \alpha_g^n \rho_g^n \bar{v}_g^n\right) A\right] \Delta t \left(\alpha_g^n \rho_g^n C_{pg}^n\right) \Big/$$

$$\left(\alpha_f^n \rho_f^n C_{pf}^n + \alpha_g^n \rho_g^n C_{pg}^n\right) \tag{395}$$

respectively.

The pump head, H, and torque, τ, are defined by means of an empirical homologous pump performance model and the pump speed, ω, is defined by a pump drive model. The derivative of the pump head with respect to the volumetric flow rate, dH/dQ, is obtained from the empirical homologous pump performance model using the assumption that the pump speed is constant.

3.1.5.4.1 Centrifugal Pump Performance Model--The basic pump performance data must be generated experimentally. Analytical programs have been developed that are reasonably successful in predicting near design pump performance for single-phase fluids. For off design operation or for operation with a two-phase fluid, the problems of analytical pump performance prediction are nearly insurmountable. The basic parameters that characterize the pump performance are the rotational speed, ω or N, the volumetric through flow, Q, the head rise, H, and the shaft torque, τ. The relationship between these four parameters can be uniquely displayed by a four-quadrant representation of such data. A typical four quadrant curve is shown in Figure 25. Both positive and negative values

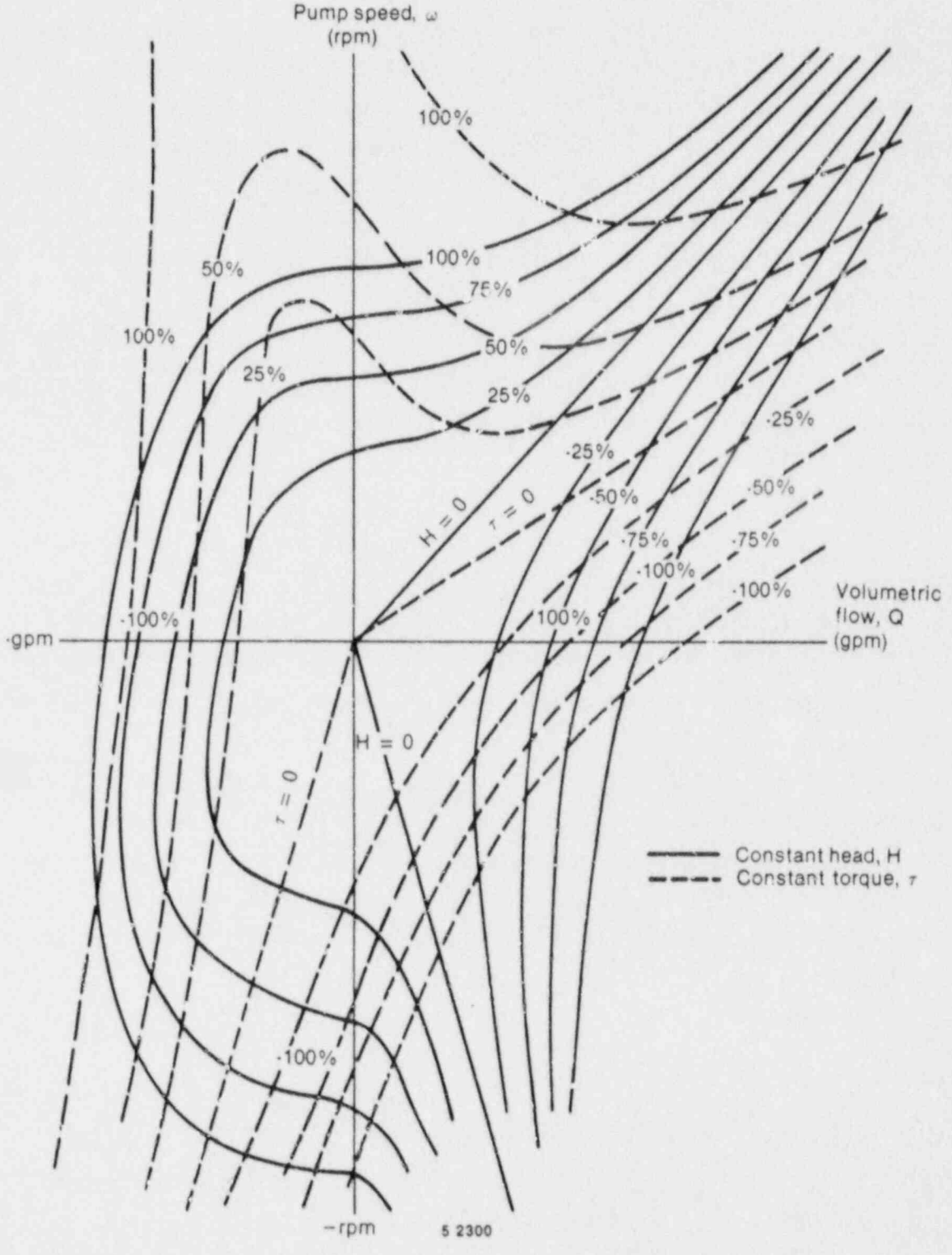

Figure 25. Typical pump characteristic four-quadrant curves.

for each of the four parameters are represented. The disadvantages in using such a data map for numerical purposes are the need for two-dimensional interpolation, the large number of points needed to define the entire range, and the fact that the map is infinite in extent. These objections can be largely overcome by use of a homologous transformation based on the centrifugal pump similarity relationships. Such a transformation collapses the four quadrant data onto a single bounded dimensionless curve having eight basic octants. Typical homologous curves for the head and torque are illustrated in Figures 26 and 27 respectively where ω_r, Q_R, H_R, and τ_R are the rated values for the pump speed, volumetric flow rate, head, and torque. respectively. The homologous transformation is not unique and not all points of Figure 25 lie on the curves of Figures 26 and 27. However, the data are closely grouped and the single curve is a good approximation for the global pump performance.

The pump model allows the user the option of accounting for cavitation or two-phase degradation effects on pump performance. The user must supply a separate set of homologous, two-phase curves for head and torque that are in the form of difference curves. Difference curves are used because analysis of available two-phase pump data indicated that when the fluid being pumped had a void fraction between 0.2 and 0.9, little head was developed by the pump being tested. Outside this range of void fraction, the pump developed head varied from zero to undegraded single-phase performance. To consider the degraded performance, a set of dimensionless homologous curves was fit to the head data. Thus the fully-degraded two-phase head was expressed as a function of the standard pump model arguments.

To consider the ranges of void fraction where the pump was able to develop head (0 to 0.2 and 0.9 to 1.0), a multiplier as a function of void fraction was used. The multiplier varied from 0 to about 1.0 as the void fraction varied from 0 to 0.2; and the multiplier varied from about 1.0 to 0 as the void fraction varied from 0.9 to 1.0.

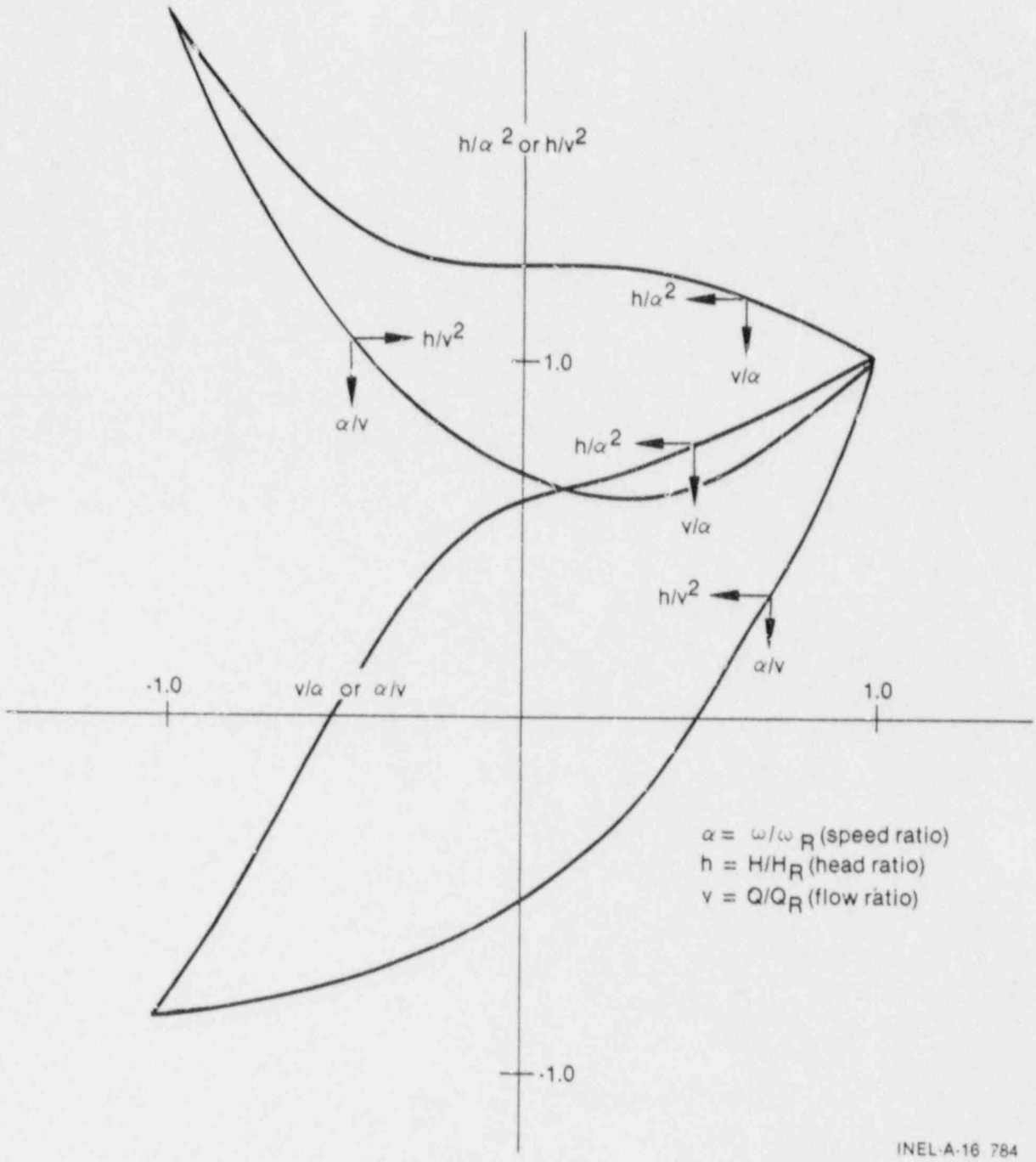

Figure 26. Typical pump homologous head curves.

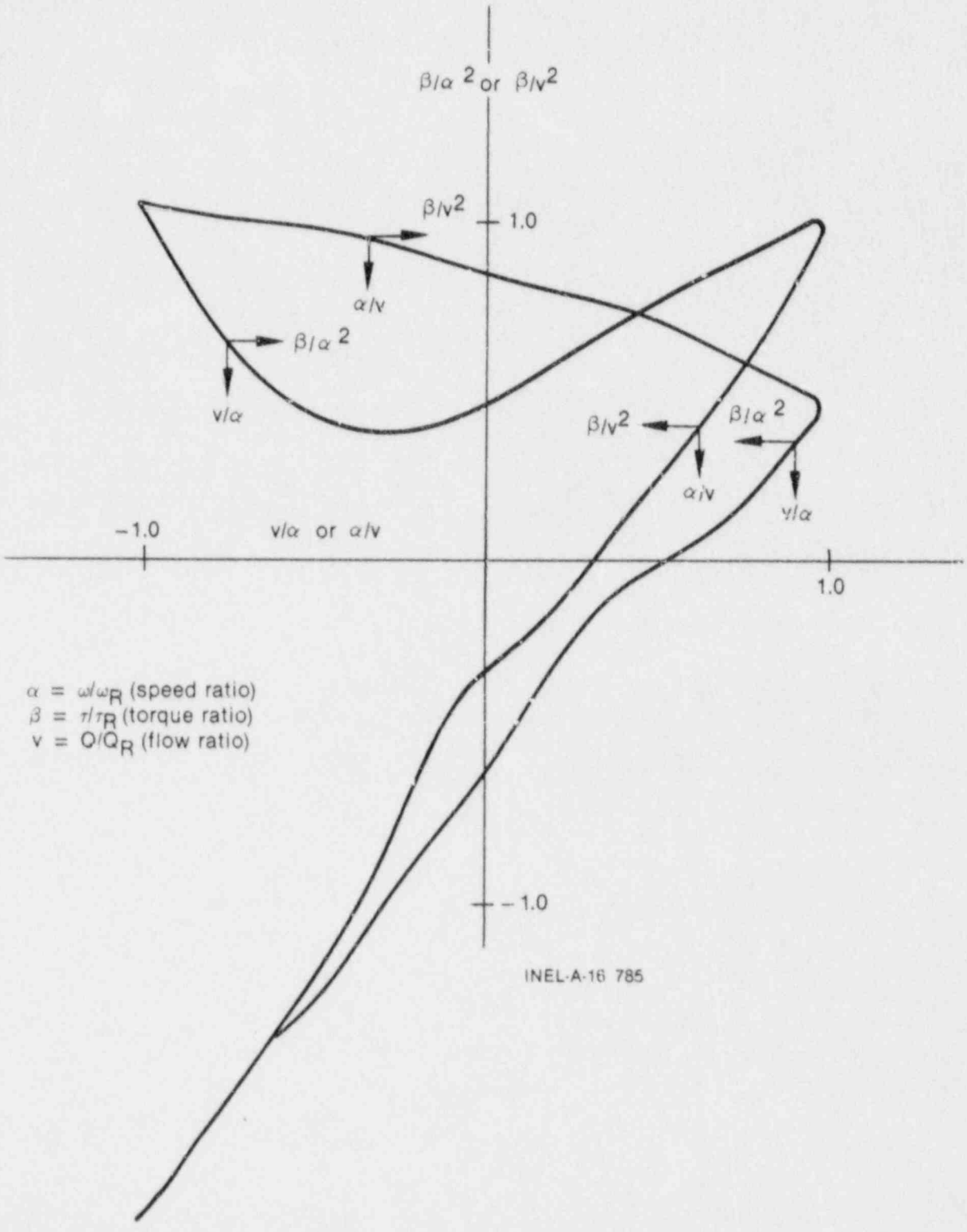

Figure 27. Typical pump homologous torque curves.

Available pump data from the 1-1/2 Loop Model Semiscale and Westinghouse Canada Limited (WCL) experiments were used in developing the two-phase pump data. Assumptions inherent in the pump model for two-phase flow include:

1. The head multiplier, $M_H(\alpha_g)$, determined empirically for the normal operating region of the pump, is also valid as an interpolating factor in all other operating regions.

2. The relationship of the two-phase to the single-phase behavior of the Semiscale pump is applicable to large reactor pumps. This assumes that the pump model of two-phase flow is independent of pump specific speed.

The single-phase pump head (dimensionless) curve for the Semiscale pump is shown in Figure 28 and the fully degraded two-phase pump head curves are shown in Figure 29. These represent complete pump characteristics (except for the reverse pump fully degraded region) for the Semiscale pump operating under two-phase conditions with the average of the void fractions of the pump inlet and outlet mixtures between 0.2 and 0.9. The lines drawn through the data were determined by least square polynomial fits to the data using known constraints.

A comparison of the two-phase data in Figure 29 with the single-phase data in Figure 28 shows that the two-phase dimensionless head ratio (h/v^2 or h/α^2) is significantly less than the single-phase dimensionless head ratio for the normal pump operation region (HAN and HVN). For negative ratios of v/α, such as those that occur in the HAD region, the pump flow becomes negative. When the pump flow is negative, the two-phase dimensionless head ratio is greater than the single-phase dimensionless head ratio. Two-phase flow friction losses are generally greater than single-phase losses, and friction is controlling in this energy dissipation region (HAD). The other regions of two-phase dimensionless head ratio data show similar deviations from single-phase data.

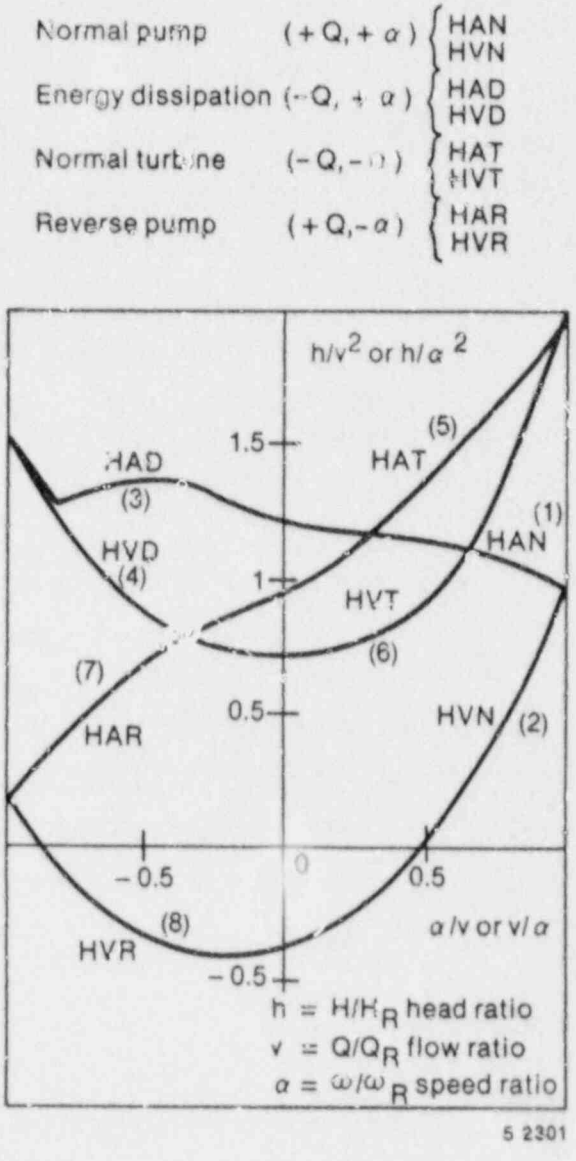

Figure 28. Single-phase homologous head curves for 1-1/2 loop MOD1 Semiscale pumps.

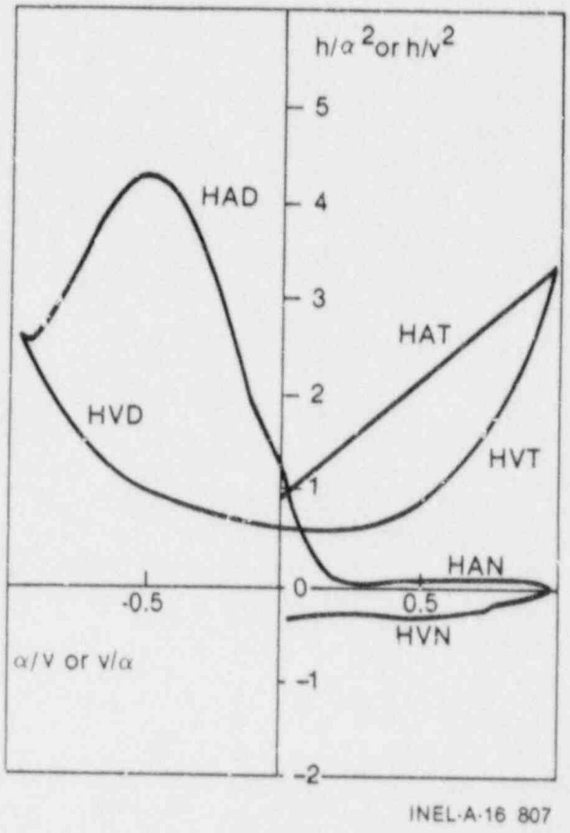

Figure 29. Fully degraded two-phase homologous head curves for 1-1/2 loop MOD1 Semiscale pumps.

Table 4 shows the difference between the single and two-phase dimensionless head ratio data as a function of v/α and α/v for the various pumping regions shown in Figures 28 and 29. The differences shown in Table 4 are for the eight curve types used for determining pump head.

The head multiplier, $M_H(\alpha_g)$, and void fraction data shown in Table 5 were obtained in the following manner. The Semiscale and WCL pump data[92] were converted to dimensionless head ratios of h/α^2 or h/v^2. Values of the dimensionless head ratios were obtained for pump speeds and volumetric flow rates within 50% of the rated speed and flow rate for the pumps. The difference between the single- and two-phase dimensionless ratios was developed as a function of the average void fractions for the pump inlet and outlet mixtures. The difference between

TABLE 4. SEMISCALE DIMENSIONLESS HEAD RATIO DIFFERENCE (single-phase minus two-phase) DATA

$x = \frac{v}{a}$ or $\frac{a}{v}$

$y = \left.\frac{h}{a^2}\right|_{1\phi} - \left.\frac{h}{a^2}\right|_{2\phi}$ or $\left.\frac{h}{v^2}\right|_{1\phi} - \left.\frac{h}{v^2}\right|_{2\phi}$

Curve Type	x	y	Curve Type	x	y
1 (HAN)	0.00	0.00	4(HVD)	-1.00	-1.16
	0.10	0.83		-0.90	-0.78
	0.20	1.09		-0.80	-0.50
	0.50	1.02		-0.70	-0.31
	0.70	1.01		-0.60	-0.17
	0.90	0.94		-0.50	-0.08
	1.00	1.00		-0.35	0.00
				-0.20	0.05
2 (HVN)	0.00	0.00		-0.10	0.08
	0.10	-0.04		0.00	0.11
	0.20	0.00			
	0.30	0.10	5 (HAT)	0.00	0.00
	0.40	0.21		0.20	-0.34
	0.80	0.67		0.40	-0.65
	0.90	0.80		0.60	-0.95
	1.00	1.00		0.80	-1.19
				1.00	-1.47
3 (HAD)	-1.00	-1.16			
	-0.90	-1.24	6 (HVT)	0.00	0.11
	-0.80	-1.77		0.10	0.13
	-0.70	-2.36		0.25	0.15
	-0.60	-2.79		0.40	0.13
	-0.50	-2.91		0.50	0.07
	-0.40	-2.67		0.60	-0.04
	-0.25	-1.69		0.70	-0.23
	-0.10	-0.50		0.80	-0.51
	0.00	0.00		0.90	-0.91
				1.00	-1.47
			7 (HAR)	-1.00	0.00
				0.00	0.00
			8 (HVR)	-1.00	0.00
				0.00	0.00

TABLE 5. HEAD MULTIPLIER AND VOID FRACTION DATA

α_g	$M_H(\alpha_g)$
0.00	0.00
0.10	0.00
0.15	0.05
0.24	0.80
0.30	0.96
0.40	0.98
0.60	0.97
0.80	0.90
0.90	0.80
0.96	0.50
1.00	0.00

the single- and two-phase dimensionless ratios was then normalized to a value between 0 and 1.0. The normalized result was tabulated as a function of the void fraction.

If the two-phase option is selected, the pump head and torque are calculated from

$$H = H_{1\phi} - M_H(\alpha_g)\,(H_{1\phi} - H_{2\phi}) \tag{396}$$

$$\tau = \tau_{1\phi} - M_\tau(\alpha_g)\,(\tau_{1\phi} - \tau_{2\phi}) \tag{397}$$

where

1ϕ = single-phase value

2ϕ = two-phase, fully degraded value, $0.2 < \alpha_g < 0.9$

M = multiplier on difference curve

α_g = average volume void fraction.

3.1.5.4.2 Centrifugal Pump Drive Model--The pump torque is used to calculate the pump speed after the pump has been shut off by the input trip signal. The speed is calculated by the deceleration equation

$$I\frac{d\omega}{dt} = \tau \quad . \tag{398}$$

The solution of this equation is

$$\omega_{t+\Delta t} = \omega_t + \frac{\tau \Delta t}{I} \tag{399}$$

where

τ = net torque

I = moment of inertia

t = time

Δt = time step

ω = angular velocity.

The rate of energy addition to the pump system is given by $\omega\tau$ and has been used in Equation (391) to calculate the pump dissipation.

The total pump torque is calculated by considering the hydraulic torque from the homologous curves and the pump frictional torque. The net torque with the drive motor shut off is

$$\tau = \tau_{hy} + \tau_{fr} \tag{400}$$

where

τ_{hy} = hydraulic torque

τ_{fr} = frictional torque.

The frictional torque is in the form of a cubic equation. The value of the frictional torque is also dependent on the sign of the pump speed. An option is available to specify whether reverse rotation of the pump is allowed.

The electric drive motor will affect the speed behavior of the pump while the motor remains connected to its power source. The net torque with the drive motor on is incorporated into the pump model by adding the value of motor torque, τ_m, to the torque summation

$$\tau = \tau_{hy} + \tau_{fr} - \tau_m \tag{401}$$

where the sign of the motor torque is the same as that of the hydraulic and frictional torque for steady operating conditions, that is, zero net torque.

Induction motors are used to drive primary coolant pumps. At constant voltage, the motor torque is an explicit function of speed. This torque/speed relationship is normally available from the motor manufacturer.

Motor torque is supplied to the pump model as a tabular function of torque versus speed as given by the manufacturer's data. A typical torque/speed curve for an induction motor is shown in Figure 30.

The capability to simulate a locked rotor condition of the pump is included in RELAP5. This option provides for simulation of the pump rotor lockup as a function of input elapsed time, maximum forward speed, or maximum reverse speed. At the time the rotor locks (and at all times thereafter), the pump speed is set equal to zero.

2.1.5.5 Turbine Component. A steam turbine is a device that converts thermal energy contained in high pressure, high temperature steam to mechanical work. The complicated configuration of a steam turbine precludes a complete first principles model, at least for the purpose of system transient calculations. A lumped parameter turbine model is used in RELAP5 wherein a sequence of turbine stages (henceforth referred to as a stage group) is treated as a single junction and volume. The stage group is then represented using modified energy, continuity, and momentum equations. An efficiency factor based upon simple momentum and energy considerations is used to represent the nonideal internal processes.

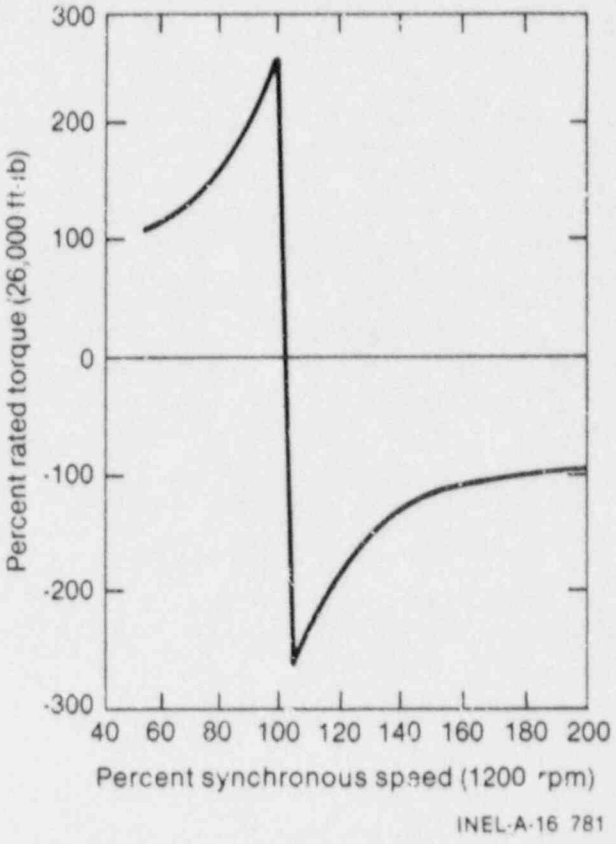

Figure 30. Torque versus speed, Type 93A pump motor (rated voltage).

A turbine can be modeled using a single stage group, i.e., a single volume and junction, or several stage groups depending upon the resolution required. If turbine steam is extracted to preheat the feedwater, then several stage groups may be needed to obtain the correct steam properties at the feedwater heating bleed points. All such steam bleed points are modeled as cross-flow junctions in the RELAP5 model.

3.1.5.5.1 Model Design--The normal unmodified volume continuity equations are used for the stage group with a representative nozzle throat area for the inlet junction and the last stator nozzle throat discharge area as the outlet junction area. It is important to use the same representative nozzle area at both junctions.

Unlike the continuity equations, the momentum equations are modified by the work extracted in the rotating blade system of each stage group. To develop the general form for the momentum equations we first consider a

steady state total energy balance for a homogeneous fluid passing through a stage group (Figure 31). We will subsequently extend this general form to that used for the two-fluid system.

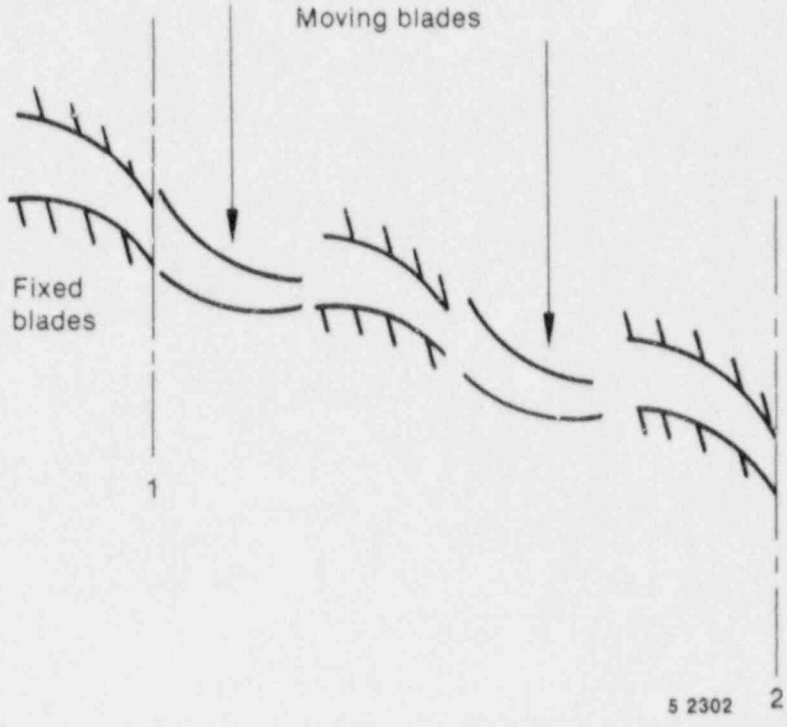

Figure 31. A schematic of a stage group with idealized flow path between Points 1 and 2.

Although the fluid particles follow a tortuous path through the turbine we can still write a total energy balance between cross sections 1 and 2 (Figure 31). For a steady state situation this gives

$$\rho vA \left(\frac{1}{2} v^2 + h\right)\Big|_1 = \rho vA \left(\frac{1}{2} v^2 + h\right)\Big|_2 + \rho vAW \qquad (402)$$

where ρ is the density, v is the velocity, h is the enthalpy, and A is the cross-sectional area. The term W represents the shaft work per mass flow rate extracted from the fluid. Heat loss is neglected in this ideal analysis. From continuity considerations ρvA is constant. Dividing Equation (402) by ρvA we obtain

$$\frac{1}{2} v_2^2 - \frac{1}{2} v_1^2 = -(h_2 - h_1) - W \quad . \qquad (403)$$

In this way the energy balance is converted into an equivalent force balance (power = force x velocity).

In this idealized process where external heat loss and internal dissipation are neglected, the process is isentropic and

$$dh = \frac{1}{\rho} dP \quad . \tag{404}$$

Integrating Equation (404) approximately between Points 1 and 2 gives

$$h_2 - h_1 = \frac{1}{\rho} (P_2 - P_1) \tag{405}$$

where ρ is an average density.

The actual work, W, produced by the fluid on the rotating blades as its momentum is changed, is usually written as an efficiency factor times the isentropic enthalpy change across the stage, and becomes

$$W = -\eta \int_{S=\text{const}} dh = -\eta \int_{S=\text{const}} \frac{1}{\rho} dP \quad . \tag{406}$$

If we assume a constant efficiency for the stage group, Equation (406) can be approximated as

$$W = -\eta \frac{1}{\rho} (P_2 - P_1) \quad . \tag{407}$$

When Equations (405) and (407) are substituted into Equation (403) we obtain

$$\frac{1}{2} v_2^2 - \frac{1}{2} v_1^2 = - \frac{(1 - \eta)}{\rho} (P_2 - P_1) \tag{408}$$

as the momentum equation for this steady state case. Equation (408) shows that only a small fraction, $(1 - \eta)$, of the pressure gradient contributes to changes in the kinetic energy of the fluid. The larger fraction, η, of the pressure gradient results in turbine work [Equation (407)].

Using Equation (408) as a prototype, the full two-fluid momentum equations which are used in the turbine model are (in differential form)

$$(\alpha_g \rho_g)\left(\frac{\partial v_g}{\partial t} + v_g \frac{\partial v_g}{\partial x}\right) = -\alpha_g (1 - n) \frac{\partial P}{\partial x}$$

$$- \alpha_g \rho_g \, \text{HLOSSG} \, v_g - \alpha_g \rho_g \, \text{FIG} \, (v_g - v_f) \qquad (409)$$

$$(\alpha_f \rho_f)\left(\frac{\partial v_f}{\partial t} + v_f \frac{\partial v_f}{\partial x}\right) = -\alpha_f (1 - n) \frac{\partial P}{\partial x}$$

$$- \alpha_f \rho_f \, \text{HLOSSF} \, v_f - \alpha_f \rho_f \, \text{FIF} \, (v_f - v_g) \quad . \qquad (410)$$

The application guidelines will be summarized in Volume 2 of this report, but it seems appropriate at this point to mention three guidelines that are related to the momentum equation development:

1. In practice, a steam turbine does not usually contain significant liquid water and the tortuous path precludes accurate modeling of the interphase drag. Therefore, it is recommended that the homogeneous option be used at all axial turbine junctions. The effect of condensation could be included in the efficiency factor if desired. At present, it is not included as the effect is usually small.

2. The fluid path through the turbine volume is very tortuous. This coupled with the large number of blades makes the standard wall friction calculation meaningless. For this reason the wall friction terms have not been shown in Equations (409) and (410). It is recommended that the turbine volume wall friction flag be set to use the zero wall friction option. If the user wants to include any momentum effects due to frictional or form losses it should be done with an appropriate user input form loss.

3. The area changes in a turbine are gradual so the smooth junction option should be used.

The inefficiency of the turbine gives rise to some dissipation that is a source of internal energy. The dissipation is a small effect and is neglected in the present turbine model formulation. The only effect on the internal energy equations is the dissipative source term due to any user input form loss.

The only equations that are modified as a result of the turbine model are the momentum equations, in which the pressure gradient terms are multiplied by the coefficient $(1 - \eta)$.

3.1.5.5.2 Efficiency Formulas--The basic efficiency formulas can be derived from velocity diagrams with assumed nozzle and blade efficiency factors. The derivations are fairly straight forward and are found in standard texts. The efficiency formulas recorded here were obtained from Reference 93. The efficiency factors for three turbine designs are described in the following paragraph.

3.1.5.5.2.1 Single-Stage Turbine---The first model considered is the most general. We consider a single row fixed blading system followed by a single row rotating blading system. Let r be the reaction fraction, i.e., the fraction of the stage energy released (enthalpy change) in the moving blade system. If r is zero we have a pure impulse stage with no pressure drop in the moving blade system, i.e., the moving blades only change the fluid flow direction. A turbine stage with nonzero r at design conditions is commonly called a reaction stage. A value of r = 0.5 is a common design.

If all blading angles are ideal and all nozzle losses are zero, the ideal efficiency, as given in Reference 93, is

$$\eta = \left[(vb - v_t) + \sqrt{(vb - v_t)^2 + rv^2}\right]\left(\frac{2v_t}{v^2}\right) \qquad (411)$$

where v is the fluid velocity at the nozzle exit, v_t is the tangental or rim velocity of the moving blades, and

$$b = \sqrt{1 - r} \quad . \tag{412}$$

In general, due to nozzle losses, entrance effects, and nonideal blading angles, the efficiency is less than that given by Equation (411). The maximum efficiency ($\eta = 1.0$) given by Equation (411) can be found by differentiation to occur when

$$\frac{v_t}{v} = \frac{0.5}{\sqrt{1 - r}} \quad . \tag{413}$$

For an impulse stage the maximum efficiency occurs at $v_t/v = 0.50$. For a reaction turbine designed with $r = 0.5$ the maximum efficiency occurs at $v_t/v = 0.707$.

In general, the actual efficiency is less than the ideal value derived above. A first approximation to the actual efficiency (see Reference 93) is to include a constant factor η_o in Equation (411) that represents the actual efficiency at the maximum point, i.e.,

$$\eta = \eta_o \frac{2v_t}{v^2} \left[(vb - v_t) + \sqrt{(vb - v_t)^2 + rv^2} \right] \quad . \tag{414}$$

Equation (414) is the general efficiency formula that is applied to a single row impulse or reaction turbine. This formula is applied to a stage group that may consist of a single blade passage or multiple blade passages. If the stage group contains multiple blade passages, the efficiency represents some average value.

3.1.5.5.2.2 Two-Stage Impulse Turbine---The second turbine design considered is a two row impulse stage, i.e., a nozzle, a moving constant area blade passage, a fixed constant area stationary passage, and a final constant area moving blade passage. This blading system is modeled

as a single stage group. This type of stage design is sometimes used as the first stage in a turbine for governing purposes. Reference 93 records the efficiency formula for this design as

$$\eta = \eta_o \frac{8v_t}{v^2}(v - 2v_t) \quad . \tag{415}$$

3.1.5.5.2.3 Constant Efficiency---The final efficiency option that is included is a constant efficiency independent of the reaction, nozzle fluid velocity, and rim speed, i.e.,

$$\eta = \eta_o \quad . \tag{416}$$

It should be noted that a turbine stage, designed to operate with a given reaction fraction r at design conditions, will have a different reaction fraction for off design conditions. The change in reaction fraction with v_t/v can be calculated [Reference 93, p. 207, Equation (14)]. For reaction stages the change is small. In all cases this change in r is neglected in the above efficiency formulas.

3.1.5.5 2.4 Power/Torque Output of Turbine---In general the relationship between power and torque for a rotating shaft is

$$P = \tau\omega \quad . \tag{417}$$

The power extracted from the fluid per mass flow rate for a given stage group is

$$\eta \int_{S=\text{const}} dh$$

so we have for the torque

$$\tau = (\rho v A)\frac{\eta}{\omega}(P_2 - P_1)/\omega \tag{418}$$

or

$$\tau = (\rho v A) \frac{\eta}{\rho} (P_2 - P_1) \frac{R}{v_t} \qquad (419)$$

where R is the mean stage radius at the nozzle and the approximation in Equation (407) has been used.

Equation (419) gives the torque that is extracted from a given stage group in terms of the stage efficiency, mean stage radius R, mean blade tangential velocity v_t, and pressure drop. This is the torque that is applied by the turbine component when it is coupled to the shaft component.

3.1.5.5.2.5 Numerical Implementation---As noted in the model design section a stage group is modeled as a single junction (j) and volume (L) (see Figure 32).

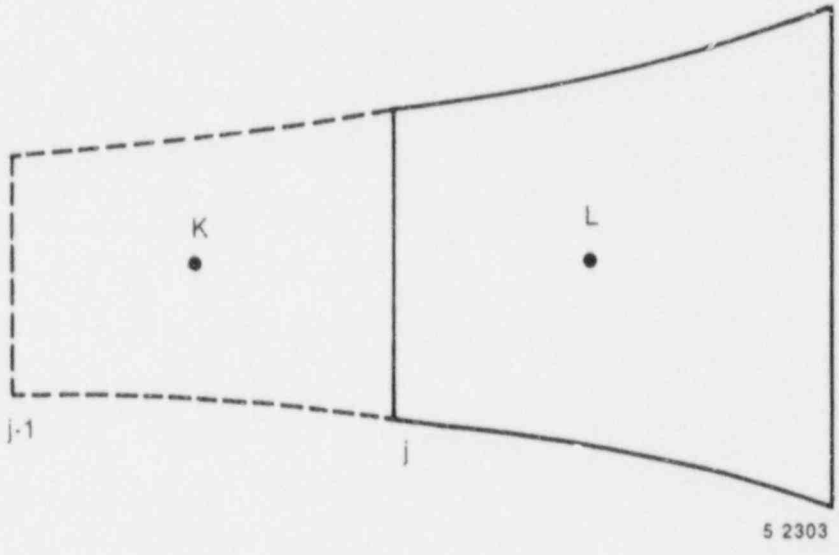

Figure 32. Schematic of lumped model for turbine stage group.

The continuity and internal energy equations from Volume 1 of this report are unchanged from their standard form. The normal finite difference form of the momentum equations for Junction j is modified in two ways:

1. The pressure gradient term in the sum and difference numerical equations is multiplied by $(1 - n)$.

2. The numerical differencing of the convective terms has been modified. At a normal junction the convective terms are approximated as

$$v\frac{\partial v}{\partial x} = \frac{1}{2} v_L^2 - \frac{1}{2} v_K^2 + VIS \quad . \tag{420}$$

The small viscous term VIS is numerically calculated so as to give a donored formulation of the momentum flux term in a straight pipe. For a variable area channel, it is formulated so that it vanishes for a variable area channel with a constant density fluid. In a turbine the area is slowly varying but the fluid experiences large pressure changes (due to the work extraction) and hence large density changes. A numerical simulation with the above convective terms used at the turbine junctions resulted in a viscous term that is larger than the kinetic energy terms. The normal viscous terms for a variable area channel are inaccurate in the turbine situation with large density changes and dominate the physical kinetic energy change. An alternative form of the convective terms which is sufficiently accurate and stable for the variable area turbine model is

$$v\frac{\partial v}{\partial x} = v_j (v_j - v_{j-1})/\Delta x \quad . \tag{421}$$

This difference form is used for all turbine junctions. If the v_j multiplying the numerical gradient is assumed to be approximately equal to $\frac{1}{2} (v_j + v_{j-1})$ then Equation (421) gives

$$v\frac{\partial v}{\partial x} = \frac{1}{2} (v_j^2 - v_{j-1}^2) \tag{422}$$

and a reasonable approximation to the kinetic energy change between j-1 and j results.

The algebraic efficiency formulas in Equations (414), (415), and (416) are coded with v, η_0, r, ω, and R (where $v_t = R\omega$) as arguments. The type of the turbine stage group is fixed at input time.

The stage torque that is applied to the shaft is calculated from Equation (419). The torques from each stage group are added using the SHAFT component that integrates the angular momentum equation. The power is calculated from Equation (417). This variable is not needed in the integration scheme but is printed in the major edits.

3.1.5.6 Valves. Valves are quasi-steady models that are used either to specify an option in a system model or to simulate control mechanisms in a hydrodynamic system. The RELAP5 valve models can be classified into two categories; (a) valves that open or close instantly and (b) valves that open or close gradually. Either type can be operated by control systems or by flow dynamics.

Valves in the first category are trip valves and check valves. The model for these valves does not include valve inertia or momentum effects. If the valve is used as a junction with an abrupt area change, then the abrupt area change model is used to calculate kinetic loss factors when the valve is open.

Valves in the second category are the inertial swing check valve, the motor valve, the servo valve, and the relief valve. The inertial valve and relief valve behavior is modeled using Newton's second law of motion. The abrupt area change model controls losses through the valve as the cross-sectional flow area varies with valve assembly movement. The motor and servo valve use differential equations to control valve movement. These two valves include the options to use the abrupt area change model to calculate losses across the valve or to use flow coefficients (C_v) input by the user. The C_v's are converted to energy loss coefficients within the numerical scheme.

Valves are modeled in RELAP5 as junction components. The types of valves are defined as follows.

3.1.5.6.1 Trip Valve--The operation of a trip valve is solely dependent on the trip selected. With an appropriate trip, an abrupt full opening or full closing of the valve will occur. A latch option is also included for latching the valve in the open or closed position.

3.1.5.6.2 Check Valve--The operation of a check valve can be specified to open or close by static differential pressure, to open by static differential pressure and close by flow reversal, or to open by static differential pressure and close by dynamic differential pressure.

All of the check valves will be opened or closed based on static differential pressure across the junction according to

$$\left(P_K + \Delta P_{K_g}\right) - \left(P_L + \Delta P_{L_g}\right) - PCV > 0, \text{ valve opens} \qquad (423)$$

where

P_K, P_L = junction from and to volume thermodynamic pressures

ΔP_{K_g}, ΔP_{L_g} = static pressure head due to gravity

PCV = back pressure required to close the valve (user input).

For a static pressure controlled check valve the valve will open if Equation (423) becomes positive and will close if Equation (423) becomes negative. If Equation (423) is zero, the valve will remain as previously defined.

For a flow controlled check valve, the valve will open if Equation (423) is positive and will close only if a flow reversal occurs such that

$GC < 0$

where GC is the dynamic pressure given as

$$GC = \frac{1}{2}(\overline{\rho v}\,\overline{v})_j = \frac{1}{2}\left[\alpha_f \rho_f v_f + \alpha_g \rho_g v_g\right]_j (\alpha_f v_f + \alpha_g v_g)_j \quad . \tag{424}$$

For a dynamic pressure controlled check valve, the valve opens if Equation (423) is greater than zero. Once the valve is open, the forces due to pressure differential and momentum hold the valve open until

$$\left(P_K - \Delta P_{K_g}\right) - \left(P_L + \Delta P_{L_g}\right) + GC - PCV \begin{cases} < 0, & \text{valve closes} \\ = 0, & \text{remains as previously defined} \end{cases} \quad . \tag{425}$$

The terms α_f and α_g are the junction liquid and vapor volume fractions, respectively, ρ_f and ρ_g are the junction liquid and vapor densities, respectively, and v_f, v_g are the junction liquid and vapor velocities, respectively.

Flow and dynamic pressure controlled valves exhibit a hysteresis effect with respect to the forces opening and closing the valve. The static pressure controlled valve, however, has no hysteresis effect.

All check valves may be initialized as either open or closed. Leakage is also allowed if the valve is closed and the abrupt area change model is used to calculate the valve form losses.

3.1.5.6.3 Inertial Valve--This valve models the motion of the valve flapper assembly in an inertial type check valve. The abrupt area change model is used to calculate kinetic form losses assuming that the

area between the flapper and the valve seat behaves as an orifice whose area changes in time as a function of the inertial valve geometry.

The motion of the flapper about the shaft axis is given by Newton's second law (angular version) as

$$\tau = I\,\alpha \tag{426}$$

where the external torques acting on the valve disk are given by

$$\tau = -\,W\,L\,\sin(\theta + \phi) - A_D\,L(\Delta P + P_{BP} + G_{head}) \tag{427}$$

where ΔP is the pressure drop across the valve, and α is the angular acceleration.

Substituting Equation (426) into Equation (427) gives

$$I\,\alpha = -\,W\,L\sin\theta - \pi R^2 L(\Delta P + P_{BP} + G_{head}) \tag{428}$$

where ϕ has been dropped by assuming the valve is a horizontal pipe. Equation (428) is then written in finite-difference form as

$$\alpha^n = \frac{1}{I} - WL\sin\theta^n - \pi R^2\,L(\Delta P^n + P_{BP} + G_{head}) \tag{429}$$

where the superscript, n, indicates the time level, $t + n\,\Delta t$. Integrating Equation (429) with respect to time yields the angular velocity

$$\omega^{n+1} = \omega^n + \alpha^n \Delta t \quad . \tag{430}$$

Similarly integrating Equation (430) gives the angular position

$$\theta^{n+1} = \theta^n + \omega^{n+1} \Delta t \quad . \tag{431}$$

The throat flow area for the valve is set by the following function[94,95]

$$A_{throat} = \begin{cases} 2\pi R^2 \tan r^{n+1} & \theta \leq 26.565° \\ \pi R^2 & \theta > 26.565° \end{cases} . \qquad (432)$$

Several options are allowed with the use of this valve such as specifying minimum and maximum flapper angular positions when the valve is closed, specifying latch or no latch options, and specifying leakage.

3.1.5.6.4 Motor Valve--This valve model has the capability of controlling the junction flow area between two control volumes as a function of time. The operation of the valve is controlled by two trips; one for opening the valve, and a second for closing the valve. A constant rate parameter controls the speed at which valve area changes. The motor valve area variation can also be specified using a general table. When the general table is specified, the constant rate parameter controls the valve stem position and the general table relates the stem position to the valve flow area. Conversely, when the general table is not specified the constant rate parameter controls the rate of change in valve area.

The abrupt area change model is used to calculate kinetic form losses with respect to the valve area. However, if the normalized valve flow area has a value less than 1.0E-10, the valve is assumed to be closed.

A second option allowed for the motor valve is the specification of valve flow coefficients, C_v. These coefficients may be specified using a general table of C_v versus normalized stem position and the smooth junction option must be specified. The conversion of C_v to an energy loss coefficient, K, is done in the numerical scheme using the formula

$$K = 2 \frac{A_{valve}^2}{C_v^2 \rho_o} \qquad (433)$$

where

ρ_o = density of water at 288.71 K (60.0°F).

Provisions also exist for applying multipliers to both stem position and C_v.

3.1.5.6.5 Servo Valve--The servo valve operation is similar to that for the motor valve. However, the valve area or stem position is controlled by a control variable rather than by a specified rate parameter. The servo valve also has the same options as the motor valve.

3.1.5.6.6 Relief Valve--For thermal-hydraulic analysis of overpressure transients it is necessary to simulate the effects of relief valves. In particular, it is desirable to model the valve dynamic behavior, including simulation of valve flutter and hysteresis effects.

To assist in understanding the relief valve model three schematics of a typical relief valve are shown in Figures 33, 34, and 35. The three schematics represent the valve in the closed (Figure 33), partially open (Figure 34), and fully open (Figure 35) modes, respectively. In the schematics, the seven main components of a relief valve are shown, which are: the valve housing, inlet, outlet, piston, rod assembly, spring, bellows, and valve adjusting ring assembly.

The numerical model of the valve simply approximates the fluid forces acting on the valve piston and the valve reaction to these forces. The model of the fluid forces is based on a quasi-steady-state form of the impulse momentum principle and the valve reaction force is based on Newton's Second Law of motion.

A qualitative understanding of the operation of the relief valve can be gained by referring again to Figures 33, 34, and 35. If the valve inlet pressure is low the valve is closed, as shown in Figure 33. As the inlet pressure increases the valve piston will remain closed until the force of

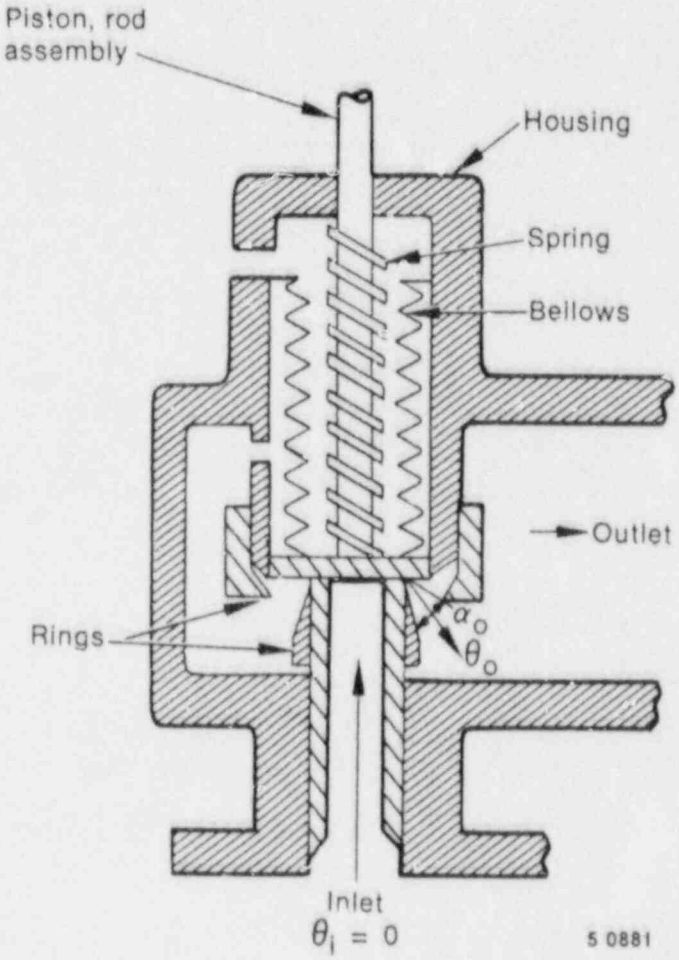

Figure 33. Schematic of a typical relief valve in the closed position.

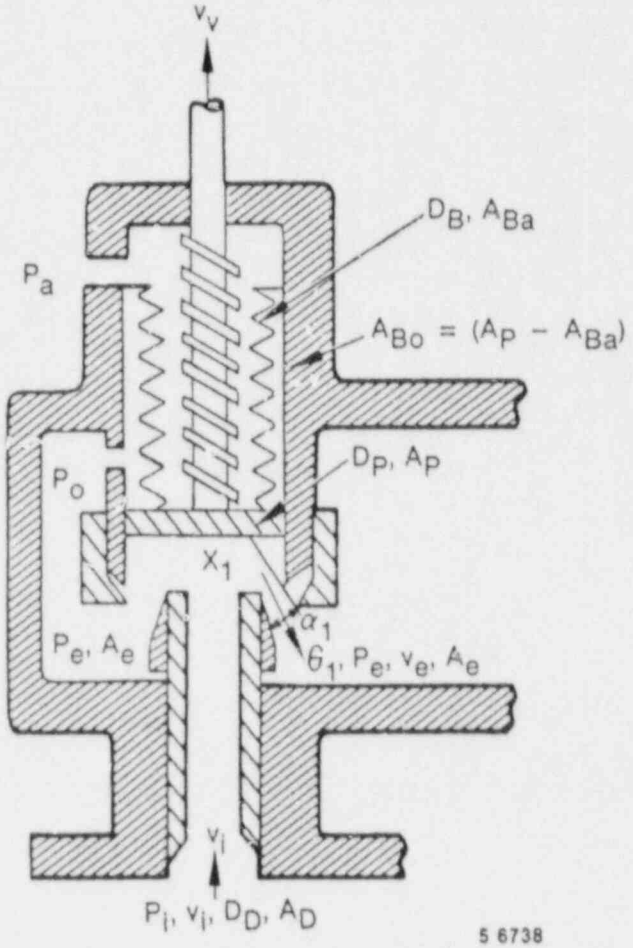

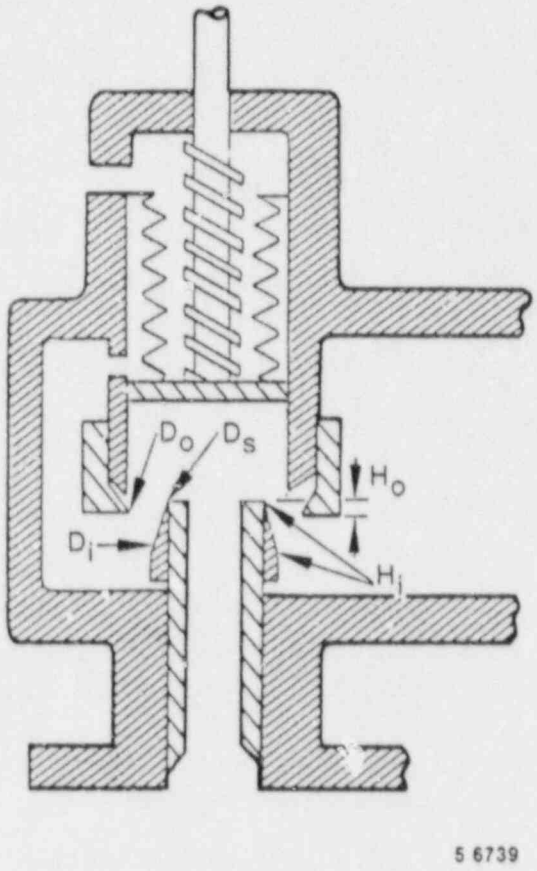

Figures 34 and 35. Schematic of a typical relief valve in the partially and fully open positions, respectively.

the upstream pressure on the valve exceeds the setpoint forces. The setpoint forces are the combined forces of the piston and rod assembly weight, the valve spring, the atmospheric pressure inside the bellows and the downstream back pressure around the outside of the bellows. Once the setpoint forces are exceeded the valve piston will begin to lift. Upon opening, the upstream fluid will begin to expand through the opening into the valve ring region. This initial expansion occurs through the angle α_0 and the flow changes direction through an average angle θ_0 as shown in Figure 33. As the flow accelerates, the momentum effects of the expansion and change in flow direction exert a thrust on the valve piston causing the valve to open further. As the valve partially opens the angle of expansion decreases to α_1 and the change in flow direction increases to θ_1 as shown in Figure 34. This effect in turn further increases the thrust on the valve piston causing it to fully open as shown in Figure 35. As these processes occur the valve reaction forces and fluid momentum forces vary in such a manner that the valve will not close until the upstream pressure decreases significantly below the valve setpoint pressure. In this respect a hysteresis effect is observed that is characteristic of relief valves.

The relief valve model consists of a set of equations designed to approximate the behavior described above. In implementing the model, the dynamic behavior of the fluid is calculated at each time step by the RELAP5/MOD2 hydrodynamic solution scheme. The resultant phasic velocities and thermodynamic properties are then utilized to solve a quasi-steady-equation approximating the fluid forces on the valve piston. The valve dynamic reaction forces are then calculated and the new time valve piston speed and position are estimated.

The relief valve model is formulated applying D'Alembert's principle in which the forces acting on the face of the valve piston are balanced, for which the valve reaction forces can be written as

$$(\text{Reaction Forces}) = F_R = m_v a_{v,x} + B\,(v_{v,x} - v_{housing}) + K_s x \qquad (434)$$

where

m_v = mass of the valve mechanism that is in motion (i.e. the valve piston, rod assembly combined with the spring and bellows)

$a_{v,x}$ = valve assembly acceleration in the x direction

B = damping coefficient

$v_{v,x}$ = velocity of the valve mechanism in the x direction

$v_{housing}$ = 0 = velocity of the valve housing

K_s = spring constant

x = piston position (i.e., x coordinate).

The positive x direction is assumed to be in the direction of fluid flow at the valve inlet. The fluid forces can be formulated by summing the forces acting over the surfaces of the fluid flow channel such that

$$\text{(fluid forces)} = F_F = (P_i A_D)_x - (P_a A_{Ba})_x - (P_o A_{Bo}) - (P_e A_e)_x - F_R \quad (435)$$

where

F_R = reaction forces

P_i = valve inlet pressure

A_D = valve piston face area exposed to the inlet flow stream

P_a = atmospheric pressure inside the bellows

A_{Ba} = valve piston area inside the bellows

P_o = valve back pressure outside the bellows

A_{Bo} = valve piston area outside the bellows

A_e = valve ring exit area

P_e = valve ring exit pressure

and where the subscript x denotes that the force component is in the x direction. Since the fluid is flowing through a channel that both expands and changes direction, the fluid undergoes a change in momentum expressed by the impulse momentum principle as

$$F_F = \Delta (mv) = \dot{m}_F (v_{e,x} - v_{i,x}) \tag{436}$$

where

$\dot{m}_F$ = mass flow rate of the fluid through the valve

$v_{e,x}$ = fluid velocity exiting through the rings

$v_{i,x}$ = fluid velocity entering the valve inlet.

Hence balancing the forces by combining Equations (434), (435) and (436) gives

$$m_v a_{v,x} + Bv_{v,x} + K_s x =$$

$$- (P_a A_{Ba}) - (P_o A_{Bo}) - (P_e A_e) \cos\theta - \dot{m}_F (v_e \cos\theta - v_i) + P_i A_D \quad . \tag{437}$$

The valve acceleration can be expressed in terms of the valve velocity as

$$a_{v,x} = \frac{dv_{v,x}}{dt} + g \tag{438}$$

where g is the acceleration of gravity.

Combining Equations (437) and (438), treating the velocity damping term and spring force position terms implicitly and integrating over the time step gives

$$m_v (v_{v,x}^{n+1} - v_{v,x}^{n}) + Bv_{v,x}^{n+1} dt + K_s x^{n+1} dt + m_v g dt = [(P_i^n A_D)$$

$$- (P_a A_{Ba}) - (P_o^n A_{BO}) - (P_e^n A_e) \cos\theta_e^n - \dot{m}_F^n (v_e \cos\theta_e^n - v_i)] dt \tag{439}$$

where the superscripts n and n+1 represent the old and new time terms, respectively.

The position term, x^{n+1}, can be written in terms of the valve velocity by considering that

$$v_{v,x} = \frac{dx}{dt} \quad . \tag{440}$$

If Equation (440) is integrated over the time step then

$$x^{n+1} = x^n + v_{v,x}^{n+1} dt \quad . \tag{441}$$

If the valve setpoint pressure is equated to $K_s x_o$ then combining Equations (439), (441) and both adding and subtracting the term $K_s x_o$ gives the numerical form of the relief valve model, for which

$$m_v (v_{v,x}^{n+1} - v_{v,x}^{n}) + [(B + K_s dt)\, v_{v,x}^{n+1} + K_s(x^n - x_o) + m_v g]\, dt$$

$$= K_s x_o dt + [(P_i^n A_D) - (P_a A_{Ba}) - (P_o^n A_{Bo}) - (P_e^n A_e)\cos\theta_e^n$$

$$- \dot{m}_F^n (v_e^n \cos\theta_e^n - v_i^n)\, dt \qquad (442)$$

where the size of the gravity term, g, is depencent on the valve orientation. For example, if the valve is oriented upward (i.e.: + x is upward) then the gravity term is expressed as $g = -|g|$.

In the numerical scheme, Equation (442) is solved for the new time valve piston velocity, v_v^{n+1}, in terms of the current time terms with superscript, n. The terms required to model the valve geometry and the valve damping, spring, and back pressure forces are input to the code as described in Volume 2, Appendix A of this report.

The characteristic relief valve hysteresis effects are inherent in the formulation of Equation (442). For example, if the valve is closed then all velocity terms are zero and $x = x_o$. Therefore, acceleration of the valve piston in the positive x direction cannot occur until the upstream force $P_i A_D$ exceeds the spring set point and valve weight. Once the valve opens and the fluid accelerates, the forces due to the change in fluid momentum aid in holding the valve open. Therefore, the valve cannot close until the combined fluid pressure and momentum terms decrease below the set point forces. Hence, the desired hysteresis is incorporated in the model.

3.1.5.7 Accumulator Model. An accumulator model is included in RELAP5/MOD2 that features mechanistic relationships for the hydrodynamics, heat transfer from the tank wall and water surface, condensation in the vapor dome, and vaporization from the water surface to the vapor dome.

3.1.5.7.1 Hydrodynamic Model--An accumulator is modeled in RELAP5 as a lumped-parameter component. This model was chosen for two reasons; the spatial gradients in the accumulator tank are expected to be small, and special treatment of the equation of state can be utilized.

The accumulator model and associated notations are shown in Figure 36. The basic model assumptions are:

1. Heat transfer from the accumulator walls and heat and mass transfer from the liquid are modeled using natural convection correlations assuming similarity between heat and mass transfer from the liquid surface.

2. The gas in the gas dome is modeled as a closed expanding system composed of an ideal gas with constant specific heat. The steam in the dome exists at a very low partial pressure and hence its effect on the nitrogen state is neglected. However, energy transport to the gas dome as a result of vaporization/condensation is included.

3. Because of the high heat capacity and large mass of water below the interface, the water is modeled as an isothermal system.

4. The model for liquid flow includes inertia, wall friction, form loss, and gravity effects.

Using these assumptions, the basic equations governing the thermal-hydraulics of the tank and discharge line for conservation of mass (nitrogen) can be written

$$M_n = \text{constant} = \rho_n V_v \tag{443}$$

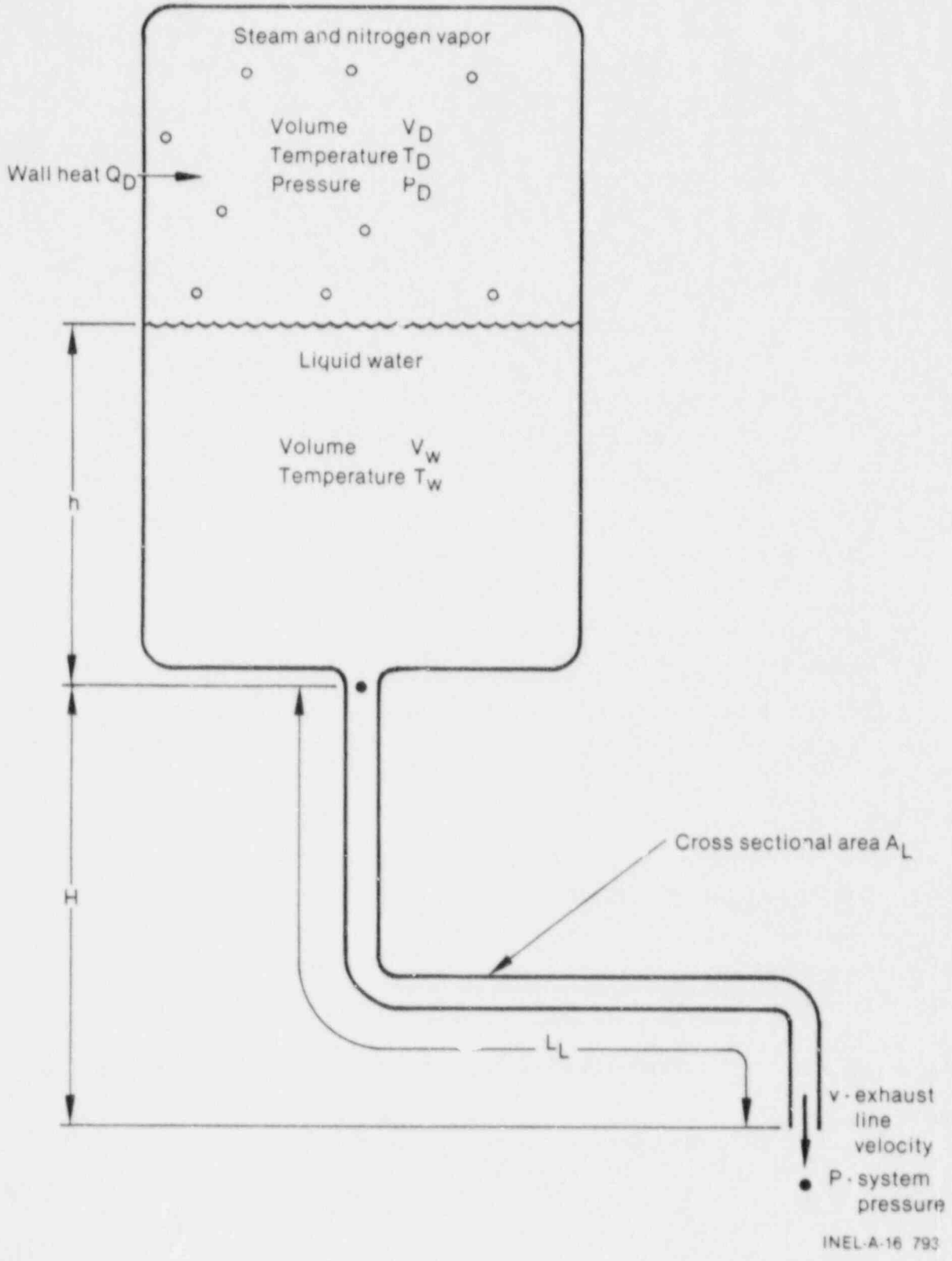

Figure 36. Typical accumulator.

where

M_n and ρ_n = gas, mass, and density, respectively

V_v = gas dome volume

for conservation of energy

Nitrogen

$$M_n \frac{\partial u_n}{\partial t} = - P_D \frac{\partial V_v}{\partial t} + \dot{Q}_D \tag{444}$$

where

u_n = nitrogen internal energy

P_D = vapor dome pressure

Q_D = heat transfer rate to the gas dome.

Wall

$$M_{wall} C_{v_{wall}} \frac{\partial T_{wall}}{\partial t} = - \dot{Q}_{wall} \tag{445}$$

where

M_{wall} = metal mass in the tank wall

$C_{v_{wall}}$ = metal specific heat

T_{wall} = mean metal temperature

$\dot{Q}_{wall}$ = heat transfer rate to the wall.

for momentum[a]

$$\rho A \left(L \frac{\partial v}{\partial t} + \frac{1}{2} v^2\right) + Fv = - A \frac{\partial P}{\partial x} + \Delta P_z \qquad (446)$$

where

A = flow channel cross-sectional area

v = velocity

F = frictional loss coefficient

ΔP_z = elevation pressure differential.

and for the gas state relationships

$$P_D V_v = M_n R_n T_D \qquad (447)$$

$$U_n = M_n C_{v_n} T_D \quad . \qquad (448)$$

Using Equations (447) and (448), the nitrogen energy equation [Equation (446)], can be rewritten as

$$M_n C_{v_n} \frac{dT_D}{dt} = - P_D v A_L + \dot{Q}_D \quad . \qquad (449)$$

Differentiating Equation (447), eliminating the constant term $M_n R_n$ and substituting the result into Equation (449) yields

---

a. Equation (446) is the combined tank and discharge line momentum equations. The wall drag coefficient, F, is given as $1/2 \rho_{wf} L_L/D A_L v$ where D = surge line diameter.

$$P_D \left(1 + \frac{R_n}{C_{v_n}}\right)\frac{dV_v}{dt} + V_v \frac{dP_D}{dt} = \frac{R_n}{C_{v_n}} \dot{Q}_D \quad . \tag{450}$$

Equations (446), (449), and (450) comprise the system of three differential equations used in the accumulator hydrodynamic model. They are used to numerically advance T_D, V_v, and P_D in time.

3.1.5.7.2 Heat Transfer to the Gas Dome--In the accumulator, energy transport by heat transfer is modeled to the gas dome using a typical connective transport equation of the form

$$Q_i = h_i A_i (T_i - T_d) \tag{451}$$

where

subscript i = thermal transport interface

h_i = convective transport coefficient

A_i = interface surface area

$T_i - T_d$ = interface to gas dome temperature difference.

It should be noted that heat and mass transfer in the accumulator surge line are neglected.

Two turbulent natural convection heat transfer models are used and combined by superposition. First, heat transfer with the cylindrical walls of the tank is considered using a turbulent natural convection correlation[96] for heat transfer within a vertical cylinder with closed ends for which

$$h_1 = 0.1 \frac{k_d}{\frac{1}{2} D_{TK}} (Gr\ Pr)^{\frac{1}{3}} \frac{L}{\delta} \tag{452}$$

and

$$A_1 = \pi D_{TK} L \tag{453}$$

where

h_1 = gas dome to cylinder heat transfer coefficient

L = gas dome cylinder length

δ = gas dome characteristic diameter

k_d = gas thermal conductivity

$\frac{1}{2} D_{TK}$ = integration interval normal to the surface of the cylinder

Gr = gas dome Grashof number

Pr = gas dome Prandtl number.

Second, heat transfer with the disk shaped ends of the cylinder is considered, where the top disk is the metal top of the tank and the bottom disk is the liquid-gas interface. For this model a turbulent natural convection correlation[56] is used for heat transfer between two horizontal disks separated vertically where, for each disk,

$$h_2 = 0.15 \frac{k_d}{L} (Gr\ Pr)^{\frac{1}{3}} \frac{L}{\delta} \tag{454}$$

and

$$A_2 = \frac{\pi D_{TK}^2}{4} \quad . \tag{455}$$

In the correlations given by Equations (452) and (455) the product of the Grashof and Prandtl numbers represents the convective thermal circulation in the gas dome, where the Grashof number represents the circulation and the Prandtl number represents the thermal diffusion. Only the Grashof number is a function of the gas dome dimensions and temperature difference for which

$$Gr = \frac{g\beta_d \left| T_i - T_d \right| \delta^3}{\nu_i^2} \tag{456}$$

where

g = acceleration due to gravity

β_d = gas isobaric coefficient of thermal expansion

$T_i - T_d$ = magnitude of the interface, gas dome difference

ν_i = gas kinematic viscosity

δ = characteristic overall diameter of the gas dome.

If the Prandtl number is written in terms of the gas dome thermal diffusivity then

$$Pr = \frac{\mu_d}{\rho_d \alpha_d} \tag{457}$$

where

ρ_d = gas density

α_d = thermal diffusivity.

The characteristic diameter is defined in terms of the typical volume to surface area ratio as

$$\delta = \frac{4\ V_d}{A_i} \tag{458}$$

where

A_i = combined gas dome cylinder, disk top, and bottom surface areas.

3.1.5.7.3 Mass Transfer to the Gas Dome--When the accumulator is in its stagnant initial condition the gas dome and liquid are in thermal equilibrium and the gas dome is at essentially 100% humidity. However, as the accumulator blows down, the gas dome expands and cools while the liquid remains essentially isothermal. As a result there is simultaneous vaporization at the liquid-gas interface and condensation in the gas dome.

At the liquid-gas interface as vaporization occurs the vapor diffuses across the temperature gradient into the gas dome. Assuming that the process can be approximated by a quasi-steady formulation, then for diffusion in a stagnant gas the mass transfer for the process can be written as

$$\dot{M}_{vap} = - \zeta A_i \frac{dC}{dx} \tag{459}$$

where

$\dot{M}_{vap}$ = rate of vapor diffusion

ζ = diffusion coefficient

A_i = surface area of the liquid-gas interface

$\frac{dC}{dx}$ = vapor concentration gradient.

The concentration can be expressed in terms of partial pressure such that

$$C = \frac{P_v}{P_d} \rho_g \tag{460}$$

where

C = vapor concentration

P_v = local vapor partial pressure

ρ_g = vapor density (saturated vapor at P_v).

Hence at the dome pressure, the concentration gradient can be written as

$$\frac{dC}{dx} = \frac{1}{P_d} \frac{dP_v \rho_g}{dx} \quad . \tag{461}$$

Combining Equations (459) and (461) and integrating gives

$$\dot{M}_{vap} L_d = - \frac{\zeta A_i}{P_d} \left(\bar{P}_v \int_{x=0}^{x=L_d} d\rho_g + \bar{\rho} \int_{x=0}^{x=L_d} dP_v \right) \tag{462}$$

where the integration is performed by parts.

Both of the differential terms $d\rho_g$ and dP_v can be written in terms of temperature differentials if 100% relative humidity is assumed so that

$$P_v = P^S (T_g)$$

where

$P^s(T_g)$ = saturation pressure at the temperature T_g.

Hence the density differential can be expanded as

$$d\rho_g = \left[\left(\frac{\partial \rho_g}{\partial P_g}\right)_T \frac{dP_g}{dT} + \left(\frac{\partial \rho_g}{\partial T}\right)_{P_g}\right] dT \tag{463}$$

where

$$\left(\frac{\partial \rho_g}{\partial P_g}\right)_T = \kappa_g \rho_g \tag{464}$$

$$\left(\frac{\partial \rho_g}{\partial T}\right)_{P_g} = -\beta_g \rho_g \,. \tag{465}$$

Combining Equations (463), (464), and (465), and substituting Clapeyron's equation for the dP_s/dT term gives

$$d\rho_g = \bar{\rho}_g \left[\kappa_g \left(\frac{h_{fg}}{T_g^s v_{fg}}\right) - \beta_g\right] dT \tag{466}$$

where Clapeyron's equation is

$$dP^s = \left(\frac{h_{fg}}{T_g v_{fg}}\right) dT \tag{467}$$

and where the term $(h_{fg}/T_g v_{fg})$ is treated as a constant. Combining Equations (462), (466), and (467) the diffusion equation can be rewritten as

$$\dot{M}_{vap} = \frac{\zeta}{L_d} \frac{A_i}{P_d} \left\{ \bar{P}_g \bar{\rho}_g \left[\kappa_g \left(\frac{h_{fg}}{T_g v_{fg}} \right) - \beta_g \right] + \bar{\rho}_g \left(\frac{h_{fg}}{T_g v_{fg}} \right) \right\} (T_f - T_w) \qquad (468)$$

where the dome average terms are evaluated at the dome average temperature, $T_g = T_d$, and where T_f is the tank top wall temperature.

Equation (468) can be made analogous to a convective equation by expressing the mass transfer coefficient as

$$h_{2s} = \frac{\zeta}{L_d} \qquad (469)$$

where

h_{2s} = mass transfer coefficient in a stagnant gas.

Then, by applying Reynold's analogy a turbulent natural convection mass transfer coefficient can be derived in terms of the heat transfer coefficient, h_2, from Equation (463) such that

$$h_{2s} = h_2 \left(\frac{\zeta}{k_D} \right) \left(\frac{\alpha_d}{\zeta} \right)^{1/3} \qquad (470)$$

Equation (470) can then be substituted in place of (ζ/L) in Equation (469) such that

$$\dot{M}_{vap} = h_2 \left(\frac{\zeta}{k_d} \right) \left(\frac{\alpha_d}{\zeta} \right)^{\frac{1}{3}} \left(\frac{A_i}{P_d} \right) \left\{ \bar{P}_g \bar{\rho}_g \left[k_g \left(\frac{h_{fg}}{T_d v_{fg}} \right) - \beta_g \right] + \bar{\rho}_g \left(\frac{h_{fg}}{T_g v_{fg}} \right) \right\} (T_f - T_w) \qquad (471)$$

which gives the rate at which water vapor is transported into the accumulator gas dome by turbulent diffusion.

Since the energy transported to the gas dome by the vaporization process must come from the liquid and since the energy per unit mass required for vaporization is h_{fg}, then the rate of energy transport to the gas dome by vaporization is

$$\dot{Q}_{vap} = \Gamma_{vap}(h_{fg})_{T_f} = \dot{M}_{vap}(h_g)_{T_f} \tag{472}$$

where Γ_{vap} is the rate of vaporization at the liquid gas interface.

In the gas dome, as the accumulator blows down, the gas cools and condensation by turbulent diffusion occurs. The rate of condensation may be approximated by assuming that the gas dome remains at 100% humidity and considering simple humidity relationships. The humidity ratio can be written as

$$w = \frac{M_g}{M_n} = \frac{N_g P_g}{N_n P_D} \tag{473}$$

where

M_g, M_n = vapor, gas masses, respectively

N_g, N_n = vapor, gas molecular weights, respectively

P_g = vapor partial pressure.

Taking the derivative of Equation (473) gives

$$\frac{dM_g}{dt} = \frac{1}{P_D}\left(M_n \frac{N_g}{N_n}\frac{dP_g}{dt} - M_g \frac{dP_D}{dt}\right) . \tag{474}$$

From Gibb's equation, the relationship between the vapor and liquid condensate in the dome is

$$V_{g_{P_g,T_D}} \frac{dP_g}{dT_D} - S_{g_{P_g,T_D}} = V_{f_{P_D,T_D}} \frac{dP_D}{dT_D} - S_{f_{P_D,T_D}} \tag{475}$$

and substituting the relationship

$$\frac{dP}{dt} = \frac{dP}{dT} \frac{dT}{dt} \tag{476}$$

into Equation (475) and rearranging gives

$$\frac{dP_g}{dt} = \frac{V_{f_{P_D,T_D}}}{V_{g_{P_g,T_D}}} \frac{dP_D}{dt} - \frac{\left(h_{g_{P_g,T_D}} - h_{f_{P_D,T_D}}\right)}{T_D V_{g_{P_g,T_D}}} \frac{dT_D}{dt} \quad . \tag{477}$$

Combining Equations (474) and (477) with Equations (449) and (450) gives

$$\frac{dM_g}{dt} = \frac{1}{P_D}\left(M_a \frac{N_g}{N_a} - M_g\right) \frac{V_{f_{P_D,T_D}}}{V_{g_{P_g,T_D}}} \frac{1}{V_v}\left[\dot{Q}_D \frac{R_n}{C_v} - P_D\left(1 + \frac{R_n}{C_v}\right) A_1 V\right] \tag{478}$$

$$+ \frac{1}{P_D} \frac{N_g}{N_a}\left(\frac{h_{g_{P_g,T_D}} - h_{f_{P_D,T_D}}}{T_D V_{g_{P_g,T_D}}}\right) \frac{1}{C_v}\left(\dot{Q}_D - P_D A_1 V\right) \tag{479}$$

and the rate of condensate formation is given as

$$\dot{M}_C = - \frac{dM_g}{dt} + \dot{M}_{vap} \quad . \tag{480}$$

The energy transported by the condensate to the interface can be expressed as

$$\dot{Q}_{m_c} = \dot{m}_c \, h_{f_{T_D}} \quad . \tag{481}$$

Also, since the condensation is taking place in the gas dome, the energy given up by the condensation process is given up to the gas dome at the rate expressed as

$$\dot{Q}_{M_c} = \dot{M}_c \, h_{fg_{T_D}} \quad . \tag{482}$$

Finally, since it is assumed that the condensate is transported to the interface at the condensation rate,

$$\dot{m}_c = \dot{M}_c \tag{483}$$

and the net energy given up to the gas dome by the condensation process can be expressed as

$$\dot{Q}_c = \dot{Q}_{M_c} - \dot{Q}_{m_c} = \dot{m}_c (h_{fg_{T_D}} - h_{f_{T_D}}) \quad . \tag{484}$$

3.1.5.7.4 Energy Transported to the Gas Dome by Combined Heat and Mass Transfer--The total energy transported to the gas dome can be rewritten by combining Equations (451), (452), (454), (472), and (484) and summing to give

$$\dot{Q}_D = (h_1 A_1 + h_2 A_2)(T_w - T_d) + h_2 A_2 (T_f - T_d) + \dot{M}_{vap} h_{g_{T_f}}$$

$$+ \dot{m}_c \left(h_{fg_{T_d}} - h_{f_{T_d}} \right) . \qquad (485)$$

3.1.5.7.5 Numerical Implementation--The numerical scheme used for the accumulator model includes special features for coupling the solution scheme to the main code in such a way that it is time step independent. This scheme, as in RELAP5, is semi-implicit and special considerations are employed to preserve the nitrogen energy and mass.

The numerical scheme uses finite difference techniques to solve the differential equations. The momentum equation is formulated by integrating Equation (446) over space and writing the time variation in difference form as

$$\left[\rho_f \left(L_{f_L} + L_{f_{TK}} \frac{AL}{A_{TK}} \right) + F_f \Delta t + \rho_g \left(L_{g_L} + L_{g_{TK}} \frac{AL}{A_{TK}} \right) + F_g \Delta t \right] v_{f_L}^{n+1}$$

$$= - \left(p^{n+1} - p_D^{n+1} \right) \Delta t + \Delta P_z \Delta t + \left[\rho_f \left(L_{f_L} + L_{f_{TK}} \frac{A_L}{A_{TK}} \right) \right.$$

$$\left. + \rho_g \left(L_{g_L} + L_{g_{TK}} \frac{A_L}{A_{TK}} \right) \right] v_{f_L}^{n} - CONVF - CONVG \qquad (486)$$

where

p^{n+1} = pressure downstream from the accumulator junction.

The inertia term is represented by

$$\rho_f \left(L_{f_L} + L_{f_{TK}} \frac{AL}{A_{TK}} \right) + \rho_g \left(L_{g_L} + L_{g_{TK}} \frac{AL}{A_{TK}} \right) \qquad (487)$$

where L_{f_L}, $L_{f_{TK}}$, L_{g_L} and $L_{g_{TK}}$ are the lengths of the liquid and gas in the surge line and tank, respectively. These terms are computed at each time step and hence vary explicitly with time having the effect that as the accumulator blows down the inertia term changes from a liquid dominant to a vapor dominant term. The liquid and gas friction terms, respectively, are formulated as

$$F_f = \frac{\rho_f}{2}\left(\lambda \frac{L_{fL}}{D_L} + K_L \frac{L_{fL}}{L_L}\right) v_{f_L}^n \tag{488}$$

for the liquid, and

$$Fg = \frac{\rho_g}{2}\left(\lambda \frac{L_{gL}}{D_L} + K_L \frac{L_{gL}}{L_L}\right) v_{g_L}^n \tag{489}$$

for the vapor, where friction is neglected in the tank and the line friction factor is assumed to be the constant turbulent-turbulent Darcy friction factor given as

$$\lambda = \left[1.74 - 2 \operatorname{Log} \frac{2\varepsilon}{D}\right]^{-2} . \tag{490}$$

The loss factor term, K_L, is assumed to be distributed over the surge line length, L_L. The term D_L is the surge line hydraulic diameter and ε is the surge line wall roughness. The elevation head term, Δp_z, is formulated as

$$\Delta P_z = - \frac{g\Delta z_{TK}\left(\rho_f L_{f_{TK}} + \frac{1}{2}\rho_g L_{g_{TK}}\right)}{L_{TK}} - \frac{g\Delta z_L\left(\rho_f L_{f_L} + \rho_g L_{g_L}\right)}{L_L} \tag{491}$$

where Δz_{TK} and Δz_L are the tank and surge line elevation changes, respectively, and g is the gravitational acceleration. The liquid and vapor momentum flux terms, CONVF and CONVG, respectively are formulated as

$$CONVF = \frac{1}{2} \rho_f \left(1 - \frac{A_L}{A_{TK}}\right)^2 \Delta t \left(v_{fL}^n\right)^2 . \quad (492)$$

if there is liquid in the tank,

$$CONVF = 0.0 \quad (493)$$

where there is no liquid in the tank,

$$CONVG = \frac{1}{2} \rho_g \left(1 - \frac{A_L}{A_{TK}}\right)^2 \Delta t \; v_{g_L}^{n\ 2} \quad (494)$$

if there is vapor in the surge line, and, finally

$$CONVG = 0.0 \quad (495)$$

where there is no vapor in the surge line. By formulation in this manner the momentum equation is solved over the pressure gradient from the centroid of the gas dome to the accumulator junction. However, the momentum of the fluid downstream from the accumulator junction is not included. Also since fluxing of the gas through the junction is not allowed, we have

$$v_{g_L}^{n,\ n+1} = v_{f_L}^{n,\ n+1} \quad (496)$$

until the accumulator empties of liquid. The effect of this formulation is that as the accumulator blows down the liquid-gas interface moves out of the accumulator tank and surge line. Thus, the centroid of the gas dome moves towards the centroid of the combined tank and surge line.

The pressure solution is obtained by combining Equations (444) and (448) and multiplying by R_n/C_{v_n}, which results in

$$M_n R_n \frac{dT}{dt} = - \frac{R_n P_D}{C_{v_n}} \frac{dV_v}{dt} + \frac{R_n}{C_{v_n}} \dot{Q}_D \tag{497}$$

where Q_D is given by Equation (485). Equations (447) and (497) are then combined resulting in

$$P_D \left(1 + \frac{R_n}{C_{v_n}} \right) \frac{dV_v}{dt} + V_v \frac{dP_D}{dt} = \frac{R_n}{C_{v_n}} \dot{Q}_D \quad . \tag{498}$$

Since the liquid is incompressible

$$\frac{dV_v}{dt} = - \frac{dV_f}{dt} = A_L v_{f_L} \tag{499}$$

and substitution in Equation (498) and expanding in nonconservative finite difference form gives

$$P_D^n \left(1 + \frac{R_n}{C_{v_n}} \right) A_L \Delta t \, v_{f_L}^{n+1} + V_v^n \left(P_D^{n+1} - P_D^n \right) = \frac{R_n}{C_{v_n}} Q_D^n \, \Delta t \quad . \tag{500}$$

The energy equation may then be solved directly for the new time gas temperature by combining Equations (447), (450), (498), and integrating, which gives

$$T_D^{n+1} = T_D^n \, e^{\left(\frac{R_n}{C_{v_n}} \ln \frac{V_v^n}{V_v^{n+1}} + \Delta t \, \frac{\dot{Q}_D^n}{P_D^n V_v^n} \right)} \quad . \tag{501}$$

3.2 Heat Structures

3.2.1 Heat Conduction Numerical Technique

Heat structures provided in RELAP5 permit calculation of the heat transferred across solid boundaries of hydrodynamic volumes. Modeling capabilities of heat structures are general and include fuel pins or plates with nuclear or electrical heating, heat transfer across steam generator tubes, and heat transfer from pipe and vessel walls. Heat structures are assumed to be represented by one-dimensional heat conduction in rectangular, cylindrical, or spherical geometry. Surface multipliers are used to convert the unit surface of the one-dimensional calculation to the actual surface of the heat structure. Temperature-dependent thermal conductivities and volumetric heat capacities are provided in tabular or functional form either from built-in or user-supplied data.

Finite differences are used to advance the heat conduction solutions. Each mesh interval may contain a different mesh spacing, a different material, or both. The spatial dependence of the internal heat source may vary over each mesh interval. The time-dependence of the heat source can be obtained from reactor kinetics, one of several tables of power versus time, or a control system variable. Symmetry or insulated conditions and tables of surface temperature versus time, heat transfer rate versus time, heat transfer coefficient versus time, or surface temperature are allowed for boundary conditions. For heat structure surfaces connected to hydrodynamic volumes, a heat transfer package containing correlations for convective, nucleate boiling, transition boiling, and film heat transfer from the wall to water and reverse transfer from water to wall is provided.

The following describes the numerical techniques for heat conduction. The integral form of the heat conduction equation is

$$\iiint_V \rho(T,\bar{x}) \frac{\partial T}{\partial t}(\bar{x},t)dV = \iiint_S k(T,\bar{x})\Delta T(\bar{x},t)d\bar{s} + \iiint_V S(\bar{x},t)dV \qquad (502)$$

where k is the thermal conductivity, s is the surface, S is the internal heat source, t is time, T is temperature, V is volume, $\bar{x}$ represents the space coordinates, and ρ is the volumetric heat capacity. The boundary condition applied to the exterior surface has the form

$$A(T)T(t) + B(T)\frac{\partial T(t)}{\partial \bar{n}} = D(T) \quad . \tag{503}$$

The $\bar{n}$ denotes the unit normal vector away from the boundary surface. Thus, if the desired boundary condition is that the heat transferred out of the surface equals a heat transfer coefficient, h, times the difference between the surface temperature, T and the sink temperature, T_s become

$$-k\frac{\partial T}{\partial \bar{n}} = h(T - T_s) \tag{504}$$

then the correspondence between the above expression and Equation (503) yields

$$A = h,\ B = k \text{ and } D = h(T_w - T_s) \quad . \tag{505}$$

In one dimensional problems, boundary conditions are applied on the left and right surfaces. In steady state problems, a valid physical problem requires that A be nonzero on at least one of the two boundary surfaces. If a transient or steady state problem has cylindrical or spherical geometry and a zero radius for the left surface (that is, a solid cylinder or sphere), the left boundary condition is normally the symmetry condition, $\frac{\partial T}{\partial \bar{n}} = 0$. Under these conditions if B is nonzero, the numerical technique forces the symmetry boundary condition, even if it is not specified.

3.2.2 Mesh Point and Thermal Property Layout

Figure 37 illustrates the placement of mesh points at temperatures to be calculated. The mesh point spacing for a rectangular problem is taken in the positive x direction. For cylindrical and spherical problems, the mesh point spacing is in the positive radial direction. Mesh points are placed on the external boundaries of the problem, at the interfaces between different materials, and at desired intervals between the interfaces, boundaries, or both.

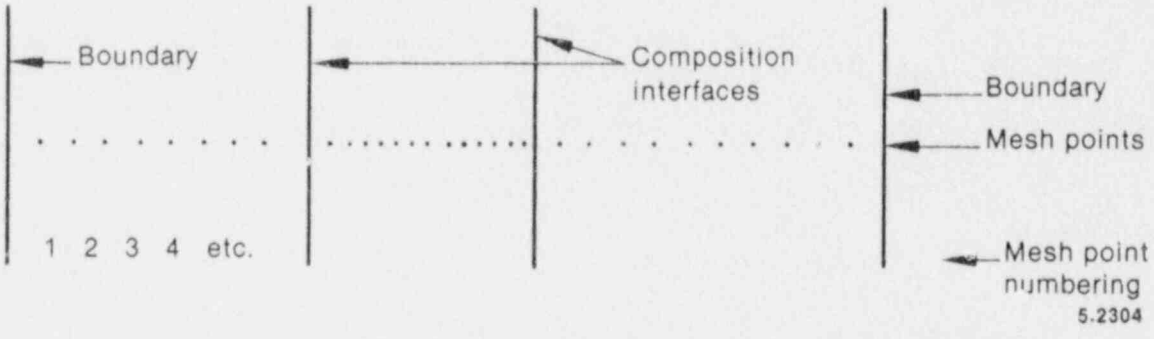

Figure 37. Mesh point layout.

Figure 38 represents three typical mesh points. The subscripts are space indexes indicating the mesh point number, and ℓ and r (if present) designate quantities to the left and right, respectively, of the mesh point. The δ's indicate mesh point spacings that are not necessarily equal. Between mesh points, the thermal properties, k and ρ and the source term, S, are assumed spatially constant, but $k_{\ell m}$ is not necessarily equal to k_{rm} and similarly for ρ and S.

To obtain the spatial-difference approximation for the m^{th} interior mesh point, Equation (502) is applied to the volume and surfaces indicated by the dashed line shown in Figure 38. For the spatial-difference approximation at the boundaries, Equations (502) and (503) are used to define the gradient along the exterior surfaces and applied to the volumes and surfaces indicated by the dashed lines shown in Figure 39. If the coefficient of the gradient in the boundary equation is zero, the surface

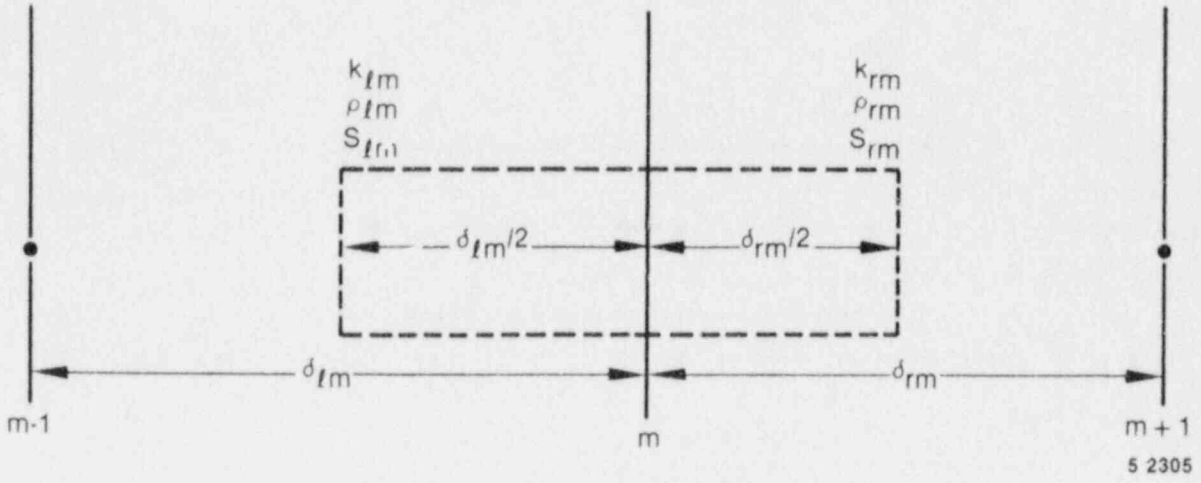

Figure 38. Typical mesh points.

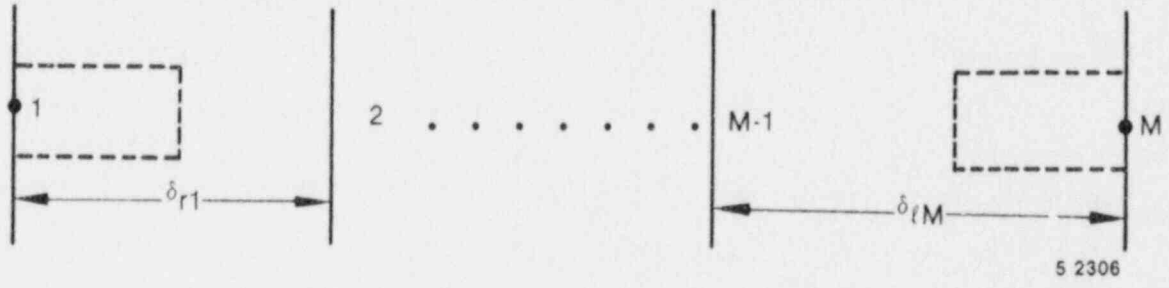

Figure 39. Boundary mesh points.

temperature is given directly from Equation (503). Since the code is one-dimensional, the dimensions of the volume for other than the x or r coordinate are set to one. For rectangular geometry, the volume is a rectangular solid. For cylindrical geometry, the volume is a cylindrical annulus, and for spherical geometry, the volume is a spherical shell.

The spatial finite-difference approximations use exact expressions for the space and volume factors and simple differences for the gradient terms.

To condense the expressions defining the numerical approximations and to avoid writing expressions unique to each geometry, the following quantities are defined.

For rectangular geometry

$$\delta^{s}_{\ell m} = \frac{1}{\delta_{\ell m}} \qquad \delta^{s}_{rm} = \frac{1}{\delta_{rm}} \tag{506}$$

$$\delta^{v}_{\ell m} = \frac{\delta_{\ell m}}{2} \qquad \delta^{s}_{rm} = \frac{\delta_{rm}}{2} \tag{507}$$

$$\delta^{b}_{m} = 1 \quad . \tag{508}$$

For cylindrical geometry

$$\delta^{v}_{\ell m} = 2\pi \frac{\delta_{\ell m}}{2}\left(x_m - \frac{\delta_{\ell m}}{4}\right) , \qquad \delta^{v}_{rm} = 2\pi \frac{\delta_{rm}}{2}\left(x_m + \frac{\delta_{rm}}{4}\right) , \tag{509}$$

$$\delta^{s}_{\ell m} = \frac{2\pi}{\delta_{\ell m}}\left(x_m - \frac{\delta_{\ell m}}{2}\right) , \qquad \delta^{s}_{rm} = \frac{2\pi}{\delta_{rm}}\left(x_m + \frac{\delta_{rm}}{2}\right) , \tag{510}$$

and

$$\delta^{b}_{m} = 2\pi x_m \quad . \tag{511}$$

For spherical geometry

$$\delta^{v}_{\ell m} = \frac{4}{3\pi}\left[x_m^3 - \left(x_m - \frac{\delta_{\ell m}}{2}\right)^3\right] , \qquad \delta^{v}_{rm} = \frac{4}{3\pi}\left[\left(x_m + \frac{\delta_{rm}}{4}\right)^3 - x_m^3\right] , \tag{512}$$

$$\delta^{s}_{\ell m} = \frac{4\pi}{\delta_{\ell m}}\left(x_m - \frac{\delta_{\ell m}}{2}\right)^2 , \qquad \delta^{s}_{rm} = \frac{4\pi}{\delta_{rm}}\left(x_m + \frac{\delta_{rm}}{2}\right)^2 , \tag{513}$$

and

$$\delta_m^b = 4\pi x_m^2 \quad . \tag{514}$$

For all geometries

$$G_m = \rho_{\ell m}\delta_{\ell m}^v + \rho_{rm}\delta_{rm}^v \quad . \tag{515}$$

The superscripts, v and s, refer to volume and surface-gradient weights. The δ_m^b is a surface weight used at exterior boundaries and in heat transfer rate equations.

3.2.3 Difference Approximation at Internal Mesh Points

Using a forward difference for the time derivative, the first term of Equation (502) for the volume of Figure 38 is approximated by

$$\iiint_V \rho(T,\bar{x})\,\frac{\partial T}{\partial t}(\bar{x},t)\,dV \approx \left(T_m^{n+1} - T_m^n\right)\frac{G_m}{\Delta t} \quad . \tag{516}$$

The superscript n refers to time; thus, T_m^n indicates the temperature at mesh point m at time t^n, and T_m^{n+1} indicates the temperature at mesh point m at time $t^{n+1} = t^n + \Delta t$. The second term of Equation (502) for the surfaces of Figure 38 is approximated by

$$\iint_S k(T,\bar{x})\Delta T(\bar{x},t)\,d\bar{s} \approx (T_{m-1} - T_m)\,k_{\ell m}\,\delta_{\ell m}^s + (T_{m+1} - T_m)\,k_{rm}\delta_{rm}^s \quad . \tag{517}$$

Note that the above expression includes the standard interface conditions of continuity of temperature and heat flow. The surface integral of Equation (502) is usually evaluated by integrating only along the exterior surfaces of the volume indicated by the dashed line in Figure 38. If, however, the volume is divided into two sub-volumes by the

interface line and the surface integrals of these sub-volumes are added, the surface integrals along the common interface cancel because of the continuity of heat flow. The continuity of temperature is implied by use of a single-valued temperature at the interface.

A contact-resistance interface condition cannot be specified directly since the temperature, instead of being continuous at the interface, is given by $q = h_c \Delta T$ where q is the heat transfer rate across the interface, h_c is the contact conductivity, and ΔT is the temperature change across the interface. This condition can be specified by defining a small mesh interval with thermal properties of $k = h_c$ and $\rho = 0$. The size of the mesh interval, δ, is arbitrary except in cylindrical or spherical geometry, where the surface and volume weights are dependent on the radius. This mesh interval is usually chosen very small with respect to the dimensions of the problem.

The space and time-dependence of the source term in Equation (502) are assumed to be separable functions

$$S(x,t) = P_f P(t) Q(x) \tag{518}$$

where P_f is the factor that relates the reactor power (or power from a table) to the heat generation rate for a particular heat structure, $P(t)$ is the time varying function and may be reactor power, power from a table, or a control variable, and $Q(x)$ is the space-dependent function. The value of $Q(x)$ is assumed constant over a mesh interval, but each interval can have a different value. The third term of Equation (502) is then approximated as

$$\iiint_V S(\bar{x},t)dV \approx \left(Q_{\ell m}\, \delta^V_{\ell m} + Q_{rm}\, \delta^V_{rm}\right) P_f P(t) \quad . \tag{519}$$

Gathering the approximations of terms in Equation (502), the basic difference equation for the m^{th} mesh point is

$$\frac{\left(T_m^{n+1} - T_m^n\right) G_m}{\Delta t} = -(T_m - T_{m-1})\, k_{\ell m} \delta^s_{\ell m} + (T_{m+1} - T_m)\, k_{rm}\, \delta^s_{rm}$$

$$+ \; Q_{\ell m}\, \delta^v_{\ell m} + Q_{rm}\, \delta^v_{rm}\; P_f P(t) \quad . \tag{520}$$

Using the symbol, ς_m to represent the right side, Equation (520) can be written as

$$\frac{\left(T_m^{n+1} - T_m^n\right) G_m}{\Delta t} = \varsigma_m \quad . \tag{521}$$

Thus far, the time superscripts for G_m and ς_m have been omitted and the procedure for approximating the temperature-dependence of the thermal properties has not been mentioned. The procedures for temperature-dependent thermal properties are discussed later. However, superscripts for thermal properties are written here even though their significance is not explained until later. For steady state, the difference approximation becomes

$$\varsigma_m = 0 \tag{522}$$

and no time superscripts are needed. For the time-dependent case, an equation of the type

$$\frac{(T_m^{n+1} - T_m^n)\, G_m}{\Delta t} = w\, \varsigma_m^{n+1} + (1 - w)\, \varsigma_m^n \tag{523}$$

is an explicit formula if w is zero, and is an implicit formula when w is nonzero. RELAP5 uses the implicit formulation with w = 1/2.

Writing Equation (523), in full, the difference approximation for the m^{th} interior mesh point for transient and steady state cases is

$$a_m^n T_{m-1}^{n+1} + b_m^n T_m^{n+1} + c_m^n T_{m+1}^{n+1} = d_m \tag{524}$$

$$a_m^n = - \frac{K_{\ell m}^n \delta_{\ell m}^s \Delta t}{\sigma + 1} \tag{525}$$

$$b_m^n = \sigma G_m^n - a_m^n - c_m^n \tag{526}$$

$$c_m^n = - \frac{K_{rm}^n \delta_{rm}^s \Delta t}{\sigma + 1} \tag{527}$$

$$d_m = \sigma a_m^n T_{m-1}^n + \sigma G_m^n + a_m^n + c_m^n T_m^n - \sigma c_m^n T_{m+1}^n$$

$$+ \Delta t P_f \left(\frac{P^{n+1} + \sigma P^n}{\sigma + 1} \right) \left(Q_{\ell m} \delta_{\ell m}^v + Q_{rm} \delta_{rm}^v \right) \tag{528}$$

and σ is 1 for transient cases and 0 for steady state cases.

3.2.4 Difference Approximation at Boundaries

To obtain the difference approximations for the mesh points at the boundaries, Equation (502) is applied to the volumes of Figure 39 with Equation (503) used to define the gradient at the surface. The second term of Equation (502) at $x = x_1$ is approximated by

$$\iint_S k(T,\bar{x}) \nabla T(\bar{x},t) \times d\bar{s} \approx - \frac{k_{r1}}{B_1} (A_1 T_1 - D_1) \delta_1^b + k_{r1} (T_2 - T_1) \delta_{r1}^s \ . \tag{529}$$

The complete basic expression for the left boundary mesh point becomes

$$\frac{(T_1^{n+1} - T_1^n)}{\Delta t} \rho_{r1} \delta_{r1}^v = - \frac{k_{r1}}{B_1} (A_1 T_1 - D_1) \delta_1^b$$

$$+ k_{r1} (T_2 - T_1) \delta_{r1}^s + Q_{r1} \delta_{r1}^v P_f P(i) \quad . \tag{530}$$

If B in the boundary condition equation is zero, the above equation is not used since the boundary condition determines the temperature. Also in that case, a divide by zero would be indicated if Equation (530) were used. Approximations for the boundary at $x = x_m$ are derived in a similar fashion. These equations for the boundary mesh points are converted to the implicit formulas in the same manner as for the interior mesh points, except that the surface temperature appearing in the boundary condition is evaluated completely at the n+1 time level. Thus, for the left boundary

$$b_1^n T_1^{n+1} + c_1^n T_2^{n+1} = d_1 \tag{531}$$

$$b_1^n = \sigma \rho_{r1}^n \delta_{r1}^v + \frac{k_{r1}^n A_1^n \delta_1^b \Delta t}{B_1^n} - c_1^n \tag{532}$$

$$c_1^n = \frac{k_{r1}^n \delta_{r1}^s \Delta t}{\sigma + 1} \tag{533}$$

$$d_1 = - \sigma c_1^n T_2^n + \sigma \rho_{r1}^n \delta_{r1}^v + c_1^n T_1^n + \frac{k_{r1}^n \delta_1^b D_1^n \Delta t}{B_1^n}$$

$$+ P_f \frac{(\sigma P^n + P^{n+1})}{\sigma + 1} \frac{Q_{r1} \delta_{r1} \Delta t}{} \tag{534}$$

In the coding, a variable, HTBCCO, is defined as $C_1^n = A_1^n T_1^n - D_1^n$. Substituting this relation into Equation (534) gives

$$d_1 = \sigma C_1^n T_2^n + \left(\delta p_{r1}^n \sigma_{r1}^v + \sigma C_1^n + \frac{k_{r1}^n \delta_1^b A_1^n \Delta t}{B_1^n} \right) T_1^n - \frac{k_{r1} \delta b_1 C_1 \Delta t}{B_1^n}$$

$$+ \frac{P_f (\sigma P^n + P^{n+1}) \, Q_{r\ell} \delta_{r\ell}^v \Delta t}{\sigma + 1} \quad . \tag{535}$$

For the right boundary,

$$a_M^n \, T_{M-1}^{n+1} + b_M^n \, T_M^{n+1} = d_M \tag{536}$$

$$a_M^n = \frac{-k_{\ell M}^n \, \delta_{\ell M}^s \, \Delta t}{\sigma + 1} \tag{537}$$

$$b_M^n = \sigma \rho_{\ell M}^n \, \delta_{\ell M}^v + \frac{k_{\ell M}^n \, A_M^n \, \delta_M^b \, \Delta t}{B_M^n} - \sigma \, a_M^N \tag{538}$$

$$d_M = - \sigma a_M^n \, T_{M-1}^n + \sigma \left(\rho_{\ell M}^n \, \delta_{\ell M}^v + a_M^n \right) T_M^n + \frac{k_{\ell M}^n \, \delta_M^b \, D_M^n \, \Delta t}{B_M^n}$$

$$+ P_f \, \frac{(\sigma P^n + P^{n+1}) \, Q_{\ell M} \, \delta_{\ell M}^v \, \Delta t}{\sigma + 1} \quad . \tag{539}$$

In the coding, a variable, HTBCCN, is defined as $C_m^n = A_M^n T_M^n - D_M^n$. Substituting this relation into Equation (539) gives:

$$dM = - \sigma a_M^n T_{M-1}^n + \left(\sigma \rho_{\ell M}^n \delta_{\ell M}^v + a_M^n + \frac{k_{\ell M}^n \delta_M^b A_M^n \Delta t}{B_M^n} \right) T_M^n - \frac{k_{\ell M}^n \delta_M^b C_M^n \Delta t}{B_M^n}$$

$$+ \frac{P_f \left(\sigma P^n + P^{n+1}\right) Q_{\ell M} \delta^v_{\ell M} \Delta t}{\sigma + 1} \qquad (540)$$

3.2.5 Solution of Simultaneous Equations

The difference approximations for the mesh points [Equations (528), (474), and (475)] lead to a tri-diagonal set of M equations. The coefficient matrix is symmetric unless the boundary condition specifies the surface temperature. In that case, the elements, c_1 and a_M, are 0, and destroy the symmetry. The solution to the above equations is obtained by

1. Form $E_1 = \frac{c_1}{b_1}$ and $F_1 = \frac{d_1}{b_1}$ (541)

2. For $E_j = \frac{c_j}{b_j - a_j E_{j-1}}$ and $F_j = \frac{d_j - a_j F_{j-1}}{b_j - a_j E_{j-1}}$

for $j = 2, 3, \ldots, M-1$ (542)

3. Form $T_M^{n+1} = \frac{d_M - a_M F_{M-1}}{b_M - a_M E_{M-1}}$ (543)

4. Form $T_j^{n+1} = - E_j T_{j+1}^{n+1} + F_j$

for $j = M-1, M-2, \ldots, 3, 2, 1.$ (544)

These procedures can be derived by applying the rules for Gaussian elimination. This method of solution introduces little roundoff error if the off-diagonal elements are negative and the diagonal is greater than the sum of the magnitudes of the off-diagonal elements. From the form of the difference equations, these conditions are satisfied for any values of the mesh point spacing, time step, and thermal properties.

3.2.6 Thermal Properties, Boundary Condition Parameters, and Iteration Procedures

The thermal conductivity, k, and the volumetric heat capacity, ρ, are considered functions of temperature and space. These thermal properties are obtained for each interval by using the average of the mesh point temperatures bounding the interval

$$k_{\ell m} = k\left(\frac{T_{r,m-1} + T_{\ell,m}}{2}\right) = k_{r,m-1} \tag{545}$$

$$k_{rm} = k\left(\frac{T_{r,m} + T_{\ell,m+1}}{2}\right) = k_{\ell,m+1} \quad . \tag{546}$$

The quantity, ρ, is treated in the same manner. The boundary condition parameters, A, B, and D, are considered functions of temperature and time. In steady state problems, no superscripts would be required for the thermal parameters, k, ρ, A, B, and D. Accordingly in Equations (528), (531), and (532), those quantities written with superscripts n or n+1/2 are ignored since they are multiplied by $\sigma = 0$, and only quantities with superscript n + 1 are used. If these quantities are not temperature-dependent, the solution of Equations (528), (531), and (532) will immediately give steady state temperatures. When these parameters are temperature-dependent, iterations are used to resolve the difficulty of obtaining thermal parameters as a function of temperature when the temperatures are unknown.

In transient problems, the thermal properties, k, ρ, A, B, and D, with superscript n are evaluated as a function of the temperatures, T^n, at the beginning of a time step. Since these are either initial temperatures or results of the last time-advancement, the corresponding thermal parameters can be determined. Those thermal parameters with superscript n + 1 are evaluated as a function of the temperatures, T^{n+1}, at the end of the time step. Since these temperatures are not available, the initial estimate of the thermal parameters is obtained using

$k^{n+1} = k^n$ and similarly for ρ, A, B, and D. The superscript n + 1/2 indicates an average of the quantities with superscript n and n + 1, or

$$\rho^{n+1/2} = \frac{\rho^{n+1} + \rho^n}{2} \quad . \tag{547}$$

If thermal parameters and boundary conditions are constant, or do not vary greatly during a time step, the temperatures obtained from the solution of Equations (528), (531), and (532) with $k^{n+1} = k^n$, etc., are satisfactory. This is presently assumed i LAP5.

3.2.7 Difference Approximation for Boundary Conditions

The development of the difference equations uses a general form for the boundary conditions, but RELAP5 uses only the following conditions,

$$-k \frac{\partial T}{\partial x} = 0 \tag{548}$$

$$-k \frac{\partial T}{\partial x} = q_T(t) \tag{549}$$

$$-k \frac{\partial T}{\partial x} = H(T - T_B) \tag{550}$$

$$T = T_T(t) \tag{551}$$

where q_T and T_T are tabular functions of time. For the first three conditions, the heat transfer rate is given directly by the boundary conditions once the surface temperature has been calculated. For the temperature boundary condition, the heat transfer rate is obtained from the difference equation. The expression for the right boundary is

$$q_M^{n+1} \delta_M^b = \frac{k_{\ell M}^n}{\sigma + 1}\left(T_{M-1}^{n+1} - T_M^{n+1}\right) \delta_{\ell M}^s + \frac{\sigma k_{\ell M}^n}{\sigma + 1}\left(T_{M-1}^n - T_M^n\right) \delta_{\ell M}^s$$

$$+ P_f \frac{(\sigma P^n + P^{n+1})}{\sigma + 1} Q_{\ell M} \delta^v_{\ell M} - \frac{\sigma \rho^n_{\ell M}}{\Delta t} \left(T^{n+1}_M - T^n_M \right) \delta^v_{\ell M} \quad . \tag{552}$$

3.2.8 Two-dimensional Conduction Solution/Reflood

A two-dimensional conduction scheme is used in the reflood model for cylindrical or rectangular heat structures. Figure 40 shows an elemental cell around the mesh point. For a cylindrical geometry, the volume elements are

$$V_1 = \pi \delta_t \delta_\ell (r_i - \delta_\ell/4)/2 \tag{553}$$

$$V_2 = \pi \delta_t \delta_r (r_i + \delta_r/4)/2 \tag{554}$$

$$V_3 = \pi \delta_b \delta_\ell (r_i - \delta_\ell/4)/2 \tag{555}$$

$$V_4 = \pi \delta_b \delta_r (r_i + \delta_r/4)/2 \tag{556}$$

and the surface elements are

$$A_1 = \pi \delta_l (r_i - \delta_\ell/4) \tag{557}$$

$$A_2 = \pi \delta_r (r_i + \delta_r/4) \tag{558}$$

$$A_3 = \pi \delta_t (r_i + \delta_r/2) \tag{559}$$

$$A_4 = \pi \delta_b (r_i + \delta_r/2) \tag{560}$$

$$A_5 = A_2 \tag{561}$$

$$A_6 = A_1 \tag{562}$$

$$A_7 = \pi \delta_b (r_i - \delta_\ell/2) \tag{563}$$

$$A_8 = \pi \delta_t (r_i - \delta_\ell/2) \tag{564}$$

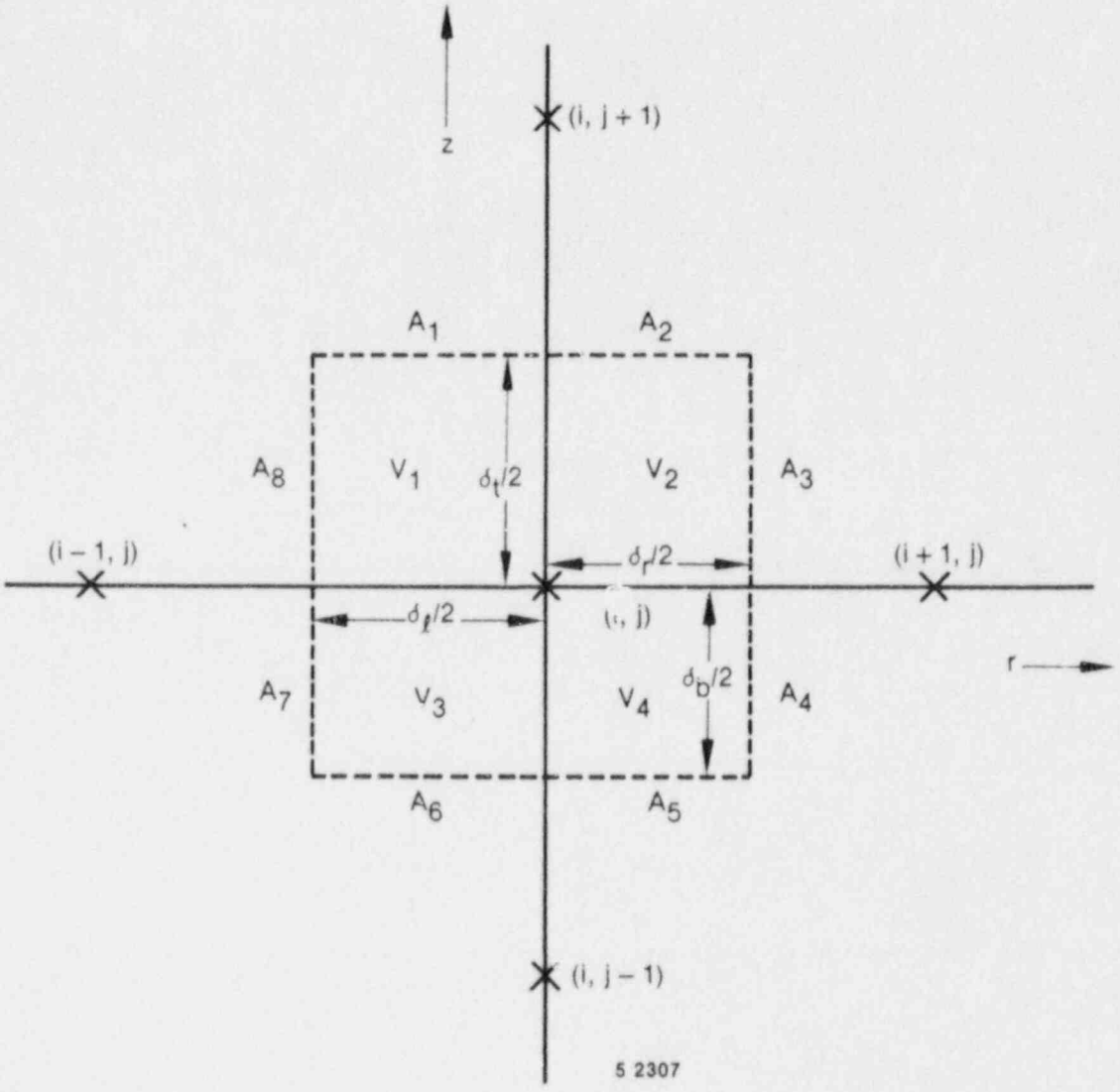

Figure 40. Volume and surface elements around a mesh point (i, j).

Integration of the heat conduction Equation (528) over the elemental cell yields the following form of finite difference equation

$$G_{ij}\left(T_{i,j}^{n+1} - T_{i,j}^{n}\right)\Big/\Delta t = a_{ij}^{L}\, T_{i-1,j} + a_{ij}^{R}\, T_{i+1,j}$$

$$+ a_{ij}^{T}\, T_{i,\,j+1} + a_{ij}^{B}\, T_{i,\,j-1} - \left(a_{ij}^{L}\right.$$

$$\left. + a_{ij}^{R} + a_{ij}^{B} + a_{ij}^{T}\right)T_{ij} + S_{ij} \quad . \tag{565}$$

By defining the material properties, ρ_{ij} and k_{ij}, at the center of the r-direction interval between mesh points (ij) and (i + 1,j), the coefficients G_{ij}, a_{ij}^{R} and a_{ij}^{T} of Equation (565) can be written as

$$G_{ij} = \rho_{i-1,j}\,(V_1 + V_3) + \rho_{ij}\,(V_2 + V_4) \tag{566}$$

$$a_{ij}^{R} = K_{ij}\,(A_3 + A_4)/\delta_r \tag{567}$$

$$a_{ij}^{T} = \left[(k_{ij} + k_{i,j+1})A_2/2 + (k_{i-1,j} + k_{i-1,j+1})A_1/2\right]\Big/\delta_t \quad . \tag{568}$$

The other two coefficients, a_{ij}^{L} and a_{ij}^{B}, are obtained by the symmetry relations

$$a_{ij}^{L} = a_{i-1,j}^{R} \tag{569}$$

$$a_{ij}^{B} = a_{i,j-1}^{T} \quad . \tag{570}$$

The space and time-dependence of the source term, S, described in Equation (518) are extended to two-dimensional cases as

$$S = P_R\, P(t)\, Q\,(r,z) \tag{571}$$

with the assumption that Q is independent of z within a heat structure. Accordingly, the heat source term S_{ij} of Equation (565) is

$$S_{ij} = P_R\, P(t)\, (Q_\ell^T\, V_1 + Q_\ell^B\, V_3 + Q_r^T\, V_2 + Q_r^B\, V_4) \quad . \tag{572}$$

Here $Q_\ell^T = Q_\ell^B$ and $Q_r^T = Q_r^B$ if the entire cell is within the same heat structure.

Equation (491) is written, of course, for an interior point (ij). For a point on the boundary, some of the coefficients a_{ij}^L, a_{ij}^R, a_{ij}^B, and a_{ij}^T should vanish. For example, at the bottom corner, a_{ij}^L and a_{ij}^B are zero. It is also obvious that some of the terms in Equations (568) and (571) disappear. Furthermore, the boundary condition must be added. To be consistent with the one-dimensional heat conduction scheme, an assumption is made that no heat is fluxed across the top and bottom ends. For the right and left boundaries, the boundary condition can be represented by one of the general forms described in Equations (548) through (551). The boundary condition specifying the surface temperature as a function of time, Equation (551), has been dropped in the two-dimensional scheme for computational efficiency.

The difference Equation (565) is solved using the alternative-direction implicit (ADI) method. The scheme is represented by two steps as follows

Step 1. Column Inversion:

$$\left(T_{ij}^{n+1/2} - T_{ij}^n\right) G_{ij} / (\Delta t/2) = a_{ij}^L\, T_{i-1,j}^n$$

$$+ a_{ij}^R\, T_{i+1,j}^n + a_{ij}^B\, T_{i,j-1}^{n+1/2} + a_{ij}^T\, T_{i,j+1}^{n+1/2}$$

$$- a^L_{ij} + a^R_{ij} \; T^n_{ij} - a^T_{ij} + a^B_{ij} \; T^{n+1/2}_{ij} + S_{ij} \; . \qquad (573)$$

Step 2. Row Inversion:

$$(T^{n+1}_{ij} - T^{n+1/2}_{ij}) \; G_{ij}/(\Delta t/2) = a^L_{ij} \; T^{n+1}_{i-1,j} + a^R_{ij} \; T^{n+1}_{i+1,j}$$

$$+ a^B_{ij} \; T^{n+1/2}_{i,j} + a^T_{ij} \; T^{n+1/2}_{i,j+1} - (a^L_{ij} + a^R_{ij}) \; T^{n+1}_{ij}$$

$$- (a^T_{ij} + a^B_{ij}) \; T^{n+1/2}_{ij} + S_{ij} \; . \qquad (574)$$

Here the superscripts n, n+1/2, and n+1 denote the values at times t, $t+\Delta t/2$, and $t+\Delta t$, respectively.

3.2.9 Fine Mesh-Rezoning Scheme

A fine mesh-rezoning scheme is implemented to efficiently use the two-dimensional conduction solution for reflood calculations. The scheme is similar to the one used in COBRA-TF[97] and is intended to resolve the large axial variation of wall temperatures and heat fluxes. The number of axial nodes in the heat structures is varied in such a way that the fine nodes exist only in the nucleate boiling and transition boiling regions.

A heat-structure geometry, which is composed of 1 to 99 heat structures as specified by users, is selected as an elementary unit for the reflood model. Figure 41 shows a typical heat-structure geometry with one fluid control volume connected to each heat structure. The dots are radial mesh points. At the initiation of the reflood model, each heat structure is subdivided into two axial intervals (Figure 42). A two-dimensional array of mesh points is thus formed. Thereafter, the number of axial intervals may be doubled, halved or unchanged at each time step according to a set of rules be discussed in the next paragraph. Figure 42 shows an example of a heat structure going through a cycle of axial nodalization variation.

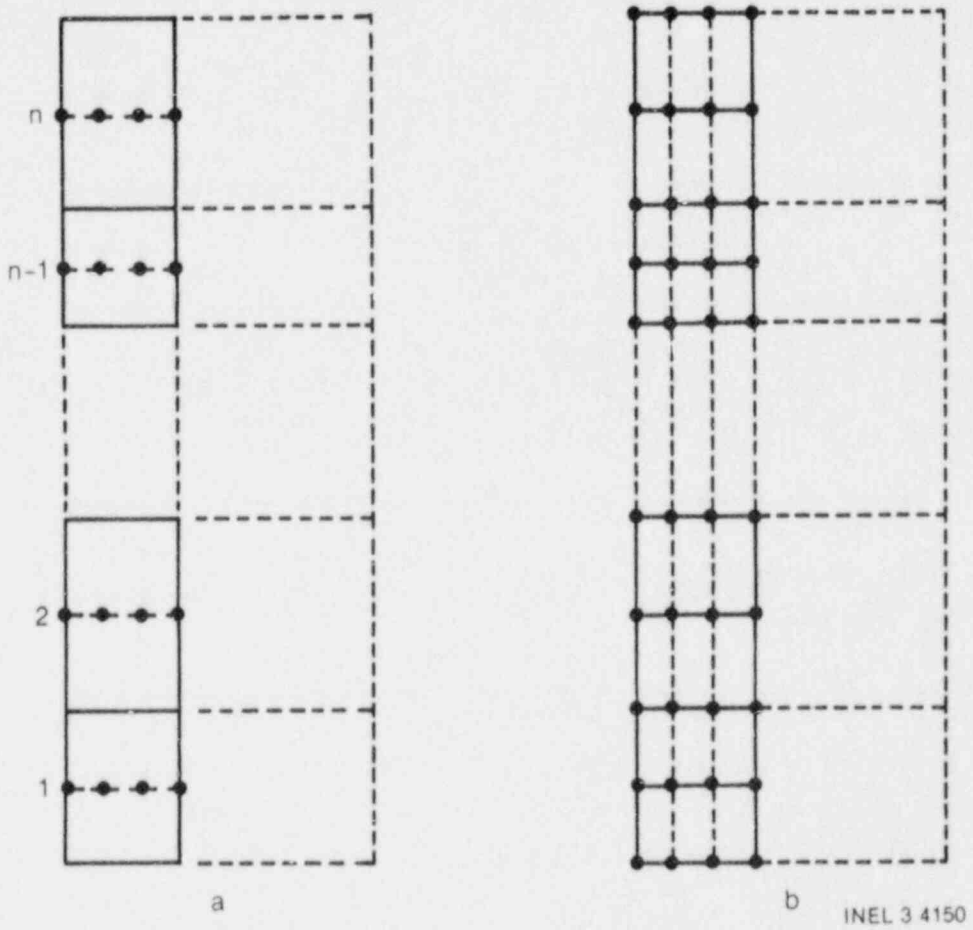

Figure 41. An elementary heat structure unit for reflood.

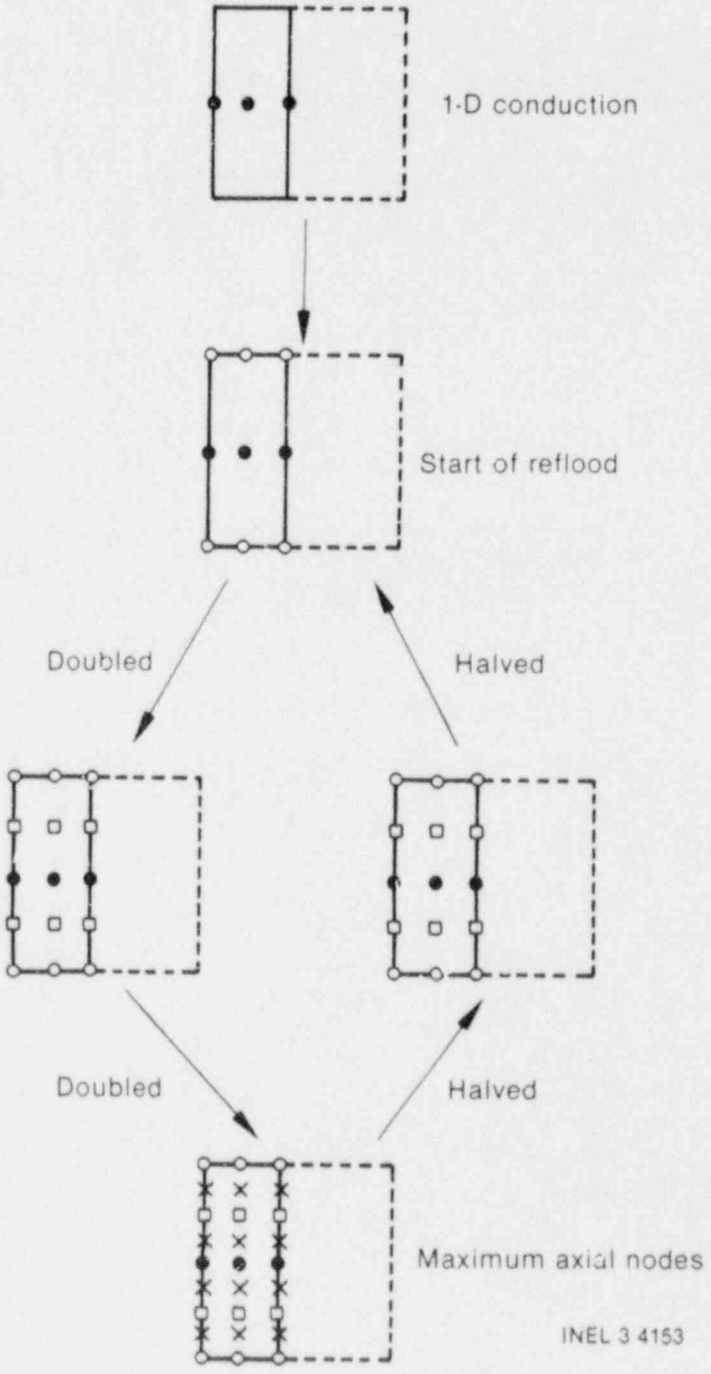

Figure 42. An example of fine mesh-rezoning process.

The number of axial mesh intervals in a heat structure depends on the heat transfer regimes in the heat structures. At each time step all heat structures in a heat-structure geometry are searched to find the positions of T_{CHF}, the wall temperature where the critical heat flux occurs, T_Q, the quench or rewetting temperature, and T_{IB}, the wall temperature at the incipience of boiling (see Section 3.1.3.4). Let us assume that T_{IB}, T_{CHF}, and T_Q are at the i-, j- and k-th heat structures and $k \geq j \geq i$. Also, let N be the number of maximum axial mesh intervals specified by the user and α_g be the void fraction in the connected control volume. The number of axial mesh intervals in a heat structure is determined according to the following rules:

1. For $\alpha_g > 0.999$ or $\alpha_g = 0$, the number is halved but not less than 2

2. For the (k+1) -th heat structure, the number is doubled but not >N/2

3. For the (i-1)-th heat structure, the number is halved but not <N/2

4. The number is doubled up to N for the heat structures between max (j+1, K) and min (j-1, i) and in the region of maximum wall temperature gradient

5. For all other heat structures, the number is unchanged.

3.2.10 Gap Conductance Model

The RELAP5/MOD2 dynamic gap conductance model[98] defines an effective gap conductivity based on a simplified deformation model generated from FRAP-T6.[99] The model employs the following assumptions: First, the fuel to cladding radiation heat transfer, which only contributes significantly to the gap conductivity under the conditions of cladding ballooning, is neglected. This is appropriate since cladding ballooning is not included in this simple model. Second, the minimum gap size is limited such that

the maximum effective gap conductivity is about the same order as that of metals. Third, the direct contact of the fuel pellet and the cladding is not explicitly considered.

Gap conductance is primarily a function of the fuel-cladding gap width and is calculated, in the FRAP-T6 model, by the equation,

$$h_g = \frac{k_g}{N} \sum_{n=1}^{N} 1/[t_n + 3.2\ (R_F + R_c) + (g_1 + g_2)] \qquad (575)$$

where

h_g = conductance through the gas in the gap (W/m^2K)

n = number of a circumferential segment

N = total number of circumferential segments = 8

k_g = thermal conductivity of gas ($W/m \cdot k$)

t_n = width of fuel-cladding gap at the midpoint of the n^{th} circumferential segment (m)

R_F = surface roughness of the fuel (m)

R_c = surface roughness of the cladding (m)

g_1, g_2 = temperature jump distance terms for fuel and cladding.

The width of the fuel-cladding gap at any given circumferential segment is calculated by the equation,

$$t_n = t_g + [-1 + (2n-1)/N]\ t_o \qquad (576)$$

where

t_g = circumferentially averaged fuel-cladding gap width (m)

t_o = as-fabricated fuel-cladding gap width (m).

The value of t_n in Equation (576) is limited between zero and $2t_g$.

The temperature jump distance terms account for the temperature discontinuity caused by incomplete thermal accommodation of gas molecules to the surface temperature. The terms also account for the inability of gas molecules leaving the fuel and cladding surfaces to completely exchange their energy with neighboring gas molecules, which produces a nonlinear temperature gradient near the fuel and cladding surfaces. The terms are calculated by

$$g_1 + g_2 = 0.024688 \left(K_g T_g^{1/2} P_g\right) \sum_i f_i a_i M_i^{1/2} \qquad (577)$$

where

T_g = temperature of gas in the fuel-cladding gap (K)

P_g = gas pressure (Pa)

f_i = mole fractions of i^{th} component of gas

a_i = accommodation coefficient of the i^{th} component of gas

M_i = molecular weight of the i^{th} component of gas.

The accommodation coefficients for helium and xenon are obtained by using curve fits to the data of Ullman:[100]

$$a_{He} = 0.425 - 2.3 \times 10^{-4} T_g \qquad \text{(Helium)} \qquad (578)$$

$$a_{Xe} = 0.740 - 2.5 \times 10^{-4} T_g \qquad \text{(Xenon)} \ . \tag{579}$$

If T_g is >1000 K, T_g is set to 1000K. The accommodation coefficients for other gases are determined by interpolation and written as

$$a_j = a_{He} + \frac{(M_j - M_{He})}{(M_{Xe} - M_{He})} (a_{Xe} - a_{He}) \ . \tag{580}$$

The circumferential averaged width of the fuel cladding gap, t_g, in Equation (576) is determined by the expression

$$t_g = t_o - u_F + u_C \tag{581}$$

where

u_F = radial displacement of the fuel pellet surface (m),

u_C = radial displacement of cladding inner surface (m).

The radial displacements, u_F and u_C, are primarily due to thermal expansion.

The radial displacement, of the fuel pellet surface, u_F, is calculated by the equation

$$u_F = u_{TF} + u_r + u_s \tag{582}$$

where

u_{TF} = radial displacement due to thermal expansion (m)

u_r = radial displacement due to uniform fuel relocation (m)

u_s = radial displacement due to fission gas induced fuel swelling and densification (m).

In the RELAP5/MOD2 model the variable u_r is assumed to be zero. The value of the variable u_s is supplied by the user. The fuel thermal expansion is obtained from the equation

$$U_{TF} = \sum_{n=2}^{N} (R_n - R_{n-1}) \, \varepsilon_{TF} \, (T_{n+1/2}) \qquad (583)$$

where

n = radial mesh point number

N = total number of mesh points in the fuel

r_n = radius of radial mesh point n

ε_{TF} = function defining thermal expansion of fuel as a function of temperature

$T_{n+1/2}$ = average fuel temperature at the center of the node between mesh points n and n+1.

The radial displacement of the inner surface of the cladding is calculated by

$$u_c = u_{TC} + u_{cc} + u_e \qquad (584)$$

where

u_{TC} = radial displacement due to thermal expansion (m)

u_{cc} = radial displacement due to cladding creepdown (m)

u_e = radial displacement due to elastic deformation (m).

The value of u_{cc} must be supplied by the user. For beginning of life fuel rods, u_{cc} is equal to zero. For fuel rods with a significant amount of burnup, a FRAPCON-2 analysis is required to determine the value of u_{cc}. The thermal expansion, u_{TC}, is obtained from

$$u_{TC} = r_{cm} \varepsilon_{TC} (T_c) \tag{585}$$

where

r_{cm} = radius of midplane of cladding (m)

ε_{TC} = function defining thermal expansion of cladding as a function of temperature

T_c = temperature of cladding at midplane (K).

The elastic deformation, u_e, is calculated by

$$u_e = r_{cm} (\sigma_h - \upsilon\sigma_z)/E \tag{586}$$

where

E = Young's modulus for the cladding (Pa)

σ_h = cladding hoop stress (Pa)

σ_z = cladding axial stress (Pa)

υ = Poisson's ratio for the cladding.

The cladding hoop and axial stress are given by

$$\sigma_n = (P_g\, r_i - P_f\, r_o)/(r_o - r_i) \tag{587}$$

$$\sigma_z = \left(P_g\, r_i^2 - P_f\, r_o^2\right)\Big/\left(r_o^2 - r_i^2\right) \tag{588}$$

where

P_f = coolant pressure (Pa)

r_i = inner radius of cladding (m)

r_o = outer radius of cladding (m).

The Poisson's ratio is obtained from the relation

$$\nu = \frac{E}{2G} - 1 \tag{589}$$

where

G = shear modulus (Pa).

The internal gas pressure P_g is determined in FRAP-T6 by a detailed plenum model. Since a plenum model is not included in the simplified approach, a static ideal gas approximation for a fixed plenum volume is used to calculate P_g, i.e.,

$$P_g = P_{g,i}\,(T_f/T_{f,i}) \tag{590}$$

where

$P_{g,i}$ = initial gas pressure in the gap (Pa)

$T_{f,i}$ = initial coolant temperature at the top of the core (K)

T_f = current coolant temperature at the top of the core (K).

The initial internal gas pressure must be supplied by the user.

The volumetric heat capacity and thermal conductivity of the fuel rod materials, except for the thermal conductivity of the gap gas, must be supplied by the user. For the computation of the gas thermal conductivity, the user is required to provide the gas composition in terms of the mole fractions of seven common gases included in the model. The properties for determining material thermal expansion and elastic deformation are calculated from permanent data within the code. No user input is needed. The user, however, should be aware that these properties are computed under the assumption that the fuel material is uranium oxide and the cladding material is zircaloy. The properties of UO_2 and zircaloy along with gas conductivity are taken from MATPRO-11 (Revision 2)[101] and are described below.

The conductivity as a function of temperature for a pure noble or diatomic gas is calculated using

$$K_g = A\, T_g^B \quad . \tag{591}$$

The constants A and B for seven common gases are given in Table 6. The thermal conductivity of a gas mixture is calculated from the expression

$$K_g = \sum_{i=1}^{N} k_i X_i \Big/ \left(X_i + \sum_{j=1}^{N} \phi_{ij}\, X_j \right) \tag{592}$$

where

$$\phi_{ij} = \left[1 + (K_i/K_j)^{1/2}\, (M_i/M_j)^{1/4}\right]^2 \Big/ \left[8\,(1 + M_i/M_j)\right]^{1/2} \tag{593}$$

TABLE 6. CONSTANTS USED IN GAS THERMAL CONDUCTIVITY CORRELATION

	Constant	
Gas	A	B
He	2.639×10^{-3}	0.7085
Ar	2.986×10^{-4}	0.7224
Kr	8.247×10^{-5}	0.8363
Xe	4.351×10^{-5}	0.8685
H_2	1.097×10^{-3}	0.8785
N_2	5.314×10^{-4}	0.6898
O_2	1.853×10^{-4}	0.8729

and

N = number of components in the mixture

M_i = molecular weight of component i

X_i = mole fraction of the component i

k_i = thermal conductivity of the component i (W/mK).

The strain function, ε_{TF} in Equation (583), of the UO_2 fuel due to thermal expansion is described by

$$\varepsilon_{TF} = 1.0 \times 10^{-5}\, T - 3.0 \times 10^{-3} + 4.0 \times 10^{-2} \exp\left(-6.9 \times 10^{-20}/k_B T\right) \qquad (594)$$

where

T = fuel pellet temperature

k_B = Boltzmann constant (1.38×10^{-23} J/K).

The radial strain function, ε_{TC} in Equation (585), for the cladding thermal expansion is given by

$$\varepsilon_{TC} = 1.5985 \times 10^{-3} + 6.721 \times 10^{-6}\, T \qquad (595)$$

for $T < 1073K$ (α phase) and

$$\varepsilon_{TC} = -4.150 \times 10^{-3} + 9.7 \times 10^{-6}\, T \qquad (596)$$

for $T > 1273K$ (β phase), where T = cladding temperature (K). In the α phase to β phase transition zone, $1073K < T < 1273K$, a table lookup is used. Some selected values are listed in Table 7.

TABLE 7. RADIAL THERMAL STRAIN OF ZIRCALOY FOR 1073 K < T < 1273 K

T(K)	ε_{TC}
1073.0	5.22×10^{-3}
1093.0	5.25×10^{-3}
1103.0	5.28×10^{-3}
1123.0	5.24×10^{-3}
1143.0	5.15×10^{-3}
1183.0	4.45×10^{-3}
1223.0	2.97×10^{-3}
1273.0	2.90×10^{-3}

Young's modulus, E, and shear modulus, G, for zircaloy cladding are approximated by neglecting the effects of oxidation, cold work, and irradiation. Young's modulus is given by

$$E = 1.088 \times 10^{11} - 5.475 \times 10^{7} T \quad (597)$$

in the α-phase and

$$E = 9.21 \times 10^{10} - 4.05 \times 10^{7} T \quad (598)$$

in the β-phase, where T is the cladding temperature (K). The shear stress, G, is given by

$$G = 4.04 \times 10^{10} - 2.168 \times 10^{7} T \quad (599)$$

in the α-phase and

$$G = 3.49 \times 10^{10} - 1.66 \times 10^{7} T \quad (600)$$

in the β-phase, where T = cladding temperature (K).

3.3 Control System

The control system provides the capability to evaluate simultaneous algebraic and ordinary differential equations. The capability is primarily intended to simulate control systems typically used in hydrodynamic systems but it can also model other phenomena described by algebraic and ordinary differential equations. Another use is to define auxiliary output quantities such as differential pressures so they can be printed in major and minor edits and be plotted.

The control system consists of several types of control components. Each component defines a control variable as a specific function of time-advanced quantities. The time advanced quantities include: hydrodynamic volume, junction, pump, valve, heat structure,

reactor kinetics, trip quantities, and the control variables themselves (including the control variable being defined). This permits control variables to be developed from components that perform simple, basic operations.

In the following equations that define the control components and associated numerical techniques, Y_i is the control variable defined by the i^{th} control component, A_j, R, and S are real constants input by the user, I is an integer constant input by the user, V_j is a quantity advanced in time by RELAP5 and can include Y_i, t is time, and s is the Laplace transform variable. Superscripts involving the index n denote time levels. The name in parentheses to the right of the definition is used in input data to specify the component.

3.3.1 Arithmetic Control Components

Constant

$$Y_i = S \qquad \text{(CONSTANT)} \qquad (601)$$

Addition-Subtraction

$$Y_i = S(A_0 + A_1V_1 + A_2V_2 + \ldots) \qquad \text{(SUM)} \qquad (602)$$

Multiplication

$$Y_i = S\ V_1\ V_2 \ldots \qquad \text{(MULT)} \qquad (603)$$

Division

$$Y_i = \frac{S}{V_1} \text{ or } Y_i = \frac{S\ V_2}{V_1} \qquad \text{(DIV)} \qquad (604)$$

Exponentiation

$$Y_i = S\ V_1^I \qquad \text{(POWERI)} \qquad (605)$$

$$Y_i = S\ V_1^R \qquad \text{(POWERR)} \qquad (606)$$

$$Y_i = S\ V_1^{V_2} \ . \qquad \text{(POWERX)} \qquad (607)$$

Table Lookup Function

$$Y_i = S\ F(V_1) \qquad \text{(FUNCTION)} \qquad (608)$$

where F is a function defined by table lookup and interpolation.

Standard Functions

$$Y_i = SF(V_1, V_2, V_3, \ldots) \qquad \text{(STDFNCTN)} \qquad (609)$$

where F can be $|V_1|$, $\exp(V_1)$, $\ln(V_1)$, $\sin(V_1)$, $\cos(V_1)$, $\tan(V_1)$, $\tan^{-1}(V_1)$, V_1, $(V1)^{1/2}$, MAX(V_1, V_2, V_3 ...), and MIN(V_1, V_2, V_3, ...) . Only MAX and MIN may have multiple arguments, such as

Delay

$$Y_i = SV_1(t - t_d) \qquad \text{(DELAY)} \qquad (610)$$

where t_d is the delay time. A user input, h, determines the length of the table used to store past values of V_1. The maximum number of time-function pairs is h+2. The delay table time increment is t_d/h. The delayed function is obtained by linear interpolation using the stored past

history. As time is advanced, new time values are added to the table. Once the table fills, new values replace values that are older than the delay time, such as

Unit Trip

$$Y_i = SU\ (\pm t_r) \qquad \text{(TRIPUNIT)} \qquad (611)$$

Trip Delay

$$Y_i = ST_r(t_r) \qquad \text{(TRIPDLAY)} \quad . \qquad (612)$$

In the above two trip related components, t_r is a trip number and if negative indicates that the complement of the trip is to be used, U is 0.0 or 1.0 depending on trip t_r (or its complement if t_r is negative) being false or true, and T_r is -1.0 if the trip is false and the time the trip was last set true if the trip is true.

No numerical approximations are involved in evaluating the algebraic components. Evaluation is by simply performing the indicated operations. In the sequence of operations that perform a time advancement of the trip, heat conduction, hydrodynamic, reactor kinetic, and control systems of RELAP5, the control system is processed last. Thus, the end of time step (n+1) values for trip variables t_r and all V_l variables except control variables Y_i are available. The control components are evaluated in component number order. As the first control variable Y_1 is being evaluated, only old time values are available for all control component variables. Once Y_1 is evaluated, the new time value is available for the remaining control variable evaluations of Y_1. In general, while Y_i is being evaluated, new time values are available for Y_k, $k < i$, and only old time values are available for Y_k, $k \geq i$.

In the example,

$$Y_{10}^{n+1} = A_0 + A_1\ T^{n+1} + A_2\ P^{n+1} + A_3 Y_8^{n+1} + A_4\ Y_{10}^{n} + A_5\ Y_{15}^{n} \qquad (613)$$

T and P, which represent a temperature and pressure from the heat structure or hydrodynamic systems, are new time values. The value Y_8 is also a new time value because it was advanced before control component 10, and Y_{10} and Y_{15} are old time values. Use of new time values when i=k (for Y_{10} in the example) is being considered.

Initialization of the algebraic control components is very similar to a time advancement. At the start of control component initialization, all other time advanced quantities have been initialized. Control component input includes an initial value and a flag that indicates if initialization is to be performed. The initialization proceeds in the order of component numbers. The initial value entered becomes the initial value if no initialization is specified. If initialization is specified, it is simply the specified computation using the available data. If component i references Y_k, $k < i$, the initialized value of Y_k is used; if $k \geq i$, the entered initial value is used.

3.3.2 Integration Control Component

The integration component evaluates

$$Y_i = S\int_{t_1}^{t} V_1 \, dt \qquad \text{(INTEGRAL)} \qquad (614)$$

where t_1 is the time the component is added to the system, and the initial value at t_1 is the input item regardless of the initialization flag.

The integral is advanced by the trapezoidal approximation,

$$Y_i^{n+1} = Y_i^n + S[V_1^n + V_1^{n+1}]\frac{\Delta t}{2} \quad . \qquad (615)$$

Both new time (n+1) and old time (n) values are available for V_1 except when it is a control variable Y_k, $k \geq i$. For the case when

$V_i = Y_k$, $k \geq i$, the V^n and V^{n+1} are instead V^{n-1} and V^n. Use of the proper values is being considered when k=i. Also, use of

$$Y_i^{n+1} = Y_i^n + S\, V_1^n\, \Delta t \tag{616}$$

is being considered when $V_1 = Y_k$, $k > i$. Use of the integral component when old time values will be used should be avoided. Consider the example

$$a = P_1 - P_2 - BV - kd \tag{617}$$

$$V = \int a dt \tag{618}$$

$$d = \int V dt \ . \tag{619}$$

This acceleration-velocity-distance system can not be advanced without use of old values. As a general rule, it is considered better to use the old value in the algebraic expression and not in the integral expressions.

Thus, using $Y_1 = a$, $Y_2 = V$, $Y_3 = d$

$$Y_1 = P_1 - P_2 - BY_2 - kY_3 \tag{620}$$

$$Y_2 = \text{INTEGRAL } (Y_1) \tag{621}$$

$$Y_3 = \text{INTEGRAL } (Y_2) \ . \tag{622}$$

3.3.3 Differentiation Control Components

Two components provide for differentiation

$$Y_i = \frac{dV_1}{dt}$$

One component evaluates the derivative by the inverse of the integration technique,

$$Y_i = \frac{2S}{\Delta t}\left(V_1^{n+1} - V_1^n\right) - Y_i^n \qquad \text{(DIFFERNI)} \qquad (623)$$

This component is not recommended since it can be unstable, requires an accurate initial value, and does not recover from a bad initial value. Deletion of this component is being considered. The recommended derivative component, uses a simple difference expression,

$$Y_i = S\,\frac{\left(V_1^{n+1} - V_1^n\right)}{\Delta t} \qquad \text{(DIFFERND)} \qquad (624)$$

Differentiation is a noisy process and should be avoided. Differentiation of control system variables can almost always be avoided. Filtering the result of differentiation of other variables should be considered. Similar to the case of the integral component, old time values are used when advancement of Y_i involves $V_1 = Y_k$, $k \geq i$.

3.3.4 Proportional-Integral Component

This component evaluates

$$Y_i = S\left[A_1 V_1 + A_2 \int_{t_1}^{t} V_1\, dt\right] \qquad \text{(PROP-INT)} \qquad (625)$$

or in Laplace transform notation,

$$Y_i(s) = S\left[A_1 + \frac{A_2}{s}\right] V_1(s) \quad . \qquad (626)$$

This component is advanced in time by

$$I^{n+1} = I^n + \left(V_1^n + V_1^{n+1}\right) \frac{\Delta t}{2} \tag{627}$$

$$Y_i^{n+1} = S\left(A_1 V_1^{n+1} + A_2 I^{n+1}\right) \quad . \tag{628}$$

The comments in the previous section concerning integration with $V_1 = Y_k$ hold for this component.

If the initialization flag is off, Y° is the entered initial value and

$$I^\circ = \frac{1}{A_2}\left(\frac{Y_i^\circ}{S} - A_1 V_1^\circ\right) \quad . \tag{629}$$

If the initialization flag is on,

$$I^\circ = 0 \tag{630}$$

$$Y^\circ_i = SA_1 V^\circ_1 \quad . \tag{631}$$

3.3.5 Lag Control Component

The lag component is defined in Laplace transform notation as

$$Y_i(s) = S\left(\frac{1}{1 + A_1 s}\right) V_1(s) \qquad \text{(LAG)} \tag{632}$$

through algebraic rearrangement,

$$Y_i(s) + A_1 s Y_i(s) = S\, V_1(s) \tag{633}$$

$$\frac{Y_i(s)}{s} + A_1 Y_i(s) = \frac{S\, V_1(s)}{s} \tag{634}$$

$$Y_i(s) = \frac{S\,V_1(s) - Y_i(s)}{A_1 s} \quad . \tag{635}$$

Transforming to the time domain gives

$$Y_i = \int_0^t [S\,V_1 - Y_i]\,dt \quad . \tag{636}$$

The above expression is advanced numerically by

$$Y_i^{n+1} = Y_i^n + \left[S(V_1^n + V_1^{n+1}) - Y_i^n - Y_i^{n+1}\right]\frac{\Delta t}{2A_1} \tag{637}$$

or

$$Y_i^{n+1} = \frac{Y_i^n\left(1 - \frac{\Delta t}{2A_1}\right) + S\left(V_1^n + V_1^{n+1}\right)\frac{\Delta t}{2A_1}}{1 + \frac{\Delta t}{2A_1}} \quad . \tag{638}$$

If the initialization flag is set,

$$Y_i^\circ = SV_1^\circ \quad . \tag{639}$$

3.3.6 Lead-Lag Control Component

The lead-lag component is defined in Laplace transform notation as

$$Y_i(s) = S\left(\frac{1 + A_1 s}{1 + A_2 s}\right)V_1(s) \qquad \text{(LEAD-LAG)} \tag{640}$$

Rearranging algebraically, this yields

$$Y_i(s) + A_2 s Y_i(s) = SV_1(s) + A_1 s\,SV_1(s) \tag{641}$$

or

$$Y_i(s) = \frac{A_1 S\, V_1(s)}{A_2} + \frac{S\, V_1(s) - Y_i(s)}{A_2 s} \quad . \tag{642}$$

Transforming to the time domain gives

$$Y_i = \frac{A_1 S\, V_1}{A_2} + \int_0^t \left(\frac{S\, V_1 - Y_i}{A_2} \right) dt \quad . \tag{643}$$

Note that the differentiation implied by the $sV_1(s)$ term has been avoided.

The above expression is advanced numerically by

$$Y_i^{n+1} = \frac{A_1}{A_2} S\, V_1^{n+1} + I^n + \left[S\left(V_1^n + V_1^{n+1} \right) - Y_i^n - Y_i^{n+1} \right] \frac{\Delta t}{2A_2} \tag{644}$$

or

$$Y_i^{n+1} = \frac{\frac{A_1}{A_2} S\, V_1^{n+1} + I^n + \left[S\left(V_1^n + V_1^{n+1} \right) - Y_i^n \right] \frac{\Delta t}{2A_2}}{1 + \frac{\Delta t}{2A_2}} \tag{645}$$

and finally

$$I^{n+1} = I^n + \left[S\left(V_1^n + V_1^{n+1} \right) - Y_i^n - Y_i^{n+1} \right] \frac{\Delta t}{2A_2} \quad . \tag{646}$$

If no initialization is specified, $I^\circ = 0$ and Y_i is the entered initial value. If initialization is specified, then

$$Y_i^\circ = SV_1^\circ \quad , \quad I^\circ = \left(1 - \frac{A_1}{A_2} \right) SV_1^\circ \quad . \tag{647}$$

For both lag and lead-lag components, if $V_l = Y_k$: $k = i$ is an error; when $k < i$, old and new values are used as indicated; if $k > i$,

V_l^n and V_l^{n+1} are really Y_k^{n-1} , Y_k^n .

3.3.7 Shaft Component

The shaft component is a specialized control component that advances the rotational velocity,

$$\sum_i I_i \frac{d\omega}{dt} = \sum_i \tau_i - \sum_i f_i \omega + \tau_c \qquad \text{(SHAFT)} \qquad (648)$$

where I is moment of inertia, τ_i is torque from component i, f_i is friction, and τ_c is an optional torque from a control component. The summations are over the pump, generator, motor, or turbine components that might be connected to the shaft and the shaft itself. The shaft and each associated component contains its own model, data, and storage for inertia, friction, and torque, and has storage for its rotational velocity. Each associated component also has a disconnect trip number. If zero (no trip) the component is always connected to the shaft. If a trip is specified, the component is connected when false and disconnected when true. Any disconnected component is advanced separately and thus can have a different rotational velocity than the shaft. All connected components have the same rotational velocity.

The shaft equation is advanced explicitly by

$$\sum_i I_i \frac{(\omega^{n+1} - \omega^n)}{\Delta t} = \sum_i \tau_i^n - \sum_i f_i^n \omega^n + \tau_c \ . \qquad (649)$$

Inertias, torques, and friction are evaluated using old time information. The torque from the control system, τ_c, would be in terms of new time values for quantities other than control variables and would use new or old time values for control variables depending on their component numbers

relative to the shaft component number. Except when a generator component is involved, the shaft component calculations consist of solving Equation (649) for ω^{n+1} separately for each component disconnected from the shaft (if any) and for the shaft and the connected components as one system. For separated components, the new rotational velocity is stored with the component data and the summations are only over terms within the component. For the shaft and the connected components, the summations are over the shaft and the connected components, and the new rotational velocity is stored as the shaft's and each connected component's rotational velocity. A tripped generator, attached or connected, is treated as described above. An untripped generator rotates at the input synchronous speed, and if connected to the shaft, the shaft and all connected components are forced to the synchronous speed.

3.4 Trip System

The trip system consists of the evaluation of logical statements. Each trip statement is a simple logical statement which has a true or false result and an associated variable, TIMEOF. The TIMEOF variable is -1.0 whenever the trip is false and contains the time the trip was last set true whenever the trip is true. This variable allows for time delays and unit step functions based on events during the transient.

Within the structure of RELAP5, the trip system is considered to be only the evaluation of the logical statements. The decision of what action is needed based on trip status resides within other models. For example, valve models are provided that open or close the valve based on trip values; pump models test trip status to determine whether a pump electrical breaker has tripped.

Two types of trip statements are provided, variable and logical trips. Since logical trips involve variable trips and other logical trips, complex logical expressions can be constructed from simple logical statements. Both types of trips can be latched or unlatched. A latched

trip, once set true, is no longer tested and remains true for the remainder of the problem or until reset at a restart. An unlatched trip is evaluated every time step.

3.4.1 Variable Trips

A variable trip evaluates the statement,

$$T_{ri} = V_i \; OP \; (V_2 + C) \quad . \tag{650}$$

The value T_{ri} is the i^{th} trip variable that may be true or false. Values V_1 and V_2 are quantities from the heat structures, hydrodynamics, reactor kinetics, control systems, or may be a TIMEOF quantity. C is a constant; OP is one of the arithmetic relational operations; (EQ) is equal; (NE) is not equal; (GT) is greater than; (GE) is greater than or equal; (LT) is less than; (LE) is less than or equal.

Trips are evaluated at the beginning of the overall RELAP5 time advancement and are evaluated in numerical order. Except for TIMEOF variables, all other V quantities have beginning of time step values and the results of the trip evaluation are independent of the evaluation order. But when a variable trip statement references TIMEOF (T_{rk}), the new value of TIMEOF is used if $k < i$.

3.4.2 Logical Trips

A logical trip evaluates,

$$T_{ri} = \pm T_{rj} \; OP \; \pm T_{r\ell} \quad . \tag{651}$$

The values T_{rj} and $T_{r\ell}$ are variable or logical trips and the minus sign if present denotes the complement of the trip value. The value OP is one of the logical operations, AND, OR (inclusive or), or XOR (exclusive or).

Logical trips are evaluated following the evaluation of variable trips and are evaluated in numerical order. When T_{rj} (or $T_{r\ell}$) is a variable trip, new trip values are used; when T_{rj} is a logical trip used in logical trip expression i, new values are used when $j < i$, and old values are used when $j \geq i$.

3.5 Reactor Kinetics

The reactor kinetics capability can be used to compute the power behavior in a nuclear reactor. The power is computed using the space-independent or point kinetics approximation that assumes that power can be separated into space and time functions. This approximation is adequate for cases in which the space distribution remains nearly constant.

The reactor kinetics model of RELAP5/MOD2 computes both the immediate fission power and the power from decay of fission fragments. The immediate power is that released at the time of fission and includes power from fission fragment kinetic energy and neutron moderation. Decay power is generated as the fission products undergo radioactive decay. The user can select the decay power model based on either an ANS Standard[102] proposed in 1973 or on the 1979 ANS Standard for Decay Heat Power in Light Water Reactors.[103]

3.5.1 Reactor Kinetics Equations

The point kinetics equations are

$$\frac{d\phi(t)}{dt} = \frac{[\rho(t) - \beta]\,\phi(t)}{\Lambda} + \sum_{i=1}^{N} \lambda_i\, C_i(t) + S \qquad (652)$$

$$\frac{dC_i(t)}{dt} = \frac{\beta\, f_i}{\Lambda}\phi(t) - \lambda_i\, C_i(t) \qquad i = 1, 2, \ldots N \qquad (653)$$

$$\psi(t) = \Sigma_f\, \phi(t) \qquad (654)$$

$$P_f(t) = Q_f \psi(t) \tag{655}$$

where

t = time

ϕ = neutron flux

C_i = number of delayed neutron precursors of group i

β = effective delayed neutron fraction

Λ = prompt neutron generation time

ρ = reactivity (only the time dependence has been indicated; however, the reactivity is dependent on other variables)

f_i = fraction of delayed neutrons of group i

λ_i = decay constant of group i

S = source

ψ = fission rate in #/s

Σ_f = fission cross section

P_f = immediate fission power in MeV/s

Q_f = immediate fission energy per fission in MeV.

3.5.2 Fission Fragment Decay Model

The 1979 standard expresses the power $P_\alpha(t)$ in MeV/s as a function of time t resulting from one fission of isotope α at t = 0 as

$$P_\alpha(t) = \sum_{j=1}^{N_\alpha} a_{\alpha j} \exp(-\lambda_{\alpha j} t) \quad . \tag{656}$$

Data are presented for three isotopes, U^{235}, U^{238}, and Pu^{239}. The parameters a and λ were obtained by fitting to fission decay power data. The fitting for each isotope used 23 groups (N_α = 23). The above expression is an impulse response to one fission and can be extended to an arbitrary fission rate $\psi_\alpha(t)$ through the convolution integral

$$P_\alpha(t) = \sum_{j}^{N_\alpha} a_{\alpha j} \exp(-\lambda_{\alpha j} t) * \psi_\alpha(t) \tag{657}$$

where the convolution operation is defined by

$$A(t)*B(t) = \int_0^\tau A(t - \tau)\, B(\tau)\, d\tau = \int_0^\tau A(\tau)\, B(t - \tau)\, d\tau \quad . \tag{658}$$

Since numerical evaluation of convolution integrals is cumbersome, a set of differential equations equivalent to the convolution integral is derived.

Assume that the power from each group is from radioactive decay of a fission fragment i. Then

$$P_{\alpha j}(t) = \lambda_{\alpha j} \gamma_{\alpha j} = a_{\alpha j} \exp(-\lambda_{\alpha j} t) \quad . \tag{659}$$

For simplification in the following derivation, the α and j subscripts are dropped and the following expressions represent an equation for one group for one isotope. From Equation (659), we have

$$\gamma(t) = \frac{a}{\gamma} \exp(-\lambda t) \quad . \tag{660}$$

Laplace transforming Equation (659), gives

$$\gamma(s) = \frac{a}{\lambda(s + \lambda)} \quad . \tag{661}$$

Rearranging Equation (661) gives

$$s\gamma(s) = \frac{a}{\lambda} - \lambda\gamma(s) \quad . \tag{662}$$

Transforming to real time yields

$$\frac{d\gamma(t)}{dt} = \frac{a}{\lambda} \delta(0) - \lambda\gamma(t) \tag{663}$$

where $\delta(0)$ is the impulse function. Applying a time dependent fission rate $\psi(t)$ in place of the single fission (impulse response), Equation (662) and (663) become

$$s\ \gamma(s) = \frac{a}{\lambda} \psi(s) - \lambda\ \gamma(s) \tag{664}$$

$$\frac{d\gamma(t)}{dt} = \frac{a}{\lambda} \psi(t) - \lambda\ \gamma(t) \quad . \tag{665}$$

Solution of Equation (664) or (665) (remembering that $P = \lambda\ \gamma$) for an impulse yields Equation (656) and a similar expression in the standard. Solution of Equation (664) or (665) for an arbitrary fission source yields Equation (658). When specifying

$$\psi(t) = 1, \quad 0 \leq t \leq T$$

$$= 0, \quad t > T \tag{666}$$

Equations (664) and (665) yield another solution given in the standard (note that the standard defines t as starting at 0 after fissioning for T seconds).

A physical model can be attached to the terms in Equation (665). The first term on the right represents production of the isotope during fission; the last term is the loss of the isotope due to decay. A more mechanistic model would provide for production of one isotope due to the decay of another (see actinide model).

As shown above, the 1979 ANS standard for decay power can be implemented by advancing the differential equations, which become

$$\frac{d\gamma_{\alpha j}(t)}{dt} = \frac{F_\gamma \, a_{\alpha j}}{\lambda_{\alpha j}} F_\alpha \, \psi(t) - \lambda_{\alpha j} \, \gamma_{\alpha j}(t)$$

$$j = 1, 2, \ldots, N_\alpha$$

$$\alpha = 1, 2, 3 \tag{667}$$

$$P_\gamma(t) = \sum_{\alpha=1}^{3} \sum_{j=1}^{N_\alpha} \lambda_{\alpha j} \, \gamma_{\alpha j}(t) \tag{668}$$

where ψ is the fission rate from all isotopes, F_α is the fraction of fissions from isotope α, and P_γ is the decay power. Summation of F_α over α is 1.0. The value F_γ is a input factor to allow easy specification of a conservative calculation. It is usually 1.0 for best estimate calculations and 1.2 was recommended for a conservative calculation with the 1973 data. The 1979 data should allow consistent use of 1.0 for F_γ.

The 1973 proposed standard as implemented in RELAP5/MOD1 used one isotope and prescribed data for 11 groups. The 1979 standard lists data for three isotopes, U^{235}, U^{238}, and Pu^{239}, and uses 23 groups for each isotope. A user option also allows only the 1979 standard data for U^{235} to be used. The data for both standards are built into the code as default data, but the user may enter different data.

3.5.3 Actinide Decay Model

In RELAP5/MOD1, the actinide model was simply the optional selection of another isotope and would be identical to using two isotopes. The MOD1 actinide default data used two groups. The RELAP5/MOD2 model uses

$$\frac{d\gamma_u(t)}{dt} = F_u \phi(t) - \lambda_u \gamma_u(t) \tag{669}$$

$$\frac{d\gamma_N(t)}{dt} = \lambda_u \gamma_u(t) - \lambda_N \gamma_N(t) \tag{670}$$

$$P_\alpha = \eta_d \lambda_u \gamma_u + \eta_N \lambda_N \gamma_N \quad . \tag{671}$$

The quantity F_u is user input and is the number of atoms of U^{239} produced by neutron capture in U^{238} per fission from all isotopes. A conservative factor if desired should be factored into F_u. The λ and η values can be user input or default values equal to those stated in the standard can be used.

The first equation describes the rate of change of atoms of U^{239}. The first term on the right represents the production of U^{239}; the last term is the loss of U^{239} due to beta decay. The second equation describes the rate of change of N_p^{239}. The production of N_p is from the beta decay of U^{239} and Pu^{239} is formed from the decay of N_p^{239}. Solution of the actinide equations, Equations (669) and (670), for the fission source given in Equation (666) yields the result quoted in the 1979 standard.

3.5.4 Transformation of Equations for Solution

The differential equations to be advanced in time are Equation (652), (653), (667), (669), and (670). (The equations are ordered in storage as listed for programming convenience and to enhance vectorization.) Multiplying by Σ_f and X, the conversion from MeV/s to watts, as needed, the equations become,

$$\frac{d}{dt}[X\,\psi(t)] = \frac{[\rho(t) - \beta]\,X\,\psi(t)]}{\Lambda} + \sum_{i=1}^{N} \lambda_i\,X\,\Sigma_f\,C_i(t) \tag{672}$$

$$\frac{d}{dt}[X\,\Sigma_f\,C_i(t)] = \frac{\beta f_i\,X\,\psi(t)}{\Lambda} - \lambda_i\,X\,\Sigma_f\,C_i(t)$$

$$i = 1, 2, \ldots, N \tag{673}$$

$$\frac{d}{dt}[X\gamma_{\alpha j}(t)] = \frac{F_\gamma\,a_{\alpha j}\,F_\alpha\,X}{\lambda_{\alpha j}}\psi(t) - \lambda_{\alpha j}\,X\,\gamma_{\alpha j}(t)$$

$$j = 1, 2, \ldots, N_\alpha$$

$$\alpha = 1, 2, 3 \tag{674}$$

$$\frac{d}{dt}[X\,\gamma_U(t)] = F_u\,X\,\psi(t) - \lambda_u\,X\,\gamma_U(t)$$

$$\frac{d}{dt}[X\,\gamma_N(t)] = \lambda_u\,X\,\gamma_U(t) - \lambda_N\,X\,\gamma_B(t)\ . \tag{675}$$

The total power P_T is the sum of immediate fission power, fission product decay, and actinide decay, and now in units of watts is

$$P_T(t) = \gamma_F\,X\,\psi(t) + \sum_{\alpha=1}^{3}\sum_{j=1}^{N_\alpha} \lambda_{\alpha j}\,X\,\lambda_{\alpha j}(t) + n_u\,q_u\,X\,q_u(t)$$

$$+ \eta_N \gamma_N X \lambda_N(t) \quad . \tag{676}$$

For solution convenience, the following substitutions are made,

$$\rho(t) = \beta\, r(t) \tag{677}$$

$$X\, \psi(t) = \psi'(t) \tag{678}$$

$$X\, \frac{\Lambda S}{\beta} = S' \tag{679}$$

$$X\, \Sigma_f\, C_i(t) = \frac{\beta\, f_i\, W_i(t)}{\Lambda\, \lambda_i} \tag{680}$$

$$X\, \gamma_{\alpha j}(t) = \frac{F_{\alpha j} F_\alpha}{\lambda_{aj}^2}\, Z_{\alpha j}(t) \tag{681}$$

$$X\, \gamma_u(t) = \frac{F_u}{\lambda_u}\, Z_u(t) \tag{682}$$

$$X\, q_N(t) = Z_N(t) \quad . \tag{683}$$

The equations to be advanced are now,

$$\frac{d\psi'}{dt}(t) = \frac{\beta}{\Lambda}\, [r(t) - 1]\, \psi'(t) + \sum_{i=1}^{N} f_i\, W_i(t) + S' \tag{684}$$

$$\frac{d}{dt}\, W_i(t) = \lambda_i\, \psi'(t) = \lambda_i\, W_i(t) \qquad i = 1, 2, \ldots, N \tag{685}$$

$$\frac{d}{dt}\, Z_u(t) = \lambda_u\, \psi'(t) - \lambda_u\, Z_u(t) \tag{686}$$

$$\frac{d}{dt} Z_N(t) = F_u Z_u(t) - \lambda_N Z_N(t) \tag{687}$$

$$P_T(t) = Q_f \psi'(t) + \sum_{\alpha=1}^{3} \sum_{j=1}^{N_\alpha} \frac{F_\gamma a_{\alpha j} F_\alpha Z_{\alpha j}(t)}{q_{\alpha j}}$$

$$+ F_u \eta_u Z_u(t) + \eta_N \lambda_N Z_N(t) \quad . \tag{688}$$

These equations are advanced using the modified Runge-Kutta method[105] described in Section 3.5.7.

3.5.5 Initialization

Two initialization options are provided. In both options, the fission rate and delayed neutrons are in steady state or equilibrium conditions, that is, their time derivatives are zero. With r(0) an input quantity,

$$W_i(0) = \psi(0) \quad i = 1, 2, \ldots, N \tag{689}$$

$$S' = -r(0) \psi(0) \quad . \tag{690}$$

The first option assumes that the fission product decay and actinides are also in equilibrium. This is equivalent to assuming that the reactor has been operating at a constant total power for an infinite period of time. The initial conditions are

$$Z_{aj}(o) = \psi(o) \quad j = 1, 2, 3, \ldots, N_a$$

$$a = 1, 2, 3 \tag{691}$$

$$Z_u(o) = \psi(o) \tag{692}$$

$$Z_N(o) = \frac{F_u}{q_u} \psi(o) \tag{693}$$

$$P_T(o) = Q\ \psi(o) \tag{694}$$

$$Q = Q_f + \sum_{\alpha=1}^{3} \sum_{j=1}^{N_\alpha} \frac{F_q\ a_{\alpha j}\ F_\alpha}{\lambda_{\alpha j}} + F_u\ \eta_u + F_u \eta_N \ . \tag{695}$$

The quantity Q, which is the total energy in MeV generated per fission, is either an input value or can be defaulted to 200 MeV. The quantity Q_f is defined from Equation (695) and the user input or defaulted data even if the second initialization option is used. The total power is an input quantity, and the source ψ is computed from Equation (694).

The second option uses a power history to determine the initial values of the fission product and actinide quantities. The power history consists of one or more periods of constant total power. For each period, the input consists of the total power, the time duration at that power, and in the case of three isotopes, the fraction of power from each isotope. The fission product and actinide differential equations, Equations (685), (686), and (687) are advanced in time starting with initial values of zero. The fission rate ψ is defined from Equation (688). The fission rate is reset to zero whenever a negative value is computed. This would occur whenever the user entered total power is less than the current fission product and actinide decay power. Thus for shutdown periods, the user may conveniently enter zero total power even though significant decay power remains. The fission product and actinide values at the end of the power history become the initial values for the transient. The initial fission rate is computed from Equation (688) using the total reactor power at the start of the transient (which may be different from the last power history value). If this fission rate is negative or zero, it is reset such that the immediate fission power is 10^{-12} times the decay power.

The differential equations for the power history calculation are advanced using the same numerical technique as for the transient advancement except for a simplified time step control. Time step control consists of starting the advancement of each history period with a time step of 1 s. The time step is doubled after each advancement. When the next advancement would exceed the time duration, the last advancement is with the remaining time. This scheme was selected since with each different power value, the solution moves toward a new equilibrium condition asymptotically and the most rapid change is at the beginning of a power change.

3.5.6 Reactivity Feedback

One of two models can be selected for reactivity feedback. The separable model is defined by

$$r(t) = r_o + r_B + \sum_i^{n_s} r_{si}(t) + \sum_i^{n_c} V_{ci} + \sum_i^{n_\rho} \left[W_{\rho i} R_\rho \; P_I(t) \; + \alpha_{Wi} \; T_{Wi}(t) \right]$$

$$+ \sum_i^{n_F} \left[W_{Fi} R_F \; T_{Fi}(t) \; + \alpha_{Fi} \; T_{Fi}(t) \right] \quad . \tag{696}$$

The quantity, r_o, is an input quantity and represents the reactivity corresponding to assumed steady state reactor power at time equal zero. The quantity, r_B, is calculated during input processing such that $r(0) = r_o$.

The quantities, r_{si}, are obtained from input tables defining n_s reactivity curves as a function of time. The quantities, V_{Ci}, are N_C control variables that can be user defined as reactivity contributions. R_ρ is a table defining reactivity as a function of the current density of water $\rho_i(t)$, in the hydrodynamic volume i; $W_{\rho i}$ is the density weighting factor for volume i. $_{Wi}$ is the equilibrium temperature of

volume i; a_{Wi} is the temperature coefficient (not including density changes) for volume i; and n_ρ is the number of hydrodynamic volumes in the reactor core. The value R_F is a table defining reactivity as a function of the average fuel temperature T_{Fi} in a heat structure; W_{Fi} and a_{Fi} are the fuel temperature weighting factor and the fuel temperature coefficient, respectively; and n_F is the number of heat structures in the reactor core.

This model assumes nonlinear feedback effects from moderator density and fuel temperature changes and linear feedback from moderator temperature changes. The name, separable, is attached to this model since each effect is assumed to be independent of the other effects. Boron feedback is not provided, but a user defined boron feedback can be implemented with the control system.

The separable model can be used if boron changes are quite small and the reactor is near critical about only one state point.

A postulated BWR ATWS accident is an example where the reactor could be nearly critical for two different state points. One point is at normal power operating conditions: high moderator and fuel temperatures, highly voided, and no boron. During accident recovery, the reactor might approach a critical condition with relatively cold moderator and fuel temperatures, with no voids, but with some boron concentration. The reactivity could be nearly critical for both states, but the contribution from the different feedback effects is vastly different. The assumptions of no interactions among the different feedback mechanisms, especially boron, cannot be justified. The tabular model defines reactivity as

$$r(t) = r_o + r_B + \sum_i^{n_s} r_{si} + \sum_i^{n_c} v_{ci}$$

$$+ R(\bar{\rho}(t), \bar{T}w(t), \bar{T}_F(t), \bar{B}(t)) \qquad (697)$$

$$\bar{\rho}(t) = \sum_{i}^{n_\rho} W_{\rho i}\, \rho_i(t) \tag{698}$$

$$\bar{T}_w(t) = \sum_{i}^{n_\rho} W_{\rho i}\, T_{Wi}(t) \tag{699}$$

$$\bar{B}(t) = \sum_{i}^{n_\rho} W_{\rho i}\, B_i(t) \tag{700}$$

$$\bar{T}_F(t) = \sum_{i}^{n_F} W_{Fi}\, T_{Fi}(t) \tag{701}$$

where B is boron density. The average quantities are obtained with the use of one weighting factor for each hydrodynamic volume and each heat structure contributing to reactivity feedback. The reactivity function R is defined by a table input by the user. In the Table 4 option, the table is four dimensional; the Table 3 option assumes no boron dependence and the table is then three dimensional.

The tabular model overcomes the objections of the separable model since all feedback mechanisms can be nonlinear and interactions among the mechanisms are included. The penalty for the expanded modeling capability greatly increases the input data requirements.

The reactivity function R is evaluated by a direct extension of the one dimensional table lookup and linear interpolation scheme to multiple dimensions. One dimensional table lookup and interpolation of the function $V = F(W)$ uses an ordered set of N_W independent variable values W_i with the corresponding values of the dependent variable V_i to determine the value of V corresponding to a search argument W. The independent variable

is searched such that W_i and W_{i+1} bracket W; an equation for a straight line is fitted to the points W_i, V_i, and W_{i+1}, V_{i+1}; and the straight line equation is evaluated for the given W.

Using subscripts 0 and 1 for bracketing independent values and corresponding dependent values, and defining $w = (W - W_0)/(W_1 - W_0)$ so that w varies from 0 through 1 as W varies from W_0 through W_1, the interpolation equations are

$$a_0 = V_0 \qquad a_1 = V_1 - V_0 \quad . \tag{702}$$

For two dimensional interpolation of $V = F(W,X)$, two sets of independent variables are used: N_W values of W_i, and N_X values of X_j. A total of $N_W N_X$ dependent values of V_{ij} are entered, one value for each combination of variables from the two sets of independent variables. Graphically, the two sets of independent variables form a rectangular grid when the W_i and X_j variables are plotted on horizontal and vertical coordinates, respectively. The dependent variables are entered corresponding to the intersections of the mesh lines. The search for bracketing values in each independent set locates a mesh rectangle and the dependent values at the four corners are used to form an interpolation equation which is the product of two straight line functions, one for each independent variable. Using 0 and 1 subscripts for the bracketing values,

$$V = \sum_{i=0}^{1} \sum_{j=0}^{1} a_{ij}\, w^i\, x^j \tag{703}$$

$$x = \frac{x - X_0}{X_1 - X_0}$$

$$a_{00} = V_{00} \quad , \quad a_{01} = V_{01} - V_{00} \quad , \quad a_{10} = V_{10} - V_{00}$$

$$a_{11} = V_{11} - V_{01} - V_{10} + V_{00} \quad .$$

This process is simply extended to three and four dimensions. Three sets of independent variables define a three dimensional rectangular grid and eight dependent quantities corresponding to the corners of a rectangular solid are used to define the interpolation equation which is the product of three straight line functions. In four dimensions, four sets of independent variables are defined and 16 dependent values are used to define the interpolation equations, which is the product of four straight line functions.

For three dimensional interpolation,

$$V = F(W, X, Y) \tag{704}$$

$$y = \frac{y - Y_0}{Y_1 - Y_0}$$

$$V = \sum_{i=0}^{1} \sum_{j=0}^{1} \sum_{k=0}^{1} a_{ijk} w^i x^j y^k$$

$$a_{000} = V_{000} \quad , \quad a_{001} = V_{001} - V_{000} \tag{705}$$

$$a_{010} = V_{010} - V_{000} \quad , \quad a_{100} = V_{100} - V_{000} \tag{706}$$

$$a_{011} - V_{011} - V_{001} - V_{010} + V_{000}$$

$$a_{101} - V_{101} - V_{001} - V_{100} + V_{000}$$

$$a_{110} - V_{110} - V_{010} - V_{100} + V_{000}$$

$$a_{111} = V_{111} - V_{011} - V_{101} - V_{110} + V_{001} + V_{010} + V_{100} - V_{000} \tag{707}$$

For four dimensional interpolation,

$$V = F(W, X, Y, Z) \tag{708}$$

$$z = \frac{z - Z_0}{Z_1 - Z_0} \tag{709}$$

$$V = \sum_{i=0}^{1} \sum_{j=0}^{1} \sum_{k=0}^{1} \sum_{l=0}^{1} a_{ijkl}\, w^i\, x^j\, y^k\, z^l \tag{710}$$

$$a_{0000} = V_{0000} \quad , \quad a_{0001} = V_{0001} = V_{0000} \tag{711}$$

$$a_{0010} = V_{0010} - V_{0000} \quad , \quad a_{0100} = V_{0100} - V_{0000} \tag{712}$$

$$a_{1000} = V_{1000} - V_{0000} \tag{713}$$

$$a_{0011} = V_{0011} - V_{0001} - V_{0010} + V_{0000} \tag{714}$$

$$a_{0101} = V_{0101} - V_{0001} - V_{0100} + V_{0000} \tag{715}$$

$$a_{0110} = V_{0110} - V_{0010} - V_{0100} + V_{0000} \tag{716}$$

$$a_{1001} = V_{1001} - V_{0001} - V_{1000} + V_{0000} \tag{717}$$

$$a_{1010} = V_{1010} - V_{0010} - V_{1000} + V_{0000} \tag{718}$$

$$a_{1100} = V_{1100} - V_{0100} - V_{1000} + V_{0000} \tag{719}$$

$$a_{0111} = V_{0111} - V_{0011} - V_{0101} + V_{0110} + V_{001} + V_{0010} + V_{0100} - V_{0000} \tag{720}$$

$$a_{1011} = V_{1011} - V_{0011} - V_{1001} + V_{1010} + V_{0001} + V_{0010} + V_{1000} - V_{0000} \tag{721}$$

$$a_{1101} = V_{1101} - V_{0101} - V_{1001} + V_{1100} + V_{0001} + V_{0100} + V_{1000} - V_{0000} \quad (722)$$

$$a_{1110} = V_{1110} - V_{0110} - V_{1010} + V_{1100} + V_{0010} + V_{0100} + V_{1000} - V_{0000} \quad (723)$$

$$a_{1111} = V_{1111} - V_{0111} - V_{1011} - V_{1101} - V_{1110} + V_{0011} + V_{0101} + V_{0110} + V_{1101} + V_{1001} + V_{1010} + V_{1100} - V_{0001} - V_{0010} - V_{0100} - V_{1000} + V_{0000} \quad (724)$$

The interpolating equations define a continuous function, that is, there is no discontinuity in the dependent quantity as any one or combination of dependent variables pass to the next bracketing pair of values.

Using N_W, N_X N_Y, and N_Z as the number of values in the four sets of independent variables, the number of data points for a three dimensional table is $N_W N_X N_Y$ and is $N_W N_X N_Y N_Z$ for a four dimensional table. Using only four values for each independent variable, a four dimensional table requires 256 data points.

3.5.7 Reactor Kinetics Numerical Procedures

The reactor kinetics equations are advanced in time using the modified Runge-Kutta Method of Cohen.[104] A first-order differential equation is written as

$$\dot{n}(t) = \alpha\, n(t) + R(n,t) \quad (725)$$

where α is constant over the time step, and $R(n,t)$ contains the remaining terms of the differential equation, including the nonconstant portion of any coefficient of $n(t)$. If the coefficient of $n(t)$ is $\beta(n,t)$, α would be $\beta[n(0),0]$, and $R(n,t)$ would contain a term of the form, $\beta[n(t),t]-\alpha\, n(t)$. Multiplying Equation (725) by an integrating factor and integrating gives

$$n(t) = n(0)\, e^{\alpha t} + \int_0^t e^{\alpha(t-\lambda)}\, R(n,\lambda)\, d\lambda \quad . \tag{726}$$

Since

$$n(0)\, e^{\alpha t} = n(0) + \int_0^t \alpha n(0)\, e^{\alpha(t-\lambda)} d\lambda, \tag{727}$$

$$n(t) = n(0) + \int_0^t [\alpha n(0) + R(n,\lambda)] e^{\alpha(t-g)} d\lambda \quad . \tag{728}$$

Letting $\lambda = ut$, then $d\lambda = t\,du$, and

$$n(t) = n(0) + t \int_0^1 [\alpha n(0) + R(n,u)] e^{\alpha t(1-u)} du \quad . \tag{729}$$

The numerical technique for advancing the solution over the time step consists of making approximations to the behavior of R(n,u) over the time step. For convenience in the following expressions, the following function is defined

$$C_{m(x)} = \int_0^1 u^{m-1}\, e^{x(1-u)} du \quad . \tag{730}$$

Stage 1:

Assume $R(n,\lambda) = R[n(0),0] = R_o$, and write $n(0)$ as n_o; then compute $n(\frac{h}{2})$,

$$n_1 = n(\tfrac{h}{2}) = n_o + \tfrac{h}{2} (\alpha n_o + R_o)\, C_1 \left(\alpha \tfrac{h}{2}\right) \quad . \tag{731}$$

Stage 2:

Assume straight-line variation of $R(n,\lambda)$ between R_o and $R_1 = R\left(n_1, \frac{h}{2}\right)$, and compute $n(\frac{h}{2})$,

$$R(n,\lambda) = R_o + \frac{2(R_1 - R_o)\lambda}{h} \tag{732}$$

$$R(n,\lambda) = R_o + (R_1 - R_o)\, u \qquad (\text{using } \lambda = u\,\tfrac{h}{2}) \tag{733}$$

$$n_2 = n\left(\frac{h}{2}\right) = n_1 + \frac{h}{2}\,(R_1 - R_o)\, C_2\left(\alpha\,\frac{h}{2}\right). \tag{734}$$

Stage 3:

Assume straight-line variation of $R(n,\lambda)$ between R_o and $R_2 = R\left(n_2, \frac{h}{2}\right)$, and compute $n(h)$,

$$R(n,\lambda) = R_o + \frac{2(R_2 - R_o)g}{h} \tag{735}$$

$$R(n,u) = R_o + 2(R_2 - R_o) \qquad (\text{using } g = uh) \tag{736}$$

$$n_3 = n(h) = n_o + h(\alpha n_o + R_o)\, C_1(\alpha h) + 2h(R_2 - R_o)\, C_2(\alpha h). \tag{737}$$

Stage 4:

Assume quadratic through points R_o, R_2, and $R_3 = R(n_3, h)$; then compute $n(h)$,

$$R(n,u) = (2R_o\ \ 4R_2 + 2R_3)\, u^2 + (-3R_o + 4R_2 - R_3)\, u + R_o \tag{738}$$

$$n_4 = n(h) = n_4 + h\,(R_4 - R_3)\,[2C_3\,(\alpha h) - C_2(\alpha h)] \quad . \tag{739}$$

Stage 5:

Assume quadratic through points R_o, R_2, and $R_4 = R(n_4,h)$; then compute n(h)

$$n_5 = n(h) = n_4 + h\,(R_4 - R_3)\,[2C_3\,(\alpha h) - C_2\,(\alpha h)] \quad . \tag{740}$$

Third-, fourth-, and fifth-order approximations are obtained by terminating the process at the end of the third, fourth, and fifth stages, respectively. RELAP5 uses only the fifth order approximation.

By direct integration, the function, $C_1(x)$, is given by

$$C_1(x) = \frac{e^x - 1}{x} \quad . \tag{741}$$

Using integration by parts, a recursion relation for $C_m(x)$ is

$$C_{m+1}(x) = \frac{mC_m(x) - 1}{x} \quad . \tag{742}$$

During machine calculations of the $C_m(x)$ functions for $X \leq 1$, excessive loss of significance occurs. For this range, $C_3(x)$ is computed from its MacClaurin series expansion

$$C_3(x) = 2\,[\frac{1}{3!} + \frac{x}{4!} + \frac{x^2}{5!} + \frac{x^3}{6!} + \frac{x^4}{7!} + \frac{x^5}{8!} + \frac{x^6}{9!} + \frac{x^7}{10!}] \quad . \tag{743}$$

C_2 and C_1 are evaluated by solving Equation (635) for $C_m(x)$.

During the advancement in time of the solution, the time increment is automatically increased or decreased to maintain a specified degree of accuracy. After the calculations for a reactor kinetics time-advancement, an empirical formula is used to estimate the error. If the error is

excessive, the time increment is halved, and the advancement calculation is redone. If the error is sufficiently small, the time interval is doubled for the next time step. If the estimated error is between limits, the same interval is used for the next time-advancement. These procedures for time step control, taken from the AIREK[105] code, are as follows

$$\omega_1 = \frac{\dot{\phi}(0)}{\phi(0)}$$

$$\omega_3 = \frac{\dot{\phi}(h)}{\phi(h)} \tag{744}$$

$\bar{\omega}$ is defined by $\phi(h) = \phi(0)e^{-\bar{\omega}h}$

$$Q = \frac{h\, C_2(\alpha h)}{1 + C_1(\alpha h)} \left[\omega_1 - 2\bar{\omega} + \omega_3\right] . \tag{745}$$

The α in Equation (745) is that of the neutron flux equation (Equation 674). The quantity, δ, is defined as the maximum (taken over all differential equations) of the quantity,

$$\frac{n_1 - n_0}{n_1} .$$

The Q_L and Q_H appearing below are 0.0001 and 0.001, respectively.

1. If $\delta < 2^{-15}$ and $Q \geq Q_L$, the program continues with the same time step

2. If $\delta < 2^{-15}$ and $Q < Q_L$, the program doubles the time step for the next advancement

3. If $\delta \geq 2^{-15}$ and

   a. $Q < Q_L$, the time step is doubled for the next advancement

   b. $Q \leq Q_H$, the same time step is used for the next advancement

   c. $Q > Q_H$, the time advancement is recalculated with half the time step.

4. The time advancement is also recomputed with the time step halved if

   a. αh of any equation >88.0

   b. negative or zero power is computed.

If the coefficient of the neutron flux in Equation (674) is negative, a subtraction is involved in determination of the derivative and a loss of significant figures can occur. If this coefficient is negative, a check is made of the number of bits lost in the subtraction. If more than nine bits are lost, the value of neutron flux computed by the current stage of the advancement procedure is discarded; instead, neutron flux is determined from the expression obtained by setting the neutron flux derivative to zero

$$D(t) = \frac{-\sum_{i=1}^{I} f_i W_i(t) - \frac{S\Lambda}{b}}{r(t) - 1} \quad . \tag{746}$$

The transfer of information between the reactor kinetics calculation and the other RELAP5 calculations is explicit. Hydrodynamic and heat conduction/transfer calculations precede reactor kinetics, and the control system calculation follows reactor kinetics. The reactor power used in hydrodynamics and heat conduction is the value at the beginning of the time

step. The reactivity used as an end-of-time step value in the kinetics advancement uses end-of-time step values from hydrodynamics and heat conduction and beginning-of-time step values from the control system.

The reactor kinetics equations are advanced at the same time step rate as the hydrodynamics and reactivity is assumed to vary linearly between time step values. The maximum time step for the reactor kinetics advancement is the hydrodynamic time step. That time step is reduced if necessary as described above.

4. SPECIAL TECHNIQUES

The semi-implicit and nearly-implicit solution methods are mass and energy conservative. The mass from the state relationship is compared to the mass from the continuity equation, and the difference is a measure of the truncation error inherent in the numerical solution. This is the main method used to control the time step and thus control the truncation error even though mass and energy are preserved in the solution scheme.

Special methods are provided in the code for use in obtaining initial conditions. These methods are based on the transient solution algorithm, but make use of an accelerated thermal transient solution technique in order to shorten the computer time required to achieve steady state.

4.1 Time Step Control

A variety of checks on solution acceptability are used to control the time step. These include material Courant limit checks, mass error checks, material properties out of defined ranges, water property errors, excessive extrapolation of state properties in the meta-stable regimes, or change in heat slab temperature of more than 50 K.

The material Courant limit check is made before a hydrodynamic advancement takes place and, thus, it may reduce the time step, but it does not cause a time step to be repeated. All of the other checks may cause all or part of the time advancement to be repeated at a smaller time step. The material Courant limit is evaluated for each hydrodynamic volume using the volume mass average velocity i.e.,

$$(\Delta t_c)_i = [\Delta x \max(\alpha_f^n , \alpha_g^n)/\max(|\alpha_f^n v_f^n| , |\alpha_g^n v_g^n|)]_i , \qquad (747)$$

$$i = 1,2, \ldots , N$$

The N volumes are sequentially divided into five subsets, i.e., (1, 6, 11, ...) volumes belong to the first subset, (2, 7, 12, ...) volumes belong to the second subset, etc. The five Courant limits for the five subsets are rearranged in ascending order, i.e.,

$$\Delta t_c^1 \leq \Delta t_c^2 \leq \Delta t_c^3 \leq \Delta t_c^4 \leq \Delta t_c^5 \quad . \tag{748}$$

Obviously, Δt_c^1 is the Courant limit for the entire system. This is the number printed at each major edit under "CRNT. DT = ". For the semi-implicit scheme, Δt_c^2 is used for limiting time step size. Thus, partial violation of the material Courant limit is allowed for this scheme. There is no user input option to select the degree of partial Courant limit violation. For the nearly-implicit scheme, five times Δt_c^2 is used for limiting the time step size for the transient mode and 10 times Δt_c^2 is used for limiting the time step size for the steady state mode.

The mass error check is made after the time step solution is nearly complete and, thus, if excessive mass error is detected then the time step is repeated at a reduced interval. Two types of mass error measures are computed. The first one is designed to check the validity of density linearization and is defined as

$$\varepsilon_m = \max \left(|\rho_{mi} - \rho_{si}|/\rho_{fi}, \; i = 1, 2, \ldots, N \right) \tag{749}$$

where ρ_m is the total density obtained from the mass continuity equation, ρ_s is the total density computed from the state relationship, and ρ_f is the liquid density computed from the state relationship. The second one is a measure of overall system mass error and is given by

$$\varepsilon_{rms} = \sum_{i=1}^{N} \left[V_i (\rho_{si} - \rho_{mi}) \right]^2 / \sum_{i=1}^{N} \left(V_i \rho_{si} \right)^2 \quad . \tag{750}$$

If either ε_m or ε_{rms} is $>2 \times 10^{-3}$, the time step is rejected and repeated with one half of the time step size. Otherwise, the time step is accepted and the next time step size is doubled if both ε_m and ε_{rms} are $<2 \times 10^{-4}$.

At any point in the solution flow if a material property is found to lie outside the defined range then the time step is halved and repeated. This process will proceed until the user specified minimum time step is reached. If the minimum time step is reached without obtaining a valid solution, then the code calculation is terminated and the last time step is repeated with a diagnostic dump printed. A program stop is encountered at completion of the step. This same procedure is applied for all property or extrapolation failures.

4.2 Mass/Energy Mitigation

The semi-implicit numerical scheme described in Sections 3.1.1.4 and 3.1.1.6 has two calculations of the new time variables α_g, U_g, U_f, X_n. These variables are first calculated in connection with a linearization of all the product terms involved in the time derivatives and are referred to as tentative new time variables [see Equations (66), (67), (68), (69) and (70)]. They are denoted by a tilde in Sections 3.1.1.4 and 3.1.1.6. This first calculation uses a numerically conservative form for all flux calculations of mass and energy but because the products in the time derivatives are linearized the quantities $\alpha_g\rho_g$, $\alpha_f\rho_f$, $\alpha_g\rho_g U_g$, $\alpha_f\rho_f U_f$, and $\alpha_g\rho_g X_n$ are not numerically conserved. These tentative new time values are only used to evaluate the interphase heat and mass transfer terms to be used in the second evaluation of the basic equations. In this second evaluation of the basic equations [see Equations (85), (87), (88), (89), and (90)], the products appearing in the time derivatives are not linearized. This second step also uses the numerically conservative form for the flux terms. Hence, the final end of time step values have been calculated using an accurate numerically conservative form of differencing.

The truncation errors in the linearization procedure may produce errors in the solu ion of pressure, phasic energies and void fraction. Since the state is computed from these basic variables, the resultant density may have some error. This error is used in the time step control presented in Section 4.1. Furthermore, the convective terms in the field equations are computed with donored properties determined by the directions of phasic velocities. There are chances that the final velocities may differ in directions from the explicit velocities used to define the donored properties. This may result in mass/energy errors due to incorrect properties used in the numerical scheme. The scheme used to handle this situation will next be presented.

The term velocity flip-flop refers to the situation in which the final velocities and the explicit velocities differ in sign. In the RELAP5 numerical scheme the pressures and final velocities are calculated using the donor properties based on the explicit velocities (see Section 3.1.1.). The velocity flip-flop implies that inconsistent donor properties were used for the pressure computation and the final mass/energy computation. This may result in bad velocity and energy solutions and large mass errors.

Let $\bar{\alpha}_{fj}$, $\bar{\rho}_{fj}$, $\bar{u}_{fj}$, $\bar{\alpha}_{gj}$, $\bar{\rho}_{gj}$, $\bar{u}_{gj}$ be the junction liquid fraction, liquid density, liquid energy, void fraction, vapor density, and vapor energy respectively, based on the explicitly velocities and $\tilde{\alpha}_{fj}$, $\tilde{\rho}_{fj}$, $\tilde{u}_{fj}$, $\tilde{\alpha}_{gj}$, $\tilde{\rho}_{gj}$, and $\tilde{u}_{gj}$ be the same variables based on the final velocities. A velocity flip-flop has occurred when one of the junctions in a system satisfies the following condition:

$$\left| \bar{\alpha}_{fj} \bar{\rho}_{fj} \bar{u}_{fj} + \bar{\alpha}_{gj} \bar{\rho}_{gj} \bar{u}_{gj} - \tilde{\alpha}_{fj} \tilde{\rho}_{fj} \tilde{u}_{fj} - \tilde{\alpha}_{gi} \tilde{\rho}_{gj} \tilde{u}_{gj} \right|$$

$$> 0.20 \left(\bar{\alpha}_{fj} \bar{\rho}_{fj} \bar{u}_{fj} + \bar{\alpha}_{gj} \bar{\rho}_{gj} \bar{u}_{gj} \right) \quad . \tag{751}$$

Under such circumstances, the pressures and final velocities are recalculated using the donor properties of the previously calculated final velocities. The solution is then accepted if no velocity flip-flop exists between the previous final velocities and new final velocities. Otherwise, the time-step size is reduced.

4.3 Steady State

A steady state initialization capability is included in RELAP5/MOD2. With this capability the transient solution algorithm is continually monitored to determine the achievement of a steady state. During this process convergence criteria are calculated and used in the steady state testing scheme. These convergence criteria are related to an overall calculational precision. This overall precision is the result of combining both the precision of the transient solution algorithm and the standard tolerance of the thermodynamic state algorithm. The following discussion describes the fundamental concepts of tests to detect steady state during transient calculations.

4.3.1 Fundamental Concepts for Detecting Hydrodynamic Steady-State During Transient Calculations

The fundamental concept of steady state is that the state of a system being modeled does not change with respect to time. In the hydrodynamic solution scheme three terms can be monitored whose variation in time include the variation of all of the other terms. These three terms are the thermodynamic density, internal energy, and pressure. Furthermore, these three terms can be combined into a single term, enthalpy. Hence, monitoring the time variation of enthalpy is equivalent to monitoring the time variation of all of the other variables in the solution scheme. For each volume cell in the system model the enthalpy can be written as

$$V_i \rho_i^n h_i^n = V_i(\rho_i^n U_i^n + P_i^n) \qquad (752)$$

where subscript i denotes the i^{th} volume element; superscript n denotes the solution time, t^n; h_i is the volume element enthalpy in units of energy per unit mass; V_i is the element volume that is constant; and ρ_i, U_i, and P_i are the thermodynamic density, internal energy and pressure, respectively, of the substance within the volume. Since volume is constant, Equation (752) can be simplified as

$$\rho_i^n h_i^n = \rho_i^n U_i^n + P_i^n \quad . \tag{753}$$

The rate of variation with respect to time of Equation (753) can be expressed numerically as

$$\left(\frac{d\rho h}{dt}\right)_i^n \sim \frac{\left(\rho_i^{n+1} U_i^{n+1} + P_i^{n+1}\right) - \left(\rho_i^n U_i^n + P_i^n\right)}{\Delta t^n} \tag{754}$$

where superscript n and n+1 denote the old and new time values, respectively. Absolute hydrodynamic steady state occurs when Equation (754) is zero for each of the volume elements in the modeled system.

In order to simplify the task of detecting steady state a system mean enthalpy can be expressed as

$$\overline{\rho h}^n = \frac{\sum_{i=1}^{NVOLS} V_i(\rho_i^n U_i^n + P_i^n)}{\sum_{i=1}^{NVOLS} V_i} \quad . \tag{755}$$

A system mean rate of change can also be formulated as

$$\overline{\left(\frac{d\rho h}{dt}\right)}^{n} = \frac{1}{\Delta t_n} \frac{\sum_{i=1}^{NVOLS}\left[V_i\left(\rho_i^{n+1}U_i^{n+1} + P_i^{n+1}\right) - \left(\rho_i^{n}U_i^{n} + P_i^{n}\right)\right]}{\sum_{i=1}^{NVOLS} V_i} \quad . \tag{756}$$

However, since the rate of change in any volume element can be positive or negative these terms would tend to cancel. Hence, a better formulation for the mean rate of change is as a mean square summation that can be written as

$$\overline{\left(\frac{d\rho h}{dt}\right)^2}^{n} = \frac{1}{\Delta t_n^2} \frac{\sum_{i=1}^{NVOLS} V_i^2\left[\left(\rho_i^{n+1}U_i^{n+1} + P_i^{n+1}\right) - \left(\rho_i^{n}U_i^{n} + P_i^{n}\right)\right]^2}{\sum_{i=1}^{NVOLS} V_i^2} \quad . \tag{757}$$

During the course of the problem solution, Equation (757) can be used to monitor the system approach to steady state because, as each volume element approaches steady state, its rate of change goes to zero and drops out of the summation. The detection of absolute steady state is therefore relatively simple, since the calculations need only be monitored until Equation (757) becomes zero. However, another property of Equation (757) is that it will fluctuate wildly, varying between small and large magnitudes. These fluctuations decrease in magnitude as the calculations proceed toward steady state. Hence, Equation (757) is not a well behaved function and it is therefore difficult to monitor its behavior. However, a well behaved function can be curve fitted to the results of Equation (757) over reasonable time intervals. An exponential function is of this type and if

$$\overline{\left(\frac{d\rho h}{dt}\right)^2}^{n} \sim y = e^{\alpha + \beta t^n + \gamma t^{n2} + \phi t^{n3}}, \quad t_0 \leq t^n \leq t \tag{758}$$

the coefficients α, β, γ, and ϕ may be computed by the method of least squares over any reasonable time interval greater than four time steps. Equation (758) has the property that it can increase to large values at small values of time and then decrease to small values as time increases and the system approaches steady state. Equation (758) represents the time smoothed root mean square (RMS) rate of change in system enthalpy.

Because the user must provide boundary conditions, controls, or trips to guide the transient solution to steady state, it may not be possible to achieve an absolute steady state. For example, a steam generator water level control may be modeled so that the water level oscillates between high and low setpoints. In addition, since numerical schemes are inexact, it may only be possible to calculate absolute steady state within a small limit of precision. For this kind of fluctuating average steady state, the RMS ($d\rho h/dt$) will approach a constant positive non-zero value. As a result, an additional method must be used to detect an average steady state over limited time intervals.

If the system $\overline{\rho h}^{\,n}$ is varying with time over the interval

$$t_1 \leq t^n \leq t_2 \tag{759}$$

its variation can be expressed approximately in the form of a straight line such that

$$H^n = b + at^n \sim \overline{\rho h}^{\,n} \ . \tag{760}$$

If the system is approaching an absolute steady state, then the line rate of change will be zero and Equation (760) will give the system time average ρh such that

$$t_1 \overline{\rho h}^{\,t_2} = b, \ t_1 \leq t^n \leq t_2 \ . \tag{761}$$

Where the superscript $t_1 \_\_ t_2$ denotes a time average over the interval $t_1 \leq t^n \leq t_2$.

The second testing method consists of monitoring the system ρh^n at the completion of each successful time step and at reasonable time intervals solving for the straight line coefficients a and b using the method of least squares.

In performing the method of least squares, the mean system enthalpy is computed at the successful completion of each time step in the interval

$$t_1 \leq t^n \leq t_2$$

and an equation expressing the sum of the squares of the differences between ρh^n and Equation (760) can be written as

$$\xi^2_{\rho_h} \Big|_{t_1}^{t_2} = \sum_{n=n1}^{n2} (\overline{\rho h}^{\,n} - b - at^n)^2 \quad . \tag{762}$$

The coefficients a and b can then be calculated by the method of least squares.

A measure of the RMS fluctuation of ρh^n with respect to the line of Equation (760) can also be computed using the mean square form of Equation (762) where

$$f^{t_1 \_\_ t_2}_{\overline{\rho h}} = \sqrt{\frac{1}{(n2 - n1)} \; \xi^2_{\rho h} \Big|_{t_1}^{t_2}} \quad . \tag{763}$$

The RMS fluctuation then represents a measure of the typical difference between the mean system enthalpy and the line of Equation (760). However, the coefficients a and b cannot be calculated with any better precision than the overall precision of the solution scheme for the entire system.

4.3.2 Calculational Precision and the Steady State Convergence Criteria

In the RELAP5/MOD2 solution scheme, at the successful completion of calculations over a time step, three fundamental variables are computed for each volume element in the system modeled. These variables are:

1. $\rho_{m_i}^{n+1}$, the thermodynamic density of the volume substance, where subscript m denotes the solution by conservation of mass

2. U_i^{n+1}, the thermodynamic internal energy of the volume substance resulting from conservation of energy

3. P_i^{n+1}, the thermodynamic pressure of the volume substance resulting from the combined solution conserving momentum, mass and energy.

The superscript n+1 denotes the new time solution at time $t^{n+1} = t^n + \Delta t^n$. Only three of these variables are required to define the thermodynamic state of the volume substance.

In RELAP5/MOD2, the thermodynamic pressure, phasic internal energies, and vapor volume fraction are used to compute the state utilizing a set of properties tables. In the resulting calculations, a thermodynamic density ρ^{n+1} is calculated corresponding to the solution results. If the pressure and overall internal energy are preserved then the precision of the calculations can be defined as

$$\varepsilon_{\rho,i}^{n+1} = \rho_i^{n+1} - \rho_{m_i}^{n+1} \tag{764}$$

for each volume element in the system. If the calculations were exact then Equation (764) would be zero. However the properties tables are limited in precision to a tolerance of ±1 in the fifth significant figure and in statistical terminology the mean expected precision would be approximately

±5 in the sixth significant figure. If the mean expected precision is considered to be a standard precision, an approximate expression can be written in terms of the properties table density as

$$\varepsilon^{n+1}_{std_{\rho},i} \sim \pm(5 \times 10^{-6})\ \rho_i^{n+1} \tag{765}$$

which is approximately ±5 in the density sixth significant figure and which represents the best expected precision for the calculational scheme.

In the steady state testing scheme, the precision of the volume enthalpy can be written as

$$\varepsilon^{n+1}_{\rho h,i} = \rho_i^{n+1} U_i^{n+1} + P_i^{n+1} - \rho_{mi}^{n+1} U_i^{n+1} + P_i^{n+1} \tag{766}$$

or

$$\varepsilon^{n+1}_{\rho h,i} = \left(\rho_i^{n+1} - \rho_{m_i}^{n+1}\right) U_i^{n+1} \quad . \tag{767}$$

Similarily, the precision of the rate of change in volume enthalpy can be written as

$$\varepsilon^{n+1}_{\left(\frac{d\rho h}{dt}\right),i} = \frac{1}{\Delta t^n}\left\{\left[\left(\rho_i^{n+1} U_i^{n+1} + P_i^{n+1}\right) - \left(\rho_i^n U_i^n + P_i^n\right)\right]\right.$$

$$\left. - \left[\left(\rho_{m_i}^{n+1} U_i^{n+1} + P_i^{n+1}\right) - \left(\rho_{m_i}^n U_i^n + P_i^n\right)\right]\right\} \tag{768}$$

which simplifies to

$$\varepsilon^{n+1}_{\left(\frac{d\rho h}{dt}\right),i} = \frac{1}{\Delta t^n}\,\varepsilon^{n+1}_{\rho h,i} \quad . \tag{769}$$

For the entire system at the current time step, a statistical precision can be defined where

$$\varepsilon_{\rho h}^{n+1} = \sqrt{\frac{\sum_{i=1}^{N\_VOLS} V_i^2 \left[\left(\rho_i^{n+1} - \rho_{m_i}^{n+1}\right) U_i^{n+1}\right]^2}{\sum_{i=1}^{NVOLS} V_i^2}} \tag{770}$$

for the system mean enthalpy and where

$$\varepsilon_{\left(\frac{d\rho h}{dt}\right)}^{n+1} = \sqrt{\frac{1}{(\Delta t^n)^2}\, \overline{\varepsilon_{\rho h}^2}^{n+1}} \tag{771}$$

for the system rate of change in enthalpy.

Simple mean differences for the entire system can also be written as

$$\bar{\delta}_{\rho h}^{n+1} = \frac{\sum_{i=1}^{NVOLS} V_i \left(\rho_i^{n+1} - \rho_{m_i}^{n+1}\right) U_i^{n+1}}{\sum_{i=1}^{NVOLS} V_i} \tag{772}$$

for the system mean enthalpy and as

$$\bar{\delta}_{\left(\frac{d\rho h}{dt}\right)}^{n+1} = \frac{1}{\Delta t^n}\, \bar{\delta}_{\rho h}^{n+1} \tag{773}$$

for the system rate of change in enthalpy.

The relationship between the mean difference and precision terms defines the uncertainty characteristics of the overall solution scheme. From Equations (770) through (773), it is obvious that

$$-\varepsilon_\eta \leq \delta_\eta \leq \varepsilon_\eta \tag{774}$$

where subscript η denotes the particular term, ρh or $d(\rho h/dt)$, being considered. In particular, if ε_η is small it can be concluded that calculations are made with a high degree of precision throughout the entire system modeled. If the mean difference term is such that

$$\delta_\eta \sim 0 \tag{775}$$

then the overall system solution is said to be unbiased. This means that the overall system mass, energy, and momentum are precisely conserved. However, if

$$\delta_\eta \sim \varepsilon_\eta \tag{776}$$

then the overall system solution is said to be biased. This means that if Equation (774) is true and

$$\delta_\eta < 0 \tag{777}$$

then the overall system solution behaves as if it were losing mass, energy, or momentum. If

$$\delta_\eta > 0 \tag{778}$$

then the system solution behaves as if it were gaining mass, energy, or momentum. In RELAP5 the size of the calculational time steps are controlled to maintain a high degree of precision which in turn limits the system bias. However, the characteristics just described can have an effect in determining time average steady state.

Since the time average straight line test defined by Equation (760) is conducted over a time interval, time average precision and mean difference terms must be calculated over the same time interval using the relationships

$$\overset{t_1 \text{---} t_2}{\underset{\varepsilon^2_{\rho h}}{}} = \frac{\sum_{n=n1}^{n2} \Delta t^n (\varepsilon^n_{\rho h})^2}{\sum_{n=n1}^{n2} \Delta t^n} \tag{779}$$

$$\overset{t_1 \text{---} t_2}{\underset{\varepsilon^2_{\frac{d\rho h}{dt}}}{}} = \frac{\sum_{n=n1}^{n2} \Delta t^n \overset{n \text{---} n}{\nu^2_{\frac{d\rho h}{dt}}}}{\sum_{n=n1}^{n2} \Delta t^n} \tag{780}$$

$$\overset{t_1 \text{---} t_2}{\underset{\delta_{\rho h}}{}} = \frac{\sum_{n=n1}^{n2} \Delta t^n \delta^n_{\rho h}}{\sum_{n=n1}^{n2} \Delta t^n} \tag{781}$$

$$\overset{t_1 \text{---} t_2}{\underset{\delta(\frac{d\rho h}{dt})}{}} = \frac{\sum_{n=n1}^{n2} \Delta t^n \delta^n_{(\frac{d\rho h}{dt})}}{\sum_{n=n1}^{n2} \Delta t^n} \tag{782}$$

where superscript $t_1 \text{---} t_2$ denotes a time average over the time interval and the summation terms n1 and n2 denote the number of time steps taken over the interval from t_1 to t_2, respectively.

Equations (779) through (782) represent the precision of the actual calculations relative to the thermodynamic state algorithm. These equations have the characteristic that if the system approaches absolute steady state both Equations (779) and (780) will become very small. Since the properties tables are limited in precision, it is useless in a practical sense to continue calculations if absolute steady state is achieved with a precision better than that for the properties tables. This

criteria can be defined by considering equations similar to Equations (779) and (780) but written in terms of the properties tables standard precision. These equations can be derived by simply substituting Equation (765) for the density difference term in the equations leading to Equations (779) and (780).

The steady state convergence criteria can then be defined by combining the calculational and standard precisions such that

$$\varepsilon^{2}_{c,\rho h} = \sqrt{\frac{1}{2}\left[\left(\frac{t_1 \text{---} t_2}{\varepsilon_{std,\rho h}}\right)^2 + \left(\frac{t_1 \text{---} t_2}{\varepsilon_{\rho h}}\right)^2\right]} \tag{783}$$

for the system mean enthalpy, and

$$\varepsilon_{c,\left(\frac{d\rho h}{dt}\right)} = \sqrt{\frac{1}{2}\left[\left(\frac{t_1 \text{---} t_2}{e_{std,\left(\frac{d\rho h}{dt}\right)}}\right)^2 + \left(\frac{t_1 \text{---} t_2}{\varepsilon_{\left(\frac{d\rho h}{dt}\right)}}\right)^2\right]} \tag{784}$$

for the system rate of change in enthalpy.

Equations (783) and (784) represent the steady state convergence criteria and it can be said that within the limits of calculational and properties precision, time average steady state is achieved when the mean rate of change in system enthalpy is within the limits of

$$-\varepsilon_{c,\frac{d\rho h}{dt}} \leq a \leq +\varepsilon_{c,\frac{d\rho h}{dt}} \tag{785}$$

where "a" is the mean rate of change in system enthalpy given by Equation (760). If Equation (785) is true and if Equation (758) is such that

$$y \leq \varepsilon_{c,\frac{d\rho h}{dt}} \tag{786}$$

then absolute steady state is achieved. If Equation (785) is true and

$$y > {}^{t_1}\underline{\hspace{2em}}^{t_2}_{\varepsilon_{c,\frac{d\rho h}{dt}}} \tag{787}$$

then the system is fluctuating and time average steady state is achieved.

4.3.3 Steady State Testing Scheme, Time Interval Control and Output

In the steady state testing scheme, the concepts discussed for detecting steady state are used and calculations are performed over time intervals composed of a number of time steps. Because the nature of each problem is different a systematic method of varying the test time intervals is performed.

These tests are performed in two parts. First the system model overall state and rate of change in state are monitored by evaluating Equations (752) through (757) and including these results in the least square terms for Equation (758). At time intervals computed internally, Equation (758) is evaluated and the current system rate of change is determined. If the rate of change in state is increasing, then a divergent condition is indicated. If the rate of change in state is decreasing or zero, then a convergent condition is indicated. Second, if a convergent condition is indicated, then calculations are performed to determine the system average state and average rate of change in state over the internally computed time intervals. These time averages are formed by obtaining successive overlapping least-square solutions for Equation (759). These successive time average values are compared and the achievement or nonachievement of a time average steady state is determined. In performing these tests the calculational precision is accounted for by using Equations (764) through (787).

In the steady state scheme, each time a solution for Equation (758) is obtained, the overall state and steady state convergence test results are printed. This printout is composed of current time results and time

smoothed results integrated over the test time interval. The current time results are (a) the state and rates of change in state resulting from Equations (755), (756), and (757), (b) the current time uncertainties resulting from Equations (770) through (773), and (c) the current time mean and root mean square (RMS) mass errors. The time smoothed results that are printed are the current time evaluation of Equation (758) and the resultant coefficients of Equation (758) determined by the least squares solution over the time interval from t_1 to the current time TIMEHY. The time, t_1, corresponds to the time at the successful completion of calculations for the first time step after problem initiation. For example, if the problem is a NEW problem then t_1, corresponds to

$$t_1 = 0 + \Delta t_1 \tag{788}$$

where Δt_1 is the first successful time step. If the problem is a RESTART problem, then t_1 corresponds to

$$t_1 = \text{TREST} + \Delta t \tag{789}$$

where TREST is the time of restart and Δt is the first successful time step after restart. If the results of the overall state tests indicate a convergent condition, then time average tests are initiated.

The time average tests consist of approximating the overall state with a set of three straight lines where each test line is fitted to the calculational results over successive test intervals. The time rates of change of these test lines are then monitored to determine time average steady state. In the testing scheme, when the time average tests are initiated, calculations continue until the successive test time interval is exceeded. At this time the first test line, Line A, is defined and its results are printed. Calculations then continue until the next successive test time interval is exceeded. At this time, the second test line, Line B, is defined for the second test interval and the third test line, Line C, is defined for the combined first and second test intervals. The results for the three test lines are then printed and tests are performed

to determine the achievement of time average steady state. If steady state has not been achieved, then test Line A is reset to Line B and the process is repeated until steady state is achieved.

In the printed edit for time average steady state tests the results for each of the three test lines are printed. The test line results are obtained by curve fitting Equation (760) over each of the line test intervals. The results printed are the endpoints of Equation (760) evaluated at the test interval start and end times and the time rate of change of Equation (760). Also printed are the time average uncertainties from Equations (779) through (782), the RMS fluctuation of system mean ρh about the line from Equation (763), and the mass error integrated over the line test interval.

In performing both the overall and time average sets of tests, calculations proceed through a logic scheme to perform tests that monitor the solution scheme's approach to steady state. After completing the logic scheme calculations, the steady state conclusions and next course of action are printed. This printout is composed of statements of the mode of convergence and the state of the system in alphanumeric terms. These statements are defined as the calculations proceed through the logic scheme. To prevent excessive printout during the overall state convergence tests, the first test for overall convergence is not performed until the completion of ten successful time steps. At this time a current test time interval is initialized as Δt_c = TIMEHY-t_1. If this test indicates a divergent condition, then the test time interval is increased and the test procedure is repeated. To increase the test time interval, three tests are performed. First, the current test time interval is halved and the time t_2 is estimated as

$$t_2 = \text{TIMEHY} + \frac{1}{2} \Delta t_c \quad . \tag{790}$$

Then Equation (758) is evaluated as $y(t_2)$. If $y(t_2)$ is greater than the current value of y, then the time t_2 is reset to

$$t_2 = \text{TIMEHY} + \Delta t_c \tag{791}$$

and Equation (758) is reevaluated, which results in resetting $y(t_2)$. If $y(t_2)$ is again >y, then the time t_2 is again reset to

$$t_2 = \text{TIMEHY} + 2\Delta t_c \quad . \tag{792}$$

In any case, the test time interval is expanded by either maintaining, halving, or doubling the current test time interval based on a projected estimate of the current time smoothed convergence function. This test procedure is then successively repeated until a convergent condition is calculated.

To provide efficiency for the time average testing scheme, upon the first occurrence of an overall state convergent condition the time average testing scheme is activated and the test time interval is redefined by estimating the time interval over which a 10% change in state will occur. This time interval is approximately

$$\Delta t_c \sim 0.1(\overline{\rho h^n})/y \quad . \tag{793}$$

However, to prevent excessively small or large intervals, the time interval is limited such that

$$10\ dt \leq \Delta t_c \leq 100\ dt \tag{794}$$

where dt is the current calculational time step. The calculations for the time average scheme then proceed with each successive test time interval specified 10% larger than the time interval just completed. As the calculations progress and approach steady state, the line segments approach a constant value within the steady state convergence criteria. When this

condition is met, the test time interval is doubled. If this condition is recursively maintained for two more successive test intervals than a final steady state has been achieved and the calculations are terminated. If the line segment tests indicate the solution is diverging from steady state the results of the time average tests are discarded. When the conditions of Equation (758) again become true, the time average tests are reinitiated and the procedure is continued until steady state is achieved.

4.3.4 Heat Structure Heat Conductance Scheme for Steady State

In both the steady state and transient solution schemes the same transient heat transfer algorithm is utilized. However, in the steady state scheme the heat structure heat capacity data input by the user is ignored. Instead, this term is evaluated as an artificially small number such that

$$\frac{\rho C_p (\Delta x)^2}{k \Delta t_{ht}} \geq 2 \qquad (795)$$

where ρC_p is the heat capacity term, Δx is the heat structure mesh interval, k is the heat structure thermal conductivity and Δt_{ht} is the heat transfer scheme calculational time step. Equation (795) corresponds to the explicit stability criteria for a transient numerical heat conduction scheme.

In a transient solution scheme, the heat capacity term is treated analogously to a thermal inertia and its magnitude determines the characteristic response time of the conduction solution. For example, ρC_p is typically quite large and on the order of 10^5 or larger. Hence, a large value of ρC_p results in a characteristic response time much greater than the hydrodynamic response time. Indeed, hydrodynamic steady state can be approximately achieved in reasonably short calculational times before large heat structures have even begun to respond.

By making the value of the heat capacity term small, the characteristic response time is made small and on the order of or less than the hydrodynamic calculational time step. The resultant solution would therefore be equivalent to a steady state solution that is "damped" and stabilized by a small thermal inertia. Hence, fluctuations of the heat structure rate of change in state are on the order of or less that the fluctuations of its hydrodynamic boundary conditions. As a result, the heat structure solution scheme will achieve time average steady state at approximately the same time as time average hydrodynamic steady state.

4.3.5 Interrelationship of Steady State and Transient Restart/Plot Records

During the course of the calculations, restart/plot records are written at the frequency specified by the user. When the code determines that steady state has been achieved, a restart/plot record is written unconditionally. Subsequent problems can then be run as restarts using any of these restart records. However, the code will treat the restart records differently depending on the type of problem using the restart record.

If a transient problem is being run by restarting from a steady state restart record, or, conversely, if a steady state problem is being run restarting from a transient restart record, the restart is treated as a new problem. In this case, only the restart record at which the problem restarts is copied and used for initial conditions. The code time step counters, statistics, and problem simulation time are reset to zero and additional restart/plot records are written as the problem progresses.

If a steady state problem is being run restarting from a steady state restart record, or, conversely, if a transient problem is being run restarting from a transient restart record then the restart is treated as a continuation of the problem. In this case, the previous restart/plot records are copied and additional records are written as the problem progresses.

5. REFERENCES

1. V. H. Ransom et al., RELAP5/MOD1 Code Manual, Volume 1 and 2, NUREG/CR-1826, EGG-2070, March 1982.

2. K. V. Moore and W. H. Rettig, RELAP2 - A Digital Program for Reactor Blowdown and Power Excursion Analysis, IDO-17263, March 1968.

3. W. H. Rettig et al., RELAP3 - A Computer Program for Reactor Blowdown Analysis, IN-1445, February 1971.

4. K. V. Moore and W. H. Rettig, RELAP4 - A Computer Program for Transient Thermal-Hydraulic Analysis, ANCR-1127, March 1975.

5. S. R. Behling et al., RELAP4/MOD7 - A Best Estimate Computer Program to Calculate Thermal and Hydraulic Phenomena in a Nuclear Reactor or Related System, NUREG/CR-1998, EG&G-2089, August 1981.

6. D. W. Hardgroves et al., CONTEMPT-LT/028--A Computer Program for Predicting Containment Pressure-Temperature Response to a Loss-of-Coolant Accident, NUREG/CR-0252, TREE 1279, August 1978.

7. J. A. Dearien et al., FRAP-T4: A Computer Code for the Transient Analysis of Oxide Fuel Rods, TFBP-TR-237, November 1977.

8. A. R. Edwards and T. P. O'Brien, "Studies of Phenomena Connected with the Depressurization of Water Reactors," Journal of British Nuclear Energy Society, 9, 1970, pp. 125-135.

9. V. H. Ransom and D. L. Hicks, "Hyperbolic Two-Pressure Models for Two-Phase Flow," Journal of Computational Physics, 53, 1984, pp. 124-151.

10. V. H. Ransom and M. P. Scofield, Two-Pressure Hydrodynamic Model for Two-Phase Separate Flow, Idaho National Engineering Laboratory, SRD-50-76, 1976.

11. M. Ishii, Thermo-Fluid Dynamic Theory of Two-Phase Flow, Direction des Etudes et Recherches of Electrucute de France, 1975.

12. F. H. Harlow and A. A. Amsden, "Flow of Interpreting Material Phase," Journal of Computational Physics, 18, 1975, pp. 440-464.

13. P. S. Anderson, P. Astrup, L. Eget, and O. Rathman, "Numerical Experience with the Two-Fluid Model RISQUE," ANS Water Reactor Safety Meeting, July 31-August 4, 1977.

14. N. Zuber, "On the Dispersed Two-Phase Flow in the Laminar Flow Regime," American Institute of Chemical Engineers, 19, 1964, pp. 897-917.

15. L. Van Wijngaarden, "Hydrodynamic Interaction between Gas and Bubbles in Liquid," Journal of Fluid Mechanics, 77, 1, 1976, pp. 27-44.

16. R. T. Lahey, Jr., "RPI Two-Phase Flow Modeling Program," Fifth Water Reactor Safety Research Information Meeting, Washington, D.C., November 7-11, 1977.

17. D. A. Drew, L. Y. Cheng, and R. T. Lahey, Jr., "The Analysis of Virtual Mass Effects in Two-Phase Flow," International Journal of Multiphase Flow, 5, 1979, pp 233-242.

18. J. A. Trapp and V. H. Ransom, "A Choked-Flow Calculation Criterion for Nonnomogeneous, Nonequilibrium Two-Phase Flows", International Journal of Multiphase Flow, 8, 6, 1982, pp. 669-681.

19. A. R. Curtis and J. K. Reid, FORTRAN Subroutines for the Solution of Sparse Sets of Linear Equations, AERE-R6844, Atomic Energy Research Establishment, 1971.

20. D. Gidaspow (Chairman), "Modeling of Two-Phase Flow," Proceedings of Round Table Discussion RT-1-2 at the Fifth International Heat Transfer Conference, Tokyo, Japan, September 3-7, 1974, also in ASME Journal of Heat Transfer, 3, 1974.

21. J. D. Ramshaw and J. A. Trapp, "Characteristics, Stability, and Short-Wavelength Phenomena in Two-Phase Flow Equation Systems," Nuclear Science and Engineering, 66, 1978, pp. 93-102.

22. E. S. Marwil, private communication, EG&G Idaho, Inc., 1983.

23. J. J. Dongarra, C. B. Moler, J. R. Bunch, and G. W. Stewart, LINPACK User's Guide, SIAM, Philadelphia, 1979.

24. H. B. Stewart, "Fractional Step Methods for Thermodynamic Calculations," Journal of Computational Physics, 40, 1981, pp. 77-90.

25. J. H. Mahaffy, "A Stability-Enhancing Two-Step Method for Fluid Flow Calculations," Journal of Computational Physics, 46, 1982, pp. 329-341.

26. V. H. Ransom, private communication, EG&G Idaho, Inc, October 17, 1975.

27. Y. Taitel and A. E. Dukler, "A Model of Predicting Flow Regime Transitions in Horizontal and Near Horizontal Gas-Liquid Flow," AIChE Journal, Vol. 22, pp. 47-55, 1976.

28. Y. Taitel, D. Bornea, and A. E. Dukler, "Modeling Flow Pattern Transitions for Steady Upward Gas-Liquid Flow in Vertical Tubes," AIChE Journal, Vol. 26, pp. 345-354, 1980.

29. M. Ishii and G. De Jarlais, "Inverted Annular Flow Modeling," presented at EG&G, July 27, 1982.

30. M. Ishii and T. C. Chawla, Local Drag Laws in Dispersed Two-Phase Flow, NUREG/CR-1230, ANL-79-105, 1979.

31. M. Ishii and K. Mishima, Study of Two-Fluid Model and Interfacial Area, NUREG/CR-1873, ANL-80-111, 1980.

32. M. A. Vince and R. T. Lahey, Jr., "On the Development of An Objective Flow Regime Indicator," International Journal of Multiphase Flow, 8, 1982, pp. 93-124.

33. D. T. Dumitrescu, "Stomung an einer Luftblase in senkrechten Rohr," Z. Angel Math. Mech. 23, 1943, 139.

34. G. B. Wallis, One-Dimensional Two-Phase Flow, McGraw-Hill Book Company, New York, 1969.

35. A. H. Shapiro and A. J. Erickson, Transactions of ASME, 79, 1957, p. 775.

36. D. Bharathan, H. T. Richter and G. B. Wallis, Air-Water Counter-Current Annular Flow in Vertical Tubes, EPRI, NP-786, 1978.

37. K. T. Chaxton, J. G. Collier, A. J. War, H.T.F.S, Correlation for Two-Phase Pressure Drop and Void Fraction in Tubes, AERE-R7162, 1972.

38. D. Chisholm, "A Theoretical Basis for the Lockhart-Martinelli Correlation for Two-Phase Flow", J. Heat-Mass Transfer, Vol. 10, pp. 1767-1778, Pergamon Press Ltd., 1967; Great Britain.

39. R. W. Lockhart and R. C. Martinelli, "Proposed Correlation of Data for Isothermal Two-Phase, Two-Component Flow in Pipes", Chemical Engineering Progress, 45, 1, 1949, pp. 39-48.

40. F. W. Dittus and L. M. K. Boelter, "Heat Transfer in Automobile Radiators of the Tubular Type," Publications in Engineering, University of California, Berkeley, 2, 1930, pp. 443-461.

41. J. C. Chen, "A Correlation for Boiling Heat Transfer to Saturated Fluids in Convertive Flow," Process Design Development, 5, 1966, pp. 322-327.

42. L. S. Tong, and J. D. Young, "A Phenomenological Transition and Film Boiling Correlation", Proceedings of the 5th International Heat Transfer Conference, Vol. IV, B 3.9, Tokyo, 1974.

43. J. C. Chen et al., A Phenomenological Correlation for Post-CHF Heat Transfer, TS-774, Dept. of M. E., Lehigh University, April 1977.

44. J. G. Collier, Convection Boiling and Condensation, London: McGraw-Hill Book Company, Inc., 1972.

45. M. L. Pomeranz, "Film Boiling on a Horizontal Tube in Increased Gravity Fields, "Journal of Heat Transfer, 86, 1964, pp. 213-219.

46. R. S. Dougall and W. M. Rohsenow, Film Boiling on the Inside of Vertical Tubes with Upward Flow of the Fluid at Low Qualities, MIT Report 9079-76, 1963.

47. M. S. Plesset and S. A. Zwick, "Growth of Vapor Bubbles in Superheated Liquids," Journal of Applied Physics, 25, 4, 1954, 493-500.

48. F. Kreith, Principles of Heat Transfer, New York: Intext Press, Inc., 1973.

49. H. C. Unal, "Maximum Bubble Diameter, Maximum Bubble-Growth Time and Bubble-Growth Rate During the Subcooled Nucleate Flow Boiling of Water Up to 17.MN/m^2," International Journal of Heat Mass Transfer, 19, 1976, pp. 643-649.

50. G. Brown, "Heat Transmission by Condensation of Steam on a Spray of Water Drops," Institute of Mechanical Engineers, 1951, pp. 49-52.

51. T. G. Theofanous, "Modeling of Basic Condensation Processes," The Water Reactor Safety Research Workshop on Condensation, Silver Springs, MD, May 24-25, 1979.

52. A. E. Bergles and W. M. Rohsenow, "The Determination of Forced-Convection Surface-Boiling Heat Transfer", Journal of Heat Transfer, Transactions of ASME, 86, 1964, p. 365.

53. W. H. McAdams, W. E. Keannel, C. S. Minden, R. Carl, P. H. Picornell and J. G. Dew, Procedings of Institute of Chemical Engineering, 41, 1949, p. 1945.

54. T. A. Bjornard and P. Griffith, "PWR Blowdown Heat Transfer," Thermal and Hydraulic Aspects of Nuclear Reactor Safety, ASME, New York, Vol. 1, 17, 1977.

55. J. Weisman, Studies of Transition Boiling Heat Transfer at Pressure from 1-4 Bar, EPRI Report NP-1899, 1981.

56. S. Wang, Y. K. Kao and J. Weisman "Studies of Transition Boiling Heat Transfer with Saturated Water at 1-4 Bar", Nuclear Engineering Design, 70, 1982, p. 223.

57. J. G. M. Andersen, "Low-Flow Film Boiling Heat Transfer on Vertical Surfaces, Part 1: Theoretical Model," and J. E. Leonard, K. H. Sun and G. E. Dix," Part 2: Empirical Formulations and Applications to BWR--LOCA Analysis," AIChE papers AIChE-53 and 54, 1976.

58. L. Arrieta and G. Yadigaroglu, Analytic Model for Bottom Reflooding Heat Transfer in Light Water Reactors, EPRI Report NP-756, 1978.

59. L. A. Bromley, "Heat Transfer in Stable Film Boiling," Chemical Engineering Progress, 46, 1950, pp. 221-227.

60. K. H. Sun, J. M. Gonzalez, C. L. Tien, "Calculations of Combined Radiation and Convection Heat Transfer in Rod Bundles under Emergency Cooling Conditions," Journal of Heat Transfer, Transactions of ASME, 98, 1976, p. 414.

61. W. L. Kirchner, Reflood Heat Transfer in Light Water Reactors, NUREG-0106, August 1976.

62. V. H. Ransom and J. A. Trapp, "The RELAP5 Choked Flow Model and Application to a Large Scale flow Test," Proceedings of the ANS/ASME/NRC International Topical Meeting on Nuclear Reactor Thermal-Hydraulics, Saratoga Springs, New York, October 5-8, 1980, pp. 799-819.

63. P. R. Garabedian, Partial Differential Equations, New York: John Wiley and Sons, 1964.

64. G. B. Whitham, Linear and Nonlinear Waves, New York: John Wiley and Sons, 1974.

65. A. H. Shapiro, The Dynamics and Thermodynamics of Compressible Fluid Flow, II, New York: Ronald, 1954.

66. V. H. Ransom and J. A. Trapp, RELAP5 Progress Summary Analytical Choking Criterion for Two-Phase Flow, CDAP-TR-013, EG&G Idaho, Inc., 1978.

67. N. Abuaf, O. C. Jones, Jr., and B. J. C. Wu, Critical Flashing Flow in Nozzles with Subcooled Inlet Conditions, BNL Informal Report, BNL-NUREG-27512, 1980.

68. M. D. Alamgir and J. H. Lienhard, "Correlation of Pressure Undershoot During Hot Water Depressurization, ASME Journal of Heat Transfer, 103, 1981, pp. 52-73.

69. O. C. Jones, Jr., "Flashing Inception in Flowing Liquids," ASME Journal of Heat Transfer, 102, 1980, pp. 439-444.

70. J. W. Burnell, "Flow of Boiling Water through Nozzles, Orifices, and Pipes," Engineering, 1947, pp. 572-576.

71. F. J. Moody, "Maximum Flow Rate of a Single Component, Two-Phase Mixture," Transactions of the American Society of Mechanical Engineers, February 1965, pp. 136-143.

72. W. M. Bryce, Improvements to the RELAP5/MOD1/014 LOCA Code: The RELAP5/MOD1/WINOO1 Code, AEEW-R-1649, May 1983, pp. 64-65.

73. N. Zuber, Problems in Modeling of Small Break LOCA, NUREG-0724, October 1980.

74. H. Rouse, "Seven Exploratory Studies in Hydraulics," Proceedings of ASCHE, Vol. 82, 1956.

75. A. Craya, "Theoretical Research on the Flow of Non-Homogeneous Fluids," La Houille Blanche, pp. 44-45, January-February 1949.

76. P. Gariel, "Experimental Research on the Flow of Non-Homogeneous Fluids," La Houille Blanche, pp. 56-64, January-February 1949.

77. B. Lubin and M. Hurwitz "Vapor Pull-Through at A Tank Drain--With and Without Dielectrophoretic Baffling," Proc. Conf. Long Term Cryo-Propellant Storage in Space, NASA Marshall Space Center, Huntsville, Alabama, p. 173, October 1966.

78. J. C. Lin, G. E. Gruen, and W. J. Quapp, "Critical Flow in Small Nozzles for Saturated and Subcooled Water at High Pressures," ASME Winter Annual Meeting, Chicago, Illinois, November 1980.

79. C. J. Crowley and P. H. Rothe, "Flow Visualization and Break Mass Flow Measurements in Small Break Separate Effects Experiments," ANS Specialists Meeting on Small Break Loss-of-Coolant Accident Analyses in LWRs, Monterey, California, August 1981.

80. J. Reiman and M. Khan, "Flow Through a Small Break at the Bottom of a Large Pipe With Stratified Flow," The Second International Topical Meeting on Nuclear Reactor Thermal-Hydraulics, Santa Barbara, California, January 1983.

81. J. A. Trapp and V. H. Ransom, RELAP5 Hydrodynamic Model Progress Summary--Abrupt Area Changes and Parallel Branching, PG-R-77-92, EG&G Idaho, Inc., November 1977.

82. J. K. Vennard, Elementary Fluid Mechanics, 4th Edition, New York: John Wiley and Sons, 1965.

83. J. Weisman, T. Ake, R. Knott, "Two-Phase Pressure Drop Across Abrupt Area Changes in Oscillatory Flow," Nuclear Science and Engineering, 61, 1976, pp. 297-309.

84. J. G. Collier, "Advanced Study Institute on Two-Phase Flows and Heat Transfer," ASI Proceedings, Istanbul-Turkey, August 1976.

85. M. M. El-Wakil, Nuclear Heat Transport, Scranton: International Textbook Company, 1971.

86. B. Harshe, A. Hussain, J. Weisman, Two-Phase Pressure Drop Across Restrictions and Other Abrupt Area Changes, NUREG-0062, University of Cincinnati, April 1976.

87. P. A. Lottes, "Expansion Losses in Two-Phase Flows," Nuclear Science and Energy, 9, 1961, pp. 26-31.

88. J. C. Lin, R. A. Riemke, V. H. Ransom, G. W. Johnsen, "RELAP5/MOD2 Pressurizer Modeling," ASME Winter Annual Meeting, New Orleans, Louisiana, December 1984.

89. D. R. Liles et al., TRAC-PF1/MOD1: An Advanced Best-Estimate Computer Program for Pressurized Water Reactor Thermal-Hydraulic Analyses, Los Alamos National Laboratory, DRAFT, December 1983.

90. J. H. Mahaffy and D. R. Liles, "Numerically Induced Pressure Excursions in Two-Phase-Flow Calculations," 2nd International Topical Meeting on Nuclear Reactor Thermal Hydraulics, Santa Barbara, California, January 11-14, 1983.

91. V. H. Ransom et al., RELAP5/MOD0 Code Description, Volume 2, Code Development Update and Sample Problems, CDAP-TR-057, May 1979.

92. EG&G Idaho, Inc., RELAP4/MOD6: A Computer Program for Transient Thermal-Hydraulic Analysis of Nuclear Reactors and Related Systems, Users Manual, CDAP-TR-003, EG&G Idaho, Inc., May 1978.

93. J. K. Salisbury, Steam Turbines and Their Cycles, Kreiger, 1950.

94. R. A. Berry, An Analysis Tool for Predicting Transient Hydrodynamics in Nuclear Piping Systems Containing Swing Check Valves, RE-A-78-261, Rev. 2, EG&G Idaho, Inc., 1978.

95. R. S. Samra, "Impact Energy Calculations for a Steam Check Valve Following a Postulated Pipe Rupture," ASME Winter Annual Meeting, December 1978, 76-WA/FE-8.

96. J. P. Holman, Heat Transfer, 4th edition, New York: McGraw-Hill Book Company, Inc., 1976, pp. 244-245, 280.

97. J. M. Kelly, "Quench Front Modeling and Reflood Heat Transfer in COBRA-TF," ASME Winter Annual Meeting, 79-WA/HT-63, New York, 1979.

98. L. J. Siefken, private communication, EG&G Idaho, Inc., 1983.

99. L. J. Siefken, C. M. Allison, M. P. Bohn, and S. O. Peck, FRAP-T6: A Computer Code for the Transient Analysis of Oxide Fuel Rods, EGG-CDAD-5410, April 1981.

100. A. Ullman, R. Acharya and D. R. Olander, "Thermal Accommodation Coefficients of Inert Gases on Stainless Steel and UO_2," Journal of Nuclear Materials 51, 1974, pp. 277-279 .

101. D. L. Hagrman, G. A. Reymann, and R. E. Mason, MATPRO-Version 11 (Revision 2), NUREG/CR-0479, TREE-1280, Rev. 2, August 1981.

102. "American Nuclear Society Proposed Standard ANS 5.1, Decay Energy Release Rates Following Shutdown of Uranium-Fueled Thermal Reactors," October 1971, revised October 1973.

103. "American National Standard for Decay Heat Power in Light Water Reactors," ANSI/ANS-5.1, 1979.

104. E. R. Cohen, "Some Topics in Reactor Kinetics," A/CONF, 15, 1958, p. 629.

105. A. Schwartz, Generalized Reactor Kinetics Code AIREK II, NAA-SR-Memo-4980, 1960.

APPENDIX A
BRIEF DESCRIPTIONS OF RELAP5/MOD2 SUBROUTINES

APPENDIX A
BRIEF DESCRIPTIONS OF RELAP5/MOD2 SUBROUTINES

RELAP5-- A computer program to simulate a nuclear reactor loss of coolant accident. The program solves coupled two-phase hydrodynamics, heat conduction, heat transfer, reactor kinetics, trip logic, and control systems.

Subroutine: ACCUM

Accumulator mass, wall heat transfer and momentum model.

Subroutine: AXISDV

Divides a plotting axis over the interval xmax - xmin into ndiv or (ndiv + 1) intervals of length xintvl. The data end points are included.

Subroutine: CELMOD

Calculates cladding Youngs modulus and Poissons ratio.

Subroutine: CHFCAL

This subroutine calculates the critical heat flux using the Zuber and Biasi CHF correlations.

Subroutine: CONDEN

Condensation heat transfer correlations.

Subroutine: CONVAR

Advance control variables over a time step.

Subroutine: CRAMER

Solves a set of simultaneous equations by Cramers' rule.

Subroutine: CTHEXPR

Calculates diametral thermal expansion of zircaloy cladding.

Subroutine: DETMNT

Determinant solution. Solution results from a Gaussian reduction of the determinant from which the diagonal is the solution.

Subroutine: DITTUS

Dittus-Boetler forced convection heat transfer correlation.

Subroutine: DOLEND

Subroutine to left justify a character string, delete extraneous blanks, and terminate the character string with a $ symbol. Termination of the string by a $ symbol is optional.

Subroutine: DTSTEP

Controls time step selection and frequency of output and plotting edits during transient advancement.

Subroutine: EQFINL

This subroutine computes the new time pressure and carries out the back substitution to obtain the new time liquid specific internal energy, vapor specific internal energy, void fraction, noncondensible quality, and boron density. It also computes the vapor generation rate and mixture density.

Subroutine: FIDIS

Computes interphase drag term for bubbles and droplets.

Subroutine: FWDRAG

Computes wall drag terms ... includes flow regimes and HTFS correlation.

Subroutine: GAPCON

Computes effective gap conductance.

Subroutine: GASTHC

Computes thermal conductivity for a mixture of gases.

Subroutine: GNINIT

Subroutine performs once-only calculations and general initialization including setting common block length and clearing them.

Subroutine: HELPHD

Subroutine to write the diagnostic print page header.

Subroutine: HIFBUB

Computes liquid HIF for bubbly flow.

Subroutine: HLOSS

Calculates void fractions at throat and downstream of an abrupt area change and associated head loss terms.

Subroutine: HTADV

Controls advancement of heat structures and computes heat added to hydrodynamic volumes.

Subroutine: HTCOND

Returns left and right boundary conditions for a heat structure.

Subroutine: HTCSOL

This subroutine finds temperature solution by back substitution.

Subroutine: HTHETA

Calculation of horizontal stratification angle.

Subroutine: HTRC1

Computes heat transfer coefficient from correlations.

Subroutine: HTRC2

This subroutine computes heat transfer coefficients for the other boundary of the reflood model.

Subroutine: HT1INP

Processes input for the HEAT1 subcode.

Subroutine: HT1SST

Solves the 1-D steady state heat problem.

Subroutine: HT1TDP

Advance one heat structure one time step by advancing transient one-dimensional heat conduction equation.

Subroutine: HT2TDP

This subroutine solves the 2-D transient heat problem and computes the radial 1-D average quantities.

Subroutine: HYDRO

This subroutine controls the advancement of the hydrodynamic calculation.

Subroutine: HZFLOW

Vapor pull-through and liquid entrainment model for stratified horizontal flow. Also adjusts donor void fractions for U-tube and inverted U-tube geometries.

Subroutine: ICMPF

Finds index, i, for component ixl. Sets ERR to .TRUE. if component has not been entered.

Subroutine: ICMPN1

Controls cross checking of component input and first pass of component initialization.

Subroutine: ICOMPN

Controls cross checking of component input and completion of component initialization.

Subroutine: ICOMPT

This subroutine checks and initializes the plot comparison data tables.

Subroutine: ICONVR

Check control system variable requests, compute initial values.

Subroutine: IEDIT

This subroutine writes a summary of the hydrodynamic volume and junction conditions after completion of input processing.

Subroutine: IELVTN

Checks input and edits elevations around each loop of each hydrodynamic system.

Subroutine: IGNTBL

Cross checks and establishes linkages for general tables and trips.

Subroutine: IHTCMP

Checks and performs referrals on geometry, compositions, source distributions, and initial temperatures between heat structures. Checks composition numbers, checks heat transfer types, and calls subroutine for steady state initialization of specified heat structures.

Subroutine: IJPROP

Computes junction properties as part of input initialization.

Subroutine: IMIEDT

Uses minor edit request file written in RMIEDT to prepare minor edit control file.

Subroutine: IMLP

Prepares multiple loop table, loads number of volumes, junctions, and components per loop, and establishes the order for processing.

Subroutine: INPUT

Controls all input data processing. If an error is found, editing for the case is completed, but all following cases only have their input listed.

Subroutine: INTERI

Process interactive input data from NPA and transfer results to NPA.

Subroutine: INVJT

Prepares inverted junction table and checks for proper number of junctions per volume.

Subroutine: IPIPE

Sets to-from pointers and initial conditions for a pipe component.

Subroutine: IPLOAD

Strip plot records from RSTIN and write plot data to PLOTFL for internal plotting.

Subroutine: IPLOT

Subroutine to check, initialize and cross reference the plot request files.

Subroutine: IPLTSI

This routine converts comparison data to SI and scales X values by CON1.

Subroutine: IPLT2D

Subroutine to check and initialize the 2-D plot requests and specifications.

Subroutine: IPUMP

Resolves table pointers and computes frictional torque if requested in pump input.

Subroutine: IRFLHT

This subroutine checks reflood input and sets up reflood indices.

Subroutine: IRKIN

Complete checking of reactor kinetic input, set pointers, and compute bias reactivity.

Subroutine: ISNGJ

Checks and sets to-from pointers for single junctions, time dependent junctions, pumps, branches, separators, and turbines.

Subroutine: ISTATE

Computes various thermodynamic properties from initial conditions for normal volumes and for time dependent volumes after interpolation for time = 0.0.

Subroutine: ITRIP

Complete checking and processing of trip data and set initial values of trip.

Subroutine: ITRSCN

Check that NUM is valid trip number in trip IR and return packed code in ICODE.

Subroutine: IUSRVR

Check user-supplied RSTPLT file variable requests for validity.

Subroutine: IVELST

Sets initial conditions for single junctions, time dependent junctions, pumps, branches, tees and pipes.

Subroutine: IVLVEL

Calculates average volume velocities by averaging the average junction velocities in and out of the volume called during hydrodynamic component initialization.

Subroutine: JCHOKE

Computation of choking criteria.

Subroutine: JPROP

Computes junction properties.

Subroutine: MADATA

Computes thermal conductivity and volumetric heat capacity for each mesh interval using the average of the temperatures of the mesh points bounding the interval.

Subroutine: MAJOUT

This subroutine prints the major edit of the transient and steady state results.

Subroutine: MDATA2

This subroutine computes the thermal conductivity and volumetric heat capacity at the center of each X-direction interval for 2-D heat conduction calculations. The subroutine is a modification of subroutine MADATA for reflood heat transfer.

Subroutine: MIREC

Transfers results of time step to save area for minor edits and edits the information if save area is full.

Subroutine: MOVER

Moves hydrodynamic variables from new to old (old to new) time values if a time advancement is successful (unsuccessful).

Subroutine: PACKER

This subroutine determines if water packing occurs, and if it does, it modifies terms used in the velocity equations.

Subroutine: PHAINT

This subroutine computes interphase drag and heat transfer. It also calculates some information for VEXPLT. (This replaces the earlier subroutines FIDRAG and MDOT).

Subroutine: PIMPLT

This subroutine carries out the back substitution to obtain the new time pressure and boron density as well as the intermediate time liquid specific internal energy, vapor specific internal energy, void fraction, and noncondensible quality. It also computes the vapor generation rate and the remainder of the source terms for the mass and energy equations used in the implicit solution scheme.

Subroutine: PLOTMD

Controls plotting using data generated in this case or obtained from a restart/plot file.

Subroutine: PLOTS

Subroutine to sort plot information and call the 2-D and 3-D plot routines.

Subroutine: PLOT2D

Subroutine to draw 2-D plots with ncurvs curves drawn on each plot.

Subroutine: PLOT3D

Plots 3-D surfaces using the DISSPLA system.

Subroutine: PLTCOM

Makes NOPLTS plots with NCURVS curves drawn on each plot for comparison.

Subroutine: PLTREC

Subroutine to store plot data on disk for internal plots.

Subroutine: PLTWRT

Write plot records on restart-plot file.

Subroutine: POLATL

Performs linear interpolation on data in LCM.

Subroutine: POLATS

Performs linear interpolation on data in SCM.

Subroutine: PREDNB

Pre-DNB forced convection heat transfer correlations.

Subroutine: PRESEQ

Using the phasic equations for mass and energy to eliminate liquid specific internal energy, vapor specific internal energy, void fraction, and noncondensible quality. This subroutine builds the matrix elements and the source vector elements for the resultant pressure equation.

Subroutine: PSATPD

Calculate saturation pressure, PRESS, and DPDT, PRESDT, for a given temperature, T, if ITYPE=1. Calculate saturation temperature, T, and DPDT, PRESDT, for a given pressure if ITYPE=2.

Subroutine: PSET

Sets array elements as required by sparse matrix solution subroutine that uses existing strategy from previous solution.

Subroutine: PSTDNB

Post-DNB forced convection heat transfer correlations.

Subroutine: PUMP

Computes pressure change and torque for pump, torque for inductive motor if present, and advances pump speed if not connected to a shaft control component.

Subroutine: PUMP2

Interpolate pump homologous curves.

Subroutine: QFHTRC

This subroutine computes reflood heat transfer coefficients using the pattern obtained in the subroutine QFSRCH.

Subroutine: QFMOVE

This is the driving subroutine for the reflood calculation.

1. Test the condition for the beginning of reflood.
2. Set up the initial axial nodes.
3. Call QFSRCH to find heat transfer patterns.
4. Perform fine mesh rezoning.
5. Call QFHTRC to find heat transfer coefficients.
6. Call HT2TDP to advance temperatures.

Subroutine: QFSRCH

This subroutine searches heat transfer patterns and determines the number of axial nodes.

Subroutine: RACCUM

Process accumulator component data.

Subroutine: RBRNCH

Process branch or separator component data.

Subroutine: RCARDS

Subroutine reads input data for the next case, writes data on disk if not last case.

Subroutine: RCDELT

Deletes an existing hydrodynamic component.

Subroutine: RCOMPN

Controls processing of hydrodynamic components.

Subroutine: RCOMPT

Subroutine to input the plot comparison data tables and curve specifications.

Subroutine: RCONVR

Process control component data.

Subroutine: RCRVSP

Subroutine to input plot curve drawing specifications and labeling. (the curve drawing specifications are packed into the last word of KURVSP.)

Subroutine: RGNTBL

Process general table data.

Subroutine: RHTCMP

Process input data and set storage for heat structures.

Subroutine: RINTRV

Process input defining interactive input and output variables.

Subroutine: RKIN

Advance space independent reactor kinetics.

Subroutine: RMADAT

Process thermal property composition data.

Subroutine: RMFLDS

Reads optional hydrodynamic system cards that specify reference volume, its elevation, fluid in system, and system name.

Subroutine: RMIEDT

Process minor edit cards.

Subroutine: RNEWP

Processes input data for new problem as opposed to restart, plot, re-edit, or strip problems.

Subroutine: RNONCN

Processes input data for constants needed in noncondensibles calculation.

Subroutine: RONOFF

Rounds value to the n^{th} significant digit.

Subroutine: RPIPE

Process pipe component data.

Subroutine: RPLOPS

Subroutine to input the plot option cards and pack the options into one word.

Subroutine: RPLOT

Process input data for plotting from a restart-plot file.

Subroutine: RPLOTF

Loads restart input files for use in plotting.

Subroutine: RPLOTN

Subroutine to input the plot header cards.

Subroutine: RPLT2D

Subroutine to input the plot request and specification cards for each plot.

Subroutine: RPMPDC

Process pump description cards for pump component.

Subroutine: RPMPMD

Process pump multiplier data for two-phase degradation.

Subroutine: RPMPVNJ

Process volume and junction data of pump component.

Subroutine: RPUMP

Subroutine that processes pump component input data.

Subroutine: RPUNIT

Subroutine to check the plot data units keyword and to input units conversion coefficients.

Subroutine: RRESTF

Reads restart input file, input data for output restart file, and copies input to output file.

Subroutine: RRKIN

Process reactor kinetics input data.

Subroutine: RRKINH

Compute initial conditions of fission product decay groups from input power history.

Subroutine: RRSTD

Read data for restart file.

Subroutine: RSIZPL

Subroutine to input the plot size specifications.

Subroutine: RSNGJ

Process single junction input data.

Subroutine: RSNGV

Process single volume input data.

Subroutine: RSTFIN

Do final actions on restart-plot file.

Subroutine: RSTREC

Writes restart records on file RSTPLT.

Subroutine: RSTRIP

Process input data for strip option.

Subroutine: RTMDJ

Process time dependent junction input data.

Subroutine: RTMDV

Process time dependent volume input data.

Subroutine: RTRIP

Process trip input data cards.

Subroutine: RTSC

Process time step control cards.

Subroutine: RTURB

Process turbine component data.

Subroutine: RUSRVR

Process user-supplied variables to be added to the RSTPLT for plotting and/or interactive mode.

Subroutine: RVALVE

Process valve input data. A valve has the same input as a single junction in addition to valve data. Valve types processed are trip valve, check valve, inertial swing check valve, motor valve, servo valve, and relief valve.

Subroutine: SCNREQ

Processes variable requests used in minor edit requests, plotting requests, trip specifications, control variables, and interactive variables.

Subroutine: SIMPLT

This subroutine computes the new time liquid specific internal energy, vapor specific internal energy, and void fraction using implicit convective terms in the mass and energy equations. It also computes the mixture density and mass flow rate.

Subroutine: SORTPR

Subroutine to sort and collect plot variable pointers.

Subroutine: SRESTF

Reads restart input file, input data for strip file, and PLOTALF and PLOTNUM records.

Subroutine: SSTAT

Controls advancement of the steady state solution.

Subroutine: SSTCHK

Subroutine to test for steady state.

Subroutine: SSTCTL

Calls the setup, advancement, and finishing subroutine for steady state.

Subroutine: SSTFIN

Re-acquire SCM-LCM space and delete all SCM files.

Subroutine: SSTSET

Protects and checks coding for steady state advancement, loads required files from disk, computes indexes of actual locations for component blocks, calls subroutines to acquire matrix solution space and controls for loading matrix, and calls subroutine to release excess space.

Subroutine: STACC

Advances energy equation and evaluates equation of state for an accumulator.

Subroutine: STATE

Controls the evaluation of the equation of state for all components.

Subroutine: STATEP

Compute equation of state and derivatives for time advanced volumes.

Subroutine: STRFIN

Do final actions on strip file.

Subroutine: STRIP

Write strip file by copying information from restart-plot file.

Subroutine: STSTEP

Controls time step selection and frequency of output and plotting edits during steady state advancement.

Subroutine: SURTEN

Computes surface tension given temperature. Formula from Schmidt, properties of water and steam in SI units, 1969.

Subroutine: SWAPLT

Subroutine to swap plot and plot comparison data table files for restart and plot runs.

Subroutine: SYSITR

Solve system of equations by iteration.

Subroutine: SYSSOL

Solves system of equations using sparse matrix subroutines.

Subroutine: TCNVSL

Set indexes for advancement of control variables.

Subroutine: THCON

Computes thermal conductivity of saturated liquid and saturated vapor, and superheated vapor, 1967 ASME tables.

Subroutine: TPAWHT

This subroutine calculates the heat transfer for the air-water mixture.

Subroutine: TRAN

Controls advancement of transient problems.

Subroutine: TRIP

Tests trip conditions and sets trip conditions and time of trip.

Subroutine: TRNCTL

Calls set up, advancement, and finish subroutines for transient problem.

Subroutine: TRNFIN

Re-acquire SCM-LCM space and delete all SCM files.

Subroutine: TRNSET

Protects and checks coding for transient advancement, loads required files from disk, computes indexes of actual locations for component and junction blocks, calls subroutines to acquire matrix solution space and controls for loading matrix, and calls subroutine to release excess space.

Subroutine: TSETSL

Obtains space and sets arrays needed to control loading and solving of pressure equations.

Subroutine: TSTATE

This subroutine processes time dependent volumes-junctions.

Subroutine: TURBST

This subroutine evaluates the turbine stage performance factors, power, and torque.

Subroutine: VALVE

Computes behavior of valves.

Subroutine: VEXPLT

This subroutine computes the explicit liquid and vapor velocities and the pressure gradient coefficients needed for the implicit pressure solution. It also computes the old time source terms for the mass and energy equations.

Subroutine: VFINL

This subroutine calls the Subroutines PRESEQ and SYSSOL, and it then computes the new velocities and mass flow rate. It also checks for bad donoring and water packing.

Subroutine: VIMPLT

This subroutine computes the new time liquid and vapor velocities using implicit coupled momentum equations. It also computes the old time source terms for the mass and energy equations.

Subroutine: VISCOG

Calculates water vapor viscosity.

Subroutine: VISCOL

Calculates liquid water viscosity.

Subroutine: VLVELA

Calculates average volume velocities from the average volumetric flow rate normalized to the volume flow area.

Subroutine: VOLVEL

Calculates the junction phasic mean abs(velocities) normalized to the volume flow area for use in the wall friction routine. Also calculates the two step linearized volume velocity coefficients and the momentum flux viscous terms for use in the momentum solution routines.

Subroutine: WRITPL

Write plot records from RSTIN to PLOTFL for internal plotting.

Subroutine: WRPLID

Write two records on RSTPLT to identify data on PLTREC records for stripping and plotting.

NRC FORM 335 (2 84) NRCM 1102 3201, 3202

U.S. NUCLEAR REGULATORY COMMISSION

BIBLIOGRAPHIC DATA SHEET

SEE INSTRUCTIONS ON THE REVERSE

1 REPORT NUMBER (Assigned by TIDC add Vol. No., if any)

NUREG/CR-4312
EGG-2396

2 TITLE AND SUBTITLE

RELAP5/MOD2 CODE MANUAL
VOLUME 1: CODE STRUCTURE, SYSTEMS MODELS AND SOLUTION METHODS

3 LEAVE BLANK

4 DATE REPORT COMPLETED

MONTH: August | YEAR: 1985

5 AUTHOR(S)

V. H. Ransom, R. J. Wagner, et al.

6 DATE REPORT ISSUED

MONTH: August | YEAR: 1985

7 PERFORMING ORGANIZATION NAME AND MAILING ADDRESS (Include Zip Code)

EG&G Idaho, Inc.
Idaho Falls, ID 83415

8 PROJECT/TASK/WORK UNIT NUMBER

9 FIN OR GRANT NUMBER

A6330

10 SPONSORING ORGANIZATION NAME AND MAILING ADDRESS (Include Zip Code)

Division of Accident Evaluation
Office of Nuclear Regulatory Commission
U.S. Nuclear Regulatory Commission
Washington, DC 20555

11a TYPE OF REPORT

Technical

b PERIOD COVERED (Inclusive dates)

12 SUPPLEMENTARY NOTES

13 ABSTRACT (200 words)

The principal objective of the RELAP5 project is to provide the United States Nuclear Regulatory Commission (USNRC) with a fast running and user convenient light water reactor system transient analysis code for use in rule making, licensing audit calculations, evaluation of operator guidelines, and as a basis for a nuclear plant analyzer. The RELAP5/MOD2 code has been developed for best estimate transient simulation of pressurized water reactors and associated systems. The code modeling capabilities are simulation of large and small break loss-of-coolant accidents, as well as operational transients such as anticipated transient without SCRAM, loss-of-offsite power, loss of feedwater, and loss of flow. A generic modeling approach utilizes as much of a particular system to be modeled as necessary. RELAP5/MOD2 extends the modeling base and capabilities offered by previous versions of the code. In particular, MOD2 contains two energy equations, reflood heat transfer, a two-step numerics option, a gap conductance model, revised constitutive models, and additional component and control system models.

14 DOCUMENT ANALYSIS - a KEYWORDS/DESCRIPTORS

b IDENTIFIERS/OPEN-ENDED TERMS

15 AVAILABILITY STATEMENT

Unlimited

16 SECURITY CLASSIFICATION

(This page) Unclassified

(This report) Unclassified

17 NUMBER OF PAGES

18 PRICE

EG&G Idaho, Inc.
P.O. Box 1625
Idaho Falls, Idaho 83415